

LIPID RAFTS IN ARABIDOPSIS THALIANA LEAVES

DISSERTATION ZUR ERLANGUNG DES NATURWISSENSCHAFTLICHEN DOKTORGRADES
DER JULIUS-MAXIMILIANS-UNIVERSITÄT WÜRZBURG

VORGELEGT VON

FATIH DEMIR

AUS MANNHEIM

WÜRZBURG 2010

Prüfungskommission

Eingereicht am: 30. September 2010

Vorsitzender: Prof. Dr. Thomas Dandekar

1. Gutachter: Prof. Dr. Rainer Hedrich

2. Gutachter: Prof. Dr. Gregory Harms

Tag des Promotionskolloquiums:

Doktorurkunde ausgehändigt am:

Acknowledgments

★ First, I would like to thank Prof. Dr. Rainer Hedrich for giving me the opportunity to carry out this research project in a vibrant and stimulating working group with great chances and responsibilities. And for his support whenever I needed it.

★ Prof. Dr. Gregory Harms for being my second referee and bearing my contempt in writing an English PhD thesis as a non-native speaker.

★ My supervisors Dr. Ines Kreuzer for the supervision of the project and being critical on lipid raft topics and Dr.es Jörg & Yvonne Reinders for teaching me mass spectrometry and the advantages of having a working pre-column which was not stiffed with lipids of all kinds. All the mass spectrometric measurements and data were acquired by a Demir-Reinders cooperation. I also greatly appreciate the technicians and PhD students in the Reinders lab in Regensburg who performed the practical sample preparation for mass spectrometry.

★ Jörg Blachutzik conducted microscopy and revealed all the nice co-localization data which appeared in our publication and also in this thesis – thanks for the bright spots on a dark background.

★ My molecular biology capacities, Dr. Dietmar Geiger & his group members for the generation of binary fusion constructs of ABI1, CPK21 and SLAH3. And of course Sönke Scherzer for conducting electrophysiological measurements of the ABI1-CPK21-SLAH3 interaction in *Xenopus laevis* oocytes.

★ Nazeer Ahmed for being so brave that he proof-read my thesis at first and refused the huge amount of dashes and semicolons. RIP all the dashes and semicolons.

★ All the gardeners & technicians of the Botany I, but especially Joachim Rotenhöfer. We saw so many fields of *Arabidopsis thaliana*, *Nicotiana benthamiana* and *Dionaea muscipula* growing and being killed by me. Thanks for organizing the plants and keeping an eye on them. I do not want to summarize the amount of biomass I destructed in the last 3.5 years.

★ Our cat Medolie who always bited me when I worked too long on this thesis – thanks for that!

★ Especially my beloved wife Liliana Demir — I hope, I can compensate all the lost hours, days, weeks which were spent on scientific work somehow, sometime, somewhere.

★ Last but not least I would like to acknowledge the financial support from the DFG Graduiertenkolleg 1342 "Lipid signalling" in form of a tax-free stipend.

Contents

List of Tables	xiii
List of Figures	xv
1. Introduction	1
1.1. Membrane structure	2
1.1.1. Components of the membrane	2
1.1.2. Singer-Nicolson model	4
1.1.3. Evidence for organization	6
1.1.4. Lipid modifications	7
1.1.4.1. Myristoylation	7
1.1.4.2. Palmitoylation	8
1.1.4.3. Prenylation	8
1.1.4.4. GPI-anchor	9
1.1.4.5. Overview of lipid modifications	9
1.1.4.6. Lipid modifications in plants	10
1.2. Lipid rafts	13
1.2.1. Sizing lipid rafts	14
1.2.2. Sterols & disruption by MCD	14
1.2.3. Model membranes	16
1.2.3.1. Cholesterol & the organizing effect	16
1.2.3.2. Visualizing lipid rafts	18
1.2.3.3. Detergent insolubility	18
1.2.3.4. Lipid modifications	20
1.2.3.5. Phytosterols & model membranes	20
1.2.4. Yeast lipid rafts	21
1.2.4.1. Mating in <i>S. cerevisiae</i>	22
1.2.4.2. Cell cycle control	23
1.2.5. Lipid rafts in animals	24
1.2.5.1. Diseases involving lipid rafts	24
1.2.5.2. Non-sphingolipids & -sterols	26
1.2.5.3. Raft sizes in animals	26
1.2.5.4. Caveolae	27
1.2.5.5. Signaling complexes in animal lipid rafts	29
1.2.5.6. Activity & affinity regulation via lipid raft localization	31

Contents

1.2.6.	Lipid rafts in plants	32
1.2.6.1.	Plant plasma membranes	32
1.2.6.2.	Evidence for organization in the plant PM	33
1.2.6.3.	Previous DRM investigations in plants	34
1.2.6.4.	Identification of a putative plant lipid raft marker	40
1.3.	Aims of the study	44
2.	Methods	45
2.1.	Membrane isolation	45
2.1.1.	Plant cultivation	45
2.1.2.	Homogenization of plant material	45
2.1.3.	Isolation of microsomal fraction	46
2.1.4.	Plasma membrane isolation	46
2.1.5.	DRM isolation	48
2.1.5.1.	Sterol depletion by MCD	48
2.1.5.2.	Detergent-treatment	48
2.1.5.3.	Sucrose density centrifugation	49
2.1.5.4.	Fractionation of the sucrose gradient	49
2.1.5.5.	Preparation of DRM samples for mass spectrometry	49
2.2.	Protein biochemistry	50
2.2.1.	Gel electrophoresis	50
2.2.1.1.	Sample preparation	50
2.2.1.2.	SDS-PAGE	51
2.2.1.3.	Gel visualization	52
2.2.2.	Western blot	53
2.2.2.1.	Transfer	53
2.2.2.2.	Antibody detection	54
2.2.3.	Protein quantification	57
2.2.4.	Precipitation methods	57
2.2.4.1.	TCA / Acetone precipitation	58
2.2.4.2.	Chloroform / Methanol precipitation	58
2.2.4.3.	Sodiumcarbonate precipitation	59
2.2.4.4.	Wang precipitation	59
2.3.	Mass spectrometry	60
2.3.1.	Sample preparation	60
2.3.1.1.	Trypsin	60

2.3.1.2.	In-gel digestion	60
2.3.1.3.	Washing of gel pieces	60
2.3.1.4.	In-solution digestion	60
2.3.1.5.	Formic acid Extraction	62
2.3.2.	Data acquisition	62
2.3.2.1.	Quantitative analysis via emPAI	62
2.3.2.2.	Data acquirement	63
2.3.2.3.	Database search parameters	64
2.3.2.4.	Data evaluation	64
2.3.2.5.	Protein data sources & lipidation predictors	64
2.4.	Molecular biology	65
2.4.1.	Bacterial cultivation	65
2.4.1.1.	DNA transformation	65
2.4.2.	DNA gel electrophoresis	66
2.4.3.	DNA purification	66
2.4.3.1.	DNA miniprep	66
2.4.3.2.	DNA midiprep	67
2.4.3.3.	DNA purification from agarose gels	67
2.4.4.	DNA quantification	68
2.4.5.	DNA sequencing	68
2.4.6.	Primer design	68
2.4.7.	PCR Amplification	68
2.4.7.1.	Colony PCR	69
2.4.7.2.	USER PCR	69
2.4.7.3.	PCR Profiles	70
2.4.8.	Restriction digest	70
2.4.9.	Particle Inflow Gun (PIG)	71
2.4.9.1.	Preparation of tungsten particles	71
2.4.9.2.	Coating of tungsten particles with DNA	71
2.4.9.3.	Transient transformation via PIG	72
2.4.9.4.	Fluorescence microscopy	72
2.4.9.5.	Analyzing co-localization experiments	72
2.4.10.	Transient expression in <i>N. benthamiana</i>	73
2.4.10.1.	Used vector constructs	73

3. Results 75

3.1. Analyzing DRMs from <i>A.th.</i> leaves	75
3.1.1. Quality control of the PM preparations	75
3.1.2. Characterization of Triton X-100 & Brij-98 DRMs	77
3.1.2.1. Quantitative analysis of protein amounts in the DRM isolation	77
3.1.2.2. Characterizing DRM isolations by sucrose gradients	78
3.1.3. Proteomic analysis of <i>A.th.</i> leaf DRMs	79
3.1.3.1. Detergent & digestion protocol effects on protein composition	80
3.1.3.2. Functional classification	81
3.1.3.3. Triton X-100 & Brij-98 specific DRM proteins	82
3.1.3.4. Molecular weight distribution	85
3.1.3.5. Transmembrane domains	86
3.1.3.6. Hydrophobicity properties	87
3.1.3.7. Identification of putative DRM-specific proteins	88
3.1.4. MCD effects on Triton X-100 DRMs	88
3.2. Investigation of candidate DRM / raft proteins	96
3.2.1. Biochemical characterization of eGFP::StRem 1.3 overexpressor	96
3.2.2. Biochemical characterization of DRMs / DSF	97
3.2.3. AtLipocalin & AtSUC1 / 2 localization	100
3.3. Transient co-expression of ABI1, CPK21 & SLAH3	103
3.3.1. Transient expression in <i>N.b.</i>	103
3.3.1.1. Assaying sterol dependency of transiently expressed CPK21	104
3.3.2. Transient co-expression in <i>N.b.</i>	105
4. Discussion	109
4.1. <i>Arabidopsis thaliana</i> DRM protein composition	110
4.1.1. DRMs enriched in signaling & transport proteins	110
4.1.2. Correlation with previous DRM studies	111
4.1.3. Post-translational modifications	114
4.1.4. Sterol-depletion by MCD identifies "true" raft members	115
4.2. Raft & non-raft markers	118
4.2.1. AtRem 1.2 / 1.3 as model lipid raft markers	118
4.2.2. AtLipocalin as a non-raft marker	119
4.3. ABI1, CPK21 & SLAH3 form a DRM-resident protein complex	120
4.3.1. Regulation of stomatal closure	120
4.3.2. ABI1, CPK21 & SLAH3 are located in DRMs	121
5. Summary	125

6.	Zusammenfassung	127
7.	Bibliography	129
A.	Protein lists	161
B.	Vector maps	201
B.1.	eGFP::StRem 1.3	201
B.2.	eGFP::AtRemorin 1.2	202
B.3.	DsRed2::AtRemorin 1.3	203
B.4.	eGFP::AtSUC1	204
B.5.	eGFP::AtSUC2	205
B.6.	eGFP::AtLipocalin	206
B.7.	DsRed2::AtLipocalin	207
B.8.	ABI1::V5	208
B.9.	CPK21::V5	209
B.10.	SLAH3::V5	210
C.	Terminology	211
Glossary		212
Acronyms		215
D.	CV	223
D.1.	Publication(s)	224
E.	Erklärung	225

List of Tables

1.1. Summary of common lipid modifications	10
1.2. Summary of previous plant DRM research	39
2.1. Homogenization buffer	45
2.2. Two-phase buffer	46
2.3. Configuration of the two-phase partitioning systems	47
2.4. 6x SDS sample buffer	51
2.5. Separation gel composition (10 mL)	51
2.6. Stacking gel composition (10 mL)	51
2.7. 5x Tris-Glycine SDS running buffer, pH 8.3	55
2.8. Simple western blot transfer buffer, pH 8.4	55
2.9. Three buffer western blot transfer system	55
2.10. PBS / TBS buffers for immunological assays	55
2.11. Antibodies	56
2.12. Usual dilutions for protein quantification	57
2.13. Washing buffers MS analysis of gel pieces	61
2.14. Solvents used by in-solution digestion	61
2.15. Solvents used by in-solution digestion	62
2.16. Solvents used in nano-HPLC	63
2.17. LB medium	65
2.18. SOB / SOC medium	65
2.19. 10x TBE buffer (pH 8.3)	66
2.20. 5x DNA sample buffer	66
2.21. TENS buffer	67
2.22. Error-prone Taq PCR reaction	69
2.23. Colony PCR	69
2.24. USER PCR	70
2.25. PCR profiles	70
2.26. Restriction digest	71
2.27. GFP / V5 fusion constructs used for N.b. infiltration	74
3.1. Protein concentrations during two-phase partitioning	77
3.2. Brij-98 specific DRM proteins	83
3.3. Triton X-100 specific DRM proteins	84
3.4. Proteins only identified in DRMs	88

List of Tables

3.5. Triton X-100 DRM proteins not detected following MCD treatment	90
3.6. Moderately MCD affected Triton X-100 DRM proteins	95
A.1. Proteins identified in the plasma membrane	162
A.2. Proteins identified in Triton X-100 DRMs	186
A.3. Proteins identified in Brij-98 DRMs	194

List of Figures

1.1. Sphingolipid content in A.th. DRMs & DSF	3
1.2. Membrane structure acc. to the Singer-Nicolson model	5
1.3. Lipid modifications on plant DRM / non-DRM proteins	11
1.4. Visualized lipid rafts containing PLAP	19
1.5. Can1 localization in MCC is dependent upon membrane depolarization	22
1.6. Shape & structure of caveolae	27
1.7. PEN1 & PEN3 interactions in lipid rafts at the plant PM	34
1.8. Publications concerning lipid rafts / microdomains	35
1.9. Potential structure of lipid rafts	36
1.10. Protein structure of the remorin proteins StRem 1.3 & AtRem 1.2 / 1.3	42
2.1. Overview of the DRM isolation procedure	50
3.1. Immunoblot analysis of PM Purity	76
3.2. Quantitative analysis of protein amounts in DRMs	77
3.3. Overview of the sucrose & protein distribution in a sucrose density gradient	78
3.4. Composition of Brij-98 & Triton X-100 DRMs	79
3.5. Functional classification of DRMs & PM	82
3.6. Molecular weight distribution of DRMs & PM	85
3.7. Transmembrane domains of DRMs & PM	86
3.8. Hydrophobicity of DRMs & PM	87
3.9. MCD effects on the DRM protein composition	89
3.10. Functional classification of strongly MCD affected Triton X-100 DRM proteins	92
3.11. MCD effects on the eGFP::StRem 1.3 overexpressor line	96
3.12. Titration of custom AtRem 1.2 / 1.3 & AtLipocalin antibody concentrations	97
3.13. Immunological characterization of A.th. DRMs & DSF	98
3.14. Co-localization studies of AtRem 1.2 / 1.3 with candidate DRM proteins	101
3.15. Statistical analysis of co-localization studies with AtRemorins	102
3.16. Transient expression of ABI1, CPK21 & SLAH3 in N.b.	103
3.17. Transient expression of CPK21 in N.b. \pm MCD treatment	104
3.18. Transient co-expression of ABI1, CPK21 & SLAH3 in N.b. DRMs	105
3.19. Transient co-expression of ABI1, CPK21 & SLAH3 in N.b. DRMs & DSF	106
3.20. Transient co-expression of ABI1::V5, CPK21::YFP and SLAH3::V5 in N.b. DRMs & DSF	107
3.21. Sterol dependency of the CPK21 and SLAH3 complex	108

List of Figures

4.1. Correlation with previous Triton X-100 DRM studies	112
4.2. Post-translational lipid modifications in DRMs	114
4.3. Post-translational lipid modifications in the PM	115
4.4. Hypothetical interactions among ABI1, CPK21 & SLAH3 at the plant PM . .	122
B.1. Vector map of eGFP::StRem 1.3 / pK7WGF2	201
B.2. Vector map of eGFP::AtRemorin 1.2	202
B.3. Vector map of DsRed2::AtRemorin 1.3	203
B.4. Vector map of eGFP::AtSUC1 / pSAT 1396 USER	204
B.5. Vector map of eGFP::AtSUC2 / pSAT 1396 USER	205
B.6. Vector map of eGFP::AtLipocalin / pSAT 1396 USER	206
B.7. Vector map of DsRed2::AtLipocalin / pSAT 2242 USER	207
B.8. Vector map of ABI1::V5 / pCambia 7	208
B.9. Vector map of CPK21::V5 / pCambia 7	209
B.10. Vector map of SLAH3::V5	210

1

Introduction

Scio me nihil scire

(Socrates)

Every cell in nature needs a delimitation of the interior cytosol against the extracellular space. This is accomplished by the plasma membrane. The plasma membrane has always been a major focus due to central functions of substance exchange through endo- and exocytosis and active and passive transport. An additional role for the plasma membrane is the perception of extracellular signals from elicitors, hormones and pH. Some well-known examples include the BRASSINOSTEROID INSENSITIVE-1 (BRI1) (Li *et al.*, 2002) and FLAGELLIN SENSITIVE-2 (FLS2) receptor (Gómez-Gómez & Boller, 2000) in *Arabidopsis thaliana* (*A.th.*). Animal & plant plasma membranes thereby exhibit a strong bias on signaling and transport functions.

In the animal field attention has been drawn to small-sized platforms ("microdomains" or "lipid rafts") with a specific lipid & protein composition (Moffett *et al.*, 2000; Simons & Ikonen, 1997; Stulnig *et al.*, 1998), which play an important role in many signaling processes (Simons & Toomre, 2000). Investigations in the plant field dealing with the lipid & protein composition of these lipid rafts revealed a similar pattern for the plant plasma membrane (Borner *et al.*, 2005; Shahollari *et al.*, 2005). However, the physiological relevance of plant lipid rafts has yet to be attributed to a specific function or structure.

1.1 MEMBRANE STRUCTURE

Right at the beginning of the 1920s it was clear that cell membranes must be comprised of a lipid bilayer (Gorter & Grendel, 1925). Lipid bilayers were thought to be constituted of phospholipids, which were polarly oriented in this bilayer exposing the hydrophilic head groups of the fatty acids to the aqueous media.

The lipid bilayer consists of two leaflets, which are facing either to the cytosolic interior or the extracellular space. Both leaflets are not similarly constituted, thus displaying differences in their lipid and protein composition. To attribute these differences in compositions, alternative models of the membrane structure have been proposed (see 1.2, p. 13).

1.1.1. Components of the membrane

Biological membranes are composed of many different lipids and proteins. For many cell types in animals, fungi & plants, the major components of the plasma membrane are phospholipids (free fatty acids, sphingolipids) and sterols (Bretscher & Raff, 1975). Cholesterol was known to be an intrinsic member of lipid vesicles for a long time (Havel *et al.*, 1955). It represents the main sterol for the animal system whereas campesterol and sitosterol are the main sterols for the plant system (Kierszniowska *et al.*, 2008); cholesterol is found only in marginal amounts in the plant plasma membrane (PM). For the plant system it has been shown that sterols are quite abundant, representing 30 – 40 mol % of the PM. A further 10 – 20 mol % are constituted by sphingolipids, whereas the rest of the PM is comprised of phospholipids (Uemura *et al.*, 1995; Warnecke & Heinz, 2003).

Regarding the lipid dynamics of membranes, thermodynamic studies demonstrated some of the first evidence for a special role of cholesterol, sphingomyelin (a major sphingolipid in animals) and cerebroside¹. When artificial membranes were enriched with cholesterol, sphingomyelin and cerebroside, the gel to liquid crystal transitions occurred at a much higher temperature ($T_m > 40\text{ °C}$) than for membranes with a lower content of cholesterol, sphingomyelin and cerebroside (Oldfield & Chapman, 1972). Correspondingly, natural membranes with a high content in cholesterol & sphingolipids show a much more ordered membrane structure.

Sphingomyelin and cerebroside represent sphingolipids which form a complex category of lipids characterized by their long-chain base (LCB) backbones ranging from 22 – 26 carbon atoms and featuring a quite low degree of saturation (Harder & Simons, 1997). This leads to long fatty acid chains which intercalate with sterols in the outer leaflet of the cellular membrane. Sphingolipids are thought to be involved in signaling processes: e.g., the

¹Cerebroside represent complex glycosphingolipids mainly located in the nervous system (Raff *et al.*, 1978).

1.1. MEMBRANE STRUCTURE

sphingolipid ceramide acts on ceramide-stimulated protein kinases and phosphatases thus regulating protein function (Divecha & Irvine, 1995).

Plant sphingolipids are a very diverse family of lipids which show a much higher heterogeneity than their animal counterparts and have not yet been investigated in full detail. The first studies on detergent-resistant membranes in *A.th.* (Borner *et al.*, 2005) revealed that there is no enrichment of sphingolipids in plant DRMs derived from *A.th.* callus, which is in contrast to the situation for sterols as will be discussed later on (cf. 1.2.6, p. 32). DRMs are characterized by an enrichment in sphingolipids & sterols which alters their separation on sucrose density gradients. This enables their isolation as a minor floating (DRMs) and a major non-floating (detergent-soluble fraction) fraction (see 2.1.5, p. 48).

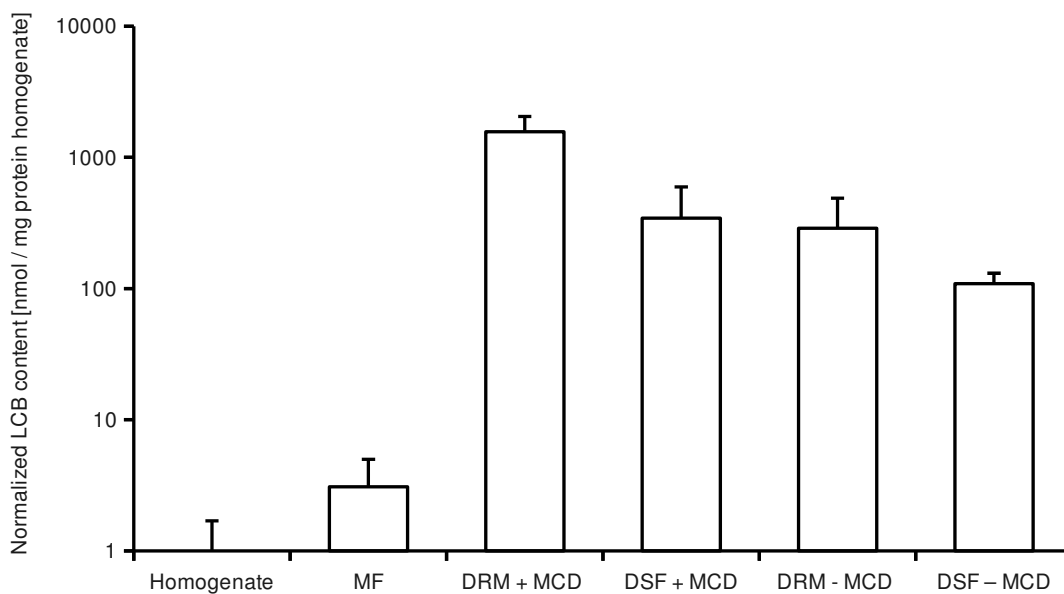


Figure 1.1.: Sphingolipid content in *A.th.* DRMs & DSF, normalized to the measurements of sphingolipids in the homogenate ($n = 6, \pm \text{SD}$). Analysis: courtesy of Markus Peer (Julius-von-Sachs Institute for Biosciences, Dept. of Pharmaceutical Biology, Univ. of Würzburg).

Own measurements of the sphingolipid content during the isolation of *A.th.* DRMs & DSF with and without methyl- β -D-cyclodextrin application revealed no major enrichment of sphingolipids in DRMs with respect to DSF (figure 1.1). A strong enrichment of sphingolipids was visible compared to the homogenate and microsomal fraction – this correlates to the findings of Borner *et al.* (2005). Interestingly, disrupting DRMs using MCD yielded no strong difference in DRM sphingolipid content. Application of MCD is the most prominent way to

disrupt DRMs by sequestering membrane sterols. Though sphingolipids & sterols both are enriched in DRMs, sphingolipids seem not to be affected by DRM disruption through MCD.

The lipids of animal plasma membranes and caveolae display no equal distribution throughout the lipid bilayer (Bergelson & Barsukov, 1977). The exoplasmic leaflet features sphingomyelin and other glycosphingolipids, whereas glycerolipids, such as phosphatidylserine and -ethanol amines, are enriched in the cytoplasmic leaflet (Simons & Ikonen, 1997). The distribution of cholesterol showed no such discrepancy. As sphingomyelin and glycosphingolipids are located at the exoplasmic surface of the cell, ordered small-sized domains might be located mainly at the cell surface. Sphingolipids intercalate into the cytoplasmic sphere of the lipid bilayer with their prolonged fatty acid chains.

Ceramide is the precursor of all sphingolipids which is subsequently converted to ceramide-1-phosphate, sphingomyelin or sphingosine (Ghosh *et al.*, 1997). All three components of this "sphingomyelin cycle" seem to be finely regulated in a manner reminding of the phosphatidylinositol (PI) cycle generating diacylglycerol (DAG) and inositoltriphosphate (IP₃). PM-located sphingomyelinase enzyme rapidly degrades sphingomyelin in the PM into cellular ceramide which acts as a lipid secondary messenger. An increase in the cellular ceramide concentrations is required for meiotic maturation in *Xenopus laevis* oocytes to proceed until the metaphase II. Astonishingly, this effect can be mimicked by treatment of arrested *Xenopus laevis* oocytes with the external application of bacterial sphingomyelinase or direct injection of ceramide. Thus intracellular levels of ceramide seem to control physiological processes like the meiotic maturation in oocytes (Ghosh *et al.*, 1997).

Thinking of the molecular crowding at the biological membranes, an approximate lipid:protein ratio of 50 could be assumed for animal membranes (Jacobson *et al.*, 2007). Estimations for the number of proteins in the membrane are in the range of 30 000 per μm^2 with a sample α -helix occupying 1 nm^2 (\varnothing 1.1 nm) and a sample lipid occupying 0.68 nm^2 (\varnothing 0.93 nm) of surface area in the membrane. Seven lipids would surround a canonical single-span transmembrane protein with only one α -helix in direct neighborhood. Further layers of lipids would fill the space between the proteins in biological membranes. Thus it may be more accurate to think of membranes as fully packed protein layers with lipids filling the gaps (Jacobson *et al.*, 2007).

1.1.2. Singer-Nicolson model

In the beginning of the 1970s the general structure of membranes was known to consist of a heterogeneous mixture of lipids and proteins (Korn, 1966). More detailed investigations by Singer & Nicolson (1972) led to the definition of the "fluid mosaic model" of membranes:

1.1. MEMBRANE STRUCTURE

proteins shall freely diffuse in the cell (plasma) membrane, which is composed of a lipid bilayer mainly constituted by phospholipids.

Structural implications of the lipids were reflected by the amphipathic organization of the lipid bilayer: lipophilic fatty acid chains face towards the inner medium of the lipid bilayer while the hydrophilic fatty acid head groups face the outer aqueous medium. According to the Singer-Nicolson model, globular and transmembrane proteins are localized in the lipid bilayer membrane without any structural or supra-molecular organization. The localization of transmembrane proteins in the lipid bilayer is driven by their amino acid sequence: lipophilic amino acids in the protein core are covered by the membrane while hydrophilic amino acids at the N- and C-termini face the cytosolic lumen / extracellular space.

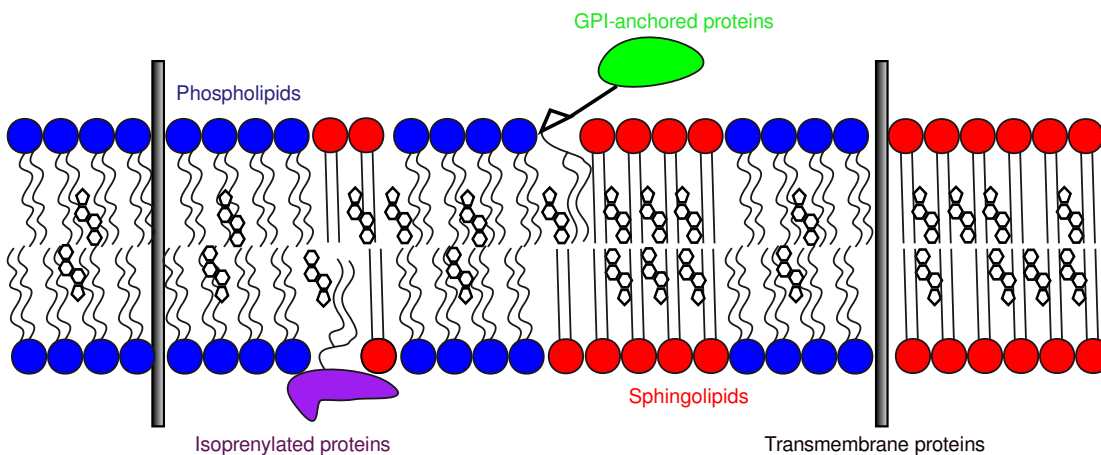


Figure 1.2.: **Membrane structure according to the Singer-Nicolson model.** The lipid bilayer structure of membranes harboring phospholipids, sterols, sphingolipids and different types of proteins: transmembrane, GPI-anchored and isoprenylated / myristoylated proteins (Singer & Nicolson, 1972). Proteins and lipids are randomly distributed on the membrane displaying no clustered organization.

Electron microscopic imaging revealed that the lipid bilayer fills up the space between protein complexes (Henderson & Unwin, 1975) providing evidence that the lipids provide the matrix in which the proteins are localized. Bretscher & Raff (1975) summarized the advantages of the fluid mosaic model without any further sub-structures to be:

- A simple distribution of lipids & proteins on the plasma membrane
- Division of membrane components during cytokinesis
- A facilitator of cell locomotion & membrane fusion

A critical point in the "fluid mosaic model" was the necessity for a controlled distribution & mobility of membrane proteins. For instance, during locomotion in animal cells or pollen tube growth in plants, the fundamental need for polarity is not explained with the plain Singer-Nicolson model.

1.1.3. Evidence for organization

First evidence for a supra-molecular organization at the plasma membrane arose from different sorting mechanisms in animal epithelial cells (van Meer & Simons, 1988). Glycero- & sphingolipids were found to be asymmetrically located at the apical and basolateral membranes of epithelial cells (cf. van Meer & Simons (1988), fig. 1.2).

It had been assumed previously, that several proteins comprise a level of self-organization (Fromherz, 1988). This self-organization may be due to the localization in special membrane domains. The isolation of Triton X-100 DRMs has proven to be useful for approximating these membrane domains (Chamberlain, 2004). First investigations of animal DRMs revealed that GPI-anchored proteins (GAPs) were enriched in the Triton X-100 insoluble phase (Brown & Rose, 1992). Further cross-linking experiments revealed clusters of GAPs to be located in special membrane domains (Brown, 1993; Friedrichson & Kurzchalia, 1998) or lipid rafts (Simons & Ikonen, 1997). To assess the sterol dependency of these membrane domain clusters, the chemical drug MCD was used to disrupt DRMs (Ilangumaran & Hoessli, 1998).

Microscopic studies also provided evidence for a macromolecular organization in the PM (Jacobson & Dietrich, 1999). Transfection of GAPs like placental alkaline phosphatase (PLAP) / Thy-1 and transmembrane proteins like viral haemagglutinin (HA) resulted in co-localization of viral HA together with PLAP / Thy-1 and also the raft marker ganglioside GM₁. The transferrin receptor which was known to be located outside of DRMs showed no such co-localization (Harder *et al.*, 1998). Co-patching of raft components was supposed to be a result of rafts having a high affinity for their kind (Jacobson & Dietrich, 1999).

Transmission electron microscopic investigations on T cell cultures added further information to the organization of rafts: abundant actin cytoskeleton staining was observed by the raft complexes (30 – 300 nm in size & enriched in cholesterol) which suggested that most – if not all – rafts are attached to the cytoskeleton (Lillemeier *et al.*, 2006).

These investigations led to different re-modeling approaches (Jacobson *et al.*, 1995; Vereb *et al.*, 2003) resulting in partially free diffusing membrane constituents which are organized and restricted by the cytoskeleton and interacting proteins, for instance by the family of tetraspanin proteins in mammals (Hemler, 2005). Lipid raft localization of some proteins is triggered by certain post-translational lipid modifications (1.1.4).

1.1.4. Lipid modifications

An important chapter for understanding the protein localization in lipid rafts are the post-translational lipid modifications. Altering certain proteins through lipid modifications surely changes their interaction properties, localization and physiological relevance.

Covalent attachment of lipid fatty acid chains to proteins is a widely known modification (Resh, 1999). The most common modifications are the attachment of C₁₄ (myristate) and C₁₆ (palmitate) saturated fatty acids.

1.1.4.1. Myristoylation

Myristoylation takes place on proteins which have the leading amino acid sequence Met-Gly: the leading methionine is removed co-translationally on nascent polypeptide chains at the ribosome and myristate is covalently bound to glycine at the second position (Wilcox *et al.*, 1987). Other proteins are myristoylated by the cytosolic enzyme *N*-myristoyl transferase (NMT) which appends a myristate to the N-terminal Gly found in the consensus sequence Met-Gly-X-X-X-Ser/Thr-.

A very often used mutational approach is the exchange of Gly at position two against another amino acid to prevent protein myristoylation and reveal the physiological importance of *N*-myristoylation (Resh, 1999). To establish a proper plasma membrane localization a sole *N*-myristoylation is not sufficient². The additional existence of a poly-basic amino acid sequence³ or a palmitoylation is necessary to allow proper plasma membrane binding (Resh, 1994). Another mechanism for tight membrane binding of myristoylated proteins are protein-protein interactions with transmembrane proteins stabilizing the myristoylated proteins in the membrane (Resh, 1999). Membrane anchorage by myristoylation can be regulated by ligand-induced conformational changes exposing the myristate to the cytosol or myristoyl-electrostatic switches (McLaughlin & Aderem, 1995). In the latter case, a phosphorylation in the poly-basic amino acids (aa) stretch, which is necessary for membrane binding (e.g. the MARCKS protein in mammalian cells is phosphorylated by protein kinase C), leads to displacement from the membrane into the cytosol (McLaughlin & Aderem, 1995). For the retinal protein recoverin, a calcium (Ca²⁺)-dependence of the membrane attachment via myristoylation was observed (Dizhoor *et al.*, 1993). Under low Ca²⁺ the hydrophobic C-terminus is occluded while elevated Ca²⁺ (> 1 μM) liberates the C-terminus containing the myristoylation site to allow tethering to the membrane.

²The binding energy of a myristate is simply too weak for a stable membrane anchorage (Resh, 2006).

³An example is the Src family of protein tyrosine kinases where a 6 amino acids long basic stretch enhances the membrane binding 3000-fold (Resh, 1999).

1.1.4.2. Palmitoylation

Palmitoylation or *S*-acylation enables membrane tethering of proteins by addition of a palmitate or other saturated long chain fatty acids such as stearate (C₁₈), oleate (cis-C₁₈), arachidonate (C₂₀) (Resh, 1999). The addition of fatty acids is mostly performed by the enzyme palmitoyl acyl transferase (PAT). However, non-enzymatic mechanisms also exist (Reverey *et al.*, 1996). A consensus sequence of the amino acids Met-Gly-Cys at the N-terminus leads to a double acylation via myristate and palmitate. Previous *N*-myristoylation at Gly2 greatly facilitates the subsequent palmitoylation at Cys3, for instance in the mammalian Src family of kinases or some G_α subunits (Resh, 1999).

Other proteins like caveolin-1 or the serotonin receptor in mammals display a different mechanism for *S*-acylation. These transmembrane proteins harbor many *S*-acylated Cys residues in or nearby their transmembrane segments. Attachment of saturated long chain fatty acids depends upon the length & sequence of transmembrane segments as well as on the length of the cytoplasmic tail (Veit *et al.*, 1996). Long cytoplasmic tails seem to favor the addition of palmitate (C₁₆) while short cytoplasmic tails favor longer stearate (C₁₈) moieties. A further class of combined lipid modifications are present in the Ras proteins from mammals. These feature a CAAX domain, a known prenylation / farnesylation motif, at their C-terminus, which must be farnesylated first before further palmitoylations at C-terminal Cys residues can take place (Hancock *et al.*, 1989).

1.1.4.3. Prenylation

Prenylation / farnesylation represents a third type of lipidation, which is performed via linkage of either a C₁₅ farnesyl or C₂₀ geranylgeranyl isoprenoid moiety to a C-terminal Cys residue inside a CAAX⁴ motif (Casey, 1995). Depending on the last residue in the CAAX motif, the cytosolic enzymes farnesyltransferase (FTase, for X = S, A, M) or geranylgeranyltransferase I (GGTase I, for all other X) perform the addition of the isoprenoid chain (Zhang & Casey, 1996). A second mechanism for farnesylation is represented by the family of guanosine triphosphate (GTP)-binding Rab proteins involved in membrane trafficking. These proteins are twice geranylgeranylated at Cys residues near the C-terminus by the enzyme GGTase II. Due to their bulky branched lipid structure, isoprenoid modifications cause the proteins to be found exclusively outside of lipid rafts (Melkonian *et al.*, 1999).

⁴Cys-Aliphatic-Aliphatic-X

1.1.4.4. GPI-anchor

While prenylation prevents raft localization, another class of lipid modification drives many proteins into lipid rafts. Attachment of glycosylphosphatidylinositol moieties to the C-terminus occurs exclusively at the endoplasmic reticulum (ER) (Casey, 1995). These GPI anchors represent a quite complex moiety consisting of a saturated phospholipid coupled to ethanolamine and sugars (Maeda *et al.*, 2007). The length of the saturated fatty acid chains linked to the GPI-anchor is responsible for raft localization (Benting *et al.*, 1999). If the length of the fatty acid chains were $< C_{16}$, the corresponding GAPs were not localized in lipid rafts. For mammalian GAPs the majority of the saturated fatty acid chains are $> C_{16}$, thus GAPs in mammals exhibit a strong enrichment in lipid rafts.

All GAPs are destined for the cell surface and represent diverse functional classes like cell adhesion, nutrient uptake and signaling. GAPs were first discovered to be located in detergent-insoluble fractions which represented a first link to small microdomains at the PM (Brown & Rose, 1992)⁵. As GAPs remain at the extracellular PM leaflet there is a necessity for linking extracellular to intracellular signals.

A fabulous example can be found in the stimulation of T-cells: cross-linking GAPs at the extracellular leaflet activates T-cells by the family of Src tyrosine kinases at the inner leaflet of the PM (Brown, 1993). The activation of T-cell receptor (TCR) signaling takes place through pre-formed microdomains containing all members of early signaling in TCRs. These members are attached to the cytoplasmic leaflet of the PM via myristoylation and palmitoylation (Drevot *et al.*, 2002).

1.1.4.5. Overview of lipid modifications

In brief, *N*-myristoylation, *S*-acylation and GPI anchors provide mechanisms for locating proteins in lipid rafts whereas prenylation presents a mechanism to exclude proteins from lipid rafts (summary in table 1.1) – at least in the animal system. All lipid modifications except *N*-myristoylation are reversible and allow fine regulation of protein function and localization in lipid rafts. Some of these lipid modifications display a cooperative effect, e.g. myristoylation facilitates palmitoylation of further Cys residues (Resh, 1994, 2006).

⁵In the past, the microdomains were called detergent-insoluble glycoproteins (DIGs) as only GAPs were found to be localized in these domains.

CHAPTER 1. INTRODUCTION

Modification	Reversible	Fatty acid chain length	Leaflet	Raft-associated
Myristoylation	○	C ₁₄	Cytosolic	●
Palmitoylation	●	C ₁₆₋₂₀	Cytosolic	●
Prenylation	●	C _{15/20}	Cytosolic	○
GPI-anchor	●	C ₁₆₋₁₈	Extracellular	●

Table 1.1.: Summary of common lipid modifications

1.1.4.6. Lipid modifications in plants

All the mammalian lipid modifications are also present in plants, but detailed investigations were never conducted concerning the lipid attachment of putative lipid raft proteins. Computational prediction tools reveal a similar situation as depicted on figure 1.3. However, there are small differences in the lipid composition of plants (Somerville & Browse, 1991). Particularly the chloroplast membranes of plants show a distinct lipid type which is not present in fungi & mammals: galactolipids representing glycerolipids containing sugar head groups like monogalactosyldiacylglycerol (MGDG) or digalactosyldiacylglycerol (DGDG) (Somerville & Browse, 1991). This class of lipids is only found in cyanobacteria and plant chloroplasts which supports the endosymbiont hypothesis that internalized cyanobacteria were the first ancestors of plant chloroplasts. Another quite different point is the sterol composition in the plant PM: cholesterol does not play a major role in plant membranes (Kierszniowska *et al.*, 2008). The plant phytosterol pool at the PM is comprised of the predominant β -sitosterol and further campesterol, cholesterol and stigmasterol (Beck *et al.*, 2007).

Upon identification of specific members of Triton X-100 DRMs during this study, an image like depicted in figure 1.3 arose where similar lipidations like in the animal system had the same localization result for plants. For example, members of the AtRab family are GTP-binding trafficking proteins which are prenylated and also additionally palmitoylated (right on figure 1.3). In this study, many proteins of the AtRab family, e.g. AtRab18 (At1g43890), could be identified to be PM-resident but not to be localized in DRMs. This may be due to their prenylation as mammals counterparts of the Ras family are also found often to be excluded from DRMs (Resh, 1999, 2006).

Proteins with many transmembrane domains (TMDs) like PEN3 (PDR8, ABC transporter G family member 36, At1g59870) are additionally palmitoylated giving rise to a putative localization in DRMs. PEN3 is involved in the export of toxic, anti-microbial compounds at powdery mildew infection sites in *A.th.* to confer non-host penetration resistance (Kobae *et al.*, 2006).

1.1. MEMBRANE STRUCTURE

The myristoylated PM protein phospholipase D (PLD) δ (At4g35790) is a member of Triton X-100 DRMs as shown in this study. PLDs are known to be PM-resident proteins which process phosphatidylcholine (PC) into phosphatidic acid (PA) upon abscisic acid (ABA) induction (Zhang *et al.*, 2004).

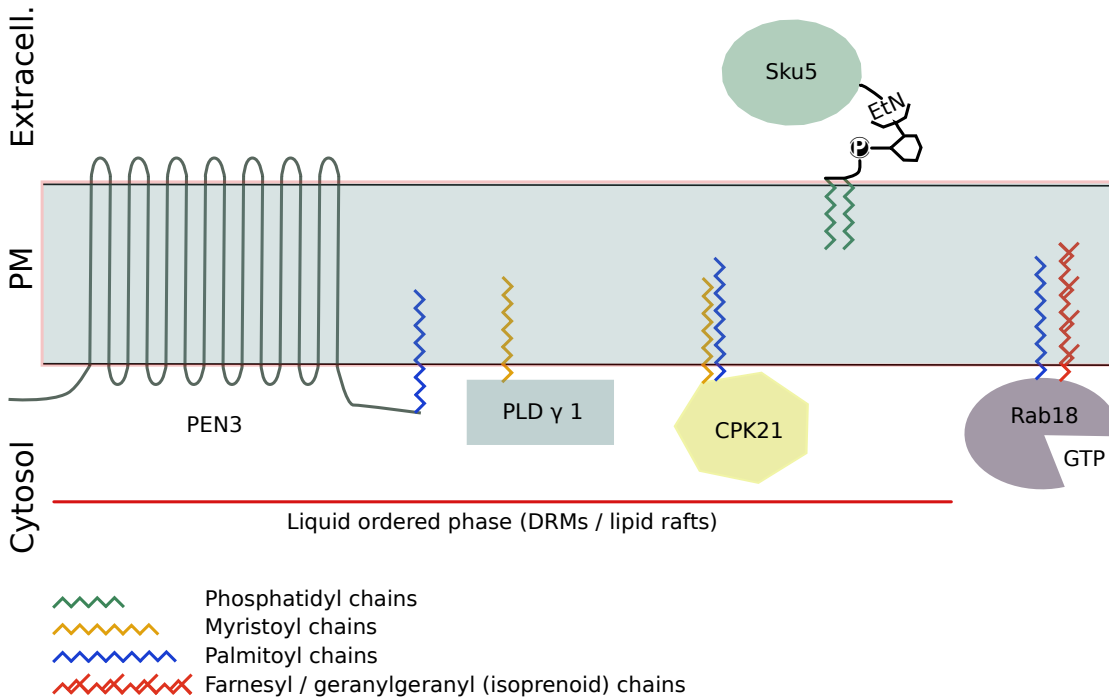


Figure 1.3.: **Lipid modifications on plant DRM / non-DRM proteins.** The plant plasma membrane with some model proteins and their lipid modifications are shown. AtRab proteins are responsible for trafficking. PEN3 is an ABC transporter involved in the secretion of anti-microbial compounds. PLD isoforms are PM-located signaling components which transform phosphatidylcholine into phosphatidic acid. Sku5 is a GAP present in the PM which is strongly involved in the growth of roots. CPK21 represents a Ca^{2+} -dependent protein kinase which is involved in the ABA-regulated drought stress regulation through anion channels of the SLAC1-family.

Like in the animal field, GAPs seem to be enriched in Triton X-100 DRMs (Borner *et al.*, 2005). A prominent member of the GAP family, AtSku5 (At4g12420) represents a putative monocopper oxidase protein (Jacobs & Roe, 2005) which is involved in directional root growth (Sedbrook *et al.*, 2002). Localization studies confirmed a PM and cell wall localization of Sku5. Sku5 mutants displayed a strong phenotype (skewed roots) which suggested a strong role for Sku5 in growth processes. Astonishingly, Sku5 represents one of the major plant Triton X-100 DRM proteins, being identified several times in proteomic investigations

CHAPTER 1. INTRODUCTION

of Triton X-100 DRMs from *A.th.* (Borner *et al.*, 2005; Kierszniowska *et al.*, 2008; Morel *et al.*, 2006; Shahollari *et al.*, 2004).

CPK21 (At4g04720) is a member of the calcium-dependent protein kinase (CPK) family which is generally involved in Ca^{2+} -mediated drought & salt stress signaling (Ma & Wu, 2007). Drought stress responses are mediated through CPK21 in a complex, ABA-dependent manner involving the protein kinase CPK21, phosphatase ABI1 and anion channels of the slow anion channel (SLAC) / SLAC1 homologue (SLAH)-family (Geiger *et al.*, 2009). Anion channels of the SLAC / SLAH-family represent two groups: the guard cell specific SLAC1 and SLAH1-4 showing distinct tissue specificity (Negi *et al.*, 2008).

The guard cell specific SLAC1 is a chloride & malate transporting S-type anion channel (Vahisalu *et al.*, 2008) involved in transpirational control through stomatal closure (Negi *et al.*, 2008). Activation of SLAC1 has been proven to be dependent on ABA and Ca^{2+} through regulation by the protein kinase CPK21 (Geiger *et al.*, 2010b) and protein phosphatase 2C ABI1 (Lee *et al.*, 2009b).

Membrane attachment of CPK21 is performed via two lipidation motifs at the N-terminus: the Gly2 residue is myristoylated and Cys3 palmitoylated. CPK21 localization in DRMs is quite comparable to the Src family of protein tyrosine kinases in mammals (Resh, 2006). Src kinases are also myristoylated, subsequently palmitoylated, display no transmembrane segment and are identified as intrinsic members of Triton X-100 DRMs (Furuchi & Anderson, 1998).

1.2 LIPID RAFTS

The term lipid rafts has been coined to describe sphingolipid- & sterol-enriched small-scale (< 200 nm), highly dynamic domains in the plasma membrane of mammalian cells (Pike, 2006; Simons & Ikonen, 1997). Specific proteins are localized in lipid rafts as a consequence of interactions between proteins, cholesterol and sphingolipids (Keller & Simons, 1998) that play a role in apical membrane trafficking of GAPs. However, the most prominent function of sphingolipid & cholesterol-enriched membrane domains is signal transduction (Ayllón *et al.*, 2002; Brown, 1993; Friedrichson & Kurzchalia, 1998; Gupta *et al.*, 2006; Prior *et al.*, 2001; Simons & Ehehalt, 2002; Simons & Ikonen, 1997).

Approaches to identify lipid raft proteins mostly begin with the biochemical characterization of DRMs. DRMs can be isolated due to their detergent-insolubility at 4 °C with non-ionic detergents like Triton X-100 (Lingwood & Simons, 2007). Triton X-100 is the preferred detergent as it has been shown to extract membranes strongly enriched with cholesterol and sphingolipids, which is a requirement for the isolation of biochemical lipid raft equivalents (Chamberlain, 2004). Other detergents like CHAPS or Brij-96 / 98 also have been utilized for the isolation of DRMs. Brij-98 especially gained much interest among researchers in the mammalian field, as it enables the extraction of DRMs at the physiologically relevant temperature of 37 °C (Campbell *et al.*, 2004). This is not possible with Triton X-100 as treatment at 37 °C leads to a complete solubilization of lipid rafts. Thereby, no differentiation between raft and non-raft complexes is possible (Chamberlain, 2004).

A critical point about the biochemical isolation of DRMs is the detergent treatment. Detergent extraction itself influences the size of DRMs (Heerklotz, 2002). Especially for Triton X-100, it has been noticed that detergent treatment itself leads to an aggregation of DRMs impairing ultrastructural investigations (Madore *et al.*, 1999). Elucidation of the Triton X-100 DRM protein composition at 4 temperature in degrees Celsius (°C) can only be a first step in understanding and identifying physiological lipid rafts, particularly as biochemically isolated DRMs cannot be equated with *in vivo* lipid rafts (Lichtenberg *et al.*, 2005). Not only aggregation of Triton X-100 DRMs but also the temperature-induced increase in raft sizes remains an issue.

1.2.1. Sizing lipid rafts

An important problem in studying lipid rafts is due to the vanishingly small size of lipid raft structures < 100 nm preventing usage of direct light microscopic investigations (Harder & Simons, 1997). Indirect measurements of raft sizes via Foerster-resonance energy transfer (FRET) (Acasandrei *et al.*, 2006; Kenworthy & Edidin, 1998) or fluorescence quenching (Ahmed *et al.*, 1997) led to a disagreement in raft sizes and the inclusion or exclusion of certain proteins in DRMs.

With the arrival of the new microscopic stimulated emission depletion (STED) technique (Hell, 2003, 2007), *in vivo* size determinations of small nanometer-scaled membrane domains became possible for the first time (Kittel *et al.*, 2006). Previous investigations relied on atomic force or electron microscopy (see 1.2.5.3, p. 26 or 1.2.6.4, p. 40). Tracking fluorescence-tagged proteins in intact cells via STED has already clarified complicated biological cases like vesicle fusion at the synaptic cleft (Willig *et al.*, 2006). In future, the extension of light microscopy below Abbe's diffraction limit will surely unveil new exciting discoveries at the nanometer-scale.

For example, 3D timelapse observations of living mammalian cells uncovered structural changes in the ER at a new resolution limit of approx. 50 nm (Hein *et al.*, 2008). Further STED applications revealed that sphingolipids & GAPs are trapped **transiently (10 – 20 ms)** in small cholesterol-rich complexes in the **living** cell plasma membrane with a mean diameter < 20 nm (Eggeling *et al.*, 2009).

Mathematical models estimated the optimum size of classical lipid rafts as protein-protein interaction platforms events to be in the very low nanometer-scale (6 – 14 nm) scaffolding signal transduction (Nicolau *et al.*, 2006). Other requirements in this model were mobility of rafts and an almost twice as slow diffusion of lipids & proteins in the rafts as for the surrounding non-raft areas. Both requirements are fulfilled by experimental evidence in model membranes consisting of the ternary cholesterol, unsaturated 1,2-dioleoyl phosphatidylcholine (DOPC) and sphingomyelin lipid system (Hancock, 2006; Nicolau *et al.*, 2006).

1.2.2. Sterols & disruption by MCD

Besides assaying the size of lipid rafts, other investigations concerning the lipid composition of lipid rafts revealed a strong dependency upon sterols (Simons & Vaz, 2004) which was studied in model membranes (see section 1.2.3) to a great extent. MCD treatment is a general approach to test how strongly certain protein complexes depend upon sterols – MCD application is the golden biochemical approach to deplete cholesterol in the mammalian system (Hao *et al.*, 2001). From a technical view, MCD represents a water-soluble cyclic

oligomer of glucose with a hydrophobic core which forms inclusion complexes with membrane-localized cholesterol (Neufeld *et al.*, 1996).

Cyclodextrins have been applied to study cholesterol trafficking in animal cells as they are effective tools for removal of newly arriving cholesterol at the PM. The uptake of cholesterol into the PM itself is dependent upon sphingolipids: when the major sphingolipid in humans, sphingomyelin, was removed from the PM of fibroblasts by treatment with the enzyme sphingomyelinase, no cholesterol efflux into cyclodextrin complexes was visible (Neufeld *et al.*, 1996). This gave rise to the assumption, that the majority of cholesterol in the animal PM is associated with sphingolipids.

An important piece of the lipid raft puzzle is delivered by Pandit *et al.* (2004a) with the help of molecular dynamics simulations: they performed 200 ns simulations of the spontaneous formation of sphingomyelin-enriched liquid-ordered (L_o) domains in an artificial ternary cholesterol, DOPC & sphingomyelin lipid system. Cholesterol favors a position at the **boundary** of the sphingomyelin-enriched L_o phase and separates the L_o phase from the liquid-disordered (L_d) phase containing DOPC. This greatly accelerates the formation of the L_o state. Structural implications from their simulations were the preference of the α -face of cholesterol to pack near the sphingomyelin molecules and the observed reduction in line tension between the L_o and L_d phase due to the cholesterol packing in between both phases. Decreasing line tension has been proven to depend on the height differences between L_o and L_d membrane phases (García-Sáez *et al.*, 2007). As sterol-enriched L_o phases represent lipid rafts, sterol depletion assays can be performed to assess lipid raft localization of proteins.

There are several sterol-disrupting agents available (filipin, MCD, nystatin and saponin) among which MCD is the most widely applied tool (Klein *et al.*, 1995; Yancey *et al.*, 1996). MCD application should lead to alleviation of a putative lipid raft protein localization in DRMs as it acts on membrane sterols without intercalating or binding to membranes (Ilangumaran & Hoessli, 1998). Pharmacological uses of MCD include the prevention of atherosclerotic plaques by lowering the levels of free cholesterol / HDLs in humans (Kilsdonk *et al.*, 1995). Regarding the mechanism of sterol depletion by MCD, it has been proposed that MCD removes cholesterol from the outer boundary and not from within sphingolipid-enriched membrane domains (Ilangumaran & Hoessli, 1998).

MCD has been used to investigate the influenza virus haemagglutinin (HA) localization in DRMs. Application of > 10 mM MCD was sufficient to remove > 90 % of cholesterol and HA from Triton X-100 DRMs (Scheiffele *et al.*, 1997). An additional finding in this study was the importance of the exoplasmic part of the TMD for correct localization in lipid rafts. Replacing cytoplasmic or exoplasmic parts of the HA TMD revealed that some kind of intrinsic sorting signal for lipid raft localization must be in the exoplasmic TMD sequence.

This intrinsic sorting signal might be lipidation through palmitoylation or interaction with the cholesterol-sphingolipid membrane domains.

Following the determination of the DRM protein composition, further studies on the physiological implications of candidate DRM proteins remain to be conducted, for instance localization of DRM proteins & interacting partners *in vivo* and circumstances where DRM localization might be altered (e.g. by sterol depletion).

Increasing pieces of evidence corroborate the lipid rafts hypothesis established by Simons & Ikonen (1997). Considering all evidence for lipid raft structure, size measurements, protein-lipid and protein-protein interactions, very small raft clusters with a dynamic constitution have to be assumed (Hancock, 2006). Or to state it with the words of Mr. Hancock (2006): "In summary, rafts exist, but their length and timescale specifications are crucially important characteristics that must be included in any definition." – this definition has not been completed in all details yet.

1.2.3. Model membranes

Studying membrane domain formation in detail is (yet) impossible in living cells. But understanding the fundamental principles behind membrane domain formation is possible using model membranes like bi-phasic lipid bilayers, small unilamellar vesicles (SUVs) or giant unilamellar vesicles (GUVs). Reconstitution experiments with model membranes frequently use a ternary lipid system consisting of DOPC as an unsaturated phospholipid, sphingomyelin representing sphingolipids and cholesterol (Simons & Vaz, 2004).

All artificial membrane studies revealed that some factors are severely affecting the emergence of membrane domains: temperature and lipid composition. Using the previously mentioned ternary lipid composition, a very simplified view of cellular membranes can be intensively studied biophysically. Every lipid species undergoes phase transitions as a function of temperature; the main / chain melting temperature T_m of a lipid is the point where the lipid bilayer is transformed from an ordered crystalline solid into a L_d state above T_m .

1.2.3.1. Cholesterol & the organizing effect

Cholesterol and sphingolipids are known to form a L_o phase which is surrounded by a liquid-disordered phase poor in cholesterol (Simons & Vaz, 2004). Cholesterol as a sterol displays a flat & rigid structure which superimposes conformational ordering on the nearest aliphatic neighbor lipid chains but without affecting the transformational mobility of the neighboring lipid (Silvius, 2003). Because of this "organizing" effect of sterols, the addition of cholesterol to model lipid bilayers leads to a $L_d \rightarrow L_o$ transition.

Both L_d and L_o phases can coexist in the same model membrane (de Almeida *et al.*, 2003) and free lipid diffusion in the L_o domains seems to be *only* 2 – 3-fold slower (Hancock, 2006). Searching for a concrete reason, Pandit *et al.* (2004a); Rietveld & Simons (1998) provided strong evidence why cholesterol addition favors the emergence of L_o domains: cholesterol is located at the boundary of sphingomyelin-rich L_o domain phases. Even more interesting, the introduction of cholesterol into sphingomyelin bilayers led to decreased Triton X-100 solubility of the cholesterol-sphingomyelin L_o domains (Li *et al.*, 2001). Detergent insolubility of these L_o phases are – at physiological concentrations of cholesterol & sphingomyelin – due to decreased in-plane elasticity in the lipid plane. Interactions between cholesterol and the saturated fatty acid chains of sphingolipids are mediated through structural implications: sphingolipids contribute hydrogen bonds from amino and carbonyl groups of their amines & hydroxyl groups to the cholesterol ring. Structural hydrogen bonding and decreased in-plane elasticity contribute to formation of physiologically relevant L_o phases in membranes (Li *et al.*, 2001).

Corresponding to the amount of cholesterol supplied to model membrane mixtures, membrane domains are beginning to appear. For the previously mentioned ternary model lipid mixture (cholesterol, DOPC and sphingolipids), 25 – 30 mol % cholesterol are sufficient to create L_o membrane domains. Supplying higher amounts of cholesterol to a 1:1 mixture of DOPC and sphingomyelin led to the appearance of big membrane domains which could be visualized by atomic force microscopy (AFM) (Rinia *et al.*, 2001). The higher the cholesterol addition, the bigger the size and area.

Upon addition of 50 mol % cholesterol, the height difference between L_o and L_d domains was reduced from 1 nm to 0.8 nm. This height difference of the L_o domains may be caused by addition of cholesterol to the surrounding L_d phase (Saslowsky *et al.*, 2002). In addition to these AFM observations, molecular dynamics simulations by Pandit *et al.* (2004b) showed that the L_d phase containing DOPC surrounding the L_o phase is perturbed at a distance of 8 nm. Below < 8 nm the order of the DOPC carbon chains is severely altered with respect to the area far away from the L_o phase.

The estimation of lipid raft sizes in model membranes via FRET revealed a complex situation (de Almeida *et al.*, 2005). Raft sizes in binary / ternary model membranes differed considerably with ternary model membranes yielding bigger raft sizes > 100 nm. Even addition of the animal lipid raft marker ganglioside GM₁ changed the raft sizes measured by FRET.

1.2.3.2. Visualizing lipid rafts

AFM enabled visualization of purified GPI-anchored PLAP protein in supported lipid bilayers consisting of DOPC and sphingomyelin (Saslowsky *et al.*, 2002). The lipid bilayers showed even a spontaneous phase separation without addition of PLAP – a sphingomyelin-enriched raft-like phase was visible which was 0.8 nm higher than the DOPC background. PLAP was efficiently targeted into rafts with and without cholesterol supplement (figure 1.4). PLAP dimers could be seen as raft protrusions of 0.8 nm height residing on a lipid bilayer with a thickness of approx. 6 nm. Almost all of the PLAP protein was directed into these raft protrusions, leaving only 10 % out of the raft area. Prior to the application of AFM, no nanometer-scale phase separations were visible in model systems. AFM studies from Veatch & Keller (2003) contributed a clear evidence for a phase separation in ternary lipid bilayers.

Another study investigated the distribution of the lipid raft marker protein ganglioside⁶ GM₁ in a ternary mixture containing cholesterol, DOPC and sphingomyelin (Yuan *et al.*, 2002). AFM observations revealed small, **40 – 100 nm in size** and 1 nm in height, GM₁-enriched microdomains in the L_o phase of the ternary lipid bilayer. This L_o phase represented a condensed domain which is cholesterol and sphingomyelin-rich, as revealed by previous investigations (Dietrich *et al.*, 2001). A comparison of the measured raft size in the ternary lipid mixture with the physiological situation in natural cell membranes (Jacobson & Dietrich, 1999) reveals a similar range of ≤ 100 nm.

1.2.3.3. Detergent insolubility

Triton X-100 solubilization mediates detergent insolubility of membranes in a concentration-, temperature- and time-dependent manner (Morandat & El Kirat, 2006). The critical time point for solubilizing an excess of model membranes without solubilizing putative lipid raft areas is reached after 30 minute (min) at 4 °C which therefore represents the standard incubation for the extraction of Triton X-100 DRMs. The lipid composition of membranes heavily alters the solubilization efficiency of Triton X-100 – Morandat & El Kirat (2006) could investigate this effect using lipids with low and high melting temperatures T_m.

Artificial DOPC vesicles (T_m = – 20 °C) were easily solubilized by Triton X-100 while combined 1,2-dipalmitoyl phosphatidylcholine (DPPC) vesicles (T_m = 41 °C) displayed resistance to Triton X-100 solubilization. This clearly indicates the importance of the lipid composition for detergent insolubility in model membranes. As the natural mammalian PM

⁶Gangliosides represent glycosphingolipids which are present in all mammalian tissues but highly enriched in the central nervous system

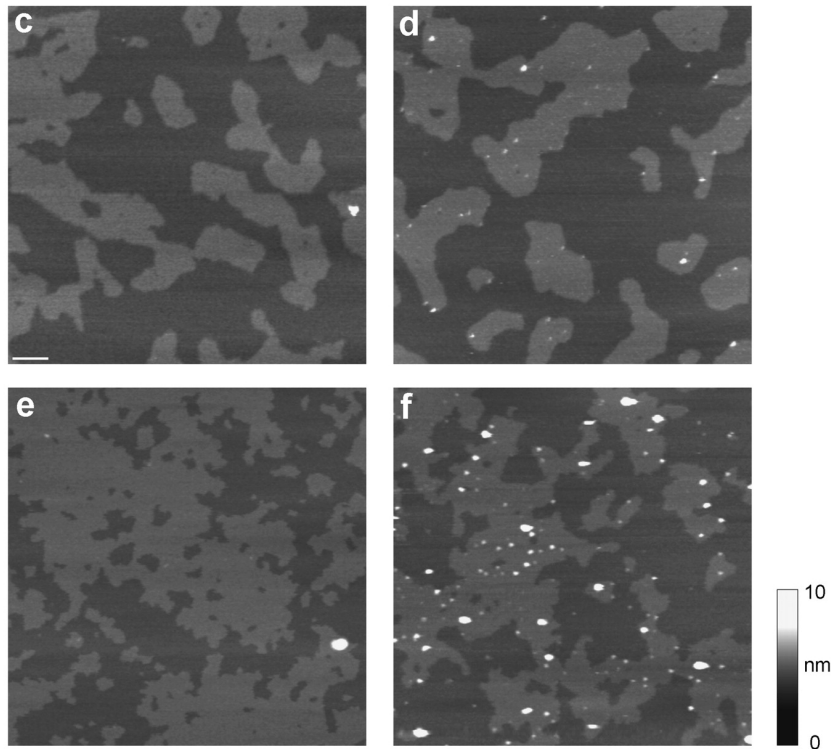


Figure 1.4.: **Visualized lipid rafts containing the GAP PLAP by AFM.**

Lipid bilayers containing DOPC & sphingomyelin (c) or cholesterol, DOPC and sphingomyelin (e) were supplied with the GPI-anchored protein PLAP (d, respectively f). PLAP was almost exclusively localized in the L_o phase. Scale bar = 5 μm

Reprinted with permission from The American Society for Biochemistry and Molecular Biology: *Journal of Biological Chemistry*, Saslowsky *et al.* (2002), © 2002

is composed with a clear bias on cholesterol and sphingomyelin, the biophysical properties of such model membranes have also been studied in further detail (Ahmed *et al.*, 1997).

Addition of 33 mol % cholesterol into model membranes promoted generation of a L_o phase. At the mammalian physiological temperature of 37 °C, cholesterol and sphingomyelin in physiological ratios led to generation of a stable L_o phase. This strengthens the hypothesis of L_o domains existing at physiological temperatures prior to detergent extraction rather than being a sole artifact of the detergent treatment.

1.2.3.4. Lipid modifications

Protein partitioning into DRMs is thought to be dependent on lipid modifications (see section 1.1.4, p. 7). Silvius (2005) applied fluorescence quenching to study partitioning of lipid modified peptides into L_d or L_o domains of a DPPC and cholesterol mixture. Isoprenylated (farnesylated / geranylgeranylated) and multiple unsaturated acyl chain peptides displayed a very low affinity for the L_o phase. In contrast to this, peptides with multiple *S*-acylations / *N*-myristoylations or a *N*-terminal palmitoylation + cholesterol significantly partitioned into the L_o phase. These results support the notion that prenylation prevents proteins from being incorporated into DRMs / physiological lipid rafts.

1.2.3.5. Phytosterols & model membranes

In all the studies made in model membranes, there is a strict usage of cholesterol as the L_o promoting sterol. Only few studies handle non-cholesterol sterols in model membranes, so there are scant details available about the raft promoting effects of phytosterols. A comparative investigation of sterol effects on a sphingomyelin bilayer revealed some differences between animal and plant sterols (Gao *et al.*, 2009). Cholesterol represents the principal sterol which is modified with an additional ethyl group at C_{24} (β -sitosterol) and an additional double bond at C_{22} (stigmasterol). Applying different spectroscopic methods, Gao *et al.* (2009) reported that cholesterol promotes more stable associations with sphingomyelin bilayers than phytosterols. The authors supposed that evolution may have selected cholesterol in homeostatic mammals to perform or establish interactions with sphingomyelin and phytosterols in heterothermic organisms like plants for lipid raft or microdomains formation. Hac-Wydro *et al.* (2010) performed studies on sphingomyelin membranes and witnessed that the phytosterols β -sitosterol and stigmasterol are contributing to L_o phases by interacting with the alkyl chains of sphingomyelin. β -sitosterol and cholesterol were also shown to affect diacylphosphatidylcholine bilayers in unilamellar vesicles at the same extent when applied at 33 mol % concentration (Gallová *et al.*, 2008).

As useful as artificial model membranes have proven to be, there is a persistent problem: all binary / ternary model membranes are symmetrical, thus having the same lipid composition on the cytoplasmic and exoplasmic leaflet. This is in contrast to the situation in living cell membranes where the cytoplasmic leaflet displays a quite different lipid composition which, for instance, is poor in sphingolipids (Simons & Vaz, 2004). Detailed studies with phytosterols in model membranes comprised of plant sphingolipids are still missing. A future challenge for all biophysicists is the establishment of a model membrane explicitly mimicking the animal / plant PM with their differing lipid composition in both leaflets.

1.2.4. Yeast lipid rafts

Even in the kingdom of fungi, there is evidence for the existence of microdomains (Alvarez *et al.*, 2007). In yeast, these microdomains are commonly referred to as "sterol-rich domains" (SRDs). SRDs are enriched in the major yeast sterol ergosterol and phosphoinositol-based sphingolipids (Alvarez *et al.*, 2007; Thomas *et al.*, 1978). Astonishingly the fungal PM seems to be majorly comprised of SRDs (Bagnat *et al.*, 2001) which makes yeast / fungi ideal organisms for investigating DRM proteins. Almost half of the PM is constituted of sterol-rich domains and can be isolated as DRMs. Additionally the yeast DRMs are exceptionally stable in the hours to days range (Lauwers & André, 2006).

Two types of PM compartments are present in the bakery yeast *Saccharomyces cerevisiae* (Grossmann *et al.*, 2007): **MCC** (**m**embrane **c**ompartment of **C**an1, an arginine / H⁺ symporter) and **MCP** (**m**embrane **c**ompartment of **P**ma1, the yeast proton ATPase). The H⁺-ATPase Pma1p is a model lipid raft protein (Bagnat *et al.*, 2001), located in MCP compartments and definitely impaired in sorting to the PM when lipid microdomains were disrupted. In contrast to evenly distributed MCP compartments at the PM, MCCs displayed a patchy appearance on the plasma membrane with a diameter of approx. 300 nm (Malínská *et al.*, 2003). These patches were very stable in temporal and spatial manners.

Heterologously expressed *Chlorella kessleri* glucose / H⁺ symporter HUP1 was localized to specific MCCs in *S. cerevisiae* (Grossmann *et al.*, 2006). The patchy appearance of MCC domains in the PM was strongly perturbed (figure 1.5) upon membrane depolarization (Grossmann *et al.*, 2007).

Fluorescently labeled HUP1-GFP showed a discrete distribution in MCC patches; after depolarization MCC proteins move out of the patches and distribute homogeneously in the PM. Approximately 20 minutes after restoration of the membrane potential, HUP1 and other MCC constituents (e.g. Can1 protein and ergosterol) move back into the original patches (Grossmann *et al.*, 2007). Using ergosterol⁷ biosynthesis mutants, Grossmann *et al.* (2007) investigated ergosterol-dependence of HUP1-GFP's patchy appearance. Ergosterol mutants displayed no patchy localization of HUP1-GFP and glucose uptake was strongly impaired. Thus, the localization of the glucose / proton symporter HUP1-GFP in *S. cerevisiae* MCC depends strongly on membrane potential and ergosterol availability.

⁷Ergosterol is the main sterol in fungi (Thomas *et al.*, 1978).

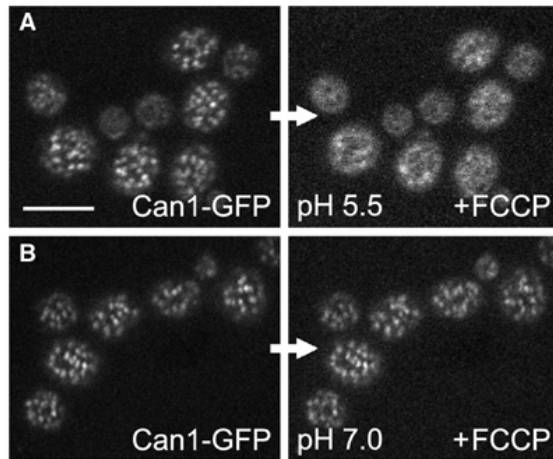


Figure 1.5.: **Can1 localization in MCC is dependent upon membrane depolarization.** Can1 dislocates from the patchy MCC compartments upon membrane depolarization via FCCP (**A**). Preventing FCCP-mediated membrane depolarization by using a pH 7 buffer also prevents the dissolution of Can1 (**B**). Reprinted with permission from Nature Publishing Group: *The EMBO Journal*, Grossmann *et al.* (2007), © 2007

The purpose of MCC may be the prevention of protein internalization as the localization of certain proteins like Can1 in MCC prevents their endocytotic recycling (Grossmann *et al.*, 2008). Can1 internalization is started upon delivery of excess substrate which leads to recruitment of Can1 outside of the MCC. Following the re-localization of Can1 outside of MCC, internalization is beginning to occur (Grossmann *et al.*, 2008).

Regarding the detergent solubility of putative yeast DRM proteins, Lauwers & André (2006) confirmed in a study with sec-mutants impaired in the secretory pathway that detergent insolubility is gained at the Golgi complex en route to the PM. If the studied permease Gap1 reaches the PM, it is localized in DRMs – but only if the nourishing medium is low on nitrogen and contains a proline source. Substrate availability alters the localization of the Gap1 permease transporter in DRMs and leads to a transition of Gap1 out of DRMs into the soluble phase.

1.2.4.1. Mating in *S. cerevisiae*

The mating process of *S. cerevisiae* presents another example of polarized protein localization: cell adhesion, fusion and signaling proteins are expressed at the tip of the mating projection upon perception of the mating pheromone α -factor (Bagnat & Simons, 2002). Proteins are

than clustered into lipid microdomains at the mating projection in a manner which is not dependent upon polarized secretion or new diffusion barriers.

Upon the emergence of cytokinesis, sterol-rich domains are located near the actomyosin-based contractile ring responsible for the final division step. Formation of two daughter cells from one parent cell is performed in an oriented manner (Rajagopalan *et al.*, 2003). Filipin stainings of dividing yeast cells reveal an enrichment in sterols at the division plane. The focal accumulation of newly synthesized membranes and cell wall building proteins at the nascent daughter cells requires a polarized organization in a manner similar to the animal system (Simons & Ikonen, 1997).

1.2.4.2. Cell cycle control

Sterol distributions and localization of the corresponding cell-division performing proteins are strictly controlled by the cell-cycle (Wachtler *et al.*, 2003). Any disruption of sterol microdomains by filipin leads to the loss of organization at the division plane. Members of the cytoskeleton, especially F-actin, are also involved in the spatial organization of the contractile division ring. In the fission yeast *Schizosaccharomyces pombe* (*S. pombe*), mutants lacking cell division protein Cdc15p show mislocalized SRDs at the lateral sides of the cells in addition to the cell tips (Wachtler & Balasubramanian, 2006). In the same study, over-expression of *cdc15*⁺ resulted in appearance of additional SRDs in the lateral cell sides in a manner which was independent of F-actin. These findings stress the importance of cell-cycle and cell division controlled sterol accumulation at the division plane.

Taken together, yeast is an ideal investigation object to study DRM protein composition, trafficking and turnover which is facilitated by the high ergosterol / sphingolipid and DRM protein content of the yeast PM. Broad availability of yeast mutant lines impaired in the secretory machinery enabled researchers to reveal the sources detergent insolubility. Some yeast DRM proteins gain their detergent insolubility at the Golgi complex such as Gap1 (Lauwers & André, 2006) or even earlier at the ER such as the PM ATPase Pma1 (Bagnat *et al.*, 2001).

1.2.5. Lipid rafts in animals

The enrichment in only one major sterol (cholesterol) greatly facilitated animal lipid raft research. Studies with cholesterol depletion by MCD as well as studies with cholesterol enrichment at the PM via supplying cyclodextrin-cholesterol complexes (Christian *et al.*, 1997) enabled researchers to investigate the effects of sterol alterations in lipid microdomains at the PM. MCD treatment does not only affect cholesterol levels, but also suppresses endocytosis through clathrin-coated vesicles (CCVs) (Subtil *et al.*, 1999). CCVs depend upon cholesterol to detach from the PM as studies with green fluorescent protein (GFP)-labeled clathrin and transferrin receptor revealed: no curvature of the vesicles was visible after sterol depletion.

Seeing the effects of sterol depletion via MCD, one has to take into consideration that cholesterol presumably occupies the boundary of the L_o phase in most cases. Hence every sterol depletion assay removes the boundaries of L_o phases (which can be assumed to represent *in vivo* lipid rafts) leading to a broadening of the L_o phase. Hao *et al.* (2001) could show this in living chinese hamster ovary (CHO) cells using fluorescently labeled lipids. Upon MCD application big sized nano- to micrometer-scaled domains were visible which were stable for a prolonged time (tens of minutes). MCD application also led to a marked reorganization in the cellular actin cytoskeleton which might occlude sterol-depletion effects on lateral protein mobility (Kwik *et al.*, 2003).

1.2.5.1. Diseases involving lipid rafts

Lipid rafts are involved in the formation of many severe disorders in animals, most prominently in HIV and the Alzheimer's disease (see Simons & Ehehalt (2002), table 1 for an exhaustive, impressive list). HIV depends upon cholesterol which has to be associated with virion particles (Campbell *et al.*, 2004) to comprise "viral lipid rafts" enriched in sphingomyelin and cholesterol. These viral lipid rafts were isolated only with the detergent Brij-98 and not with Triton X-100. Replacing cholesterol with raft-disrupting sterol analogues like 4-cholestenone or coprostanol decreases HIV infectivity to a great degree.

This is due to a malfunction in the membrane fusion step as the HIV1 gp41 Env protein favors membrane fusion with membranes containing cholesterol. At the early steps of HIV infection, HIV particles cluster & enter the cells via surface nucleolin localized in lipid rafts (Nisole *et al.*, 2002). The gp41 Env protein of HIV-1 contains a specific sequence near its transmembrane domain which has been demonstrated to interact with membrane cholesterol and sphingomyelin (Sáez-Ciri3n *et al.*, 2002). Future antiviral therapeutics will use this

structural information on a specific cholesterol-binding motif in one of the most important HIV-1 proteins for generation of specific therapeutic antibodies.

The involvement of lipid rafts in many human diseases depicts the importance of these focal accumulation points for signaling & transport functions. *Helicobacter pylori* is a gram-negative bacterium colonizing the intestinal tract in humans and being known to cause gastric ulcers and stomach cancer. Intoxication occurs via acid-activated monomeric vacuolating toxin (VacA) which depends upon lipid rafts (Schraw *et al.*, 2002).

VacA oligomerizes at the PM if no acid-activation takes place – but in oligomerized form, VacA cannot intoxicate the host cells. Lipid raft localization of monomeric VacA was only visible after acid-activation. Upon sterol depletion by MCD, no internalization or intracellular localization of VacA was observable. Only if VacA is acid-activated in the stomach, the monomeric form penetrates into the host cells possibly causing ulcers or even stomach cancers.

Another prominent example involving lipid rafts is the Alzheimer's disease. Pathogenesis of Alzheimer's disease is directly linked to the fate of amyloid precursor protein (APP): APP is proteolytically cleaved either into amyloid-promoting β -amyloid or into non-amyloid-promoting APP_{sec} fragments. β -amyloid leads to the formation of brain lesions intrinsic for Alzheimer's disease. Application of cholesterol reducing reagents (lovastatin⁸ & MCD) led to a reduction of β -amyloid by 70 % while leaving APP_{sec} fragments unaffected.

APP cleavage is mediated through BACE (β -secretase enzyme) which co-localized with APP into complexes enriched in GAPs but depleted of the non-raft marker transferrin receptor (Simons & Eehalt, 2002). Amyloid plaque generation depends on the lipid raft association of BACE and APP since experiments where both components were cross-linked via antibodies led to a strong stimulation in the β -amyloid production. Another link for a putative lipid raft localization was contributed by the fact that β -amyloid interacts physically with the known raft-marker ganglioside GM₁ (Choo-Smith *et al.*, 1997).

⁸Lovastatin inhibits cholesterol biosynthesis.

1.2.5.2. Non-sphingolipids & -sterols

Not only cholesterol and sphingolipids alter the protein composition in lipid microdomains. Polyunsaturated fatty acids (PUFA) also modulate protein activity and localization in the cytoplasmic leaflet of lipid rafts. Protein tyrosine kinases of the Src family have been shown to depend upon PUFA moieties like myristoyl and palmitoyl acyl chains (Stulnig *et al.*, 1998). Src kinases are normally bound to the membrane via palmitoylation, however if the Src kinase Lck is lacking acylation sites, localization in DRMs is altered. Lck is no longer conducting signals if localized outside of DRMs thus underlining the importance of proteins in the cytosolic leaflet of DRMs (Stulnig *et al.*, 1998).

1.2.5.3. Raft sizes in animals

Investigations in animals concerning raft sizes have led to many contradicting results: experiments applying single-dye tracking (SDT) methodology followed fluorescently labeled saturated and mono-unsaturated lipid molecules to observe lipid-specific membrane domains (Schütz *et al.*, 2000). The saturated lipid probe (DMPE) localized 100-fold more in defined, small raft-like areas while the mono-unsaturated lipid probe (DOPE) diffused freely within the membrane showing no confined localization.

This confirmed the general assumption that unsaturated phospholipids are excluded from lipid rafts (Simons & Ikonen, 1997). Observed raft-like domains enriched in DMPE had a mean size of 0.7 μm , covered approx. 13 % of the membrane area and exhibited spatial-temporal stability. No free diffusion of the raft-like domains was observed. Only uni-directional movements were visible which resulted in dissolving of old domains and new assembly at another fixed position. Restriction of the free mobility of raft-like domains has been proposed to be dependent upon the cytoskeleton (Jacobson & Dietrich, 1999).

Other high resolution single particle tracking approaches following single proteins provided a much smaller size for rafts. Pralle *et al.* (2000) observed rafts as small cholesterol-sphingolipid enriched entities with a diameter ≤ 100 nm in the mammalian PM. Another finding in this study was the slowed diffusion of GPI-anchored and transmembrane proteins in rafts relative to non-raft GAPs. Following MCD sterol depletion these differences were no longer visible. Determination of raft sizes led to small entities (radius $r = 26 \pm 13$ nm) stable for several minutes.

1.2.5.4. Caveolae

Caveolae⁹ represent a subset of animal lipid rafts which form special flask-shaped PM invaginations on some mammalian cell types, first discovered in the 1950s (Yamada, 1955). These invaginations are small-sized (50 – 100 nm), stable and morphologically easy to recognize via microscopic techniques (Harder & Simons, 1997). A specific class of proteins was found to be heavily concentrated in these caveolae: caveolins (Rothberg *et al.*, 1992). Caveolins represent 21 – 25 kilo Dalton (kDa) proteins with N- and C-terminal hydrophilic domains being located in the cytosol and a hydrophobic intermembrane domain in the center of the protein (Okamoto *et al.*, 1998; Parton & Simons, 2007). Both cytoplasmic termini display post-translational modifications: the C-terminus is palmitoylated (figure 1.6) and the N-terminus bears a phospho-tyrosine residue (Cohen *et al.*, 2004).

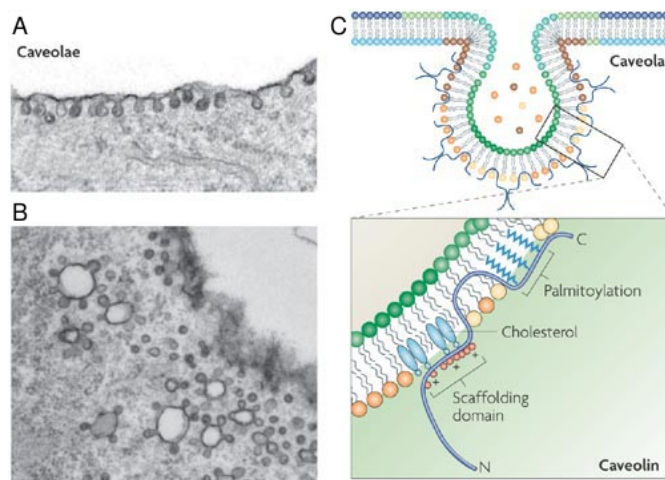


Figure 1.6.: **Shape & structure of caveolae in adipocytes.**

A & B: Electron micrographs showing surface-labeled caveolae as flask-shaped invaginations at the plasma membrane (**A**) or in intracellular pools (**B**).

C: Structure of caveolin featuring both cytosolic N- & C-termini and the hydrophobic intermembrane domain forming a hairpin in the membrane bilayer.

Adapted by permission from Macmillan Publishers Ltd: *Nature Reviews Molecular Cell Biology*, Parton & Simons (2007), © 2007

Three major members of this caveolin protein family are known: caveolin-1 & caveolin-2 are located in adipocytes, endothelial tissue and fibroblastic cells whereas caveolin-3 is specifically expressed only in the sarcolemma of smooth muscle cells. Mutational analyses using truncated and fluorescently labeled caveolin-1 revealed a 20 aa N-terminal membrane attachment domain (N-MAD) to be responsible for proper caveolae localization of caveolin-

⁹Caveolae: *small caves*

CHAPTER 1. INTRODUCTION

1. A shorter portion of the N-MAD (amino acids KYWFYR) was sufficient to gain plasma membrane localization of GFP fusion constructs (Cohen *et al.*, 2004).

Availability of caveolin knockout mice lacking caveolin-1 expression enabled whole organism studies of caveolin expression: caveolin-1 $-/-$ mice displayed impaired nitric oxide and calcium signaling (Drab *et al.*, 2001) resulting in physical limitations for the mice like reduced swimming capacity. Caveolin-3 is involved in the formation of a special form of muscle dystrophy, limb-girdle muscular dystrophy (LGMD). Functional caveolin-1/2/3 form oligomers of 14 – 16 monomers at the membrane of caveolae. Caveolin-1 and caveolin-2 form even stable hetero-oligomers with a size > 400 kDa.

The high enrichment in cholesterol and sphingolipids is important for a determinative protein localization in caveolae. Cholesterol accounts for more than 30 % of the membrane lipids in caveolae. Caveolin protein itself highly depends upon the cholesterol content for insertion into the PM (Okamoto *et al.*, 1998). Cholesterol depletion in caveolae by MCD leads to a dramatic change in the activation status of signaling proteins like the Extracellular Signal-related Kinase (ERK) which is involved in the MAP kinase cycle (Furuchi & Anderson, 1998). Interestingly caveolin-1 also transports cholesterol from the ER to the PM and expression of all caveolins is strictly transcriptionally controlled by the cholesterol content in cells due to sterol-binding promoter elements (Okamoto *et al.*, 1998).

Targeting proteins into caveolae is dependent upon the acylation status of proteins, for instance the endothelial nitric-oxide synthase (eNOS) displays an exclusive localization in caveolae when myristoylated & palmitoylated (Shaul *et al.*, 1996). Dynamic post-translational modifications may play a role in localization of proteins in caveolae. Cholesterol & sphingolipids seem to attract many lipid-anchored proteins (GPI and acyl anchors) into caveolae. Especially GPI-linked proteins were shown to be clustered within caveolae (Harder & Simons, 1997).

Some signaling complexes are also found to be preformed at the caveolae membrane: all members of a mitogen-activated kinase (MAP) kinase pathway are located in caveolae of unstimulated human fibroblasts¹⁰ (Liu *et al.*, 1997). Exogenous application of platelet-derived growth factor (PDGF) led to the activation of MAP kinases in caveolae through tyrosine phosphorylation over 11 involved molecules. Supplying PDGF to isolated caveolae also led to activation of this signaling cascade. Therefore, the authors were prompted to assume that all elements of this MAP kinase activating cascade are pre-concentrated in caveolae. Caveolin-1 itself also exhibits signaling functions upon transfection with the simian virus 40 (SV-40) as emerged in the studies involving dominant negative caveolin mutants (Roy *et al.*, 1999).

¹⁰Fibroblasts: cells responsible for the production of extracellular matrix components in animals.

Signaling proteins of the Ras family have also been localized in caveolae (Prior *et al.*, 2001). H-Ras transfer into caveolae & lipid rafts was mediated by palmitoylation and farnesylation but the localization of H-Ras in lipid rafts was highly dynamic. Upon loading with GTP H-Ras dissociated from rafts due to conformational changes. After GTP-driven release of H-Ras into the bulk PM, Raf-1 kinase was activated and participated in a MAPK kinase pathway (Prior *et al.*, 2001; Roy *et al.*, 1999).

Not only signaling proteins are interacting with caveolae. Transport proteins were also shown to locate in caveolae of endothelial cells. The endothelial volume-regulated anion channel (VRAC) is involved in the regulation of cell volume and known processes regulated by VRACs are proliferation and angiogenesis (Trouet *et al.*, 2001b). Activation of VRAC was impaired upon transfection with caveolin-1 Δ 1-81 (Trouet *et al.*, 2001b). When transfection was performed only with intrinsic full-length caveolin-1, VRAC displayed normal activation characteristics. More interestingly, VRAC was inhibited by a raft-located isoform of c-Src protein tyrosine kinase which was double acylated (Trouet *et al.*, 2001a).

To summarize, caveolae represent stable, light microscopically visible plasma membrane invaginations in mammals where pre-concentrated signal transduction & transport complexes are localized. These special invaginations are highly enriched in cholesterol, glycosphingolipids and GAGs. Unfortunately, there are no direct plant equivalents known for these specific structures.

1.2.5.5. Signaling complexes in animal lipid rafts

In general GPI-linked signaling proteins are enriched in animal caveolae & lipid rafts (Zajchowski & Robbins, 2002) emphasizing the important role of lipid modifications (see section 1.1.4, p. 7). GAGs are clustered into lipid microdomains, for instance placental alkaline phosphatase (PLAP) (Schroeder *et al.*, 1994). Altering the lipid environment in artificial liposomes led to a loss of detergent-insolubility of PLAP (disappearance out of Triton X-100 DRMs) if the lipid environment features DOPC, a low T_m lipid. If the artificial membranes were build with DPPC (a high T_m lipid) detergent-insolubility was visible. This reported a direct relationship of PLAP localization in DRMs and the lipid environment. Especially as GAGs feature many unsaturated fatty acid chains, this might be an explanation for the enrichment of GPI-anchored proteins in DRMs. GAGs favor a more rigid membrane environment containing sphingolipids and sterols.

Lipid rafts or specialized membrane compartments play an important role particularly for signaling processes in the animal immune system. T cell activation depends strongly on the correct localization of activated TCR and corresponding interacting molecules in lipid rafts (Xavier *et al.*, 1998). Disrupting functional lipid rafts by sterol depletion via MCD or sterol

CHAPTER 1. INTRODUCTION

dispersion by filipin led to suppression of T cell activation. Detailed investigations revealed that the TCR is recruited into lipid rafts where a tetraspanin CD4:Lck tyrosine kinase complex activated the TCR (Xavier *et al.*, 1998).

Post-translational lipid modifications play a key role in recruiting of proteins into and out of lipid rafts (Melkonian *et al.*, 1999). More than half of the proteins in Madin-Darby canine kidney (MDCK) DRMs were specifically acylated (e.g. palmitoylated) in contrast to cytoskeleton contaminations which were not acylated. Palmitoylation is a post-translational modification guiding transmembrane proteins into rafts: cytoplasmic attachment of one or two palmitoyl chains confers raft localization of the B-cell receptor in mammals (Brown, 2006). The palmitoylation of the involved tetraspanin CD81 led to surface presentation of the B-cell receptor which subsequently activated a consecutive signaling cascade.

Astonishingly, prenylated proteins were excluded from DRMs. Experiments with Rab5 and H-Ras as multiple lipid-modified, prenylated proteins exposed that sole hydrophobicity was not sufficient to trigger DRM localization (Melkonian *et al.*, 1999). Another example is represented by G_{α} subunits which are normally located in DRMs by myristoylation and palmitoylation anchors. By introduction of additional unsaturated fatty acid chains, these subunits lost their DRM localization though the hydrophobicity increased (Moffett *et al.*, 2000).

It had previously been proposed by Kusumi & Sako (1996) that the cytoskeleton might play a key role in partitioning the PM. Single-particle tracking methods allowed to observe non-free protein floating which was restricted to certain areas. More recent quantitative proteomics data from B cells supported this notion: B cell antigen receptors were ligated by antigen binding which led to coalescence of lipid rafts incorporating several signaling receptors (Gupta *et al.*, 2006). Activation of the B cell antigen receptors mediated threonine dephosphorylation at Thr567 and dislocation of the adaptor protein ezrin from lipid rafts.

Subsequently, ezrin detached from the actin cytoskeleton and lipid rafts were transiently uncoupled from the actin cytoskeleton. Constitutively active ezrin attached raft / non-raft areas in the PM to the actin cytoskeleton which inhibited the coalescence of lipid rafts in B cell receptors. Thereby, ezrin mediated the lipid raft formation in B cell antigen receptors by detachment from the underlying actin cytoskeleton.

Another study confirming the involvement of cytoskeleton components into lipid raft formation concentrated upon IgE-Fc ϵ RI¹¹ receptor complexes. IgE-Fc ϵ RI co-localized with the GAP Thy-1 and Src-family tyrosine kinase Lyn in small patches at the PM (Holowka *et al.*, 2000). Concomitant F-actin stainings displayed the same localization after cross-linking, in-

¹¹Fc ϵ RI represents the tetrameric high affinity receptor at the surface of IgE antibodies involved in the immune system response to allergies and parasites.

dicating a regulatory role for stimulated F-actin polymerization in clustering IgE-Fc ϵ RI & Lyn. Dynamic incorporation of Fc ϵ RI and Lyn in DRMs strongly depended upon the regulation by the F-actin cytoskeleton.

To summarize, several important signaling events in the animal immune response are directly linked to the formation of lipid rafts and / or the pre-concentration of several signaling components in distinct membrane domains which are organized by the cytoskeleton (Brown, 2006; Gupta *et al.*, 2006; Holowka *et al.*, 2000; Xavier *et al.*, 1998).

1.2.5.6. Activity & affinity regulation via lipid raft localization

Not only signaling events are involving lipid rafts. Transporter activity is also finely regulated by localization in lipid rafts. For instance, the activity of the metabotropic glutamate receptor DmGluRA in *Drosophila melanogaster* (D.m.) was strictly regulated by localization in sterol-rich membrane domains (Eroglu *et al.*, 2003). Placing DmGluRA in liposomes lacking ergosterol inhibited ligand binding at all.

In Liposomes supplied with ergosterol, a high affinity state of DmGluRA was present in DRMs which exhibited a 50 times higher affinity than the corresponding low affinity state which localized outside of DRMs. Increasing the sterol content in the membrane led to an increasing amount of high affinity DmGluRA in DRMs. Thereby, regulation of DmGluRA transport activity was mediated by localization in cholesterol-rich membrane domains.

The same applied also to the shaker-like potassium channel Kv2.1 which was localized in rat brain and HEK 293 cell lipid rafts (Martens *et al.*, 2000). Disrupting the sterol-rich membrane environment of Kv2.1 via MCD application strongly displaced the ion channel out of lipid rafts and affected electrophysiological properties: the midpoint of Kv2.1 inactivation was shifted by > 30 mV towards hyperpolarization without altering channel activation or peak intensity. Thus, ion channel activity seemed to be regulated by lipid-protein interactions taking place in lipid rafts.

1.2.6. Lipid rafts in plants

Lipid rafts in plants have not been investigated to such an extent as animal lipid rafts – after the first isolations of Triton X-100 DRMs from *Nicotiana tabacum* (*N.t.*) by Peskan *et al.* (2000) further studies were conducted on *A.th.* revealing a similar pattern for the DRM protein composition as for animals: enrichment of proteins fulfilling signaling, trafficking and transport functions.

As the main structural components of animal lipid rafts are cholesterol and sphingomyelin, corresponding plant counterparts must exist. Cholesterol does not play an important role in the plant PM and is substituted by β -sitosterol, campesterol and stigmasterol as the major plant sterols. Experiments signified a correlation between ABA-induced membrane permeability and plant sterols in artificial lipid bilayers consisting of two kinds of PCs (Stillwell *et al.*, 1990). The addition of 5 mol % β -sitosterol and campesterol to artificial membranes strongly decreased ABA-induced membrane permeability for the fluorescent anion carboxyfluorescein to the same extent as cholesterol did, thus inhibiting ABA effects on the membrane. As Stillwell *et al.* (1990) put it: "From these experiments a possible role is suggested for plant sterols in controlling the mode of action of ABA". Other studies also confirmed that β -sitosterol and cholesterol have similar effects on artificial lipid bilayers: there were no differences in the additional surface area introduced by both sterols to lipid bilayers and in the number of coordinated water molecules (Gallová *et al.*, 2008).

1.2.6.1. Plant plasma membranes

In response to many external signals like microbe-associated molecular patterns (MAMPs) / pathogen-associated molecular patterns (PAMPs) dynamic protein complexes appeared to be located in distinct structures at the plant PM, for instance at papillae formed upon pathogen attack (Assaad *et al.*, 2004) or during FLS2 receptor signaling (Chinchilla *et al.*, 2007; Robatzek *et al.*, 2006). Recently, it could be shown that *Pseudomonas syringae* decreased β -sitosterol levels in plants in favor of increasing stigmasterol levels which in turn promoted susceptibility to pathogens (Griebel & Zeier, 2010). Altering sterol composition of the PM might thus be a mechanism for pathogens to successfully attack plants.

Many proteomic investigations have elucidated the protein composition of plant PMs (Alexandersson *et al.*, 2004; Marmagne *et al.*, 2004, 2007; Nelson *et al.*, 2006): some studies concentrated on GAPs (Borner *et al.*, 2003; Elortza *et al.*, 2003, 2006), others were interested in the identification of phosphoprotein isoforms (Nühse *et al.*, 2003, 2004) and the effects of (a)biotic stress on salt-induced (Malakshah *et al.*, 2007) or sucrose-induced (Niittylä *et al.*, 2007) phosphorylation patterns of PM proteins. In all investigations, the plant PM has

proven to be enriched in signaling, trafficking and transport proteins which underlines the importance of the PM as a gateway for molecule and signal traversal. From a structural view, GAPs were also found to be enriched in the extracellular leaflet of *A.th.* PMs (Sherrier *et al.*, 1999). This is in line with the mammalian PM though there is no such strong emphasis on signaling in plant GAPs.

1.2.6.2. Evidence for organization in the plant PM

Polar transport in plants has been studied for a long time, especially the PIN family of auxin transporters. PIN1 and PIN2 are major auxin transporters in the root of *A.th.* whereas PIN3 is highly expressed in leaves (Zappel & Panstruga, 2008). Sterol-deficient mutants displayed clearly reduced polar auxin transport – for PIN2 it has extensively been studied that sterols affect its polar localization at the PM (Men *et al.*, 2008). In *cpi1-1* sterol mutants, PIN2 displayed wrong localization due to compromised endocytosis which subsequently led to a failure in root gravitropism. Upon cytokinesis, PIN2 was equally distributed to both daughter membranes, but removed from one of these daughter membranes by endocytotic mechanisms. In contrast, PIN2 localization was stable on both daughter membranes in *cpi-1* sterol mutants emphasizing the importance of the sterol composition for correct PIN2 distribution / localization. The endocytosis of PIN2 has been shown to be dependent upon sterols and CCVs (Men *et al.*, 2008).

PEN3 (PDR8, ABC transporter G family member 36, At1g59870) represents a transporter for toxic secondary metabolites to the apoplast. It is involved in the plant response to pathogen attack by powdery mildew (Stein *et al.*, 2006). Interestingly, PEN3 localization at the PM is changed upon pathogen attack: uninfected leaves display a uniform PM localization while infected leaves show focal accumulations at penetration sites (Stein *et al.*, 2006). Stainings with the polyene compound filipin revealed a strong enrichment of sterols at these focal accumulation sites surrounding the fungal appressoria. PEN3 expression was shown to be strong in hydathodes, stomata and to be induced by infection with avirulent and virulent bacterial pathogens (Kobae *et al.*, 2006).

Upon induction, defense response genes like *PR-1* and *AtRbohD / F* were highly up-regulated in *pen3* mutant plants (Kobae *et al.*, 2006). The plant response to pathogen attack is based on a complex of PEN1 (a PM syntaxin, Assaad *et al.*, 2004), PEN2 (glycoside hydrolase, located in peroxisomes), PEN3 (ABC transporter for the toxic compounds), VAMP722 (vesicle-associated membrane protein 722) and further adaptor proteins which are gathered at the entry site of the pathogen (Lipka *et al.*, 2008). The members of this defense complex (figure 1.7) recognized the pathogen (PEN1), produced antimicrobial compounds (PEN2) and exported these toxic metabolites (PEN3).

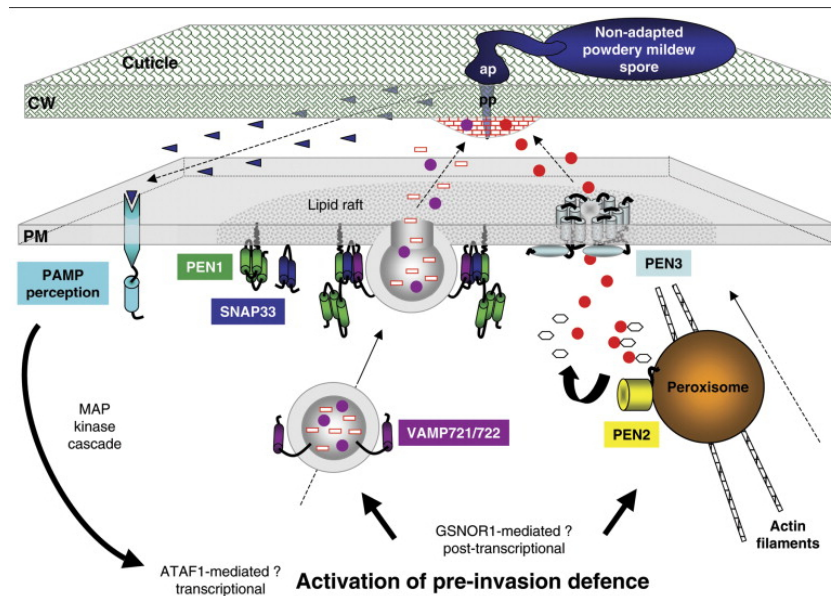


Figure 1.7.: **PEN1 & PEN3 interactions in lipid rafts at the plant PM.** Upon attack by non-adapted powdery mildew, lipid raft-localized PEN1 & PEN3 mediate the defense response by secretion of antimicrobial compounds. Reprinted with permission from Elsevier: *Current Opinion in Plant Biology*, Lipka *et al.* (2008), © 2008

Remorins represent another family of proteins located in spatially distinct domains at the plant PM. Detailed information on remorins can be found in section 1.2.6.4, p. 40.

1.2.6.3. Previous DRM investigations in plants

Figure 1.8 depicts the tremendous amount of lipid raft publications in the animal field. More than 1000 publications every year during the last decade underline the importance of lipid rafts. Especially during virus entry into host cells (e.g. HIV-1), lipid rafts are often used as entry doors (Nisole *et al.*, 2002). With the help of the non-ionic detergent Brij-98, virion-associated rafts could be analyzed for their protein content (Gil *et al.*, 2006).

However, for the plant kingdom there is no huge amount of lipid raft data available. But our knowledge about plant lipid rafts is growing, e.g. by identification of a putative, plant-specific raft marker (cf. section 1.2.6.4) or by detailed analyses of plant DRMs for dependency upon sterols. Differences in the protein composition of plant DRMs upon the application of (a)biotic stress stimuli are currently under investigation.

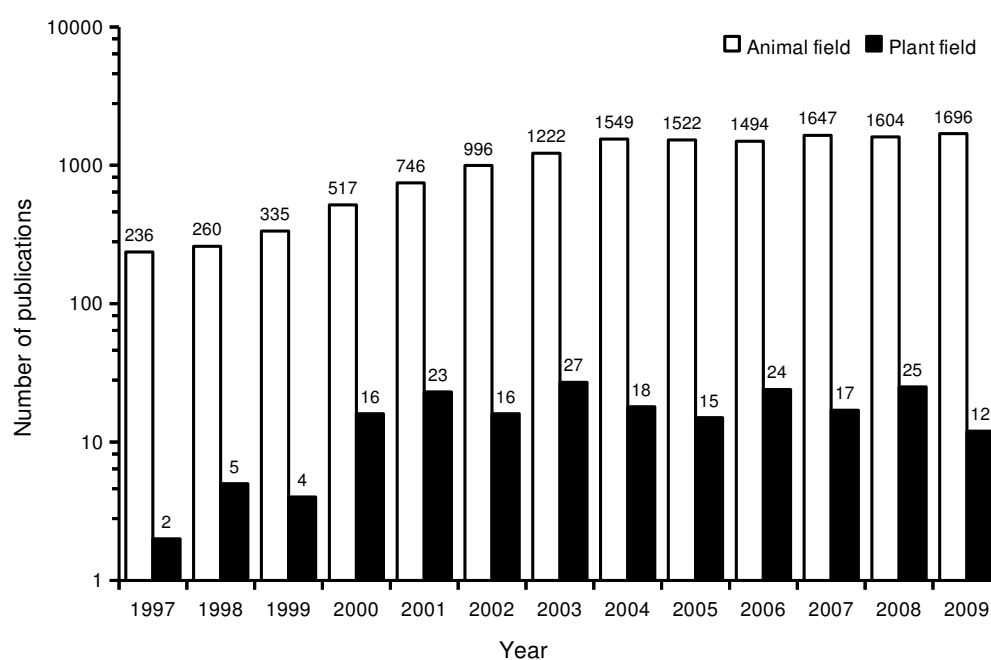


Figure 1.8.: **Publications concerning lipid rafts / microdomains.** Source: ISI Web of Knowledge, publications tagged with the keywords "DRMs", "lipid rafts" or "microdomains" (©Thomson Reuters, 2010).

First investigations on the subject of plant DRMs / lipid rafts performed in the beginning of the century: Peskan *et al.* (2000) identified a G-protein coupled receptor in low density Triton X-100 DRMs. Following this first evidence for plant DRMs, Mongrand *et al.* (2004) performed a proteomic analysis of *N.t.* leaves resulting in the identification of the protein NtRac5 which was heavily enriched in Triton X-100 DRMs together with the NADPH oxidase NtRbohD upon elicitation with cryptogin.

In the same study, StRem 1.3 from potato was reported to localize in Triton X-100 DRMs and, for the first time, the lipid composition of plant DRMs was analyzed. Plant DRMs were shown to be enriched in sphingolipids & sterols and depleted in unsaturated phospholipids like animal DRMs (Mongrand *et al.*, 2004). Different detergent:protein ratios were titrated to gain insights into the optimum ratio at which maximum enrichment in sphingolipids & sterols and maximum depletion of phospholipids occurred. Two-fold enrichment of sphingolipids & sterols was observed for a detergent:protein ratio of 15:1 (w/w). At this ratio, phospholipids were depleted by 50 % and the loss of DRM protein content was acceptable. Supplemented detergent led to no further enrichment in sphingolipid & sterols. Thus, the authors proposed using a fixed detergent:protein ratio of 15:1 in plant DRM studies.

CHAPTER 1. INTRODUCTION

First in-depth investigations of *A.th.* Triton X-100 DRM protein composition in cotyledons revealed an enrichment in certain signaling proteins comparable with the situation in animals (Shahollari *et al.*, 2004): leucin-rich repeat (LRR) protein kinases, β subunits of heterotrimeric G-proteins and several GTP-binding proteins were identified. One of these LRR protein kinases was transiently up-regulated during recognition of the endophytic fungus *Piriformospora indica* (Shahollari *et al.*, 2005). Another pair of DRM localized LRR protein kinases (At1g13230 & At5g16590) was shown to be necessary for the plant response against the fungus *P. indica*. Pii-2 (At1g13230) mutants displayed no DRM localization of At5g16590 and no response to the fungus (Shahollari *et al.*, 2007). Pii-2 and At5g16590 seem to modulate the *P. indica-A.th.* interaction.

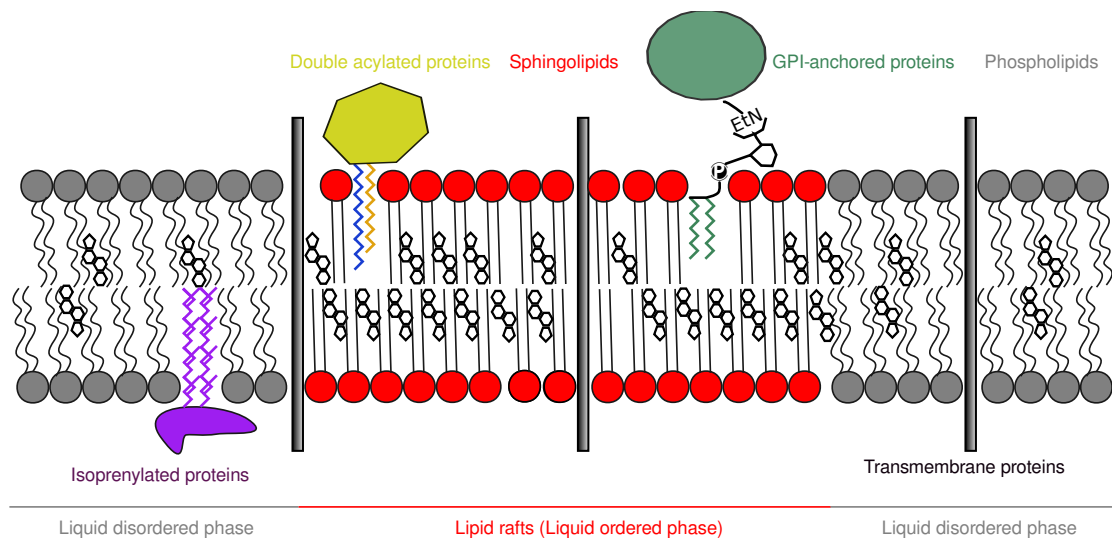


Figure 1.9.: **Potential structure of lipid rafts.**

A schematic presentation of the PM containing lipid rafts. Lipid rafts are considered to represent a liquid ordered (L_o) area due to their high sterol and sphingolipid contents: these molecules leave only small room for free diffusion of proteins. GPI-anchored and acylated (myristoylated / palmitoylated) proteins are strongly enriched in this L_o phase. In contrast, prenylated proteins are enriched in the non-raft L_d phase.

Further evidence for phytosterol- and sphingolipid-enriched lipid domains in plants was contributed by Borner *et al.* (2005). Isolation of Triton X-100 DRMs from *A.th.* callus membranes yielded enrichment in specific proteins inside the DRMs with respect to the microsomal membrane fraction. Among those proteins were GAPs, P-type ATPases, multidrug resistance (MDR) proteins, a plant homologue of flotillin and proteins of the stomatin family which are induced by the hypersensitive response.

Phytosterol and sphingolipid content was remarkably higher in DRMs¹². The overall composition of sterols did not alter between microsomal membrane fractions and the PM: β -sitosterol and campesterol were as abundant in the DRMs as in the microsomal membrane fraction.

GAPs were further studied intensively by generation of a transgenic GAP: PAT-GPI4. PAT-GPI4 was constructed by the GPI-anchor of AtAGP4¹³ and a bacterial phosphinothricin acetyl transferase (PAT) which was known to have no intrinsic plant sorting signals. The fusion protein localized clearly to the PM and into DRMs suggesting an important sorting signal function for the GPI-anchor in plants. AtSku5 (At4g12420) and GPDL1¹⁴ (At5g55480) represented *natural* GAPs which were among the enriched DRM proteins as revealed by difference gel electrophoresis. In brief, GAPs seemed to be strongly enriched in Triton X-100 DRMs isolated from *A.th.* callus membranes (Borner *et al.*, 2005).

A complete inventory of Triton X-100 DRMs from *N.t.* BY-2 cell cultures resulted in the identification of 145 proteins (Morel *et al.*, 2006). Cell wall metabolism, signaling and trafficking proteins were strongly enriched in DRMs. The role of specific lipids in DRMs was studied using *fad2* and *Fad3*⁺: the amount of DRM proteins decreased strongly due to a malfunction in regulating the degree of fatty acid saturation (Laloi *et al.*, 2007). DRMs isolated from the Golgi apparatus and PM were strongly enriched in sterols, sterylglucosides, glucosylceramides and displayed depletion of phospholipids. Emergence of DRMs started at the Golgi apparatus and was not visible in the ER as witnessed after treatment of leek seedlings with fenpropimorph¹⁵.

The first quantitative analysis of sterol dependency in *A.th.* DRMs resulted in the identification of a core set of strictly sterol-dependent proteins (Kierszniowska *et al.*, 2008). Sterol dependency was tested by application of 30 mM MCD to PM preparations from *A.th.* cell cultures. It has been shown that MCD treatment does not only lower cholesterol levels in the plant PM but also depletes the phytosterols campesterol, β -sitosterol and stigmasterol in a concentration-dependent manner. GAPs were among the DRM proteins which were depleted by MCD treatment, again resembling the situation for animal lipid rafts. Functionally, these GAPs were attributed to cell wall anchoring like AtSku5 and fasciclin-like arabinogalactan proteins. Other MCD responsive DRM proteins were the *A.th.* remorins AtRem 1.2 / 1.3.

¹²The phytosterol:protein ratio was 4-fold and sphingolipids:protein ratio 5-fold enriched in DRMs compared to the total / microsomal membrane fraction.

¹³Arabinogalactan protein 4 is a GPI-anchored protein at the apoplastic face of the PM involved in the attachment to the matrix.

¹⁴Glycerophosphodiesterase-like 1 protein

¹⁵Fenpropimorph is a sterol biosynthesis inhibitor which prevents the formation of Δ^5 sterols in the Golgi apparatus, thus stopping the delivery of glucosylceramides to the PM / DRMs. The amount of PM DRMs decreased greatly after treatment with fenpropimorph.

CHAPTER 1. INTRODUCTION

Signaling proteins were also depleted by MCD but were suggested to be dynamic members of DRMs as their level of depletion was lower (Kierszniowska *et al.*, 2008).

A further quantitative proteomics approach used metabolic labeling with ^{14}N / ^{15}N to investigate the cryptogein effects on *N.t.* BY-2 DRMs (Stanislas *et al.*, 2009). Cryptogein represents a low molecular weight protein from the oomycete *Phytophthora* inducing a hypersensitivity-like response in *N.t.* involving the NADPH oxidase NtRbohD (Simon-Plas *et al.*, 2002). NtRbohD had been investigated earlier to be localized in *N.t.* DRMs. The said oxidase strictly relies on the DRM sterol composition (Roche *et al.*, 2008) and is responsible for the production of reactive oxygen species (ROS) after cryptogein treatment (Simon-Plas *et al.*, 2002). Quantitative proteomics revealed 4 dynamin proteins being depleted and a specific 14-3-3 protein being induced by cryptogein treatment (Stanislas *et al.*, 2009).

Studying the protein composition in DRMs after different biotic and abiotic stimuli in a quantitative manner has been further continued by a study of Minami *et al.* (2009). Cold-acclimation in *A.th.* seedlings was analyzed for changes in DRM lipid and protein composition. After cold-acclimation more free sterols and significantly less proteins were found in DRMs. Some DRM proteins showed a decrease after cold-acclimation (actins, tubulins, V-type H^+ -ATPase) while others were enriched (aquaporins, P-type H^+ -ATPase and AtRem 1.3). Interestingly, AtLCN / AtLipocalin (At5g58070) was used as a cold-induced PM marker in this study and showed no appearance in DRMs according to immunoblotting experiments. This might render AtLipocalin a putative non-raft marker for plants.

Taken together, plant lipid rafts have a similar lipid and protein composition as their animal counterparts (figure 1.9, p. 36). Future investigations of plant DRMs are expected to improve our knowledge concerning changes in the lipid & protein composition upon application of (a)biotic stimuli.

Table 1.2.: Summary of previous plant DRM research

Publication	Object	Outline
Peskan <i>et al.</i> (2000)	<i>N.t.</i> leaves	Heterotrimeric G-protein subunit β was located in low-density Triton X-100 DRMs
Mongrand <i>et al.</i> (2004)	<i>N.t.</i> leaves	Proteomic analysis revealed enrichment of specific proteins in Triton X-100 DRMs (NtRac5)
Shahollari <i>et al.</i> (2004)	<i>A.th.</i> cotyledons	Triton X-100 DRMs were enriched in signaling components (especially kinases and LRR receptor-like kinases)
Borner <i>et al.</i> (2005)	<i>A.th.</i> callus membranes	First profound analysis of the lipid composition of Triton X-100 DRMs. DIGE analysis showed differential enrichment / depletion of proteins
Shahollari <i>et al.</i> (2005)	<i>A.th.</i> seedling roots	A receptor kinase accumulated in Triton X-100 microdomains in response to the endophytic fungus <i>Piriformospora indica</i>
Morel <i>et al.</i> (2006)	<i>N.t.</i> BY-2 cells	Proteomic analysis of Triton X-100 DRMs: signaling, trafficking and cell wall metabolism showed a significant increase in their relative importance. In total 145 proteins were identified
Laloi <i>et al.</i> (2007)	<i>A.th.</i> & <i>Allium porrum</i> (A.p.) seedlings	Triton X-100 DRMs showed enrichment in sterols, sterylglucosides and glucosylceramides. Synthesis of DRM lipids starts in the Golgi apparatus, not in the ER. Fatty acid desaturase-deficient <i>A.th.</i> <i>fad2</i> and <i>Fad3</i> ⁺ plants displayed a dramatic decrease in the amount of DRMs
Raffaele <i>et al.</i> (2007)	Plants	Remorins represent a plant-specific protein family with coiled-coil domains. Representatives of the family are present in <i>A.th.</i> , <i>Medicago truncatula</i> (<i>M.t.</i>) and <i>Solanum tuberosum</i> (<i>S.t.</i>). StRem 1.3: canonical member of the family.
Kierszniowska <i>et al.</i> (2008)	<i>A.th.</i> cell culture	Quantitative analysis of DRMs treated with the sterol-disrupting agent MCD. Cell wall-related proteins represented true core raft proteins whereas signaling components were variable components of DRMs
Roche <i>et al.</i> (2008)	<i>N.t.</i> BY-2 cells	MCD depleted PM sterols by approx. 50 % and redistributed NtRbohD out of DRMs
Minami <i>et al.</i> (2009)	<i>A.th.</i> seedlings	Cold acclimation decreased gradually DRM amount, quantitatively changing protein expression. Membrane transport, trafficking and cytoskeleton interactions were strongly biased upon cold acclimation.
Stanislas <i>et al.</i> (2009)	<i>N.t.</i> BY-2 cells	Quantitative analysis of DRMs after elicitor treatment with cryptogein showed a higher abundance for a 14-3-3 signaling protein.

1.2.6.4. Identification of a putative plant lipid raft marker

Remembering the huge amounts of known animal lipid raft proteins (Src family of protein tyrosine kinases, caveolin-1, flotillins) there has been a lack of a plant lipid raft "marker" protein. Evidence accumulating during the last years point to the family of remorin proteins in *A.th.*, *M.t.* and *S.t.* These proteins have the potential to represent golden lipid raft markers in plants.

The remorin protein was first identified as an unspecific, lysine-rich DNA-binding protein (Dbp) in *A.th.* which was auxin-induced 10-fold after 8 h (Alliotte *et al.*, 1989). Due to the highly charged structure of Dbp¹⁶ this protein displayed significantly altered migration on sodium-dodecylsulfate polyacrylamide gel electrophoresis (SDS-PAGE) gels: the protein has a molecular weight of 21 kDa, but migration can be observed at approx. 36 kDa because of the high glutamic acid and lysine content. Expression of this *A.th.* remorin AtRem 1.3 (Dbp) was shown to be induced by wounding and dehydration (Reymond *et al.*, 2000).

Later investigations in *S.t.* identified the potato protein pp34 as a PM-associated protein which seemed to be involved in viral movement (Reymond *et al.*, 1996). Pp34 was known to bind galacturonides and displayed multiple threonine phosphorylation sites (Jacinto *et al.*, 1993). The protein migrated anomalously on SDS-PAGE gels like the *A.th.* Dbp protein with a molecular weight of approx. 34 kDa. Both proteins, Dbp and pp34, shared 67 % amino acid identity, had the same enrichment in glutamic acid and lysine residues in their sequence and intriguingly a proline-rich N-terminus (22 % proline content). As the potato protein pp34 lacked any TMDs but interacted with the PM, the name **remorin** was proposed as remora represents a fish which attaches itself to the surface of other larger organisms (Reymond *et al.*, 1996). A specific function could be attributed to the *S.t.* remorin at that time: the binding of oligogalacturonides, structural and regulatory members of the extracellular matrix of plants.

Further investigations identified remorins also in *Solanum lysopersicum* (Bariola *et al.*, 2004) where they were identified as coiled-coil forming oligomeric and filamentous proteins in chemical cross-linking studies applying glutaraldehyde. Coiled-coil domains are known to facilitate protein-protein interactions, e.g. protein oligomerization (Kohn *et al.*, 1997). The expression of the tomato remorin was strong in apical tissues, leaf primordia and vascular traces. Immunolocalization of remorin at the root tip of tomato disclosed distinct, clustered PM structures which resembled microdomains in mammals. It was assumed that these structures may be constituted of oligomerized remorins. In the same year, Mongrand *et al.* (2004) identified the potato remorin StRem 1.3 as a member of Triton X-100 DRMs. This

¹⁶Dbp corresponds to AtRem 1.3 (At2g45820) according to recent naming schemes (Raffaele *et al.*, 2007).

finding supported the notion that remorin proteins are localized in microdomains at the plant PM.

Additional evidence for incorporation of remorin proteins into membrane domains was delivered by proteomic studies of DRMs conducted in *A.th.* seedlings (Shahollari *et al.*, 2004) and *A.th.* cell cultures (Kierszniowska *et al.*, 2008). Remorin proteins were also identified to be enriched in the rice PM upon salt stress (Malakshah *et al.*, 2007). In a quantitative proteomics study, Minami *et al.* (2009) identified AtRem 1.3 as a DRM protein which is strongly induced upon cold acclimation after 48 h.

Microarray data support a strong induction of AtRem 1.3 upon drought stress (Bray, 2002) and pathogen attack (Journot-Catalino *et al.*, 2006). Yeast two-hybrid screens revealed a direct interaction of AtRem 1.3 with the two-response gene regulator ARR4 which is induced by ABA and cytokinin (Yamada *et al.*, 1998). Taken together, AtRem 1.3 seems to be heavily involved in different stress responses and / or signaling processes.

Searching for physiological functions of StRem 1.3 it was discovered that StRem 1.3 played a role in the entry of viral movement proteins of potato virus X (Raffaele *et al.*, 2009a). Biochemical approaches identified StRem 1.3 as an intrinsic DRM constituent, attached to the cytosolic leaflet of the PM in *S.t.* and susceptible to sterol depletion via MCD application (Raffaele *et al.*, 2009a). Studying the localization of StRem 1.3, GFP-tagged full length StRem 1.3 was transiently expressed in *N.t.* leaves. StRem 1.3 displayed a discontinuous labeling of the PM – it clearly localized to "patchy" structures at the PM where single fluorescent structures were measured to be approx. 600 nm in size. Performing immunolocalization by gold-coated antibodies the size of StRem 1.3 structures could be narrowed down to small clusters with a mean diameter of 76.5 ± 21.6 nm. These clusters were only visible at the cytosolic side of the DRMs. Following MCD treatment these small clusters dispersed to the whole PM displaying no aggregated localization anymore.

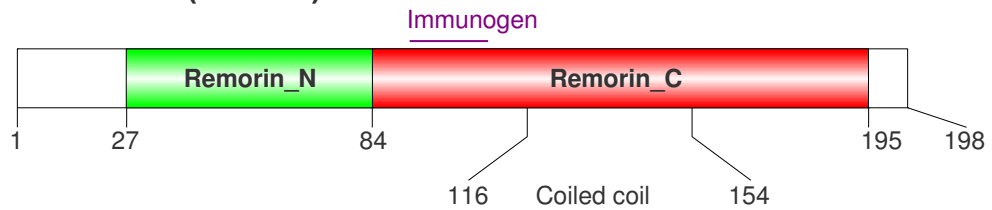
Virus infection studies with transgenic *Solanum lysopersicum* (*S.l.*) transiently expressing StRem 1.3 resulted in a reverse relationship between StRem 1.3 expression levels and movement of potato virus X (PVX) (Raffaele *et al.*, 2009a). PVX was shown to interact with StRem 1.3 in yeast two-hybrid systems and to co-localize with StRem 1.3 in the PM and plasmodesmata (PD) upon virus infection. Thus, the authors concluded that StRem 1.3 is involved in plant-pathogen interactions.

Supporting evidence for the involvement of remorin proteins in plant-pathogen interactions was found in a study addicted to identify proteins specifically induced by the bacterial AvrRpm1 effector (Widjaja *et al.*, 2009).

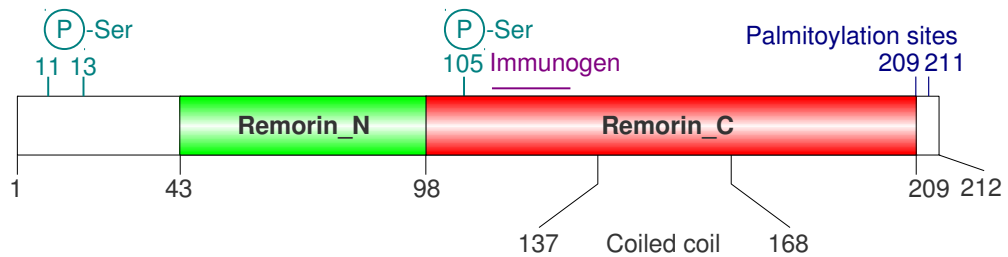
CHAPTER 1. INTRODUCTION

Four proteins were found to be early signaling components in response to bacterial AvrRpm1 and the corresponding cognate disease resistance protein RPM1¹⁷, one of these proteins was AtRem 1.2 (At3g61260). Phospho-isoforms of AtRem 1.2 were detected to be differentially regulated during the AvrRpm1:RPM1 interaction. This study emphasized the putative phosphorylation-dependent regulation of AtRem 1.2 in response to pathogen attack.

StRem 1.3 (P93788)



AtRem 1.2 (Q9M2D8)



AtRem 1.3 (O80837)

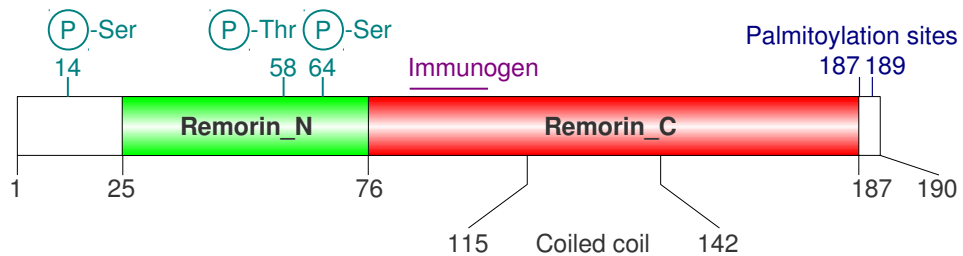


Figure 1.10.: **Protein structure of the remorin proteins StRem 1.3 & AtRem 1.2 / 1.3.**

Depicted remorins display a strong proline-rich N-terminus and coiled-coil oligomerization domains at the C-terminus as they all belong to the remorins of group 1b (Raffaele *et al.*, 2007). *A.th.* remorins feature putative palmitoylation sites at their C-terminus. The immunizing peptide for the production of custom antibodies is marked as "Immunogen" (see 2.11, p. 56 for details).

¹⁷RPM1: resistance to *Pseudomonas syringae* pv. *maculicola* 1

Besides their role in plant-pathogen interactions, the involvement of remorin proteins in *Medicago truncatula* (*M.t.*) rhizobia symbiosis has recently been postulated (Lefebvre *et al.*, 2010). A specific remorin in *M.t.* was strongly (1000-fold) induced upon bacterial infection and spatially limited to nodules, thus the authors named this protein MtSYMREM1 (*Medicago truncatula* symbiotic remorin 1). MtSYMREM1 was shown to oligomerize at the host PM surrounding the bacteria and facilitating the release of rhizobia into the host cytoplasm. Interactions of MtSYMREM1 with receptor-like protein kinases (RLKs) involved in the signal perception of bacterial molecules could be visualized by bi-molecular fluorescence complementation (BiFC). Lack of MtSYMREM1 abolished the symbiosis between *M.t.* and the symbiont *Sinorhizobium meliloti* indicating that MtSYMREM1 might organize the plant-microbe synergy.

The remorin family is grouped into different clades according to the protein length and composition of N- / C-termini (Raffaele *et al.*, 2007). Most prominent AtRem 1.2 / 1.3 and StRem 1.3 belong to the group 1b (see figure 1.10). These three remorin proteins are expressed throughout the plant with their highest expression level present in leaves (Raffaele *et al.*, 2007). StRem 1.3 expression studies highlighted an increased remorin protein level in mature & aging tissues and in the source parts of the leaves, coinciding with mature and branched plasmodesmata (Raffaele *et al.*, 2009b).

AtRem 1.2 / 1.3 are always present in proteomic analyses of *A.th.* (Kierszniowska *et al.*, 2008; Minami *et al.*, 2009; Shahollari *et al.*, 2004) due to their high expression level throughout the whole plant (Raffaele *et al.*, 2007). MCD treatment depleted AtRem 1.2 / 1.3 from DRMs in *A.th.* cell cultures (Kierszniowska *et al.*, 2008) and *A.th.* leaves (the study herein): it is therefore tempting to promote AtRem 1.2 / 1.3 as model DRM / lipid raft proteins for *A.th.*

Physiological relevance of the *A.th.* remorins has not been demonstrated yet, but there is evidence for their involvement in drought stress regulation on the level of stomatal opening: AtRem 1.2 is member of a RIN4 complex regulating PM-ATPase activity in response to pathogen attack as detected via mass-spectrometric techniques (Liu *et al.*, 2009a). In addition to the microarray data (Bray, 2002; Journot-Catalino *et al.*, 2006), biochemical investigations indicate a very important role for the remorin protein family. These studies pinpoint that remorins are regulated by plant hormones and seem to be involved in the plant response to pathogens and, most importantly, strictly localized into membrane domains at the PM.

1.3 AIMS OF THE STUDY

The *Arabidopsis thaliana* system always gathered much interest as a model-organism for plant biology – nevertheless no proteomic analysis of leaf DRM proteins had been performed yet. Leaves have a central role in regulating the drought stress response in plants: control of stomatal opening / closure and transpiration is conducted herein. Many proteins take part in the control of the plant's water status: signaling proteins (members of the CPK family), ion channels (SLAC1 / SLAH family) and proton transporters. It was therefore tempting to investigate the proteomic composition of DRMs from *A.th.* leaves (mainly consisting of mesophyll cells). The usage of different non-ionic detergents like Brij-98 and Triton X-100 should clarify if the protein composition of *A.th.* DRMs depends upon the detergent used for the isolation of DRMs. Different digestion approaches (standard in-gel procedure in addition to in-solution tryptic digest) were applied to add a further layer of proteomic data. After the establishment of a proteomic data set, further investigations were performed to identify putative lipid raft proteins among the DRM proteins.

An investigative approach to test the localization of certain proteins in membrane domains was the application of the sterol-depleting reagent methyl- β -D-cyclodextrin (MCD). As lipid raft proteins are supposed to be strongly dependent upon a sterol-enriched microenvironment, MCD removal of sterols should result in a substantially different DRM protein composition. Thus, a sterol-depletion of Triton X-100 isolated DRMs minimizes the set of DRM proteins to a "core" set of candidate proteins which would be strongly depending upon sterols. Identifying important signaling components for the regulation of drought stress adaptation in *A.th.* leaf mesophyll DRMs was the central aim of this work. No investigation of Triton X-100 DRMs in *A.th.* leaves was performed up to now, also the usage of another non-ionic detergent like Brij-98 was novel.

The identification of a central signaling protein involved in drought stress regulation, CPK21, led to the discovery of a lipid raft-resident ABA-regulated protein complex consisting of the protein kinase CPK21, protein phosphatase 2C ABI1 and anion channel SLAH3. CPK21 as a raft-resident member of this complex has been investigated with biochemical and mass spectrometric methods for strict sterol dependency. Localizing the ABI1-dependent protein complex through transient expression in *Nicotiana benthamiana* should help to clarify two questions: (I) Does CPK21 build a protein complex with the anion channel SLAH3 located in lipid rafts? (II) Is this protein complex affected by addition of the protein phosphatase 2C ABI1?

2

Methods

2.1 MEMBRANE ISOLATION

2.1.1. Plant cultivation

A.th. ecotype Columbia-0 were grown at 22 °C on soil under a short-day light regime (8 hours light / 16 hours darkness) with a photon-flux of 200 μ E and a relative humidity of 50 %. Plants were harvested after 6-8 weeks when leaves were grown to full size.

2.1.2. Homogenization of plant material

Leaves including petioles were homogenized using a Waring Blender (Waring Laboratory & Science Inc., Torrington, USA) with appropriate amounts of homogenates buffer (HB) and polyvinylpolypyrrolidone (50 g chunks of leaves were blandered using 100 mL of HB + 4 g of PVPP). 10 pulses of 20 seconds were performed for homogenization of the plant material until no big chunks of plant leaves were visible. To avoid protease activity, complete, **EDTA-free** protease inhibitor cocktail tablets (Roche Applied Biosciences, Mannheim, D) were used in minute amounts.

Ingredient	Final concentration	For 1 L
Sucrose	330 mM	112.9 g
1 M Tris-HCl pH 7.4	50 mM	50 mL
0,5 M EDTA pH 8	3 mM	6 mL
DTT (fresh)	1 mM	0.154 g

additionally: fresh 4 % w/v PVPP powder

Table 2.1.: Homogenization buffer

CHAPTER 2. METHODS

The homogenates was filtered through Miracloth membranes (Merck Bioscience, Darmstadt, D) to avoid non-homogenized clumps. Cleared homogenates were subjected to isolation of the microsomal endomembranes fraction.

2.1.3. Isolation of microsomal fraction

A low speed centrifugation of 15 000 g force units in average (g_{av}) / 9 207 rpm was performed for 31 minutes in a JA-10 rotor / Avanti-XP centrifuge (Beckman Coulter, Krefeld, D) at 4 °C. After centrifugation cell wall components, nuclei, cell debris, mitochondria and partly chloroplasts were pelleted and removed from the microsomal fraction.

The supernatant was filtered through Miracloth membranes and centrifuged 1 h at 4 °C, 100 000 g_{av} / 36 000 rounds per minute (rpm) in a Beckman Coulter 45Ti rotor / Optima-L 100 K ultra centrifuge. Pellets containing the microsomal fraction were re-suspended in two rounds of 4 milliliter (mL) two-phase buffer (TPB), supplied with the corresponding amounts of complete Protease inhibitor cocktail tablet (**EDTA-free**) and homogenized in a potter membrane homogenizator (Sartorius, Göttingen, D). Homogenized microsomal fractions were further purified to PM or stored frozen at -20 °C.

Ingredient	Final concentration	For 100 mL
43 % w/w Sucrose	9.5 %	22 mL
2 M KCl	6 mM	300 μ L
0,2 M K^+P_i pH 7.8	5 mM	2.5 mL
Complete protease inhibitor cocktail		

Table 2.2.: Two-phase buffer

2.1.4. Plasma membrane isolation

Aqueous two-phase partitioning (see Yoshida *et al.* (1983) and Larsson (1988) for reviews) yielded highly pure PM preparations from microsomal endomembranes fractions. Using the different miscibility of membrane fractions in the two used polymers the PM was purified in the upper polyethylene glycol 3350 phase.

A maximum of 5 g microsomal endomembranes fraction was loaded on 27 g two-phase partitioning systems with a 6.5 % w/w PEG-3350 / dextran T-500, 5 mM K^+P_i pH 7.8 and 6 mM KCl constitution – the first system was re-partitioned with a fresh upper phase to recover the majority of the lost PM vesicles¹. Overloading the first two-phase partitioning

¹A major loss of PM vesicles occurs at the first partitioning, see Mitra *et al.* (2009) for details.

2.1. MEMBRANE ISOLATION

system with a too high content of microsomal fraction (>50 mg of protein) resulted in a saturation of the separating systems and a loss of PM at the end.

Two separate system compositions were used: a more stringent 6.5 % PEG-3350 / Dextran T-500, 6 mM KCl system which yields much purer PM preparations at the cost of very less protein – the other isolation setup with 6.4 % PEG-3350 / Dextran T-500, 3 mM KCl retrieved much more PM protein (approx. $\frac{1}{3}$ more) but these isolations were more contaminated with chloroplastic traces. The *stringent* 6.5 % PEG-3350 / Dextran T-500, 6 mM KCl system was used for mass spectrometric identification approaches and accordingly for western blot assays and lipid determinations.

PM isolations performed on mutant plant lines were purified using the more *relaxed* 6.4 % PEG-3350 / Dextran T-500, 3 mM KCl setup.

	6.5 % PEG / Dextran	6.4 % PEG / Dextran
20 % w/w Dextran T-500	11.7 g	11.34 g
40 % w/w PEG-3350	5.85 g	5.67 g
43 % w/w Sucrose	5.94 mL	5.94 mL
2 M KCl	82 μ L (6 mM)	41 μ L (3 mM)
0.2 M K ⁺ P _i pH 7.8	675 μ L	
H ₂ O	ad 27 g	

Table 2.3.: Configuration of the two-phase partitioning systems

Each isolation of PM was done in 2 rounds of 3 purification steps where the first extracted upper PEG-3350 phase containing the PM was subsequently purified with the help of two further prepared systems. The normally discarded first lower Dextran T-500 phase was re-extracted with 2 further systems to recover the majority of the PM occurring during the first two-phase partitioning. Final PEG-3350 phases containing the purified PM were diluted at least two-fold with two-phase buffer (TPB) before centrifugation at 4 °C, 100 000 g_{av} for 1 hours (h).

Further purification of the PM was performed with an alkaline lysis of the PM vesicles by 0.1 M sodiumcarbonate for 15 min. on ice followed by an ultra centrifugation at 100 000 g_{av} , 4 °C for 1 h. Re-suspending the resulting pellet in an appropriate volume of Tris-DTT buffer (50 mM Tris pH 8, 1 mM DTT freshly added and protease inhibitor cocktails), the PM is ready for further applications. Typically 0.6 mg PM vesicles were prepared from approx. 80 g of fresh leaves – freshly prepared microsomal fractions led to a higher PM recovery after the two-phase partitioning.

2.1.5. DRM isolation

Isolation of DRMs was performed via continuous sucrose gradient density ultra centrifugation after detergent treatment / sterol depletion. According to the nature of DRMs containing high amounts of sterols and sphingolipids, the floating density of DRMs was altered in sucrose gradient density ultra centrifugation. DRMs were obtained as a gray opaque band at a sucrose concentration of around 30 %. Proteins which were not resistant to detergent treatment remained at the bottom of the sucrose gradient and were visible as a pellet fraction (DSF).

2.1.5.1. Sterol depletion by MCD

Sterol depletion was achieved by 25 mM MCD treatment at 37 °C for 30 minutes under continuous shaking. Ultra centrifugation (100 000 g_{av} at 4 °C for 1 h in a Beckman-Coulter TLA-55 rotor) separated sterol-depleted PM in shape of a gray-yellow pellet from the sterol-containing supernatant. Sterol-depleted and non-treated PM were subjected to detergent-treatment.

2.1.5.2. Detergent-treatment

Treating PM with the non-ionic and mild detergents Triton X-100 or Brij-98 enabled the isolation of DRMs – all steps were taken out on ice. 1 mg of purified PM were homogenized freshly in a tissue homogenizator and brought to such a volume that the final detergent concentration was 1 % v/v for each of the detergents (Brij-98 solutions need heating over a long time to dissolve and keep stable for just 1-2 days). Ideally the detergent to protein ratio should be 15 : 1 (15 mg detergent, e.g. 150 μ L 10 % v/v Triton X-100 : 1 mg protein) to gain the maximum enrichment of sterols without losing too much protein (Mongrand *et al.*, 2004).

After detergent addition, the sample was incubated for **exactly** 30 min on ice: longer incubation led to a non-specific protein solubilization by the detergent. This has proven to prevent the isolation of any specific membrane fractions such as DRMs (Morandat & El Kirat, 2006).

Finally 60 % w/v sucrose was added to the detergent-treated sample to yield a 48 % w/v sucrose concentration, e.g. detergent-solubilization assay volume: 1200 μ L, 4800 μ L of 60 % w/v sucrose was applied. The mixture was put into the Beckman-Coulter polycarbonate ultra centrifugation tube before laying the sucrose gradient on top of the sample.

2.1.5.3. Sucrose density centrifugation

Isolation of the DRMs was achieved by continuous sucrose density centrifugation in a swing-out Beckman-Coulter SW 32 Ti rotor / Beckman-Coulter Optima-L 100 K ultra centrifuge at 100 000 g_{av} (28 500 rpm), 4 °C for 18 hours. The continuous sucrose gradient was poured with a gradient mixing chamber containing 2 chambers each of approx. 15 mL volume – one chamber for the low (15 % w/v) and another chamber for the high (45 % w/v) sucrose solutions used to build up the gradient. Under continuous stirring the sucrose solutions were mixing in a concentration dependent manner building up a continuous sucrose gradient from 45 % to 15 % w/v sucrose upon the sample.

After ultra centrifugation a gray to white opaque band was occurring in the middle of the sucrose gradient showing the floating DRMs ("lipid rafts"). If >1 mg of PM proteins were loaded onto the gradient a small pellet might be seen at the bottom of the gradient where the majority of the proteins shall reside after being solubilized by Triton X-100 or Brij-98 treatment.

2.1.5.4. Fractionation of the sucrose gradient

Fractions of the sucrose gradient were taken in 1.5 mL volumes beginning from the top. Each fraction was tested for sucrose (refractometer) and protein concentration (microplate BCA assay) to determine additional information where the opaque band containing DRMs is located. Upon characterization of the protein distribution in exemplary sucrose gradient, three pools were observed of the sucrose gradient fractions:

1. Top pool: all fractions from the top of the gradient
2. DRMs pool: 3-4 fractions containing the opaque band (approx. 30-36 % w/v sucrose)
3. DSF pool: all fractions below the opaque DRM band (majority of the protein)

Half of each pool was precipitated via TCA / acetone precipitation and again subjected to protein determination before being loaded onto polyacrylamide gels to perform western blots or visual staining protocols of the DRM proteins.

2.1.5.5. Preparation of DRM samples for mass spectrometry

Samples to be analyzed via mass spectrometry were solubilized directly in 2x SDS sample buffer containing DTT and handled like described in 2.3.1.2.

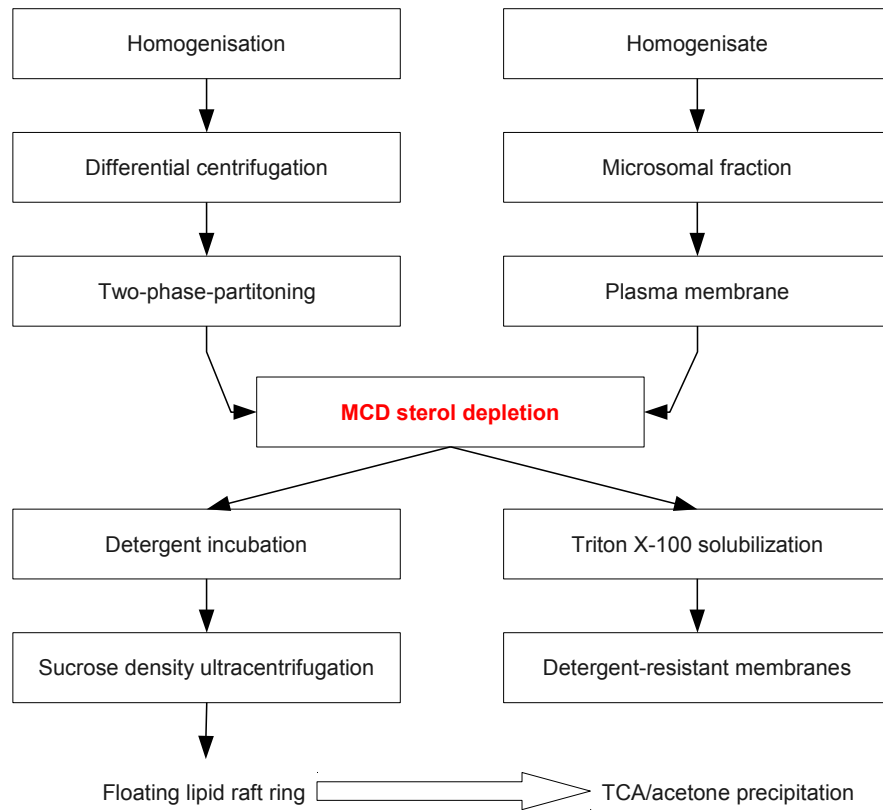


Figure 2.1.: Overview of the DRM isolation procedure

2.2 PROTEIN BIOCHEMISTRY

2.2.1. Gel electrophoresis

2.2.1.1. Sample preparation

Samples were mixed with 6x SDS sample buffer containing (modified from Laemmli, 1970) DTT for reducing gel electrophoresis (or without DTT for non-denaturing protein complex analysis), incubated over night (o/n) at 15 °C with gentle agitation, then incubated at 37 °C for 60 min and finally boiled for 6 min. at 95 °C to denature the proteins. After cooling the samples at room temperature (RT), a brief centrifugation was carried out to remove any debris and the resulting supernatant was applied onto the gel.

2.2. PROTEIN BIOCHEMISTRY

Ingredient	Concentration
Tris-HCl pH 6.8, 0.4 % SDS	0.3 M
Bromphenolblue	0.02 %
Glycerol	37 %
SDS	10 %
optionally: 0.2 M DTT	

Table 2.4.: 6x SDS sample buffer

2.2.1.2. SDS-PAGE

Discontinuous SDS-PAGE was used for protein separation & identification according to Laemmli (1970).

Manually poured gels were composed like detailed below; separation gel was covered with H₂O and allowed to polymerize for 30 minutes. Afterward the water was drained off and the separation gel was overlaid with the stacking gel. Here a 15 minutes polymerization was accomplished.

	8 %	10 %	12 %
H ₂ O	5.4 mL	4.9 mL	4.4 mL
4x Tris-HCl/SDS, pH 8.8 (1.5 M Tris-HCl; 0.4 % SDS)	2.5 mL	2.5 mL	2.5 mL
Rotigel polyacrylamide stock	2 mL	2.5 mL	3 mL
10 % (NH ₄) ₂ S ₂ O ₈ (APS)	50 µL	50 µL	50 µL
TEMED	5 µL	5 µL	5 µL

Table 2.5.: Separation gel composition (10 mL)

	Amount
H ₂ O	6.6 mL
4x Tris-HCl/SDS, pH 6.8 (0.5 M Tris-HCl; 0.4 % SDS)	2.5 mL
Rotigel polyacrylamide stock	0.8 mL
10 % (NH ₄) ₂ S ₂ O ₈ APS	100 µL
TEMED	10 µL

Table 2.6.: Stacking gel composition (10 mL)

Custom-made protein gels were run at 10 mA / gel for 15 minutes and at 25 mA / gel for 45 further minutes until the bromphenol blue band leaves the gel.

Alternatively 8-16 % Pierce Precise Protein Gels (Thermo Fisher Scientific, Bonn, D) were used with a polyacrylamide gradient 8 - 16 % which allowed a better separation of protein bands. These gels were constantly run with 90 V for 90 minutes at 4 °C in the cold room to achieve best resolution for the protein bands (avoiding diffusion based migration which can occur at room temperature).

Gels were washed 3 × 5 minutes with Millipore H₂O to remove residual SDS from the running buffer as it can interfere with subsequent western blot transfer and / or staining techniques.

2.2.1.3. Gel visualization

Gels were favorably stained via Coomassie Brilliant Blue staining (Imperial Blue staining by Pierce [Thermo Fisher Scientific, Bonn, D]) for 2 hours and subsequently destained with Millipore H₂O until no background staining of the gel was visible. Alternatively a convenient silver staining was performed to obtain low abundance protein signals according to Blum *et al.* (1987).

Unfortunately, the silver staining highly depends on the amino acid sequence of the proteins visualized: proteins missing ionic amino acids may not be visible at all (Nielsen & Brown, 1984). Syrový & Hodný (1991) suggested that Coomassie Brilliant Blue G-250 stainings provide more accurate protein visualization. Thus, Coomassie Brilliant Blue stainings were used to for gels containing samples for mass-spectrometric analysis.

2.2.2. Western blot

2.2.2.1. Transfer

Western blotting was usually done with a isotachoelectrophoresis 3 buffer system according to (Kyhse-Andersen, 1984) to obtain greater molecular weight and hydrophobic proteins whereas detection of soluble proteins could be carried out with a single transfer buffer system.

Transfer onto a Hybond-P Polyvinylidene fluoride (PVDF) membrane (GE Healthcare Europe, Munich, D) was accomplished in 1 h at 70 mA / 4 °C conditions for self-made protein gels – pre-cast gels were transferred for **1 h at 20 V / 100 mA / 4 °C** or alternatively 50 min. at 20 V / 100 mA / RT according to their smaller gel area.

After gel electrophoresis, the PVDF membrane is moisturized using 100 % methanol for 1 min then washed with Millipore purified H₂O (H₂O MQ) for 5 min and incubated in the corresponding transfer buffer (anode buffer 2) for at least 20 min at RT to wash off any bound SDS from the gel. Whatman paper was also put for at least 5 min into the corresponding transfer buffer before assembling the western blot "sandwich". The western blot "sandwich" was structured like this:

- Cathode (-)
- 3 sheets of Whatman paper in cathode buffer
- PVDF membrane
- Polyacrylamide gel
- 2 sheets of Whatman paper in anode buffer 2
- 3 sheets of Whatman paper in anode buffer 1
- **Anode (+)**

Following the transfer of proteins a blocking step is necessary to saturate the unbound binding capacity of the polyvinylidene fluoride (PVDF) or Nitrocellulose (NC). Several alternative blocking approaches are possible, but the mostly used blocking buffers contain either 5 % non-fat dry milk or 3 % bovine serum albumin (BSA) in PBS supplied with 0.05 % Tween-20 (PBS-T) / TBS supplied with 0.05 % Tween-20 (TBS-T). BSA is indicated when the usage of phospho-specific antibodies are planned since non-fat dry milk masks signals due to the milk-intrinsic casein. In this work 3 % BSA in PBS-T / TBS-T was used for blocking of PVDF membranes.

2.2.2.2. Antibody detection

Immunodetection was performed using primary antibodies according to the overview table 2.11 for at least 1 h at RT with custom made antibodies from GenScript Inc. (GenScript Inc., Piscataway, USA) and/or commercially available antibodies from AgriSera (AgriSera AB, Uppsala, S) and Abcam (Abcam plc, Cambridge, UK). For samples containing very low amounts of antigen (e.g. DRMs with low protein amount), the primary antibody incubation was accomplished o/n. All used primary antibodies were raised in rabbits.

After incubation with primary antibody three consecutive washing steps (each 5 min) were carried out using Phosphate-buffered saline (PBS) or Tris-buffered saline (TBS) buffers supplied with 0.05 % Tween-20 (a mild non-ionic detergent to loosen weak interactions). For detection, the Horseradish peroxidase (HRP)-system was applied (α -rabbit primary antibody coupled to HRP raised in goats, supplied by Pierce) at dilutions of 1:20 000 - 1:35 000 for 1 h at RT. A standard dilution of 1:30 000 was applied for the secondary antibody.

A prolonged washing step of 15 min followed the secondary antibody incubation – after three additional washing steps (each 5 min) the HRP-detection was performed using highly sensitive HRP substrate ("SuperSignal West Pico" by Pierce) according to manufacturer's instructions (in brief: 5 min incubation in the dark of a 1:1 mixture of peroxide and luminol enhancer solutions).

Signal emission was imaged by sensitive X-ray Amersham Hyperfilm ECL from GE Healthcare. Exposure times of 1, 5 and 15 min were applied, longer exposure times up to o/n were performed where necessary.

2.2. PROTEIN BIOCHEMISTRY

	Concentration
Tris	0.125 M
Glycine	0.96 M
SDS	0.5 %
H ₂ O	ad 1000 mL

Table 2.7.: 5x Tris-Glycine SDS running buffer, pH 8.3

	Concentration	Amount
Tris	25 mM	3 g
Glycine	200 mM	14.4 g
Methanol	15 %	150 mL
H ₂ O		ad 1000 mL

Table 2.8.: Simple western blot transfer buffer, pH 8.4

	Cathode buffer	Anode buffer 1	Anode buffer 2
Tris	25 mM	300 mM	25 mM
ϵ -Aminocaproic acid	40 mM	-	-
Methanol	20 %	20 %	20 %
Final pH	7.6	10.4	10.4

Table 2.9.: Three buffer western blot transfer system

	TBS	PBS
Tris	50 mM	-
NaCl	150 mM	13.7 mM
KCl	-	0.27 mM
Na ₂ HPO ₄	-	10 mM
KH ₂ PO ₄	-	0.2 mM
Final pH	7.4	7.4

Table 2.10.: PBS / TBS buffers for immunological assays

Table 2.11.: Antibodies used in investigation

Target protein	Target compartment	Supplier	Product no.	LOT no.	Source	Type	Dilution [¶]
AtRem 1.2 / 1.3	PM / Lipid rafts	GenScript*	Custom (78120.1)	78120002090409ZW	Rabbit	Polyclonal affinity-purified	1 µg / mL
AtLipocalin	PM	GenScript*	Custom (78120.4)	78120005090409WJ	Rabbit	Polyclonal affinity-purified	1 µg / mL
V-type ATPase	Tonoplast	Agrisera [†]	AS07 213	0707	Rabbit	Polyclonal serum	1:1 000
P-type ATPase	PM	Agrisera [†]	AS07 260	0805	Rabbit	Polyclonal serum	1:1 000
RNA pol I	Nucleus	Agrisera [†]	AS07 225	0707	Rabbit	Polyclonal affinity-purified	1:1 000
UGPase	Cytoplasm	Agrisera [†]	AS05 086	0801	Rabbit	Polyclonal serum	1:1 000
Sec21p	Golgi	Agrisera [†]	AS08 327	0807	Rabbit	Polyclonal serum	1:1 000
Sar1	ER	Agrisera [†]	AS08 326	0807	Rabbit	Polyclonal serum	1:1 000
VDAC1	Mitochondria	Agrisera [†]	AS07 212	0903	Rabbit	Polyclonal affinity-purified	1:1 000
Toc75	Chloroplast outer env.	Agrisera [†]	AS06 150	0704	Rabbit	Polyclonal serum	1:1 000
RbcL	Chloroplast stroma	Agrisera [†]	AS03 037-10	0907	Rabbit	Polyclonal affinity-purified	1:10 000
AtPDR8 (PEN3)	PM / Lipid rafts	Agrisera [†]	AS09 471	0910	Rabbit	Polyclonal serum	1:1 000
GFP	GFP	Abcam [‡]	ab6556-25	758496	Rabbit	Polyclonal affinity-purified	1:2 500
V5	V5	Invitrogen [§]	R960-25		Mouse	Monoclonal affinity-purified	1:5 000

[¶]Dilution used for immunoblot detection via ECL

[‡]Abcam plc, Cambridge, UK

[†]Agrisera AB, Vännäs, S

*GenScript Inc, Piscataway, USA

[§]Invitrogen GmbH, Darmstadt, D

^{||}Final working concentration 0.2 µg / mL

2.2.3. Protein quantification

Proteins in solution were quantified in macroscale via Roti Nanoquant (a Coomassie Brilliant Plus-based assay, Bradford, 1976), according to the manufacturer's instructions (Carl Roth, Karlsruhe, D). Quantification of minute samples was done with the Pierce BCA protein assay kit (Thermo Fisher Scientific, Bonn, D) microplate protocol which is based on the biconchic acid detection technique (Smith *et al.*, 1985). A working reagent : sample ratio of 10 : 1 was used (250 μ L BCA working reagent + 25 μ L unknown sample) for microplate assays. In general the BCA protein determination allowed a more exact quantification of microsomal fraction and PM proteins. Corresponding BSA samples ranging from 0 – 500 μ g / mL protein should be run in at least duplicates along with the sample measurements to guarantee identical conditions. Upon each measurement, a fresh linear fit BSA calibration was performed by which the protein concentration was calculated.

Microplate BCA assay was incubated in a 37 °C incubator for 30 minutes and allowed to cool down to RT before being measured.

Fraction	Dilution in microplate assay	Dilution in macro assay
Homogenate	1 : 40	1 : 40
Microsomal fraction	1 : 40	1 : 40
PM	1 : 10	1 : 10
DRM fraction	1 : 2.5	1 : 5

Table 2.12.: Usual dilutions for protein quantification

Microplate measurements of protein content were done in a Thermo Fisher Scientific Luminoskan (Thermo Fisher Scientific, Dreieich, D) plate reader with a 571 nm filter for the BCA assay and a 571 / 490 nm filter set for the Bradford protein assay.

2.2.4. Precipitation methods

Different precipitation methods were used to purify proteins from a heterogeneous mixture of sugars, lipids and other contaminants (e.g. DRMs fractions). The fastest method to precipitate and isolate proteins from solution was the chloroform / methanol extraction which can be done in 10 minutes, but was limited to a maximum volume of 200 μ L for the sample being purified.

A more gentle precipitation method was applied to purify PM fractions before DRM isolation: the alkaline sodiumcarbonate treatment according to (Fujiki *et al.*, 1982) eliminated big proportions of soluble proteins from the PM vesicles by alkaline PM vesicle disruption.

For bigger volumes a combined approach with trichloroacetic acid (TCA) and acetone is used which also recovers much more protein (Cabib & Polacheck, 1984; Sivaraman *et al.*, 1997). Alternatively a Wang precipitation (2.2.4.4) can be performed which is also based upon TCA / acetone.

2.2.4.1. TCA / Acetone precipitation

TCA (working solution: 100 % freshly prepared by weighing 1 g TCA into 430 μ L H₂O supplied with 1 mM DTT) was added to a final concentration of 10 % v/v to the sample and incubated on ice for at least 2 h (for improved protein precipitation: o/n, Sivaraman *et al.*, 1997) followed by a centrifugation at 20 000 g_{av} at 4 °C for $\frac{1}{2}$ hour. Samples derived from DRM isolations were washed once more with a 10 % TCA v/v in H₂O solution, incubated on ice for 1 h followed by a centrifugation at 20 000 g_{av} at 4 °C for $\frac{1}{2}$ hour. This additional TCA washing step helped to remove the residual sugar which is a major contaminant of protein samples derived from sucrose density gradients. Xu *et al.* (2003) revealed that TCA precipitation denatured proteins by reinforcing molten globule changes. Washing of the produced pellet was performed twice with 500 - 1000 μ L of ice-cold 100 % acetone, vortexed, incubated shortly on ice and centrifuged again at 20 000 g_{av}, 4 °C for 15 min.

The final TCA / acetone pellet was re-suspended directly in 1x SDS sample buffer containing DTT – if the color of the sample was not blue, 1-5 μ L of 1 M Tris pH 8 were added until the pH indicator bromphenolblue shows a blue color in the sample. Alternatively the TCA / acetone pellet might be re-suspended in a Tris-DTT buffer (50 mM Tris, 1 mM DTT, pH 7.4) complemented with protease inhibitor cocktails.

2.2.4.2. Chloroform / Methanol precipitation

The chloroform (CHCl₃) / methanol precipitation was a versatile technique to isolate membrane bound proteins via hydrophobic / hydrophilic interactions Wessel & Flügge (1984) - Ferro *et al.* (2000) used this approach to isolate chloroplast envelope proteins. Starting with an aqueous protein solution of 100 / 200 μ L volume, 4 volumes methanol were added, samples vortexed, 1 volume of chloroform added, samples again being vortexed and after the addition of another 3 volumes of H₂O the sample was vigorously vortexed yielding a milky white solution indicating the presence of proteins.

After a 3 min. centrifugation at 14 000 g_{av} at RT an interphase containing white protein flakes was visible – the chloroform supernatant containing lipids and sugars was discarded and another 4 volumes (in respect to the original starting sample volume) of methanol were added upon vortexing. Subsequently another 3 min. centrifugation at 14 000 g_{av} (RT)

resulted in a small bright protein pellet which was air-dried for several minutes before being re-suspended in the buffer of choice.

Other combinations of chloroform / methanol might be used for isolation of more hydrophobic proteins (e.g. 6 chloroform / 3 methanol) but the general procedure remained the same (Ferro *et al.*, 2000; Vertommen *et al.*, 2010). Different ratios of chloroform / methanol did not lead to a more successful precipitation of PM proteins.

2.2.4.3. Sodiumcarbonate precipitation

Solutions were combined with ice-cold, freshly prepared 0.2 M sodiumcarbonate (Na_2CO_3), pH 11 supplied with protease inhibitor tablets and incubated at 4 °C for 15 min. If existing pellets should be purified by this technique, only 200 μL of 0.1 M sodiumcarbonate, pH 11 were sufficient to proceed further. Following an ultra centrifugation at 100 000 g_{av} , 4 °C for an hour (47 000 rpm with a Beckman-Coulter TLA-55 rotor in a Beckman-Coulter Optima XP micro ultra centrifuge) the membrane fraction appeared as a cloudy yellow-to-green pellet – carefully all of the supernatant was removed. Re-suspension of the pellet in an appropriate buffer should be accompanied by an homogenization in a potter to produce an evenly distributed protein solution.

2.2.4.4. Wang precipitation

Samples were mixed with 10 % TCA in ice-cold acetone, vortexed and centrifuged for 3 min. at 14 000 g_{av} in the cold. Washing of the pellet was done with 0.1 M ammoniumacetate ($\text{NH}_4\text{C}_2\text{O}_2\text{H}$) in 80 % methanol and afterward with 80 % acetone. After air-drying of the sample a 1 : 1 mixture of phenol pH 8 and sds buffer (30 % sucrose, 2 % SDS, 0.1 M Tris pH 8, freshly supplied with 5 % β -mercaptoethanol) was applied and centrifuged for 5 min. at 14 000 g_{av} at RT.

The upper phase was precipitated for at least 2 hours (better: over night) with 0.1 M ammoniumacetate in 80 % methanol at - 20 °C and pelleted for 3 min. at 14 000 g_{av} in the cold. Subsequent washes with ice-cold 100 % methanol and 80 % acetone led to a pellet suitable for two-dimensional gel electrophoresis (Hurkman & Tanaka, 1986; Wang *et al.*, 2003).

2.3 MASS SPECTROMETRY

2.3.1. Sample preparation

2.3.1.1. Trypsin

A complete Trypsin/P (Promega Inc, USA) package was re-suspended in 1 mL of 1 mM HCl and aliquoted into 25 μ L fractions. Each trypsin aliquot was mixed with 175 μ L washing buffer A yielding a 12.5 ng / μ L trypsin solution.

2.3.1.2. In-gel digestion

Samples to be digested in-gel were pelleted via 0.1 M Na_2CO_3 precipitation, obtained pellets were incubated in 2x SDS sample buffer over night at 15 °C with soft agitation. Upon SDS gel electrophoresis the samples were diluted to 1x SDS sample buffer and run on pre-cast Pierce gradient gels 8 - 16 % (Thermo Fisher Science, Bonn, D) at 100 volt (V) for 1 h.

Gels were washed twice with H_2O to remove excess SDS and subsequently the very sensitive Coomassie Blue based staining "Imperial Blue" by Pierce (Thermo Fisher Science, Bonn, D) was performed. After staining the gel lane was cut into 37 - 54 pieces depending on the complexity of the stained samples. Gel pieces were dried under vacuum at 60 °C and frozen at - 80 °C until further analysis or directly washed.

Trypsin digested the proteins in the gel pieces at least for 4 h, mostly over night (o/n) at 37 °C with 8 μ L of Trypsin working solution (100 ng / gel piece).

2.3.1.3. Washing of gel pieces

Two alternating washes of each 100 μ L buffer A 50 mM ammonium bicarbonate (NH_4HCO_3) and 100 μ L 25 mM ammonium bicarbonate in 50 % Acetonitrile (MeCN) were followed by a reduction (100 μ L 10 mM dithiothreitol at 56 °C) / alkylation (100 μ L 5 mM iodoacetamide at RT in the dark) to provide carbamidomethylated cysteines (improves the efficiency of the tryptic digest). Subsequently two washes with buffer A / B were accompanied by a vacuum drying at 60 °C.

2.3.1.4. In-solution digestion

Dimethylsulfoxide (DMSO)-assisted in-solution digestion provided an alternative to in-gel digestion after gel electrophoresis – some proteins being problematic in SDS-PAGE due to their very polar / hydrophobic structure could be resolved via tryptic digestion in solution.

2.3. MASS SPECTROMETRY

	Buffer A	Buffer B	Reduction buffer	Alkylation buffer
NH ₄ HCO ₃	50 mM (0.2 g)	25 mM	50 mM	50 mM
DTT	-	-	10 mM (0.077 g)	-
IAA	-	-	-	5 mM (0.057 g)
Acetonitrile	-	50 %	-	-
	ad 50 mL			

Table 2.13.: Washing buffers MS analysis of gel pieces

The starting point for an in-solution digestion was a vacuum dried membrane fraction which was re-suspended in 40 μ L of 60 % DMSO v/v in 50 mM ammonium bicarbonate. After a brief centrifugation and very profound pipetting to resolve the membranes in the organic solvent DMSO, 4 μ L of a 200 mM DTT solution in 50 mM NH₄HCO₃ were added and incubated for 1 h at 37 °C under vigorous shaking.

	Re-suspension buffer	Trypsin buffer A	Trypsin buffer B
DMSO	60 %	-	-
NH ₄ HCO ₃	50 mM	100 mM	50 mM
Trypsin/P	-	25 ng / μ L	12.5 ng / μ L

Table 2.14.: Solvents used by in-solution digestion

After cooling of the samples to RT, 4 μ L of a 100 mM IAA solution in 50 mM ammonium bicarbonate were applied during shaking in the incubator for a further hour in the **dark**. To stop alkylation further 2 μ L of 200 mM DTT were added to fix excessive IAA at 37 °C for 20 min.

The tryptic digest was started with 40 μ L of trypsin buffer A for at least 4 hours (alternatively: over night). Addition of 1 μ L 0.5 M CaCl₂ improved the tryptic digestion efficiency according to (Shevchenko *et al.*, 1997). Incubation with trypsin was accomplished at 37 °C in an shaking thermomixer.

1st tryptic digest

A second tryptic digestion was started with the addition of 20 μ L trypsin buffer B for at least 4 hours at 37 °C or, alternatively, over night. One the tryptic digests could be done for 4 hours if the other digestion step is performed over night to ensure complete tryptic digestion in the organic solvent DMSO.

2nd tryptic digest

Following tryptic digestion the sample was vacuum dried at 60 °C for approx. 45 min to evaporate DMSO and all volatile buffers like ammonium bicarbonate. Deep-freezing of the sample in liquid N and storage at - 80 °C was possible without any protein loss.

CHAPTER 2. METHODS

Re-suspending the dried in-solution digest in 40 μ L of in-solution digestion solvent A was followed by a microcon centrifugation cleanup for 30 min at 14 000 g_{av} RT with a microcon cutoff size of 10 kDa (all digested peptides were smaller and should pass the filtration membrane). The filtrate was subjected to strong cation exchange chromatography on a 300 μ m inner diameter, 15 cm custom PL-SCX column (particle size: 5 μ m, pore size: 1000 \AA ; Polymer Laboratories, Darmstadt, D) with a flow rate of 1.7 mL / min for 50 min. A binary gradient of 5 to 95 % solvent B was run with a starting phase of 5 min with 5 % solvent B and 95 % solvent A was hold for 2 min – followed by an inversion to 5 % solvent B and 95 % solvent A for the equilibration of the column for the next fraction.

After the first 5 min retention phase a fraction was captured every minute, vacuum dried at 60 $^{\circ}$ C and stored frozen at - 20 $^{\circ}$ C. Every fraction was solubilized in 20 μ L 5 % formic acid (FA) and subsequently applied to RP (Reversed Phase) chromatography.

	In-solution digestion solvent A	In-solution digestion solvent B
KH_2PO_4	20 mM	20 mM
NaCl	-	0.25 M
Acetonitrile ²	-	25 %
pH (per phosphoric acid)	3	5.5
	ad 1 L	

Table 2.15.: Solvents used by in-solution digestion

2.3.1.5. Formic acid Extraction

Extraction of the tryptically digested peptides was done with 50 μ L of a 5 % FA : acetonitrile (MeCN) solution, a RT incubation of 15 min; supernatants were taken off and evaporated down to approx. 5 μ L in MS glass vials (15 - 30 min). Adding 5 % FA up to 15 μ L in volume was the last step in FA extraction of peptides.

2.3.2. Data acquisition

2.3.2.1. Quantitative analysis via emPAI

Quantitative evaluation of protein abundance was performed via label-free emPAI quantification (Ishihama *et al.*, 2005, 2008). The emPAI methodology was based upon the presence of tryptically digested peptides in the sample with respect to the potentially observable number

of digested peptides. For easier handling of values, a logarithmic scale was applied to the protein abundance index (PAI) to gain emPAI values:

$$PAI = \frac{N_{\text{observed peptides}}}{N_{\text{observable peptides}}}$$

$$emPAI = 10^{PAI} - 1$$

With the help of the emPAI values, the molecular protein content and weight could be calculated according to these formulas:

$$Protein\ content\ (mol\ \%) = \frac{emPAI}{\sum emPAI} \times 100$$

$$Protein\ content\ (weight\ \%) = \frac{emPAI \times M_r}{\sum emPAI \times M_r} \times 100$$

2.3.2.2. Data acquisition

An Ultimate 3000 nano-high-performance liquid chromatography (HPLC) MS (Dionex, Idstein, Germany) was used for identification of proteins – 0.1 % trifluoroacetic acid (TFA) concentrated the samples on a 100 µm inner diameter, 2 cm C₁₈ column (nanoseparations, Nieuwkoop, Netherlands) with a flow rate of 8 µL / min. Peptides were separated on a 75 µm inner diameter, 15 cm C₁₈ PepMap column (Dionex, Idstein, Germany) with a flow rate of 300 µL / min using a 2 h binary gradient from 5 to 50 % solvent B (solvent A: 0.1 % FA; solvent B: 0.1 % FA, 84 % acetonitrile).

A LCQ DecaXP^{Plus} ion trap mass spectrometer (ThermoElectron, Dreieich, Germany) or Quad-TOF (Time Of Flight) QSTAR XL[®] (Applied Biosystems, Darmstadt, D) acquired repeatedly one full-MS and three / two tandem-MS spectra (ion trap / Quad-TOF) from the nano-HPLC separated samples. The tandem-MS spectra were recorded from the most intensive ions in the respective full MS scan.

	Solvent A	Solvent B
FA	0.1 %	0.1 %
Acetonitrile	-	84 %

Table 2.16.: Solvents used in nano-HPLC

2.3.2.3. Database search parameters

All tandem-MS result peak files from an ESI-QUAD-TOF / ESI nano-HPLC tandem mass spectrometry were run on a Mascot daemon using the Mascot algorithm (Version 2.2; Matrix Science Ltd., London, UK) with the TAIR v9 protein database, Trypsin/P as protease.

Allowed fixed modification was carbamidomethylation (C) and variable modifications were oxidized methionines (N) and pyroglutamic acid for N-terminal glutamic acids (pyro-Glu at N-term. Q). Peptide and fragment mass tolerance were set to ± 1.5 Da for the ion trap and ± 0.2 Da for the Quad-TOF, max. missed cleavages to 2 and only singly, doubly and triply charged ions were analyzed.

2.3.2.4. Data evaluation

After manual inspection proteins with more than 2 **uniquely** identified peptides were automatically approved – proteins yielding only 2 uniquely identified peptides were manually verified (selection criteria: ions score > 32). No single peptide match was considered. All critical entries near the significance threshold were manually controlled for inclusion in the data analysis. The overall false discovery rate (fdr) was below 5 %.

2.3.2.5. Protein data sources & lipidation predictors

Data about the identified proteins was gathered from the Uniprot consortium (<http://www.uniprot.org>, Jain *et al.*, 2009) and TAIR (<http://www.arabidopsis.org>, Swarbreck *et al.*, 2008) and supplied with additional hydropathicity data according to the grand average of hydropathicity (GRAVY) index (Kyte & Doolittle, 1982). Protein names and functions were manually curated according to publications, TAIR information and Uniprot annotations.

Lipidation motifs were assigned due to detailed investigations in publications and where no published information was available, computational prediction tools were used. Myristoylation motifs were queried on the plant myristoylation predictor available on <http://plantsp.genomics.purdue.edu/plantsp/html/myrist.html> (Podell & Gribskov, 2004). Putative GPI-anchor motifs were searched via http://mendel.imp.ac.at/gpi/gpi_server.html (Eisenhaber *et al.*, 1999).

S-acylated residues were predicted with the help of the computational prediction software Csspalm version 2.0.4 using low thresholds (<http://csspalm.biocuckoo.org/>, Ren *et al.*, 2008). Identification of prenylation motifs (farnesylation / geranylgeranylation) was performed with WoLF PSORT version 0.2 (<http://www.wolfpsort.org>, Horton *et al.*, 2007).

2.4 MOLECULAR BIOLOGY

2.4.1. Bacterial cultivation

Transformation and selection were performed on the chemically competent E.coli strain XL1 Blue MRF' with the following genotype $\Delta(mcrA)183 \Delta(mcrCB-hsdSMRmrr)173 endA1 supE44 thi-1 gyrA96 relA1 Lac$. Cultivation of bacteria was done in LB medium supplied with the corresponding antibiotic reagent each at a final concentration of 50 $\mu\text{g} / \text{mL}$ (ampicillin for pSat USER and kanamycin for pCambia USER vectors).

Ingredient	Amount
Trypton	10 g / L
Yeast extract	5 g / L
NaCl	10 g / L
	15 g / L Agar-Agar danish for Agar plates

Table 2.17.: LB medium

2.4.1.1. DNA transformation

Deep-frozen XL1 Blue MRF' aliquots (each 50 μL) were gently thawed on ice and supplied with 2-3 μL of a ligation / USER reaction (maximum additive volume $\frac{1}{10}$). Following a 30 minutes incubation on ice the bacteria are heat shocked at 42 °C for 60 seconds (s). 400 μL of SOC medium were applied to enable growth of bacteria at 37 °C for at least 60 minutes under normal agitation in a incubator shaker.

After a brief centrifugation at RT the supernatant was reduced to approx. 50 μL in volume to allow re-suspension of the pelleted bacteria. Bacteria were plated on pre-warmed, light-safe ampicillin or kanamycin-containing LB / Agar petri dishes and cultivated over night at 37 °C.

Ingredient	Amounts
Trypton	20 g / L
Yeast extract	5 g / L
NaCl	0.5 g / L
MgSO ₄	5 g / L
	20 mM glucose freshly added for SOC medium

Table 2.18.: SOB / SOC medium

CHAPTER 2. METHODS

2.4.2. DNA gel electrophoresis

Separation of DNA fragments via TBE gel electrophoresis is based upon the negatively charged phosphate backbone chains of the DNA which leads to migration of the DNA from the minus to the plus pole of the electrophoresis chamber. Agarose is used as the separating matrix for DNA fragments according to their size. The optimal resolution of the DNA separation is dependent upon the pore size which itself depends on the agarose content.

One percent agarose gels allow ideal separation of DNA ranging from 500 – 7 000 bp whereas two percent agarose gels are better suited for the resolution of 200 – 4 000 bp fragments. For extremely small DNA fragments (<1 000 bp) 3 % gels are best.

Size determination of the electrophoresed material depended upon home-brewn λ -Pst marker (λ DNA over night digested with PstI). DNA Gels were run with a constant voltage of 100 V for 30 - 60 min.

Ingredient	Amounts
Tris	0.9 M
Boric acid	0.9 M
EDTA	20 mM

Table 2.19.: 10x TBE buffer (pH 8.3)

Visualiation of the DNA bands is based upon UV illumination of ethidiumbromide containing gels (agarose gel solutions were pre-mixed with 0.1 mg / mL ethidiumbromide and stored at 60 °C).

Ingredient	Amounts
Bromphenol blue	0.25 %
Xylencyanole	0.25 %
EDTA	100 mM
Glycerol	50 %

Table 2.20.: 5x DNA sample buffer

2.4.3. DNA purification

2.4.3.1. DNA miniprep

Single grown colonies of a transformation were inoculated o/n in 5 mL LB (+ respective antibiotics) at 37 °C with an agitation of 500 rpm in a bacteria incubator. 1.5 mL of the o/n

culture were briefly centrifuged for 1 min and the supernatant was poured off leaving approx. 50 μ L of solution to vigorously vortex the bacteria pellet with the resting LB media. After re-suspension a alkaline lysis of the bacterial cells according to Birnboim & Doly (1979) was done.

Briefly summarized: 400 μ L of freshly made TENS buffer were added to lyse cells yielding a clear solution. Adding 200 μ L 3 M Sodiumacetate (pH 5.2) neutralizes and leads to precipitation of proteins and chromosomal DNA. After a 5 min incubation on ice and 5 min centrifugation on a benchtop Eppendorf centrifuge (Eppendorf, Hamburg, D) supernatants were mixed with 600 μ L isopropanol, pelleted for 10 min and washed once with 500 μ L ethanol (70 %) (5 min centrifugation). Remaining ethanol was aspirated at 37 °C for 15 - 30 minutes. Pellets were re-suspended in 50 μ L of TE buffer (10 mM Tris-HCl, pH 7.5; 1 mM EDTA).

Ingredient	Amounts
TE buffer	9.4 mL
10 % SDS	0.5 mL
10 M NaOH	0.1 mL
RNAse	100 μ g / mL

Table 2.21.: TENS buffer

2.4.3.2. DNA midiprep

High quality and quantity demands of the particle inflow gun (PIG) require a high volume DNA isolation from 100 mL over night 37 °C bacteria culture using the "Qiagen Plasmid Plus Midi Kit" (Qiagen, Hilden, D). The final elution volume was according to the manufacturer's instructions (200 μ L). After quantification of the DNA amount and purity Midi DNA solutions were stored at 4 °C in the fridge for several months.

2.4.3.3. DNA purification from agarose gels

Electrophoresed DNA fragments need to be purified before usage in ligations / USER reactions. Melting of the cut agarose gel slices at 60 °C for 5 min in a chaotropic buffer containing guanidine hydrochloride was followed by an affinity purification on silicate beads with the "Qiaquick Gel Extraction Kit" (Qiagen, Hilden, D). The final elution volume was 50 μ L.

2.4.4. DNA quantification

Examination of DNA content was performed in a GeneQuant II photometer (Amersham Biosciences, Karlsruhe, D) via measuring the optical density (OD) at the following wavelengths: 230 nm (organic solvents), 260 nm (nucleic acids), 280 nm (aromatic amino acids), 320 nm (RNA). The ratio $\frac{260}{280}nm$ allows an assessment of protein contaminations: values above 1.8 are acceptable, above 1.9 would be ideal. A 1 : 70 dilution (70 μ L volume) was used for all measurements.

2.4.5. DNA sequencing

Chain termination by dideoxyribonucleotides was used for sequencing of DNA constructs (Sanger *et al.*, 1977) in an in-house ABI Prism 3100 Avant Genetic Analyser (Applied Biosystems, Karlsruhe, D) by the team members of the sequencing lab. Automated laser fluorescence (ALF) technology was used to non-radioactively label DNA probes. Hybridization of DNA samples was accomplished by using pre-defined sequencing primer attachment sites (T7, M13) in the multiple cloning sites (MCS) of the vector constructs. Sequence analysis was done with the free molecular biology software "A plasmid editor" v 1.17 for Linux (<http://www.biology.utah.edu/jorgensen/wayned/ape/>).

2.4.6. Primer design

Primers were designed with "A plasmid editor" v 1.17 for Linux which uses the "nearest neighbor" method for calculating annealing temperatures. Manufacturing of primers was carried out by Metabion (Martinsried, D). USER oligonucleotides were prefixed with *GGCT-TAAU* for the forward (5' \rightarrow 3' primer) (fwd) and suffixed with *TAATTTGG* for the reverse (3' \rightarrow 5') primer (rev) primers. In general an annealing temperature of at least 60 $^{\circ}$ C was desirable.

2.4.7. PCR Amplification

Amplification of polymerase chain reaction (PCR) products for cloning was carried out using the *Pyrococcus furiosus* C_x polymerase (Pfu C_x) polymerase in a total reaction volume of 50 μ L. Simple control amplifications were also done in a 50 μ L reaction volume according to the error-prone Taq PCR. PCR reactions were either carried out on "Mastercycler personal" (Eppendorf, Hamburg, D) or "Primus Thermocycler" (MWG-Biotech, Ebersberg, D) PCR multiplexers.

2.4. MOLECULAR BIOLOGY

Ingredient	Final concentration
Taq PCR buffer (10x, Biotherm)	5 μ L
MgCl ₂ (25 mM)	5 μ L
dNTPs (10 mM)	1 μ L
Fwd primer (10 μ M)	1 μ L
Rev primer (10 μ M)	1 μ L
Template DNA	1 μ L
Taq DNA polymerase (Biotherm)	1 μ L
H ₂ O	ad 50 μ L

Table 2.22.: Error-prone Taq PCR reaction

2.4.7.1. Colony PCR

Amplifying inserts for control PCR reactions were done with a 1 : 100 dilution of individual clones in PCR H₂O which was briefly heated to 99 °C to degrade and lyse the cells. After cooling to RT 1 μ L of the colony dilution was taken into reaction with the Taq DNA polymerase (Biotherm).

Ingredient	Amount
Taq PCR buffer (10x, Biotherm)	5 μ L
MgCl ₂ (25 mM)	5 μ L
dNTPs (10 mM)	1 μ L
Fwd primer (10 μ M)	1 μ L
Rev primer (10 μ M)	1 μ L
1 : 100 diluted colony	1 μ L
Taq DNA polymerase (Biotherm)	1 μ L
H ₂ O	ad 50 μ L

Table 2.23.: Colony PCR

After PCR amplification a DNA control gel is run on which the amplified insert fragment should be visible. Colony PCR are useful for a quick control of correct insertions of the desired insert into vector. For a more stringent control, a restriction digest (section 2.4.8) can reveal if fragments have been inserted rightly into the vector.

2.4.7.2. USER PCR

For a directed vector construction, the USER enzyme was used as already previously described (Geu-Flores *et al.*, 2007; Nour-Eldin *et al.*, 2006). In brief, pre-constructed USER vectors

CHAPTER 2. METHODS

containing the desired tags were mixed with PCR amplification product and USER enzyme and incubated for 25 min at 37 °C and further 25 min at 25 °C (reaction scheme: 2.4.7.2).

Ingredient	Amount
USER vector	2 µL
PCR fragment	6 µL
TE buffer	6 µL
USER enzyme	1 µL

Table 2.24.: USER PCR

The final constructed USER vector construct is further transformed into chemically competent MRF' bacteria like described in section 2.4.1.1.

2.4.7.3. PCR Profiles

PCR profiles for amplification of USER cloning compatible fragments were done via Pfu C_x DNA polymerase in the same manner as normal PCR amplifications using the Biotherm Taq DNA polymerase except for the elongation time. Pfu C_x elongation was allowed for approx. 1 kilo base pairs (kb) / min where Biotherm Taq DNA polymerase was allowed for approx. 5 kb / min.

Step	Taq PCR	Pfu C _x PCR	gDNA PCR
Initial denaturation (98 °C)	2 min	2 min	15 min
Denaturation (98 °C)		1 min	
Primer annealing (primer specific)		30 s	
Elongation (72 °C)	depending on insert length		
Finish (72 °C)	depending on insert length		

Table 2.25.: PCR profiles

2.4.8. Restriction digest

Restriction digests are useful controls of DNA transformation into bacteria: depending on the resulting fragment sizes, correct incorporation of the insert can be assayed. All the restriction enzymes used belonged to the family of bacterial endonucleases type II (Pingoud & Jeltsch, 2001). These endonucleases recognize a short, often palindromic, sequence of 4 to 8 base pairs (bp) and depend upon the presence of Mg²⁺ for their endonuclease activity (Kostreva & Winkler, 1995).

Classical applications for restriction digests are control experiments of DNA miniprep extractions to check whether the insert + vector fusion was performed correctly. Almost any vector used for cloning has multiple cloning site (MCS) which harbor many restriction sites where restriction enzymes cut. Together with a restriction site in the insert fragment, one experiment can control whether the insert was inserted correctly.

Normally a double digestion with two restriction enzymes was performed at once to check for (carefully chosen) multiple restriction sites. This also allowed the detection of many fragments on the same DNA gel.

Ingredient	Amount
DNA miniprep	5 μ L
Restriction enzyme	0.2 μ L
Restriction buffer (10x)	1.5 μ L
H ₂ O	7.3 μ L

Table 2.26.: Restriction digest

2.4.9. Particle Inflow Gun (PIG)

PIG (Klein *et al.*, 1988a,b; Vain *et al.*, 1993) allowed transient transformation of native *Arabidopsis thaliana* ecotype Columbia-0 (Col-0) leaves with fluorescently labeled proteins of interest. Protein-coupled fluorescence could be subsequently detected via confocal microscopy. Confocal microscopy was conducted on a Zeiss Pascal 5 LSM setup (Carl Zeiss Microimaging, Jena, D).

2.4.9.1. Preparation of tungsten particles

50 mg of tungsten particles (Biorad, Dreieich, D) were sterilized with 2 washes of 500 μ L ethanol (EtOH) (100 %) followed by a 2 min centrifugation. Resting EtOH was aspirated and 1 mL of sterile H₂O was added to yield a 50 μ g / mL stock solution of tungsten particles. This stock solution could be stored at 4 °C for several weeks.

2.4.9.2. Coating of tungsten particles with DNA

100 μ L of the 50 μ g / mL tungsten particle stock solution was supplied with 10 μ g of DNA (or 2x 10 μ g of DNA for double-impact bombardments) and mixed via vortexing. Under vigorous vortexing (approx. 2-3 min) 100 μ L CaCl₂ (2.5 M) and 40 μ L spermidin (0.1 M) were added. Upon application of 200 μ L EtOH (100 %, ice-cold) vortexing helped to mix

all components well before a final addition of 400 μL EtOH (100 %, ice-cold) started DNA precipitation.

CaCl_2 helped to stabilize the DNA structure while spermidin acted as a DNA carrier to improve the rate of DNA precipitation on the tungsten particles.

The DNA precipitation on the tungsten particles was carried out at $-20\text{ }^\circ\text{C}$ for at least 1 h. Coated tungsten particles were centrifuged for 1 min at RT and the supernatant was carefully removed. Re-suspension of the tungsten-DNA complexes with 100 μL H_2O led to 10 possible transformations with each 10 μL of the tungsten-DNA complexes. For each transformation, 500 μg of tungsten particles and 2 μg DNA were used.

2.4.9.3. Transient transformation via PIG

A.th. leaves were transformed with a home-build particle inflow gun apparatus at a pressure of 8 – 9 bar and a chamber underpressure of 0.8 bar. Leaves were incubated in standard round petri dishes filled with normal tap water for approximately 16 h at room temperature in the dark.

2.4.9.4. Fluorescence microscopy

Images of proteins which were fluorescence labeled with eGFP and *Discosoma* sp. red fluorescent protein 2 (DsRed2) were obtained employing a Zeiss LSM5 Pascal confocal microscope (Carl Zeiss Microimaging, Jena, D). The applied excitation wavelengths were 488 nm for eGFP and 534 nm for DsRed2.

Corresponding emission wavelengths for each fluorophore were detected with filter sets supplied by the manufacturer. Images were recorded using a 40x / 1.2W C-Apochromat or 63x / 1.25 oil Plan-Neofluar objective with a confocal pinhole set to 1 – 1.5 airy units.

2.4.9.5. Analyzing co-localization experiments

Co-localization studies were performed with fluorescence tagged (eGFP or DsRed2) proteins and analyzed with the help of the software ImageJ (<http://rsb.info.nih.gov/ij>, Abramoff *et al.*, 2004; Collins, 2007). Analyzes were performed for Pearson's and Spearman's ranks according to French *et al.* (2008) using their ImageJ plugin.

Pearson's and Spearman's coefficients >0 indicate a tendency towards co-localization while coefficients <0 indicate a tendency towards separation. A perfect co-localization would gain a Pearson's rank of 1.0.

2.4.10. Transient expression in *N. benthamiana*

To elaborate putative protein interactions among ABI1, CPK21 and SLAH3, transient expression studies in *N. benthamiana* (N.b.) were performed according to previous investigations (Lee *et al.*, 2009a; Romeis *et al.*, 2001). In brief, *Agrobacterium tumefaciens* GV3101 strains were transformed with fusion constructs bearing GFP- or V5-tagged ABI1 (At4g26080), CPK21 (At4g04720) & SLAH3 (At5g24030), grown on YEB + Kan + Rif + Gent plates for 2d at 28 °C.

Single colonies were inoculated in 100 mL YEB + Kan + Rif + Gent media o/n, centrifuged for 10 min at 1 500 g_{av} , 20 °C and taken up in 15 mL of a special "agromix buffer" consisting of 150 μ M acetosyringone, 10 μ M $MgCl_2$ and 10 μ M MES-KOH pH 5.6.

The cultures were grown for 1 – 2 h at 28 °C until an OD_{600} of 0.5 – 0.8 was reached. Cultures were pooled in equal amounts for co-transformation, 19K cultures (Voinnet *et al.*, 2003) were added to suppress gene silencing (Te *et al.*, 2005) and infiltrated into young, 6 – 7 weeks old leaves of N.b. with the help of a 5 mL syringe without a needle. Almost every second leaf of N.b. plants was infiltrated and for one experimental setup at least 20 N.b. plants were necessary.

After three days of expression, leaves were harvested as described in section 2.1, p. 45 and the corresponding DRMs / DSF were isolated from following co-expression approaches:

- Kinase CPK21 + anion channel SLAH3
- Phosphatase ABI1 + kinase CPK21 + anion channel SLAH3

These two different approaches aimed to clarify localization of the kinase CPK21 and anion channel SLAH3: whether both or one of these proteins are situated in DRMs. If this should be the case, then application of the protein phosphatase 2C 56 (ABI1) should alleviate localization of kinase and / or anion channel from DRMs. Protein localization was tested via western blotting with GFP or V5 antibodies against the fusion constructs.

2.4.10.1. Used vector constructs

Tagging target proteins with the cyan fluorescent protein (CFP) / yellow fluorescent protein (YFP)-tag increased their molecular weight by approx. 27 kDa while adding a V5-tag increased the molecular weight by 25 kDa. Appropriate molecular weights are listed in table 2.27. In the first experiments ABI1, CPK21 & SLAH3 were fused C-terminally to either CFP (pCambia 31 vector backbone, ABI1::CFP) or YFP (pCambia 41 vector backbone, CPK21::YFP and SLAH3::YFP).

CHAPTER 2. METHODS

C-terminal fusions were mandatory as CPK21 and SLAH3 did not reach the PM if N-terminal fusions were used (previous work in the group of Dietmar Geiger, Julius-von-Sachs Institute for Biosciences, Univ. of Würzburg, D). Especially as CPK21 harbored two lipidation motifs directly at the N-terminus (Gly2 for myristoylation and Cys3 for palmitoylation), no N-terminal fusion constructs were used.

Later, the constructs were cloned into V5-tagged vectors to allow simultaneous detection of CPK21::YFP and SLAH3::V5 without obtaining intercepting signals. Therefore, ABI1 and SLAH3 were transferred into pCambia 6 and pCambia 7 binary vectors containing a C-terminally fused V5-tag to allow immunodetection using V5 antibodies in parallel with CPK21::YFP detection using GFP antibodies.

Protein name	AGI	MW [kDa]	MW + V5-Tag [kDa]
Protein phosphatase 2C 56 (ABI1)	At4g26080	47.5	72.5
Calcium-dependent protein kinase 21 (CPK21)	At4g04720	65	90
SLAC1-homologue 3 (SLAH3)	At5g24030	72	97

Table 2.27.: **GFP/V5 fusion constructs used for N.b. infiltration.** The approx. molecular weights are declared for the V5-tagged variants, the GFP-tagged variants gained a further increase in molecular weight by 2 kDa.

3

Results

3.1 ANALYZING DRMs FROM *A.TH.* LEAVES

The isolation of DRMs from purified PMs of *A.th.* mesophyll cells disclosed a diverse protein constitution. Beginning with the quality assessment of the purified PM, the protein composition in DRMs was analyzed with different detergents, different digestion protocols and refined via MCD treatment to identify "core" DRM proteins. This "core" set of DRM proteins was investigated for physiological interactions & relevance in plant drought stress response.

3.1.1. Quality control of the PM preparations

PM isolations are always prone to contaminations. Ribosomal proteins represent the major contaminants of PM isolations which have also been observed in the animal system (Hesketh, 1996; Medalia *et al.*, 2002). Another major source for contaminations in the plant field are chloroplasts (Widjaja *et al.*, 2009). The purity of the PM isolation with the 6.5 % Dextran T-500 / PEG-3350 / 6 mM KCl setup was assessed using immunoblot analysis with corresponding specific antibodies against compartment markers of the cytosol, ER, mitochondria, vacuole and PM.

The purification progress was visualized and analyzed from four fractions for their purity: the crude extract of the plants (homogenates), microsomal fraction, PM fraction and a mitochondrial fraction. Microsomal fractions contain all endomembranes and the PM, including the ER, vacuolar and mitochondrial contaminations.

UGPase as a cytosolic marker (Kuras *et al.*, 2007; Martz *et al.*, 2002) could only be found in the crude extract and was not detectable in any of the other fractions. Mitochondrial contaminations were detected using a VDAC1 antibody (Gibala *et al.*, 2009) in the microsomal fraction and, of course, concomitantly in the mitochondrial fraction. Sar1, a marker of the

CHAPTER 3. RESULTS

ER (Pimpl *et al.*, 2000), was only detectable in the microsomal fraction. The V-H⁺ ATPase antibody (Reuveni *et al.*, 2001) depicted presence of vacuolar portions in the microsomal but not in the PM fraction. Minor chloroplastic contaminations were detected (Prins *et al.*, 2008).

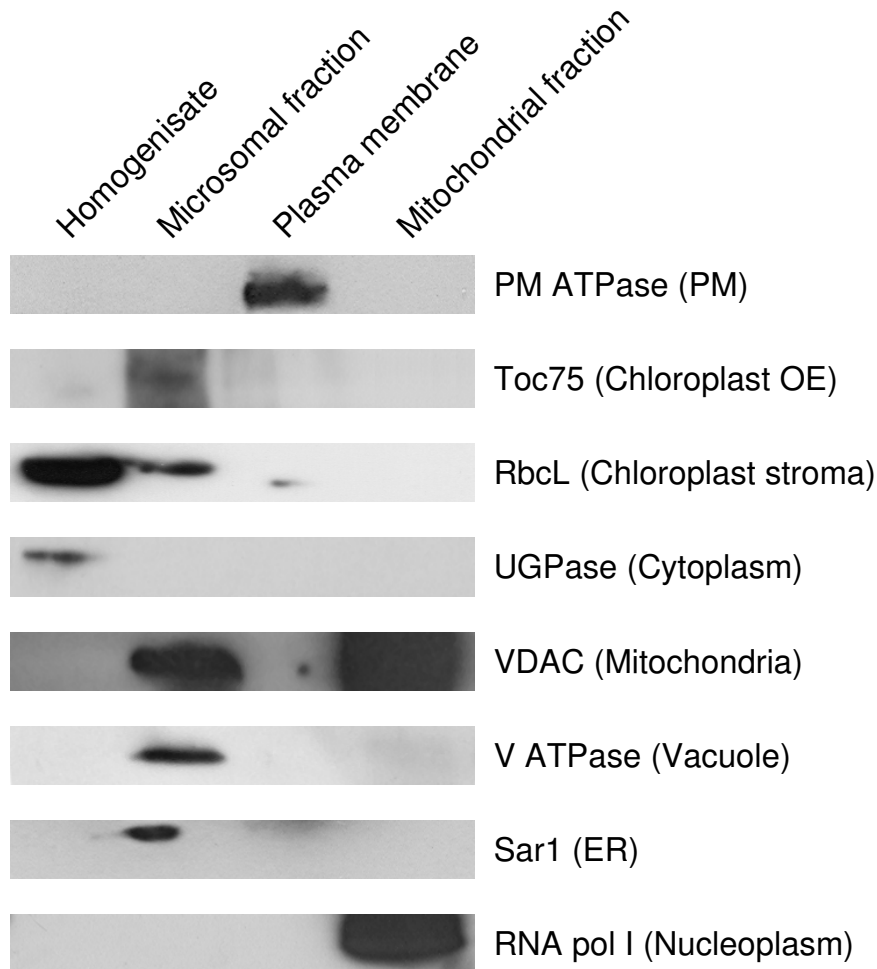


Figure 3.1.: **Immunoblot control of PM purity.** 10 μg of each fraction was loaded on a 8 - 16 % gradient polyacrylamide gel and subsequently blotted onto a PVDF membrane. Proteins were detected using specific antibodies against compartment markers (for details, see table 2.11, p. 56).

Positive detection of the PM was successful using a PM-H⁺ ATPase antibody (Page *et al.*, 2009). The PM-H⁺ ATPase was strongly enriched in the PM fraction. Thus, it was tempting to assume that PM fractions isolated with the 6.5 % Dextran T-500/PEG-3350 setup were of high purity and suitable for isolating DRMs without many contaminations.

3.1.2. Characterization of Triton X-100 & Brij-98 DRMs

3.1.2.1. Quantitative analysis of protein amounts in the DRM isolation

The isolation of pure PM and corresponding DRMs led to an enormous loss of protein during purification. Table 3.1.2.1 gives a short overview of the protein concentrations normalized per g fresh weight. Every purification step resulted in a quantitative protein loss of at least 90 %.

Fraction	Depletion	Protein [$\frac{mg}{g \text{ fresh weight}}$]	SE
Homogenate		13.1346	0.6886
Microsomal fraction (MF)	13.4	0.9801	0.0395
Plasma membranes (PM)	72	0.0136	0.0009
Detergent-resistant membranes (DRMs)	6.5	0.0021	0.0002
Detergent-soluble fraction (DSF)	3	0.0046	0.0003

Table 3.1.: Protein concentrations obtained from the 6.5 % PEG-3350 / Dextran T-500 two-phase partitioning setup for *N.b.* (n = 8). SE = standard error.

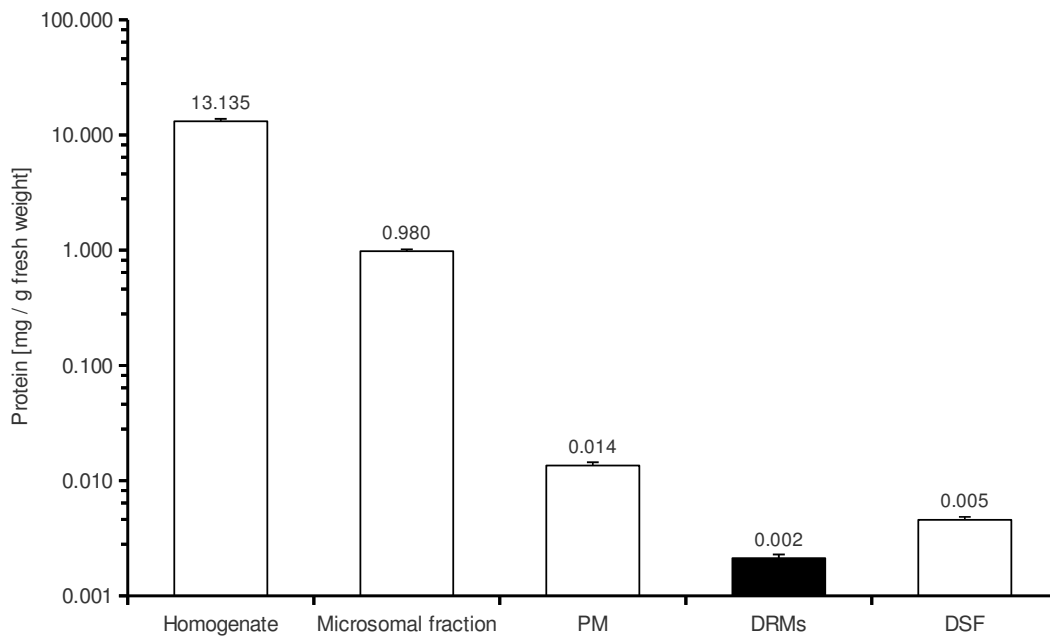


Figure 3.2.: **Quantitative analysis of protein amounts in DRMs.** Depicted are the protein concentrations in the corresponding fractions in mg protein per g fresh weight (n = 8 independent isolations + SE).

Figure 3.2 depicts the tremendous loss of protein for the isolation of DRMs. Especially the sequestration of the PM from microsomal fractions (MF) resulted in only **1.4 %** of the MF being isolated as highly pure PMs. Generation of 100 µg DRMs from *A.th.* or *N.b.* leaves required at least 50 g of fresh material (approx. 20 *N.b.* plants).

3.1.2.2. Characterizing DRM isolations by sucrose gradients

Sucrose density gradients were used to separate DRMs from the bulk of the PM. To assess the distribution of sucrose and protein concentrations across the gradient, 17 – 18 fractions were taken (each 1.5 mL) and analyzed for their sucrose & protein content. Sucrose content was determined using an optical refractometer and protein concentrations were detected using a microplate BCA protein assay.

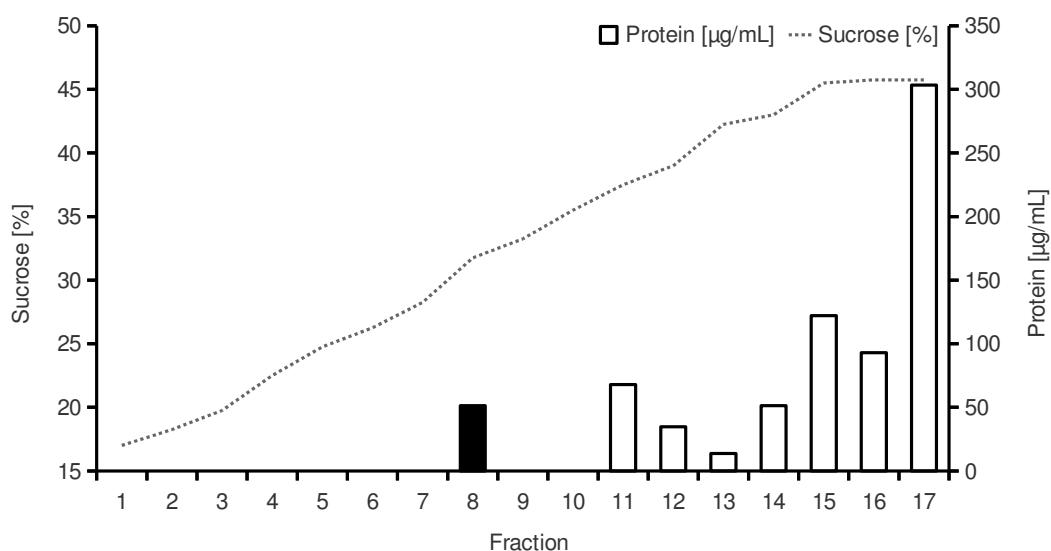


Figure 3.3.: **Overview of the sucrose & protein distribution in an exemplary sucrose density gradient.** Fraction 8 represents the DRMs (black bar).

An exemplary sucrose gradient is depicted in figure 3.3. The sucrose concentration increased from 15 % at the top of the gradient to approx. 50 % sucrose at the bottom. Any perturbation in the gradient could influence the resulting opaque DRM band.

The vast majority of the proteins in sucrose gradients were located in the bottom fractions representing the DSF. Even a small protein pellet could be seen at the bottom. Only a minor amount of the proteins were located in DRM fractions at ≈ 30 % sucrose (for instance, fraction 8 in figure 3.3 represented 7 % of the total proteins).

3.1.3. Proteomic analysis of A.th. leaf DRMs

Proteomic analysis led to the identification of 246 Brij-98 & Triton X-100 DRM proteins in total. The majority of these proteins were known or predicted PM residents.

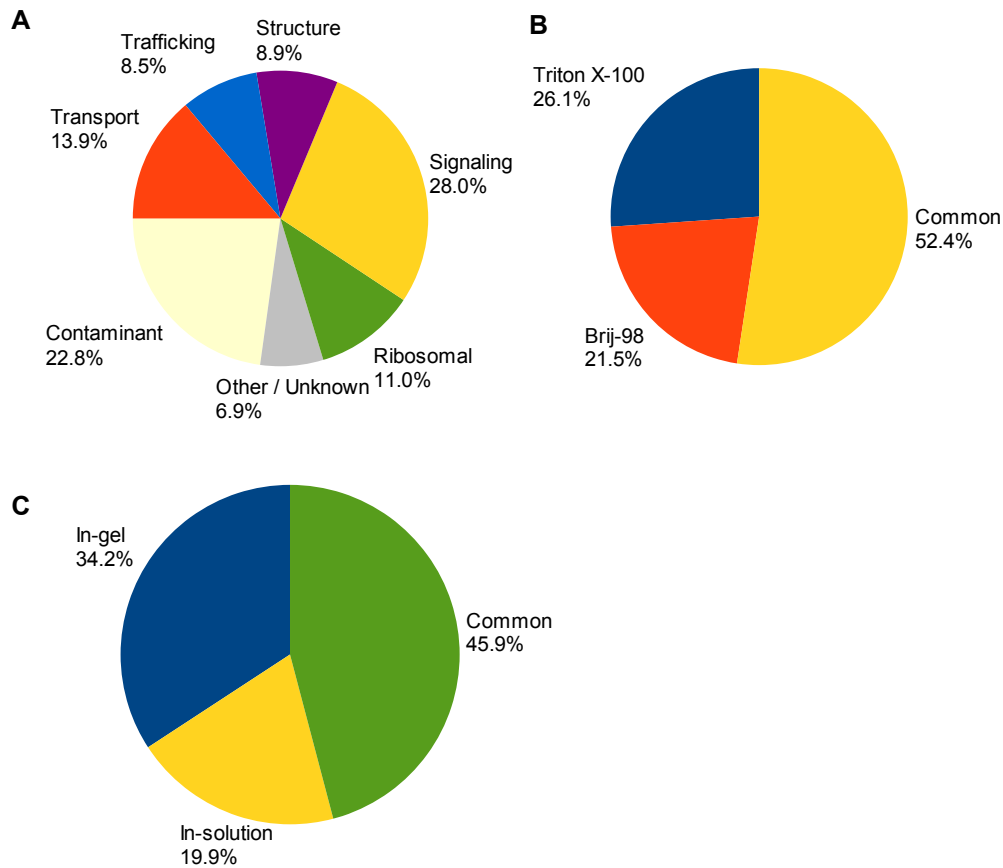


Figure 3.4.: **Composition of Brij-98 & Triton X-100 DRMs.**

A: Proteins fulfilling signaling (28 %) and transport (13.8 %) functions were the main functional groups in DRMs.

B: The majority of the DRM proteins were isolated by Triton X-100 treatment (78.5 %). Brij-98 treatment retrieved only 21.5 % specific DRM proteins.

C: In-gel & in-solution digestion protocols retrieved different subsets of DRM proteins. Most of the identified DRM proteins could be isolated by in-gel digestion.

As visible on figure 3.4A the majority of the 246 DRM proteins could be assigned to signaling (28 %) and transport (13.9 %) functions. 22.8 % of the identified DRM proteins were contaminations; this was in the same range as comparable investigations (Borner *et al.*, 2005). Major contaminations came from chloroplasts (29 proteins, 11.8 % of total identified

proteins) and the ER. Ribosomal proteins formed another big cluster of proteins which were possibly connected to the cytoskeleton (Hesketh, 1996; Medalia *et al.*, 2002) in polysomal structures and could be declared to not present contaminations.

3.1.3.1. Detergent & digestion protocol effects on protein composition

Parallel isolation of DRMs via the non-ionic and mild detergents Brij-98 and Triton X-100 revealed an interesting pattern. It can be concluded that Triton X-100 remains the golden standard for the isolation of DRMs. Detergent treatment with Triton X-100 resulted in the identification of 78.5 % of the total 246 DRM proteins (fig. 3.4B). Brij-98 treatment yielded only a small pool of Brij-98 specific DRM proteins (21.5 %). An overlapping fraction of more than 50 % which could be detected via both detergents. There were small differences in the protein subsets – these will be presented later on.

The application of different digestion protocols displayed a similar situation (figure 3.4C). More than half of the proteins were detected by both techniques, every digestion approach delivered a quarter of specific proteins. In-gel digestion represents the state-of-the-art method to conduct mass spectrometry (MS) analysis of complex protein samples. In-solution digestion leads to a different subset of proteins than in-gel digestion (Gaspari *et al.*, 2007). Therefore, both digestion approaches were combined:

1. In-gel digestion: DRMs were applied on SDS-PAGE gels & separated acc. to molecular weight. This reduced sample complexity enabled MS identification of proteins.
2. In-solution digestion: DRMs were directly digested in buffer, followed by SCXC fractionation and subsequent MS protein identification of SCXC separated fractions.

Most of the identified DRM proteins were detected following in-gel digestion (80.1 %). Only a minority of 19.9 % could be exclusively identified by in-solution digestion. Almost half of the DRM proteins (45.9 %) were observed following both digestion protocols.

However, there was an outstanding difference between both digestion techniques. Transport proteins were detected to a much higher degree following in-gel digestion. In-gel digestion retrieved 32 whereas in-solution digestion yielded only 21 transport proteins. Effects from the digestion techniques could not be observed for all the other functional categories.

Some proteins were specifically retrieved by one digestion method. For instance, CPK21 was only detected after in-gel digestion whereas dehydrin ERD10 was only identified by in-solution digestion. Thus, in-gel digestion of Triton X-100 DRMs remains the golden standard.

3.1.3.2. Functional classification

The identified 246 Brij-98 & Triton X-100 DRM and 741 PM proteins were manually classified into the following functional groups, according to existing database annotations & publications¹:

Signaling

Proteins involved in signal transduction: kinases, phosphatases, receptors

Transport

Proteins responsible for the traverse of substances across the PM: ABC transporters, aquaporins, H⁺-ATPases, ion channels

Trafficking

Proteins involved in delivery of proteins to target membranes: Rab family of GTPases, vesicle-associated membrane proteins and secretion assistant proteins

Structure

Structural components bound to the PM: the cytoskeleton (actin / tubulin), phragmoplast and adaptor proteins

Other / Unknown

Miscellaneous proteins not categorized into the other categories

Ribosomal

Individual members of polysomal and ribosomal complexes

Contaminations

Proteins not located or bound to the PM in any circumstance: chloroplastic components, for instance, ribulose-1,5 bisphosphat-carboxylase / -oxygenase (RuBisCO)), mitochondrial proteins, transcription factors

The functions of the PM and the corresponding DRMs were quite comparable (figure 3.5). A strong enrichment in signaling proteins was inevitable for the PM representing almost $\frac{1}{3}$ of all identified proteins. Brij-98 treatment yielded more signaling and transport proteins than Triton X-100 treatment while displaying less contaminations. Triton X-100 seemed to favor identification of ribosomal proteins. The isolation of DRMs resulted in a higher proportion of signaling & transport proteins than the corresponding PM.

¹Evidence from publications was given priority over computational annotations whenever available.

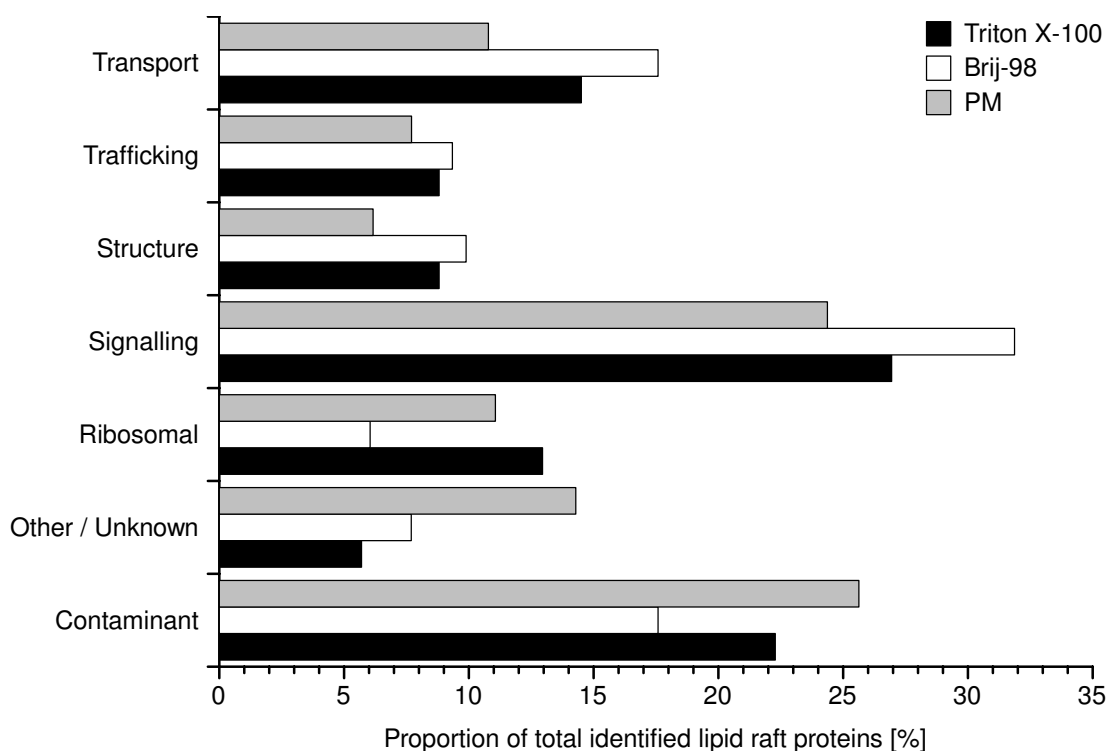


Figure 3.5.: **Functional classification of DRMs & PM.** A major bias on signaling functions in the PM (gray) and in Brij-98 (white) / Triton X-100 (black) DRMs was observed.

3.1.3.3. Triton X-100 & Brij-98 specific DRM proteins

Some proteins among the 246 identified DRM proteins were specifically identified only by Brij-98 or Triton X-100 treatment. Detergent treatment with Brij-98 yielded only 53 (21.5 %) Brij-98-specific proteins while Triton X-100 treatment resulted in the identification of 64 (26.1 %) Triton X-100-specific proteins. Every detergent retrieved specific contaminations and ribosomal proteins, which were not detectable with the other detergent. However, these contaminating and ribosomal proteins are not listed in the tables 3.2 (p. 83), respectively table 3.3 (p. 84), which contain detergent-specific proteins to avoid excess protein lists.

Upon comparison of protein properties, Brij-98 DRMs displayed a higher molecular weight and more transmembrane domains than proteins in Triton X-100 DRMs. Brij-98 treatment enriched proteins with a lower isoelectric point (pI) and a higher GRAVY value. All this pointed to Brij-98 DRM proteins being larger in size, more hydrophobic and composed of less charged amino acids.

3.1. ANALYZING DRMS FROM A.TH. LEAVES

Table 3.2.: **A selection of Brij-98 specific DRM proteins.** Brij-98 specific contaminations and ribosomal proteins are not listed.

AGI	Name	MW [kDa]	TMDs	Classification
At1g71880	Sucrose transport protein AtSUC1	54.9	12	Transport
At2g36910	ABC transporter B family member 1 (MDR1/PGP1)	140.6	12	Transport
At2g39480	ABC transporter B family member 6 (MDR6/PGP6)	155.9	12	Transport
At3g18830	Polyol transporter 5 (AtPLT5)	58.1	12	Transport
At4g16370	Probable oligopeptide transporter 3 (AtOPT3)	82.1	16	Transport
At3g46830	Ras-related protein RABA2c	23.8	0	Trafficking
At3g45600	Tetraspanin 3	31.9	4	Structure
At4g12730	Fasciclin-like arabinogalactan protein 2 (Fla2)	43.5	0	Structure
At2g17120	LysM domain-containing GPI-anchored protein 2 precursor	37.7	0	Signaling
At4g23160	Cysteine-rich receptor-like protein kinase 8	75.4	1	Signaling
At4g23220	Cysteine-rich receptor-like protein kinase 14	73.9	1	Signaling
At4g23250	Cysteine-rich receptor-like protein kinase 17	76.4	1	Signaling
At4g26690	Probable glycerophosphoryl diester phosphodiesterase 2	82.6	0	Other
At4g27520	Early nodulin-like protein 2	35.1	0	Other

Treating PMs with Brij-98 led to a short list of specific proteins. Especially transport proteins with many transmembrane domains were present in Brij-98 DRMs, for instance the ABC transporters PGP1 & PGP6 or AtSUC1. Other prominent members were cysteine-rich receptor-like protein kinases (CRKs) which are supposed to be induced by pathogen attack and ROS (Chen, 2001).

Some GAPs were also identified exclusively in Brij-98 DRMs, e.g. the early nodulin-like protein 2 and glycerophosphoryl diester phosphodiesterase 2.

CHAPTER 3. RESULTS

Table 3.3.: **A selection of Triton X-100 specific DRM proteins.** Triton X-100 specific contaminations and ribosomal proteins are not listed.

AGI	Name	MW [kDa]	TMDs	Classification
At1g13210	Putative phospholipid-transporting ATPase 11	136.6	10	Transport
At5g06530	ABC transporter G family member 22 (AtWBC23)	82.9	6	Transport
At1g04750	Vesicle-associated membrane protein 721 (AtVAMP721)	24.8	1	Trafficking
At1g10630	ADP-ribosylation factor A1F	20.6	0	Trafficking
At1g04820	Tubulin alpha-2/alpha-4 chain	49.5	0	Structure
At1g49240	Actin-8	41.9	0	Structure
At4g14960	Tubulin alpha-6 chain	49.5	0	Structure
At5g09810	Actin-7	41.7	0	Structure
At1g18890	Calcium-dependent protein kinase 10 (CPK10)	61.5	0	Signaling
At1g70530	Cysteine-rich receptor-like protein kinase 3	71.6	1	Signaling
At3g25070	RPM1-interacting protein 4	23.4	0	Signaling
At4g11530	Putative cysteine-rich receptor-like protein kinase 35	74.1	1	Signaling
At4g12980	Auxin-responsive protein, putative	42.2	0	Signaling
At4g17530	Ras-related small GTP-binding protein RAB1c	22.3	0	Signaling
At4g26080	Protein phosphatase 2C 56 (ABI1)	47.5	0	Signaling

Many of the Triton X-100-specific DRM proteins possessed no transmembrane domain at all that were predicted to be located in the PM. A member of the CPK family, CPK10 occurred only in Triton X-100 DRMs. CPK10's attachment to the PM is performed via a lipid myristoylation anchor.

Members of the cytoskeleton like actin-7 / 8 and tubulin α -2 / 4 / 6 were identified only in Triton X-100 DRMs. Another interesting finding was localization of an ABA-signal transduction protein in DRMs: the protein phosphatase abscisic acid insensitive 1 (ABI1).

3.1.3.4. Molecular weight distribution

As seen on figure 3.6 the overall distribution of DRM proteins' molecular weights varied only to a little degree. Proteins with a higher molecular weight > 75 kDa were more present in Brij-98 DRMs; contrary to this, Triton X-100 DRMs were enriched in small proteins with a molecular weight < 25 kDa.

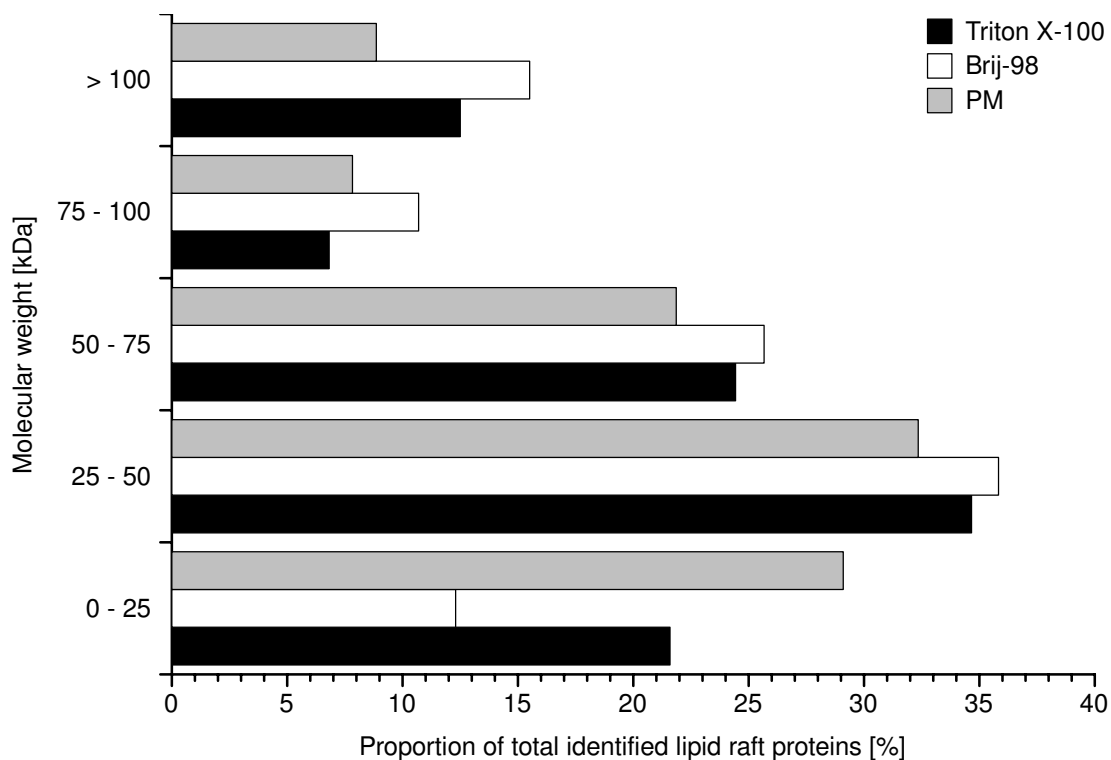


Figure 3.6.: Molecular weight distribution of Brij-98 (white), Triton X-100 (black) DRMs & corresponding PM (gray). Brij-98 treatment resulted in the identification of higher molecular weight DRM proteins while Triton X-100 retrieved smaller DRM proteins.

In general, DRM proteins displayed a homogenous distribution after Brij-98 and Triton X-100 treatment – the distribution was also quite comparable to the PM used for the isolation of these DRMs.

3.1.3.5. Transmembrane domains

The majority of the DRM proteins displayed no transmembrane domain at all (figure 3.7). Triton X-100 DRMs were specifically enriched in proteins without any predicted or known transmembrane domain at all. Brij-98 treatment allowed the identification of intrinsic PM proteins with more transmembrane domains. Especially in the range of multi-transmembrane proteins Brij-98 was the detergent of choice.

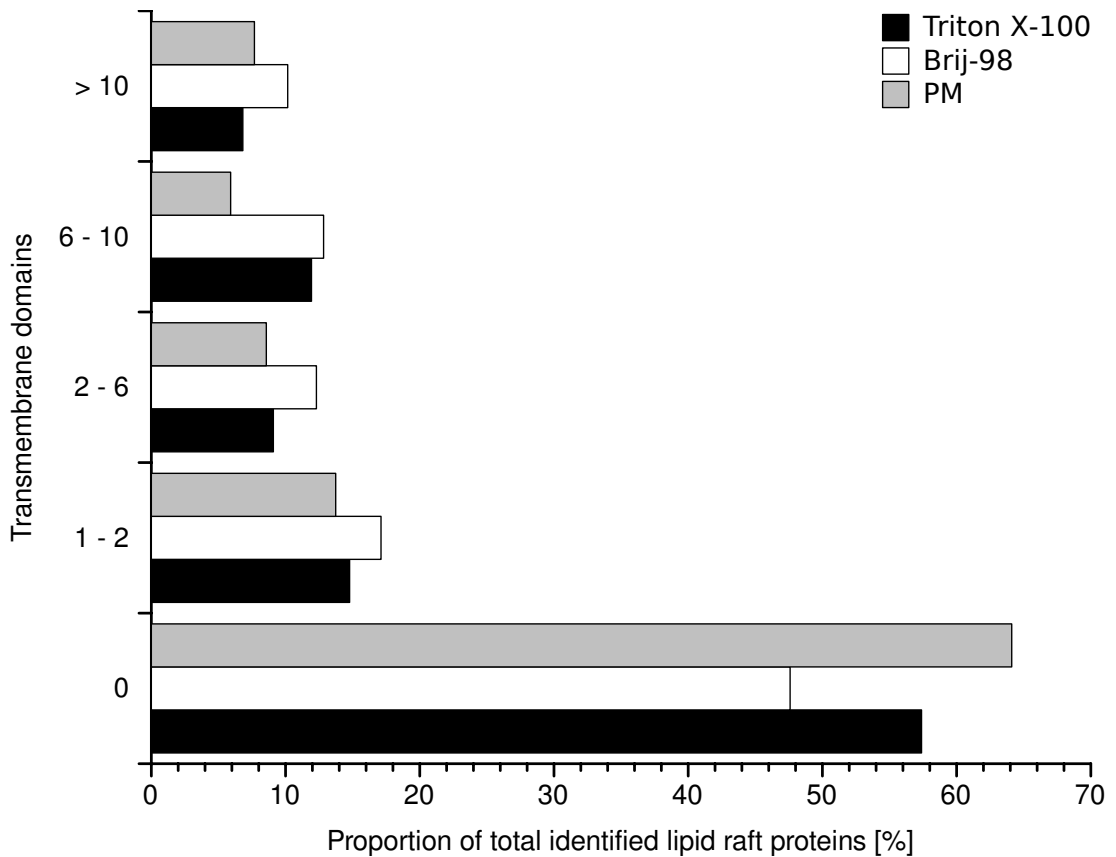


Figure 3.7.: Analysis of the TMDs of identified PM (gray) & DRM proteins (Brij-98 in white, Triton X-100 in black). After Brij-98 detergent treatment substantially more transmembrane proteins were identified while Triton X-100 application resulted in the identification of more proteins with no transmembrane domain.

A consideration to be taken is the fact that PM proteins could also be tethered to the PM via lipid attachments (e.g. palmitoylation / prenylation) & GPI-anchors which would not be visible as a transmembrane domain.

3.1.3.6. Hydrophobicity properties

A characteristic feature of PM proteins is the strong tendency towards hydrophobicity as calculated by the GRAVY index of hydrophobicity (Kyte & Doolittle, 1982). Surprisingly, majority of the identified proteins in the PM & DRMs (figure 3.8) had a low hydrophobicity (indicated by an index ≤ 0). This correlated with the analysis of molecular weights (figure 3.6) and TMDs (figure 3.7). The majority of DRM proteins were rather small and had no TMD.

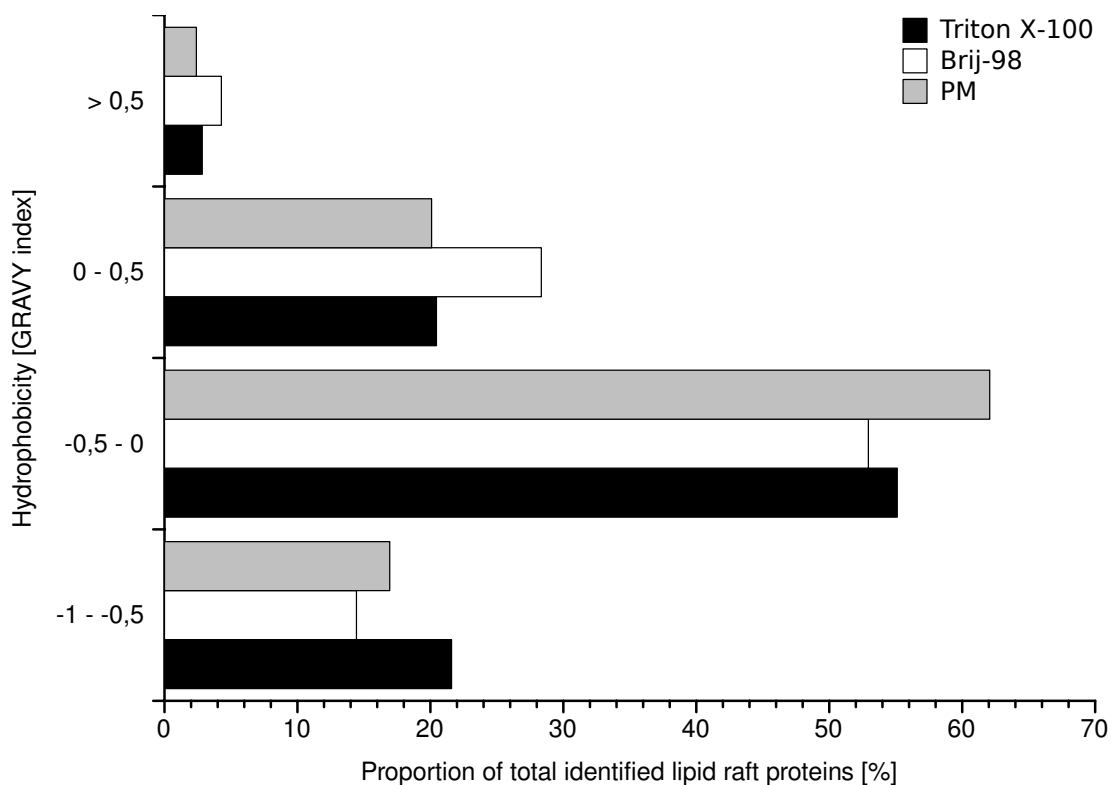


Figure 3.8.: Analysis of the hydrophobicity based on the GRAVY index displayed no great differences except a little bias on Brij-98 DRM proteins being more hydrophobic. The GRAVY index is an indicator for the hydrophobic nature of a protein: more negative values indicate less hydrophobicity (Kyte & Doolittle, 1982).

The PM and Triton X-100 DRMs displayed a similar hydrophobicity distribution whereas Brij-98 treatment triggered identification of slightly more hydrophobic DRM proteins.

CHAPTER 3. RESULTS

3.1.3.7. Identification of putative DRM-specific proteins

Before analyzing DRMs for their protein composition, purified PMs were analyzed (complete listing: table A.1, p. 162). During the isolation of DRMs from purified PMs, some weakly expressed proteins might be lost and not identified in DRMs. On the other hand, there were also proteins identified in DRMs, which were not identified in the corresponding PMs, which might be an evidence for their enrichment in DRMs.

AGI	Uniprot	Protein name	Classification
At3g09790	Q39256	Polyubiquitin	Other
At1g48830	Q9C514	40S ribosomal protein S7-1	Ribosomal
At2g24090	Q8VZ55	50S ribosomal protein L35	Ribosomal
At3g60770	P59223	40S ribosomal protein S13-1	Ribosomal
At1g48210	Q93Y19	Serine/threonine protein kinase-like protein	Signaling
At1g51805	Q9C8I7	Leucine-rich repeat receptor-like protein kinase	Signaling
At1g53430	Q9LPF9	Leucine-rich repeat receptor-like protein kinase	Signaling
At2g37050	Q2V2T0	Uncharacterized protein At2g37050.2	Signaling
At3g57530	Q6NLQ6	Calcium-dependent protein kinase 32 (CPK32)	Signaling
At4g08850	Q8VZG8	Leucine-rich repeat receptor-like protein kinase	Signaling
At5g10020	Q0WR59	Probable inactive receptor kinase	Signaling
At5g12250	P29514	Tubulin beta-6 chain	Structure

Table 3.4.: **Proteins only identified in DRMs and not in the PM by mass spectrometry.**

The majority of the DRM-specific proteins were devoted to signaling functions. Only in-solution digested protein identifications were compared.

Table 3.4 depicts signaling proteins being enriched in DRMs. In the corresponding PM samples these proteins were not detectable (at least, in a mass spectrometric approach). The calcium-dependent protein kinase **CPK32** might be an interesting candidate to be investigated in further studies.

3.1.4. MCD effects on Triton X-100 DRMs

The chemical compound MCD was applied (cf. section 2.1.5.1, p. 48) to further dissect the identified Triton X-100 DRM proteins for intrinsic lipid raft proteins. MCD treatment removes cholesterol and plant sterols by more than 50 % (Kierszniowska *et al.*, 2008) from membranes resulting in a disruption of DRMs. If some proteins were depending strongly on their sterol-rich environment, these proteins have a high likelihood of no longer being detected after disruption of the DRMs.

3.1. ANALYZING DRMS FROM A.TH. LEAVES

MCD treatment resulted in the identification of two different sub-pools of Triton X-100 DRM proteins (figure 3.9). One set of DRM proteins were not detectable in mass spectrometric analysis at all after MCD application (furthermore called "strongly affected", corresponding to 38 % of the identified Triton X-100 DRMs in this experimental setup). Another pool of proteins was detected to a much weaker extent after MCD treatment according to the emPAI index (23.1 % "moderately affected" proteins). The emPAI index represents a label-free quantitative analysis technique (cf. section 2.3.2.1, p. 62).

Based upon the abundance of the tryptic-digested peptides, the emPAI index was a rough quantitative estimation method. Due to the label-free nature of the emPAI abundance index, the interest focused on the Triton X-100 DRM proteins, which were not detectable anymore.

Triton X-100 DRM proteins which were not detected following treatment with 25 mM MCD are listed in table 3.5 (p. 91).

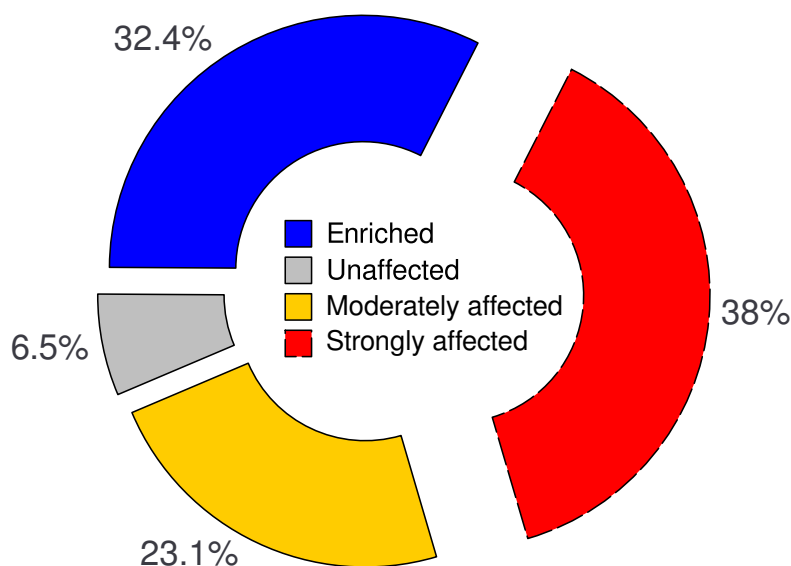


Figure 3.9.: **MCD effects on the DRM protein composition.** The majority of the DRM proteins were affected by methyl-β-D-cyclodextrin (MCD) treatment: more than half of the proteins were negatively affected.

The proteins, which remained in the DRMs after sterol depletion, are considered to not depend on sterols and were, thus, considered to be relatively "enriched" in DRMs after MCD treatment. These proteins could be attributed to contaminations and highly expressed transport proteins like the water transport facilitators (aquaporins). Highly expressed PM proteins like the aquaporins might be just co-purified during the DRM isolation procedure. After the depletion of sterol-dependent DRM proteins, these co-purified proteins remained in the DRMs and were overrepresented in the proteomic analysis.

Table 3.5.: **Triton X-100 DRM proteins strongly affected by MCD treatment.**

Proteins not detectable via mass spectrometry after 25 mM MCD treatment.

AGI	Protein name	MW [kDa]	TMDs	MCD [†]	Classification
At1g13440	Glyceraldehyde-3-phosphate dehydrogenase	36.9	0	○	Contaminant
At1g18890	Calcium-dependent protein kinase 10 (CPK10)	61.5	0		Signaling
At1g21250	Wall-associated receptor kinase 1	81.2	1		Signaling
At1g22710	Sucrose transport protein SUC2	54.5	12		Transport
At1g23410	Ubiquitin	8.5	0		Other
At1g49240	Actin-8	41.9	0	○	Structure
At1g51805	Leucine-rich repeat (LRR) receptor-like kinase	95.8	0		Signaling
At1g53440	LRR receptor-like kinase	108.8	2		Signaling
At1g72150	Patellin-1	64	0	○	Trafficking
At2g01250	60S ribosomal protein L7-2	28.2	0	○	Ribosomal
At2g23810	Tetraspanin 8	22.1	0		Structure
At2g31880	LRR receptor-like kinase	71.1	0		Signaling
At2g37710	Putative receptor protein kinase	75.5	0		Signaling
At2g39730	Ribulose biphosphate carboxylase/oxygenase (RuBisCO) activase (chloroplastic)	51.1	0		Contaminant
At3g02520	14-3-3-like protein GF14 nu (GRF7)	29.8	0		Signaling
At3g07160	Callose synthase 9	222.1	16	○	Structure
At3g09440	Heat shock cognate 70 kDa protein 3	71.1	0	○	Contaminant
At3g09740	Syntaxin-71	29.1	1	○	Trafficking
At3g11130	Clathrin heavy chain, putative	27.6	0	○	Contaminant
At3g24550	Proline Extensin-Like Receptor Kinase 1	69.3	0	○	Signaling
At3g26650	Glyceraldehyde-3-phosphate dehydrogenase A	42.5	0		Contaminant
At3g45140	Lipoxygenase 2 (AtLOX2)	102.1	0		Contaminant

Continued on next page ...

AGI	Protein name	MW [kDa]	TMDs	MCD [†]	Classification
At3g45780	Phototropin-1	111.7	0		Signaling
At3g51550	Receptor-protein kinase-like protein	98.1	0	○	Signaling
At3g61260	AtRem 1.2	23.1	0	●	Signaling
At3g63260	MLK/Raf-related protein kinase 1 (AtMRK1)	42.6	0	●	Signaling
At4g04720	Calcium-dependent protein kinase 21 (CPK21)	59.9	0		Signaling
At4g08850	Leucine-rich repeat receptor-like protein kinase	115.4	2	○	Signaling
At4g11530	Cysteine-rich receptor-like protein kinase 35 (CRK35)	74.1	1		Signaling
At4g22485	Uncharacterized protein	68.2	0		Unknown
At4g31700	40S ribosomal protein S6-1	28.4	0	○	Ribosomal
At5g09810	Actin-7	41.7	0	○	Structure
At5g43470	Disease resistance protein RPP8	104.7	0		Contaminant
At5g44020	Vegetative storage protein-like	31.1	0		Contaminant
At5g48380	LRR receptor-like protein kinase	69.1	0	○	Signaling
At5g49760	LRR receptor-like protein kinase	104.7	0	●	Signaling
At5g56000	Heat shock protein (HSP81-4)	80.1	0	○	Contaminant
At5g57110	Calcium-transporting ATPase 8, P-type	116.2	10	●	Transport
At5g57350	ATPase 3, P-type	104.4	10	○	Transport
At5g62670	ATPase 11, P-type	105.2	10	○	Transport
AtCg00830	50S ribosomal protein L2 (chloroplastic)	29.9	0		Contaminant

[†]MCD responsive proteins according to the study of Kierszniowska *et al.* (2008): filled circles (●) represented proteins negatively affected by MCD treatment; empty circles (○) were unaffected according to their study.

CHAPTER 3. RESULTS

Among the Triton X-100 DRM proteins which were not detected after MCD treatment (table 3.5), signaling proteins represented 41.5 % of the undetected DRM proteins (figure 3.10). All other functional classes (trafficking, transport) were affected to a much weaker extent.

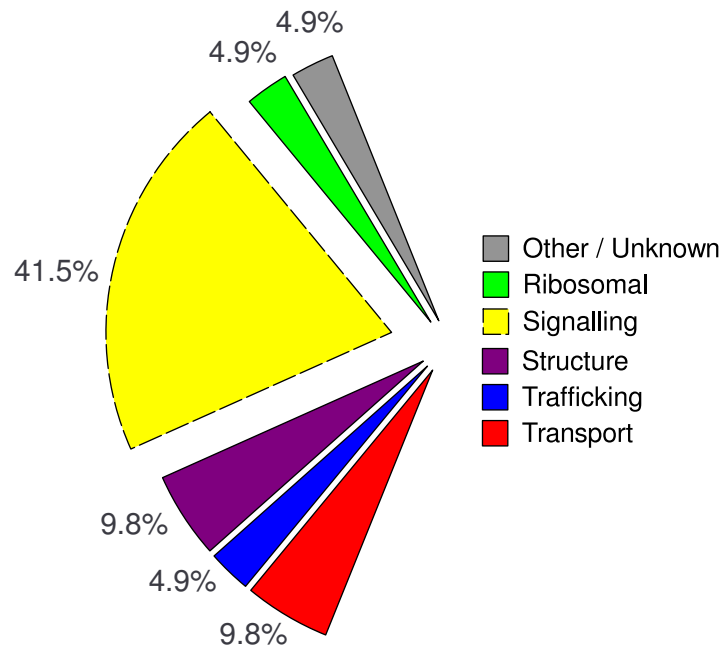


Figure 3.10.: **Functional classification of strongly affected Triton X-100 DRM proteins.** Signaling proteins represented the major class of proteins which were no longer detectable following MCD treatment.

Kinases represented many of the strongly affected signal transduction components. Two Ca^{2+} -dependent protein kinases (CPKs) 10 and 21 were no longer detected after MCD treatment. CPK21 has already been identified in proteomics studies as a member of Triton X-100 DRMs isolated from *A.th.* seedlings (Shahollari *et al.*, 2007).

Anion channels of the SLAC1(-homologue) family are known to interact with the CPK21 (Geiger *et al.*, 2010b). Thus, further investigations with CPK21 and the anion channel SLAH3 (**SLAC1-homologue 3**) were carried out (see section 3.18, p. 105).

Other proteins which were not detected after MCD treatment were structural components like actin-7 / 8 (At5g09810 / At1g49240) and callose synthase 9 (At3g07160), which has been shown to be involved in callose deposition into the secondary cell wall (Jacobs *et al.*, 2003). It is interesting that such a protein requires a sterol-rich microenvironment as callose deposition represents a defense mechanism against (a)biotic stress (Zhu *et al.*, 2010).

3.1. ANALYZING DRMS FROM A.TH. LEAVES

For the animal system it was known that membrane microdomains are organized partially by tetraspanin proteins (Nydegger *et al.*, 2006) and attached to the cytoskeleton, especially in caveolae (Morone *et al.*, 2006). *A.th.* tetraspanin 8 displayed strong sterol-dependency as revealed by MCD treatment. It may be speculated that tetraspanin proteins are also involved in membrane domain organization at the plant PM.

Another strikingly affected protein was AtRem 1.2 (At3g61260), which has also been found to be depleted after MCD treatment by Kierszniowska *et al.* (2008). Proteins of the remorin family are canonical lipid raft proteins for the plant kingdom which display a strong dependence upon sterols. While MCD treatment affected AtRem 1.2 strongly, AtRem 1.3 (At2g45820) was still detected but to a much weaker extent in Triton X-100 DRMs after MCD application. The complete absence of AtRem 1.2 but not of AtRem 1.3 could be attributed to the lower expression level of AtRem 1.2 which might have led to the loss of detection while AtRem 1.3 was still detectable.

MCD treatment strongly affected six LRR receptor-like protein kinase located in Triton X-100 DRMs (At1g51805, At1g53440, At2g31880, At4g08850, At5g48380, At5g49760). Up to now, no detailed information on function & interaction partners for all of these LRR receptor-like protein kinases is available. At2g31880 is expressed in response to *Pseudomonas syringae* infection while At5g48380 (BAK1-interacting receptor-like kinase 1) plays a negative regulatory role in plant resistance signaling (Gao *et al.*, 2009).

Transport proteins were affected by MCD treatment to a minor degree: only ATPases 3, 8, 11 and the sucrose transporter AtSUC2 were not detected after 25 mM MCD application. These transport proteins might perhaps be depending upon sterol-rich environments. AtSUC2 was further investigated for co-localization with AtRem 1.3 (cf. 3.2.3, p. 100) as it was strongly affected by MCD and displayed a strong localization in Triton X-100 DRMs.

Only very few proteins were identified directly in the supernatant after MCD treatment (cf. 2.1.5.1, p. 48). These proteins were detected in the MCD supernatant[†]:

- Protein phosphatase ABI1 (At4g26080)
- Two plasma membrane intrinsic proteins (PIPs) (At2g45960, At3g53420)
- Putative harpin-induced protein (NHL3, At5g06320)
- Large subunit of RuBisCO (AtCg00490)

None of the strongly MCD affected DRM proteins located in the MCD supernatant. Only DRM proteins which were moderately affected by MCD treatment occurred in the MCD

[†]Listed in order of abundance according to the emPAI index (cf. 2.3.2.1, p. 62)

supernatant. Strongly MCD affected DRM proteins were detected neither in DRMs nor in the MCD supernatant. Thus, it may be proposed that proteins, which are strongly affected by MCD treatment, dislocate into DSF fractions.

Signaling and transport proteins represented the majority of the only moderately MCD affected Triton X-100 DRM proteins. Proteins fulfilling signaling functions were not as dominant among the moderately MCD affected proteins as for the strongly MCD affected Triton X-100 DRM proteins (table 3.5). Among the transport proteins, ATP-binding cassette (ABC) auxin transporter ABCB19 / PGP19 (At3g28860) was negatively affected by MCD application. PGP19 is supposed to play a role in the fine-regulation of PIN1-mediated auxin transport in membrane microdomains (Titapiwatanakun *et al.*, 2009). The localization of PIN1 in membrane microdomains was negatively affected in a mutant *abcb19* line. It has been supposed that ABCB19 stabilizes PIN1 localization in PM membrane microdomains.

MCD application has also affected strongly PEN3 localization in Triton X-100 DRMs. PEN3 (At1g59870) represents an ABC transporter and was shown to be involved in non-host resistance to pathogens (Stein *et al.*, 2006). Physiological relevance of PEN3 localization in membrane microdomains has been attributed to transport of anti-microbial substances across the PM (Lipka *et al.*, 2008). PEN3 participated in a pathogen-response complex together with the PM syntaxin PEN1 (At3g11820) which was also negatively affected by MCD (for more details, see section 1.2.6.2, p. 33).

A slight homologue of PEN3, Mlo (Mildew resistance locus o) has been located in membrane microdomains. Mlo takes part in a complex which accumulates at fungal appresoria upon pathogen attack (Bhat *et al.*, 2005). This shares similarity with the situation in animal host cells upon bacterial or viral attack (Chazal & Gerlier, 2003; Conner & Schmid, 2003).

Phospholipase D δ represented an important lipid signaling protein which was also affected by MCD. The phospholipase D δ has been shown to be involved in generation of the lipid secondary messenger PA. PA interacts with the protein phosphatase 2C ABI1 (Zhang *et al.*, 2004) and the NADPH oxidase (Zhang *et al.*, 2009).

Interactions of PA with these important ABA signal transduction or ROS producing proteins underlines the importance of combined lipid and protein signaling in the plant PM.

Table 3.6.: Triton X-100 DRM proteins only moderately affected by MCD treatment.

Proteins were identified to a weaker extent in the mass spectrometric analysis after the 25 mM MCD treatment.

AGI	Protein name	MW [kDa]	TMDs	MCD [†]	Fold depletion			Classification
					emPAI	Mascot score	Seq. coverage	
At1g04750	Vesicle-associated membrane protein 721 (AtVAMP721)	24.8	1		1.61	1.06	1	Trafficking
At1g04820	Tubulin alpha-2/alpha-4 chain	49.5	0	○	1.59	1.18	2.01	Structure
At1g07930	Elongation factor 1-alpha	49.5	0		1.31	0.67	0.98	Contaminant
At1g15690	Pyrophosphate-energized vacuolar membrane proton pump 1	80.9	13	○	3.22	1.44	2.84	Contaminant
At1g30360	Dehydrin ERD4	81.9	0		1.78	1.49	1.47	Signaling
At1g59870	ABC transporter G family member 36 (PEN3/PDR8)	165.1	14	○	1.59	1.64	1.31	Transport
At1g76180	Dehydrin ERD14	20.8	0	●	2	1.23	2.14	Signaling
At2g18960	ATPase 1, P-type	104.2	10	○	2.05	1.63	1.67	Transport
At2g20990	Synaptotagmin A	61.7	0		2.22	2.09	2.33	Signaling
At2g37170	Aquaporin PIP2-2	30.5	6		1.34	1.01	1.56	Transport
At2g43030	50S ribosomal protein L3-1 (chloroplastic)	29.4	0		1.48	1.04	1.11	Contaminant
At2g45820	AtRem 1.3	20.1	0	●	2.61	2.2	1.63	Signaling
At3g08510	Phosphoinositide phospholipase C 2	66.1	0	○	1.84	1.15	1.35	Signaling
At3g08580	ADP,ATP carrier protein 1 (mitochondrial)	41.5	6	○	1.31	1.12	1.2	Contaminant
At3g11820	Syntaxin-121 (PEN1)	37.1	1		1.64	1.15	1.26	Trafficking
At3g14840	Receptor-like serine/threonine kinase	114.7	2		6	3.91	4.67	Signaling
At3g25920	50S ribosomal protein L15 (chloroplastic)	29.7	0		2.96	1.68	2.31	Contaminant
At3g28860	ABC transporter B family member 19 (MDR11/PGP19)	136.8	11		4.6	1.97	2.57	Transport
At4g01310	50S ribosomal protein L5 (chloroplastic)	28.3	0		3.93	1.41	2.1	Contaminant
At4g23400	Probable aquaporin PIP1-5	30.6	6		1.28	0.75	1.08	Transport
At4g26080	Protein phosphatase 2C 56 (ABI1)	47.5	0		1.62	0.79	1.04	Signaling
At4g30190	ATPase 2, P-type	104.4	10	○	2.07	1.68	1.7	Transport
At4g35100	Aquaporin PIP2-7	29.7	6		1.58	1.01	1.46	Transport
At4g35790	Phospholipase D δ	98.1	0		2	1.57	3.09	Signaling
AtCg00490	Ribulose bisphosphate carboxylase large chain	52.1	0		1.63	1.07	1.22	Contaminant

[†]MCD responsive proteins acc. to Kierszniowska *et al.* (2008): filled circles (●): negatively affected by MCD treatment; empty circles (○): unaffected.

3.2 INVESTIGATION OF CANDIDATE DRM / RAFT PROTEINS

Following the generation of a Brij-98 & Triton X-100 DRM protein inventory, the physiological localization and relevance of the identified "candidate" DRM proteins was elucidated via transient expression studies. Identification of AtRem 1.2 / 1.3 as lipid raft marker proteins allowed co-localization assays of the proteins under investigation together with fluorescence labeled AtRem 1.2 / 1.3.

3.2.1. Biochemical characterization of eGFP::StRem 1.3 overexpressor

For further studies, stable transgenic *A.th.* lines expressing eGFP-tagged potato remorin StRem 1.3³ were used to isolate DRMs and to test the hypothesis that StRem 1.3 localization in DRMs is strongly dependent on a sterol-rich environment. In a previous study by Raffaele *et al.* (2009a) StRem 1.3 was identified as a lipid raft marker protein for *S.t.* localized in microdomains of approx. 75 nm in diameter. Applying fluorescently labeled StRem 1.3, a "patchy" pattern was visible on the PM.

Highly purified PM was prepared from stable transgenic *A.th.* eGFP::StRem 1.3 plants using a 6.5 % PEG-3350 / Dextran T-500 setup. This PM was subjected to a 30 min treatment with 25 mM MCD at 37 °C and subsequently DRMs were isolated from MCD treated and non-treated PM fractions.

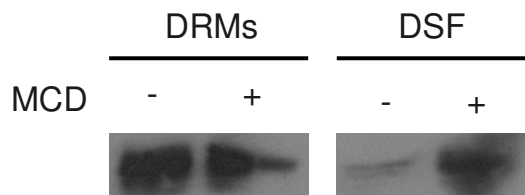


Figure 3.11.: **MCD effects on the eGFP::StRem 1.3 overexpressor line.** Sterol-depletion led to re-localization of fluorescently labeled StRem 1.3 from DRMs to DSF. 15 µg protein fractions were loaded, detection was performed with GFP primary antibody (1:2 500) and goat α-rabbit HRP secondary antibody (1:25 000).

Figure 3.11 displayed strong sterol dependency of eGFP-tagged StRem 1.3 localization in DRMs. Following MCD treatment, the signal strength decreased in DRMs and increased in the DSF. Depleting sterols led to the dissociation of eGFP::StRem 1.3 from DRMs. This was an additional piece of evidence that StRem 1.3 represents a lipid raft marker protein displaying strong sterol dependency.

³Vector maps, cf. appendix, section B, p. 201

3.2.2. Biochemical characterization of DRMs / DSF

The localization of putative lipid raft marker proteins AtRem 1.2 / 1.3 and non-raft marker AtLipocalin, DRMs and DSF were examined by isolating them from highly pure *A.th.* PM. Additionally, sterol dependency of AtRem 1.2 / 1.3 and AtLipocalin localization was assessed using MCD treatment. These investigations were carried out using custom polyclonal antibodies (cf. figure 3.12 and table 2.11, p. 56).

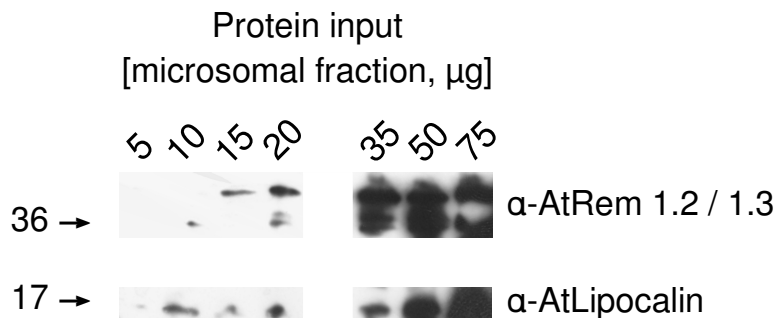


Figure 3.12.: **Titration of custom AtRem 1.2 / 1.3 & AtLipocalin antibody concentrations for immunodetection.** Increasing amounts of *A.th.* microsomal fractions were blotted and detected with a 1 µg / mL solution of affinity-purified AtRem 1.2 / 1.3 or AtLipocalin antibodies. Antibody detection was performed for 1 h at RT followed by incubation with a secondary α-rabbit HRP antibody at a dilution of 1:30 000 (1 h, RT).

Investigations on the ideal antibody concentration (figure 3.12) revealed the AtLipocalin antibody to react very well with ≥ 10 µg of microsomal fraction. At least 20 µg of microsomal fraction were required to gain signals for the AtRem 1.2 & 1.3 antibody. Both AtRem 1.2 & 1.3 were detected in parallel on western blots featuring *A.th.* material as the custom AtRem antibody was generated in rabbits after immunization with a peptide containing a consensus sequence of AtRem 1.2, 1.3 & StRem 1.3.

Due to the very hydrophilic sequence of the remorin proteins, these proteins always migrate at a much higher molecular weight than expected. The molecular weight of AtRem 1.2 / 1.3 was approx. 21 kDa, but AtRem 1.2 / 1.3 signals were detected at 36 kDa. This has also been reported by co-researchers working with the potato StRem 1.3 (Bariola *et al.*, 2004; Raffaele *et al.*, 2009a). StRem 1.3 displayed the same discrepancy between apparent molecular weight on SDS-PAGE gels (36 kDa) and theoretical molecular weight (24 kDa).

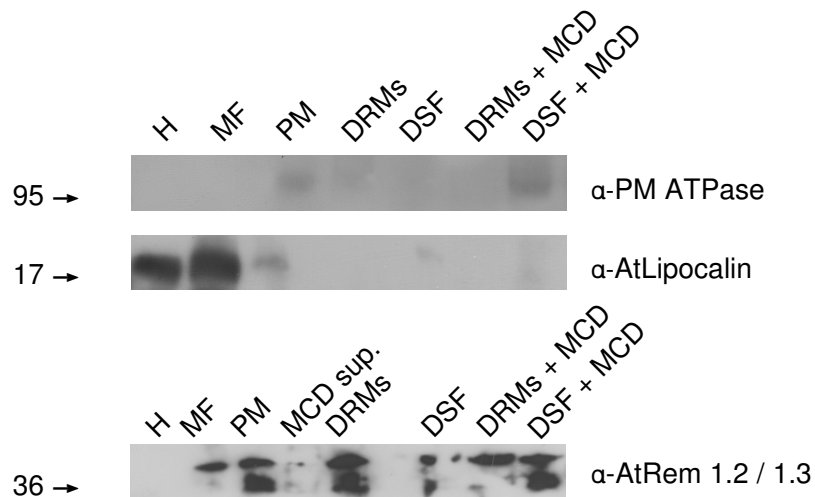


Figure 3.13.: **Immunological characterization of *A.th.* DRMs & DSF using *AtLipocalin* and *AtRem 1.2 / 1.3* antibodies.** Equal amounts of protein (15 μ g) were loaded, DRMs were isolated from the concomitantly loaded PM.

AtLipocalin was only present in homogenate, microsomal fraction and PM. *AtRem 1.2 / 1.3* displayed strong presence in the PM and DRMs. Upon MCD application, *AtRem 1.2 & 1.3* dislocated at least partially from DRMs into the DSF.

Abbreviations: H = homogenate, MF = microsomal fraction, PM = plasma membrane, DRMs = Detergent-resistant membranes, DSF = Detergent-soluble fraction, MCD sup. = MCD supernatant, DRMs / DSF + MCD = DRMs / DSF after MCD treatment.

In addition to the expected *AtRem 1.2 & 1.3* signals, a single band of approx. 55 kDa was detected. The nature of this additional signal could not be investigated in this study, but might represent a phospho-isoform of *AtRem 1.2 & 1.3*. This additional band at 55 kDa always appeared first, long before both *AtRem 1.2 & 1.3* bands were visible on the western blots.

On the titration immunoblot (figure 3.12) this 55 kDa signal was already present in 15 μ g of microsomal fraction whereas the *AtRem 1.2 / 1.3* signals were detected only in ≥ 20 μ g of the microsomal fraction. As phospho-isoforms of *AtRem 1.2* have already been identified to be present in high abundance after stimulation (Widjaja *et al.*, 2009), remorin phospho-isoforms might have been present in the experiments conducted in this study.

Figure 3.13 depicts clearly that *AtLipocalin* was strongly expressed and localized in homogenate, microsomal fraction and only weakly in the PM. No *AtLipocalin* signal could be detected in DRMs, but a faint signal was present in the DSF. After MCD treatment no signal was present in DRM / DSF fractions. This signal distribution correlated with the assumption that a non-raft marker would not be located in DRMs but maybe partially in DSF.

3.2. INVESTIGATION OF CANDIDATE DRM / RAFT PROTEINS

AtRem 1.2 & 1.2 displayed a strong presence in the PM and in DRMs / DSF. A slight dislocation from DRMs into DSF was visible upon MCD treatment (figure 3.13). Almost no AtRem 1.2 / 1.3 signal was detected in the corresponding supernatant after MCD treatment (cf. 2.1.5.1, p. 48).

As a loading control, PM H⁺-ATPases were present in the PM and DRMs. After treatment with 25 mM MCD, the signal for the PM proton ATPases disappeared from DRMs and appeared in the DSF. The antibody used for detection of the PM H⁺-ATPase was generated against a common peptide sequence found in many *A.th.* PM H⁺-ATPases (ATPases 1,2,3,4,6,7,8,9).

Thus, western blot signals must be interpreted with caution as a pool of PM H⁺-ATPases was detected at once but not individual H⁺-ATPases. However, the loading control displayed the expected localization for H⁺-ATPases being present in DRMs & the PM.

3.2.3. AtLipocalin & AtSUC1 / 2 localization

The *A.th.* remorins AtRem 1.2 & 1.3 represent model lipid raft markers as they were detected multiple times in independent proteomic analyses (Borner *et al.*, 2005; Kierszniowska *et al.*, 2008; Morel *et al.*, 2006) and were proven to be strongly sterol-dependent in *A.th.* cell cultures (Kierszniowska *et al.*, 2008).

MCD depletion experiments on Triton X-100 DRMs isolated from *A.th.* leaves (tables 3.5, p. 91 and 3.6, p. 95) also confirmed a strong sterol-dependency of AtRem 1.2 & 1.3. Transient expression of AtRem 1.2 & 1.3 in *A.th.* leaves displayed a patchy appearance at the PM (Jörg Blachutzik, personal communication) resembling membrane microdomains in animals (Lillemeier *et al.*, 2006) and yeasts (Grossmann *et al.*, 2006, 2007).

Sucrose-proton symporters AtSUC1 / 2 were detected clearly in Brij-98 & Triton X-100 DRMs and represented ideal candidates for co-localization studies with AtRem 1.2 & 1.3. AtSUC1 / 2 were characterized to be involved in phloem unloading and to be localized in the PM (Truernit & Sauer, 1995).

In search of a non-raft marker, several proteins were detected in PM preparations used for the isolation of Brij-98 & Triton X-100 DRMs but not in the resulting DRMs: one of these PM proteins was an outer membrane protein of the lipocalin family.

Lipocalin proteins are quite ubiquitously expressed proteins at the PM, mostly localized at the extracellular leaflet. They build complexes with macromolecules, bind to specific cell-surface receptors and small hydrophobic molecules, e.g. lipids. Lipocalins are involved in the sensory perception in mammals (Flower, 1996).

However, in plants, not much is known about functions and structures of lipocalins. Only AtLipocalin (AtTIL) has been investigated for physiological roles (Charron *et al.*, 2008). AtLipocalin was involved in the modulation of oxidative stress. Knock-out plants were very sensitive to sudden temperature drops and transfer into light when they had been grown in darkness. Other functions for AtLipocalin have been proposed in the field of thermotolerance, acting against lipid peroxidation which was induced by severe heat shock (Chi *et al.*, 2009). The membrane attachment of AtLipocalin has not been investigated in detail yet, but it was shown to be susceptible to alkaline release from membranes by treatment with 0.1 M Na₂CO₃ (Chi *et al.*, 2009).

Because AtLipocalin (At5g58070) lacked any identification in DRMs, it was used as a non-raft marker for transient co-expression studies in *A.th.* leaves to obtain a negative control. It has been already used in a comparative, quantitative proteomics study as a PM-resident cold-induced protein which was not present in DRMs (Minami *et al.*, 2009).

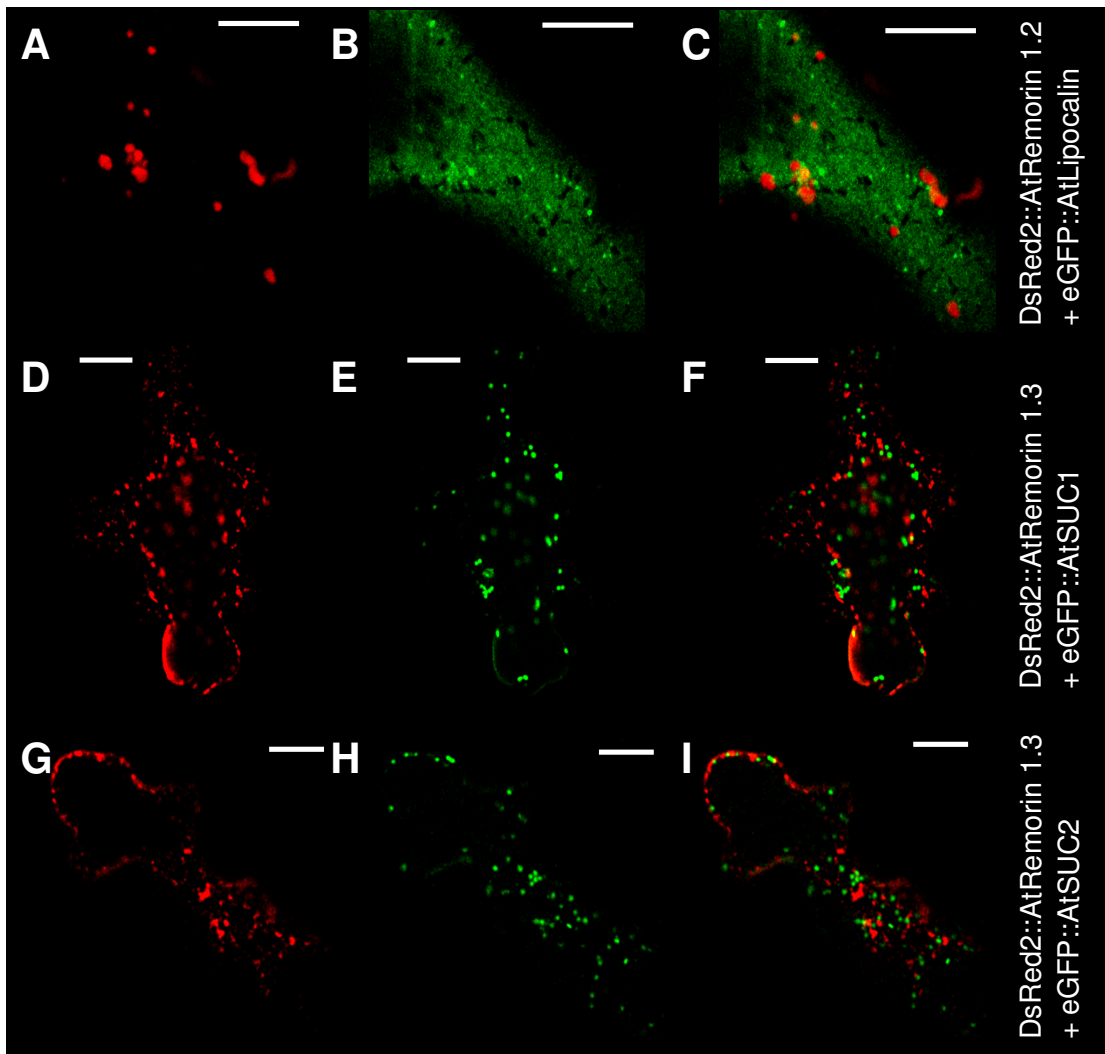


Figure 3.14.: **Co-localization studies of the DRM marker proteins AtRem 1.2 / 1.3 with candidate proteins.** DRM marker protein AtRem 1.2 tagged with eGFP and AtRem 1.3 tagged with DsRed2 were transiently co-expressed with sucrose transporters AtSUC1 / AtSUC2 identified in DRMs and the putative non-raft marker AtLipocalin.

A-C: AtRem 1.2 (**A**) did not co-localize with AtLipocalin (**B**, merge in **C**). Sucrose transporters AtSUC1 (**D-F**) and AtSUC2 (**G-I**) displayed no co-localization with DsRed2::AtRem 1.3 (scale bars = 10 μ m).

As expected, the putative non-raft marker AtLipocalin did not co-localize with AtRem 1.2 (figure 3.14, **A-C**); AtLipocalin (**B**) did not show any co-staining with AtRem 1.2 (**A**, merge in **C**). eGFP::AtLipocalin stained uniformly the PM whereas DsRed2::AtRem 1.2 showed patchy structures.

CHAPTER 3. RESULTS

Transient expression of eGFP-labeled AtSUC1 / 2 together with AtRem 1.3 revealed both proteins to be visible in patchy structures, but AtSUC1 / 2 were partially located in the cytosol / ER. The fluorescence was not overlapping in the regions of the PM marked by AtRem 1.2 / 1.3. Thus, it can be assumed that AtSUC1 / 2 were not located in the same *in vivo* lipid rafts like AtRem 1.2 / 1.3 though they were identified in the same Triton X-100 DRMs.

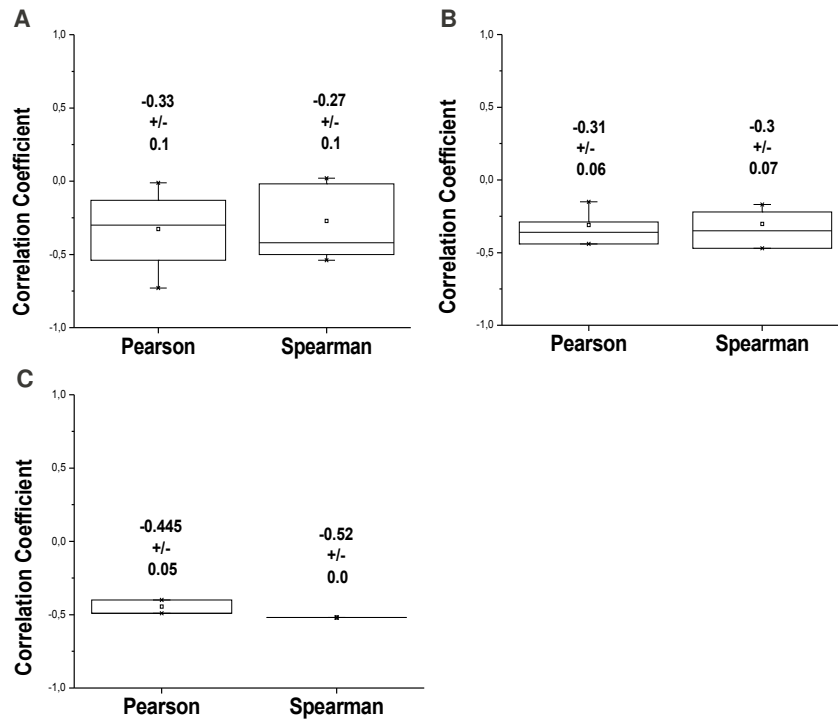


Figure 3.15.: **Statistical analysis of co-localization studies with AtRem 1.2 / 1.3.** DRM marker proteins AtRem 1.2 / 1.3 did not show any co-localization with AtLipocalin (At5g58070, **A**, $n = 6$ independent experiments \pm SE) or AtSUC1 (**B**, $n = 4$) / AtSUC2 (**C**, $n = 2$). Pearson's and Spearman's coefficients < 0 indicate a tendency towards signal separation whereas coefficients > 0 indicate a tendency towards co-localization.

Statistical analysis (figure 3.15) revealed that neither AtLipocalin nor AtSUC1 / 2 co-localized with AtRem 1.2 / 1.3. All co-localization analyses resulted in a Spearman's / Pearson's rank < -0.3 . Ranks < 0 indicate a strong tendency towards separation of both fluorescently labeled proteins (French *et al.*, 2008). Thus, no lipid raft localization could be attributed to AtLipocalin and the sucrose- H^+ symporters AtSUC1 / 2. AtLipocalin seemed to be a valuable non-raft marker for co-localization studies.

3.3 TRANSIENT CO-EXPRESSION OF ABI1, CPK21 & SLAH3

CPK21 was an intrinsic member of DRMs which was highly susceptible to MCD treatment. Further investigations to uncover physiological lipid raft localized protein complexes were started by testing known interaction partners of CPK21. An anion channel of the SLAC1-homologue family, SLAH3 (At5g24030) was shown to interact with CPK21 (Geiger *et al.*, 2010b). Another interaction partner of CPK21 was the central ABA-signaling protein phosphatase 2C, 56: ABI1 (At4g26080). ABI1 plays an important role in stomatal closure, drought stress regulation and has already been studied for a long time (Gosti *et al.*, 1999; Leung *et al.*, 1994, 1997; Meyer *et al.*, 1994). To assess the localization of ABI1, CPK21 and SLAH3 in DRMs / DSF, transient (co-)expression studies in *N.b.* leaves were conducted.

3.3.1. Transient expression in *N.b.*

Upon transient expression of ABI1::CFP, CPK21::YFP and SLAH3::YFP (using binary pCambia vectors suitable for transformation) highly pure PM and DRMs were isolated from infiltrated *N.b.* leaves. Western blot analysis of PM fractions in figure 3.16A & B revealed clear PM-resident signals for CPK21 and SLAH3. CPK21 was clearly detected in DRMs.

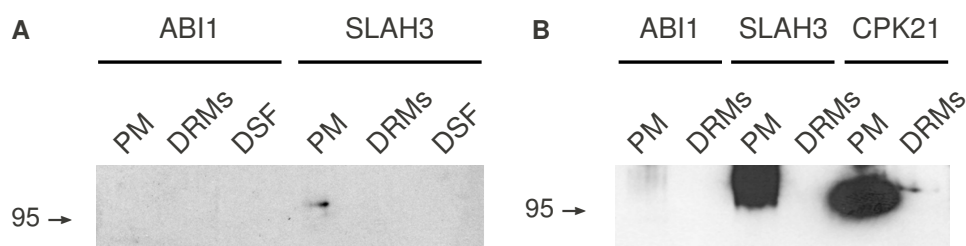


Figure 3.16.: **Transient expression of ABI1, CPK21 & SLAH3 in *N.b.* PM and DRMs / DSF isolated from these PM preparations.**

A: Expression of ABI1::CFP in *N.b.* led to no PM, DRMs or DSF localization (fusion protein: 75 kDa). SLAH3::YFP (fusion protein: 100 kDa) was clearly detectable in the PM but not in DRMs or DSF. Protein load = 1.6 µg.

B: CPK21::YFP (fusion protein: 90 kDa) and SLAH3::YFP were clearly detected in the PM but only CPK21 was present in DRMs. Protein load = 5 µg.

After all single expression studies, only CPK21::YFP and SLAH3::YFP reached the PM whereas no ABI1::CFP signal was visible in the PM. Only CPK21::YFP gave rise to an immunoblot signal in DRMs, supporting the notion from mass spectrometric data that CPK21 resides in DRMs. In contrast to this, ABI1::CFP was identified only in mass spectrometric

measurements and not on western blots with infiltrated PM & DRMs. Therefore, ABI1::CFP localization in DRMs might be highly transient and dependent upon presence of other proteins. ABI1 might regulate other proteins in DRMs and dissociate immediately after the interaction.

3.3.1.1. Assaying sterol dependency of transiently expressed CPK21

For further confirmation of the strong sterol dependency of CPK21 from suggestions in the mass spectrometric data, an immunoblot was performed on DRMs / DSF isolated from CPK21::YFP infiltrated *N.b.* plants. If CPK21 localization in DRMs was strongly affected by MCD, then CPK21 would very likely be a strongly sterol-dependent member of *A.th.* DRMs, as mass spectrometric data suggested.

To test this in more detail, transiently expressed CPK21::YFP was subjected to MCD treatment, and DRMs / DSF were isolated. CPK21 signal strength in DRMs should decrease after MCD treatment if CPK21 was an intrinsic member of lipid rafts which depends upon sterols.

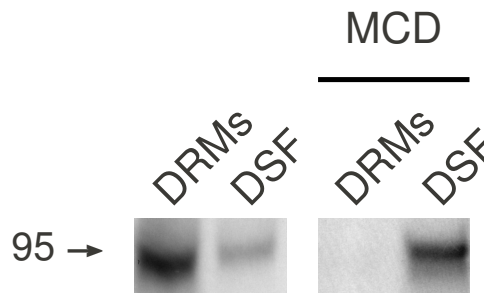


Figure 3.17.: **Transient expression of CPK21::YFP in *N.b.* ± MCD treatment.**

The majority of CPK21::YFP located in DRMs whereas after MCD treatment no CPK21::YFP signal was detected in DRMs. CPK21::YFP traversed from DRMs into DSF upon MCD application. Protein load = 20 µg.

MCD treatment strongly affected CPK21::YFP localization in infiltrated *N.b.* plants. Before MCD application, most of the CPK21::YFP signal was detected in Triton X-100 DRMs. But after treatment with 25 mM MCD for 30 min at 37 °C, no CPK21::YFP signal remained in Triton X-100 DRMs (figure 3.17, right panel). All CPK21::YFP disappeared out of DRMs into the DSF fraction.

Thus, CPK21 localization in Triton X-100 DRMs exhibited a strong sterol-dependency.

3.3. TRANSIENT CO-EXPRESSION OF ABI1, CPK21 & SLAH3

3.3.2. Transient co-expression in *N.b.*

As single expression studies in *N.b.* revealed that only CPK21 was located in Triton X-100 DRMs (cf. 3.3.1, p. 103), co-expression studies with combinations of ABI1, CPK21 and SLAH3 were performed. It was supposed to see an interaction between CPK21 and SLAH3 as electrophysiological studies revealed CPK21 to activate the anion channel SLAH3 (Geiger *et al.*, 2010a).

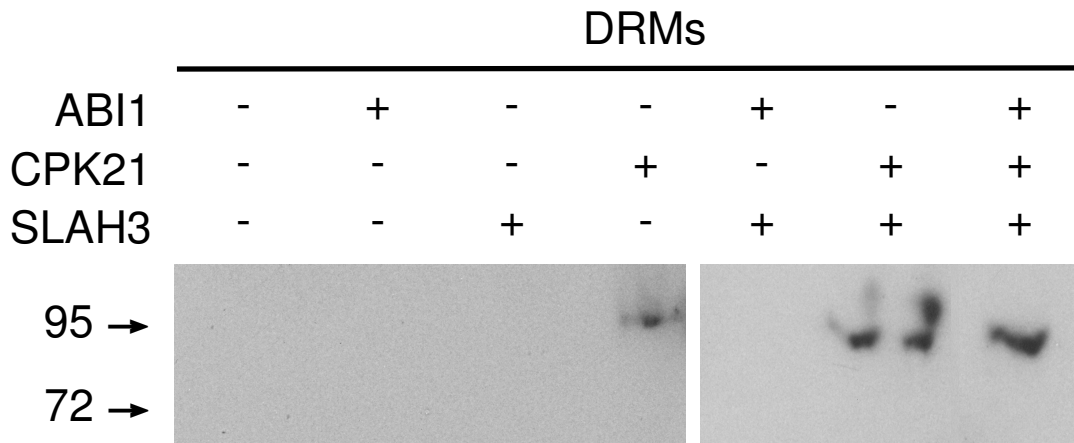


Figure 3.18.: **Transient co-expression of ABI1, CPK21 & SLAH3 in *N.b.* DRMs.**

Comparing the expression of ABI1, CPK21 and SLAH3 in *N.b.* PM revealed only CPK21::YFP to be clearly expressed in Triton X-100 DRMs.

Co-expression of ABI1::YFP and CPK21::YFP led to no DRM signal, while CPK21::YFP and SLAH3::YFP displayed two signals at approx. 90 & 100 kDa in DRMs. Additional ABI1::YFP expression released the higher 100 kDa signal from Triton X-100 DRMs. Protein load = 25 µg.

Figure 3.18 indicates a putative interaction of CPK21::YFP and SLAH3::YFP in DRMs of *N.b.* Two signals at approx. 90 and 100 kDa were visible which could be attributed to CPK21::YFP at 90 kDa and SLAH3::YFP at 100 kDa. Single infiltrations only displayed a localization of CPK21::YFP in Triton X-100 DRMs while all other constructs were not located in DRMs.

The kinase CPK21::YFP seemed to trigger the anion channel SLAH3::YFP into DRMs. An additional co-expression of CPK21::YFP and SLAH3::YFP together with ABI1::CFP should potentially alleviate the DRM localization of SLAH3::YFP. As seen on the right panel in figure 3.18, ABI1 addition induced dislocation of the anion channel SLAH3 out of DRMs. Only CPK21::YFP remained in DRMs. Investigating the signal traversal for CPK21::YFP

CHAPTER 3. RESULTS

and SLAH3::YFP upon ABI1::CFP addition required a further assay, where DRMs and DSF of infiltrated *N.b.* leaves were compared.

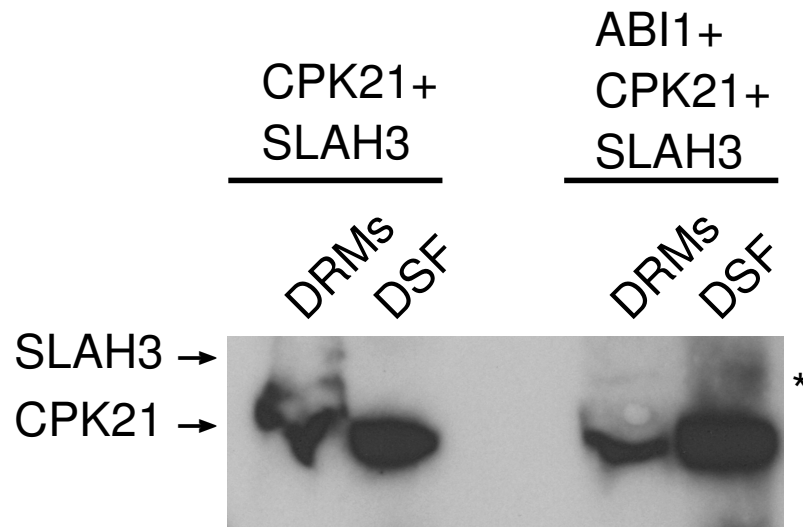


Figure 3.19.: **Transient co-expression of ABI1, CPK21 & SLAH3 in DRMs & DSF of *N.b.* leaves.**

CPK21::YFP co-expressed with SLAH3::YFP resulted in the appearance of two bands in Triton X-100 DRMs representing CPK21 & SLAH3 but only CPK21 was present in the DSF.

Additional expression of ABI1::CFP led to disappearance of the SLAH3 signal in DRMs and traversal of SLAH3 into the DSF (indicated by asterisk). Protein load = 25 μ g.

CPK21::YFP and SLAH3::YFP interacted in Triton X-100 DRMs, but additional expression of the phosphatase ABI1::CFP diminished the SLAH3::YFP signal from DRMs. This led to transition of SLAH3::YFP from Triton X-100 DRMs into the DSF. CPK21 in DRMs was not affected by additional ABI1 expression. Thus, the alteration of SLAH3 localization should be a direct effect of the protein phosphatase 2C, ABI1.

The visualization of the ABI1-dependent SLAH3 re-localization was improved by slightly altering the co-expression system. A V5-tag was fused C-terminally to ABI1 and SLAH3 instead of the CFP / YFP fluorescent tags. This step enabled separate detection of ABI1::V5, CPK21::YFP and SLAH3::V5 upon co-expression with different antibodies on different western blots.

3.3. TRANSIENT CO-EXPRESSION OF ABI1, CPK21 & SLAH3

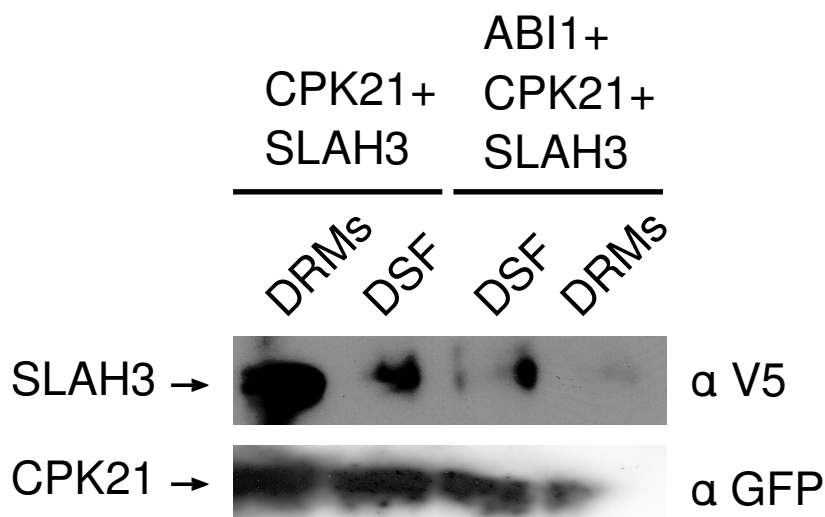


Figure 3.20.: **Transient co-expression of ABI1::V5, CPK21::YFP and SLAH3::V5 in N.b. DRMs & DSF.**

Co-expressed ABI1::V5 dislocated SLAH3::V5 signals from Triton X-100 DRMs into DSF. Only a very faint signal was detected for SLAH3::V5 in DRMs whereas a stronger signal located in the DSF.

CPK21::YFP gave an almost equal signal in co-expression studies with SLAH3::V5. Upon additional co-expression of ABI1::V5, CPK21::YFP was concentrated in Triton X-100 DSF and displayed only a weak signal in DRMs. Protein load = 25 µg.

Co-expression of YFP- and V5-tagged constructs enabled the parallel detection of ABI1::V5, CPK21::YFP and SLAH3::V5 fusion constructs on separate immunoblots (figure 3.20). Upon co-expression of CPK21::YFP and SLAH3::V5, the SLAH3::V5 fusion construct was detected mainly in Triton X-100 DRMs and only to a little extent in the DSF. However, the amount of SLAH3::V5 in Triton X-100 DRMs was clearly reduced when ABI1::V5 was additionally co-expressed. Thus, additional presence of ABI1::V5 led to the dissociation of SLAH3::V5 from Triton X-100 DRMs into the DSF.

When CPK21::YFP and SLAH3::V5 were expressed alone, SLAH3::V5 was strongly present in Triton X-100 DRMs. Concomitantly, CPK21::YFP was also affected by ABI1::V5 expression as it was detected mainly in the Triton X-100 DSF after ABI1::V5 co-expression.

To examine sterol dependency of the CPK21 and SLAH3 complex in DRMs, sterols of PMs co-expressing CPK21::YFP and SLAH3::V5 were disrupted using MCD. Subsequently, MCD-treated and non-treated DRMs and DSF were isolated.

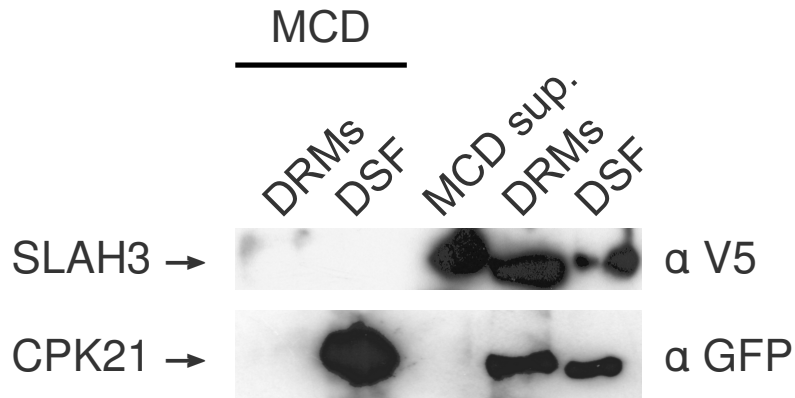


Figure 3.21.: **Sterol dependency of the CPK21::YFP and SLAH3::V5 complex.**

Co-expressed CPK21::YFP and SLAH3::V5 were both detected in DRMs and DSF. After MCD treatment, CPK21::YFP localized exclusively into the DSF while SLAH3::V5 was strongly present in the MCD supernatant. SLAH3::V5 remained only to a very little extent in the DRMs after MCD application. Protein load = 25 µg.

The supernatant of the ultra centrifugation after MCD treatment and corresponding DRMs and DSF ± MCD treatment were applied on an immunoblot (figure 3.21). CPK21::YFP co-expressed with SLAH3::V5 displayed a similar distribution like CPK21::YFP alone (figure 3.17, p. 104). Prior to MCD treatment, CPK21 and SLAH3 were present in DRMs and DSF. After MCD application, CPK21 exclusively located into the DSF and was not detected neither in DRMs nor in the MCD supernatant.

In contrast to this, sterol depletion affected SLAH3::V5 in a different manner. Before sterol depletion SLAH3::V5 was mostly present in DRMs and to a smaller extent in the DSF. As DRMs were disrupted by MCD, SLAH3::V5 was only weakly present in DRMs. The majority of the SLAH3::V5 signal appeared in the MCD supernatant.

Regardless of the re-distribution of CPK21 and SLAH3 after sterol depletion, both proteins were no longer present in DRMs. While CPK21 redistributed from DRMs exclusively to the DSF, SLAH3 was mainly present in the MCD supernatant and not in the DSF. Therefore, CPK21 and SLAH3 both depend upon a sterol-rich membrane environment to build the CPK21 / SLAH3 protein complex in DRMs.

4

Discussion

Proteomic analyses always deliver a first snapshot of the protein composition in a certain compartment. Uncovering the protein composition provides an impression about the status of the protein machinery in the cells, far beyond the information obtained by simple transcriptional analysis. The major advantages of proteomic studies are the detection of multiple splicing isoforms, alternative translation initiation sites and elucidation of post-translational modifications like lipidation, phosphorylation or ubiquitylation (Peck, 2005). The technical advancements in the last decades enabled researchers to investigate the protein composition of GAPs in the plant PM (Borner *et al.*, 2003) and organelle proteomes (Jones *et al.*, 2009; Lilley & Dupree, 2007; Whiteman *et al.*, 2008) as well as phosphorylation status of the plant PM (Chen *et al.*, 2010).

Even quantitative analyses of protein phosphorylation patterns in the plant PM upon abiotic salt stress (Malakshah *et al.*, 2007) or sucrose-induction (Niittylä *et al.*, 2007) have been performed. Differential phosphorylation patterns disclose potential regulation sites in proteins, for instance does the phosphorylation state of H⁺-ATPase residue Thr881 regulate the activity of this proton pump (Niittylä *et al.*, 2007). This phosphorylated residue had not been detected in the numerous previous studies regarding the H⁺-ATPase which did not apply mass spectrometric methodology. Investigations of the quantitative changes in phosphorylation patterns and protein composition will surely broaden our knowledge of the complex protein ensemble within the plant cell (Chen & Harmon, 2006).

In the study herein, the protein composition of Brij-98 and Triton X-100 DRMs was investigated. To no surprise, signaling components represent the largest group of proteins in PM DRMs of *A.th.* All information gained from proteomic analyses of DRMs are just hints for the *in vivo* lipid raft protein composition. Thus, physiological investigations on DRM protein complexes are necessary to reveal further information about the physiological relevance of identifying proteins biochemically in DRMs.

4.1 ARABIDOPSIS THALIANA DRM PROTEIN COMPOSITION

The strong enrichment in signaling proteins for DRMs obtained from *A.th.* PMs is inevitable as the PM and corresponding microdomains are pathways from the intracellular to the extracellular space. Traversal of substances and signals through the PM needs adequate platforms. Hence, a strong enrichment of signaling and transport proteins in Brij-98 and Triton X-100 DRMs is concomitant with a high content of signaling and transport proteins in the underlying bulk plasma membrane.

4.1.1. DRMs enriched in signaling & transport proteins

Among the transport proteins, three big clusters were present: ABC transporters, aquaporins and ATPases. The high abundance of these protein clusters in previous Triton X-100 DRM studies (Kierszniowska *et al.*, 2008; Minami *et al.*, 2009; Morel *et al.*, 2006; Shahollari *et al.*, 2005) surely results from their high expression level in the PM. Mass spectrometric analyses of protein compositions always obtain the most highly expressed proteins as a matter of signal-to-noise ratio. Proteins, which are less abundant, are not detected with crude HPLC MS technology, for instance, redox system components (Lüthje *et al.*, 2009). Therefore, affinity-purification has been proven to be a solution for this abundance problem. Affinity-tag purification uncovered a low abundance protein complexes involved in pathogen defense. RIN4, a putative interactor of the LRR protein kinase RPS2¹, was identified by this approach (Qi & Katagiri, 2009).

Signaling proteins like CPKs and LRR protein kinases were strongly enriched in Brij-98 and Triton X-100 DRMs. This is a common phenomenon among plant DRM proteomic studies (cf. section 4.1.2). Especially the cluster of LRR protein kinases is strongly present in DRMs (Shahollari *et al.*, 2004, 2005). Many of these LRR protein kinases have not been attributed to a specific function in planta yet. The flagellin receptor FLS2 (flagellin sensitive 2) represents an important LRR protein kinase which is responsible for initiation of the plant immune response to bacterial attack (Chinchilla *et al.*, 2007). Due to their localization in lipid rafts at the PM, FLS2 receptor complexes could represent plant equivalents to animal pathogen recognition complexes (Robatzek, 2007).

In mammals, signaling kinases were found to be strongly enriched in a quantitative proteomic investigation of DRMs (Foster *et al.*, 2003). A further degree of enrichment (> 10-fold for Lyn protein tyrosine kinases with respect to untreated DRMs) was achieved by MCD treatment. DRMs in mammals and plants display an inevitable bias on signaling proteins, mainly protein kinases.

¹Response to *Pseudomonas syringae* 2

4.1.2. Correlation with previous DRM studies

Previously conducted plant DRM studies all concentrated on Triton X-100 DRMs. No other detergents like Brij-98 were used for the generation of plant DRMs though other detergents (Chamberlain, 2004) are widely used in mammalian research (Heffer-Lauc *et al.*, 2007; Karacsonyi *et al.*, 2005; Staneva *et al.*, 2005), for instance in the field of HIV research (Campbell *et al.*, 2004) or neurobiology (Gil *et al.*, 2006). The ability to isolate mammalian DRMs at the physiological temperature of 37 °C disclosed proteins involved in neurotransmitter release to be located in Brij-98 DRMs (Gil *et al.*, 2006).

For the first time, DRMs in plants have also been isolated with Brij-98 in addition to Triton X-100. As plants are heterothermic organisms with no constant physiological temperature, DRM isolations with both detergents were carried out at 4 °C. Comparing the protein composition between Brij-98 and Triton X-100 DRMs revealed only minor differences: Brij-98 seems to be "less" effective in solubilizing membranes. The presence of proteins with a higher molecular weight and more TMDs are valuable indicators for this hypothesis.

Mammalian Brij-98 DRMs displayed a slightly decreased cholesterol & sphingolipid enrichment in comparison to Triton X-100 DRMs (Schuck *et al.*, 2003). Triton X-100 has also been more effective in solubilization of specific DRM marker proteins in animals (Schuck *et al.*, 2003). If Brij-98 is less effective in solubilizing the bulk PM, more proteins will remain in the detergent-insoluble area which is isolated as DRMs after detergent treatment.

The additional extraction of Brij-98 DRMs did not lead to a completely different set of DRM proteins given the extraction parameters used in this study: 1 % v/v final detergent concentration, 15:1 ratio of detergent to protein and incubation at 4 °C for 30 minutes.

Comparing the resulting DRM protein list with previous publications discloses a big degree of overlap with the work of Kierszniowska *et al.* (2008) on *A.th.* cell cultures and Minami *et al.* (2009) on *A.th.* seedlings. In these studies rather comprehensive lists of DRM proteins (340 in Kierszniowska *et al.*, 2008 and 98 in Minami *et al.*, 2009) have been published which might have led to the high degree of overlap. Both surveys and the investigations performed by this study utilized state-of-the-art HPLC MS methodology for protein identification.

It may be reasonable to attribute the high number of identified DRM proteins to the usage of comparable technology. Signaling and transport proteins were also enriched in the DRMs isolated from *A.th.* seedlings (Minami *et al.*, 2009) comparable to the situation in this study. The same was pertinent for other studies on *A.th.* seedlings (Shahollari *et al.*, 2004, 2005). But for DRMs of *A.th.* cell cultures, ABC transporters and cell wall anchoring / linking proteins were the most prominent functions (Kierszniowska *et al.*, 2008). In particular, after MCD-induced sterol depletion these functional groups were strongly affected.

Many of the identified 246 Brij-98 and Triton X-100 DRM proteins in this study were not spotted in DRMs by other researchers in the field. Almost half of the DRM proteins (120 proteins, 48.8 %) were not identified in previous analyses of *A.th.* DRMs (Borner *et al.*, 2005; Kierszniowska *et al.*, 2008; Minami *et al.*, 2009; Mongrand *et al.*, 2004; Morel *et al.*, 2006; Shahollari *et al.*, 2004, 2005). This high number of newly detected DRM proteins may be due to the fact that this is the first study investigating Brij-98 & Triton X-100 DRMs in *A.th.* leaves. Hence, the "new" DRM proteins may be attributed to the effects of the tissue specific isolation of DRMs in leaves comprised mainly of mesophyll cells. Using an additional non-ionic detergent like Brij-98 surely contributed to the identification of novel DRM constituents in *A.th.*

Comparing only the identified Triton X-100 DRM proteins with previously conducted research resulted in a total of 88 (45.6 %) novel Triton X-100 DRM proteins. A high degree of overlap (figure 4.1) was repeatedly present with the studies of Kierszniowska *et al.* (2008) and Minami *et al.* (2009). Thus, the majority of the novel identified DRM proteins may have emerged from utilizing a novel tissue for the isolation of DRMs.

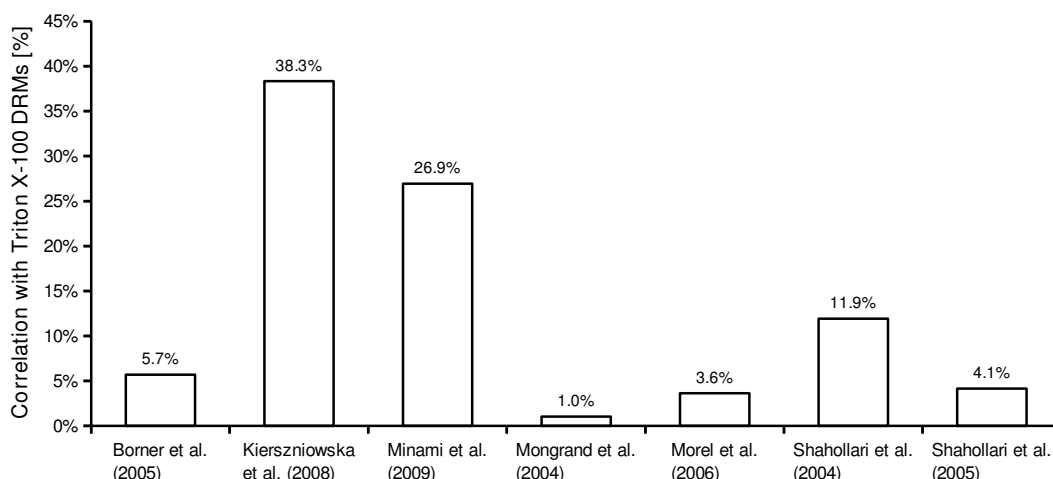


Figure 4.1.: **Correlation with previous Triton X-100 DRM studies.** The percentage of common Triton X-100 DRM proteins with previous DRM investigations is depicted. A high degree of overlap was present with studies conducted by Kierszniowska *et al.* (2008) on *A.th.* cell cultures and Minami *et al.* (2009) on *A.th.* seedlings. However, the amount of commonly identified DRM proteins with the other investigations was rather low.

A lower number of common DRM proteins is visible for the investigation on *A.th.* callus membranes by Borner *et al.* (2005): potential differences in the applied techniques may have led to this great difference. Borner *et al.* (2005) applied DIGE analysis to detect depleted /

4.1. ARABIDOPSIS THALIANA DRM PROTEIN COMPOSITION

enriched proteins in DRMs. DRM proteins were identified by HPLC MS analysis of excised 1D SDS-PAGE protein bands. The isolation of DRMs was not performed from purified PM fractions but from total membrane pellets (microsomal fractions). Substantial differences in DRMs isolated from total membrane pellets and PMs could not be spotted yet but it may be tempting to propose a higher degree of purity for PM DRMs.

Using *N.t.* BY-2 cells, Morel *et al.* (2006) detected a substantial enrichment of cell wall-associated, signaling and trafficking proteins in DRMs relative to the PM. 145 DRM proteins were identified by in-gel and additional in-solution digestion, techniques which were also used in a comparable manner in this study (cf. 2.3.1.2). However, the identified DRM proteins were annotated with respect to different known plant databases, resulting in a very low number of *A.th.* DRM proteins which were common between this study and Morel *et al.* (2006). Looking at the list of identified DRM proteins, some familiar protein families like ABC transporters, CPKs and cytoskeleton components also arose in this study.

Summarizing all these proteomic investigations of Triton X-100 DRMs, two proteins are regularly spotted in DRMs: AtSku5 (Borner *et al.*, 2005; Kierszniowska *et al.*, 2008; Minami *et al.*, 2009; Morel *et al.*, 2006; Shahollari *et al.*, 2004, 2005) and AtRem 1.3 (Kierszniowska *et al.*, 2008; Minami *et al.*, 2009; Shahollari *et al.*, 2004).

AtSku5 represents an extracellular GPI-anchored protein putatively involved in cell wall processes. AtRem 1.3 is a PM protein localized at the cytosolic leaflet and attached to the PM via palmitate anchors as indicated by two putative palmitoylation sites at the C-terminus. The presence of both an extracellularly located and cytosolically attached PM protein as members of the DRMs might be representative for two very important classes of lipid raft functions: structural cell wall organization (Sedbrook *et al.*, 2002) and scaffolding / signaling (Raffaele *et al.*, 2009a).

One interesting aspect is the differential enrichment of signaling and cell wall / structure proteins between studies conducted in cell cultures (Kierszniowska *et al.*, 2008; Morel *et al.*, 2006) and whole plant tissues. *A.th.* seedlings (Minami *et al.*, 2009; Shahollari *et al.*, 2004, 2005), callus membranes (Borner *et al.*, 2005) and leaves (this study) displayed a strong enrichment of signaling functions in DRMs. In contrast to this, cell cultures were enriched for cell wall anchoring / structure proteins in DRMs. It may be speculated that DRMs are devoted to signaling functions in whole plants whereas cell cultures might display this enrichment to a slighter extent.

4.1.3. Post-translational modifications

One characteristic feature of animal lipid rafts is the high amount of lipid modified proteins. While prenylation drives proteins to be located outside of lipid rafts, myristoylation and palmitoylation seem to be involved in the regulation of raft localization for several mammalian proteins (Melkonian *et al.*, 1999). Lipid modifications enhance the affinity of certain proteins (e.g. c-Src protein tyrosine kinase in mammals or CPK21 in plants) for lipid rafts due to the addition of saturated fatty acid chains (see section 1.1.4, p. 7 for a detailed overview on the lipidation mechanisms).

To consider the role of lipid modifications in lipid raft localization of DRM proteins, lipid modifications of identified DRM and PM proteins were analyzed (figure 4.2 and 4.3).

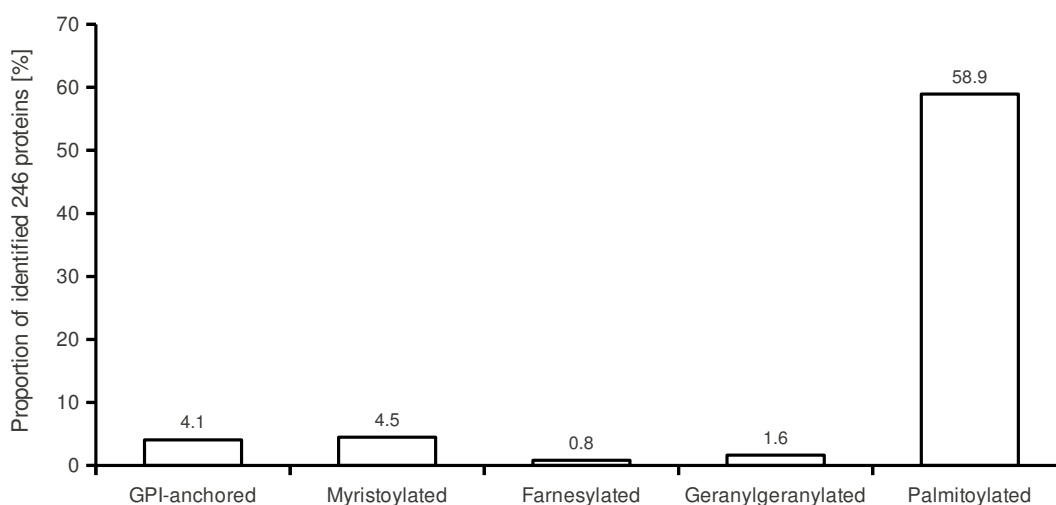


Figure 4.2.: **Post-translational lipid modifications in Brij-98 & Triton X-100 DRMs.** Palmitoylation represented by far the most prominent lipid modification of DRM proteins.

The major lipid modification in plant Brij-98 & Triton X-100 DRMs was palmitoylation / S-acylation (58.9 %, figure 4.2). All other lipidations were predicted to a much lesser extent. Myristoylation and GPI-anchorage also play important roles in targeting proteins into DRMs. Only very few prenylated proteins were present in DRMs supporting a similar notion like in animals: prenylation prevents DRM localization of proteins (Melkonian *et al.*, 1999).

For the majority of the identified DRM proteins, lipid modifications were computationally predicted as no experimental evidence was available. This is an important point to consider, as protein lipidations *in vivo* were only studied for a very small number of plant proteins.

4.1. ARABIDOPSIS THALIANA DRM PROTEIN COMPOSITION

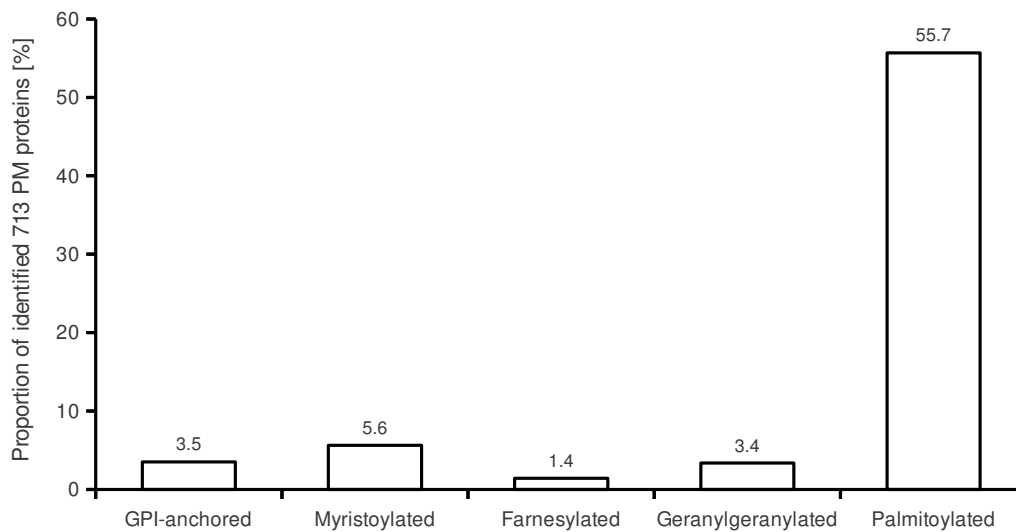


Figure 4.3.: **Post-translational lipid modifications in the PM.** For the PM fraction used to isolate Brij-98 and Triton X-100 DRMs the same pattern of lipidations occurred. The majority of the PM proteins were predicted to be palmitoylated.

Figure 4.3 depicts a similar situation for the PM concerning lipidation. As for DRMs (figure 4.2), palmitoylation presents the major post-translational lipid modification in the PM. However, farnesylated and geranylgeranylated proteins were enriched in the PM with respect to DRMs. Only 2.4 % of the DRM proteins (all Ras-related proteins involved in protein trafficking) but 4.8 % of the PM proteins (Ras-related proteins, many AtRab trafficking proteins and G protein subunit γ) were prenylated. This highlights a depletion of prenylated proteins after the isolation of DRMs from PMs specifically excluding certain signaling and trafficking proteins in a similar manner as in the mammalian system (Melkonian *et al.*, 1999).

4.1.4. Sterol-depletion by MCD identifies "true" raft members

Depletion of sterols by MCD revealed some proteins to strictly depend upon sterol-enriched microdomains. As lipid rafts are supposed to be enriched in saturated phospholipids, sphingolipids and sterols (Simons & Ikonen, 1997), this depletion of sterols could be a hint for the identification of *in vivo* lipid raft proteins (Scheiffele *et al.*, 1997; Simons *et al.*, 1998). Contrary to the situation in fungi or mammals, where only one major sterol (ergosterol or cholesterol) constitutes the biological membranes, plants feature a very distinct sterol composition with a mixture of phytosterols (Hartmann, 1998).

These sterols have been studied for their effects on water permeability in soybean PC bilayers (Schuler *et al.*, 1991). The two major phytosterols sito- and stigmasterol apparently have different roles in maintaining membrane integrity. Sitossterol was very efficient in reducing PM permeability while stigmasterol exhibited no significant effect (Schuler *et al.*, 1991). Another piece of evidence for a differential role for the major phytosterols is present at the regulation of the plant PM H⁺-ATPase. The activity of the proton ATPase was subject to many studies (Sussman, 1994). In one of these investigations, Grandmougin-Ferjani *et al.* (1997) discovered that cholesterol and stigmasterol play an important role in modulating the transporter activity while sitosterol and other phytosterols displayed inhibitory effects. Thus, specific phytosterols seem to regulate H⁺-ATPase activity in addition to protein phosphorylations (Morsomme & Boutry, 2000) and protein complex formation (Liu *et al.*, 2009a).

Sterol disruption by MCD is widely used for the identification of sterol-dependent processes. An intact sterol environment is required for polar PIN2 localization after cytokinesis as shown in the sterol biosynthesis mutant *cpi1-1* (Men *et al.*, 2008). As an alternative to the use of sterol biosynthesis mutants, acute sterol depletion by the chemical reagent MCD may be applied (Dietrich *et al.*, 2002; Rodal *et al.*, 1999; Subtil *et al.*, 1999). MCD treatment leads to perturbation of cholesterol & sphingolipid-enriched domains at the PM (Ilangumaran & Hoessli, 1998; Ohvo *et al.*, 1997).

Investigations on the MCD effects on the plant PM uncovered a similar situation as for the mammalian PM (Roche *et al.*, 2008). Treating *N.t.* BY-2 cells with 20 mM MCD decreased the amount of free sterols in the PM by 50 % and led to dissociation of a plant lipid raft marker, the *N.t.* NADPH oxidase NtRbohD, from DRMs (Roche *et al.*, 2008). A comparable MCD effect could be observed in *A.th.* cell cultures which were treated with varying concentrations of MCD (Kierszniowska *et al.*, 2008). Using MCD concentrations above 20 mM, a clear reduction in the amount of sterols at the PM was observed.

Comparing the protein composition in *A.th.* cell culture DRMs before and after MCD treatment in a quantitative proteomics approach, Kierszniowska *et al.* (2008) discovered a core set of lipid raft proteins comprised mainly of GAPs. Signaling proteins were observed as more variable constituents of DRMs and were considered as stimulation-dependent members of biochemically isolated DRMs by the authors. But these variable constituents may trigger important processes for the plant like cytokinesis, plant defense signaling and polar transport.

In this study, signaling proteins were strongly impaired by MCD treatment and dislocated from DRMs. Especially the protein phosphatase ABI1, AtRem 1.2 & 1.3 and the protein kinase CPK21 were affected. These proteins disappeared from DRMs and did partially relocate to the DSF or to the MCD supernatant. ABI1, AtRem 1.3 and P-type H⁺-ATPase 2 were not completely removed from DRMs but could be spotted in the MCD supernatant.

4.1. ARABIDOPSIS THALIANA DRM PROTEIN COMPOSITION

MCD treatment also affected LRR protein kinases severely. Among these LRR protein kinases, the BAK-1 interacting receptor-like kinase 1 (BIR1, At5g48380) was present. BAK1 is a LRR protein kinase present at the cell surface (Heese *et al.*, 2007) and functions together with another receptor-like kinase, BRI-1, in brassinosteroid signaling (Li *et al.*, 2002; Nam & Li, 2002). BAK1 is also responsible for recognition of the bacterial elicitor flagellin in a receptor complex together with FLS2. BAK1 activates plant defense signaling by dimerizing with FLS2 upon flagellin perception (Chinchilla *et al.*, 2007). BIR1 exhibited a strong phenotype in knock-out plants (Gao *et al.*, 2009). Knocking out BIR1 led to extensive cell death, constitutive defense response and suppression of MAPK4 activity. Thus, Gao *et al.* (2009) suggested an important role for BIR1 in negative regulation of plant resistance signaling.

Unfortunately, no FLS2 or BAK-1 could be identified directly in the Brij-98 and Triton X-100 DRMs. But one has to keep in mind, that the DRMs isolated in this study were not elicited / untreated. It may be assumed that without bacterial elicitation, expression levels of BAK-1 and FLS2 might be just too low to be identified by MS. Further studies comparing the protein composition in DRMs before and after bacterial elicitation may shed more light on whether plant defense complexes are located in DRMs. Quantitative proteomic analysis of intrinsic bacterial *avrRpm 1* type III effector expression revealed an enrichment of certain phospho-isoforms after elicitation, for instance AtRem 1.2 (Widjaja *et al.*, 2009).

Despite all the advantages of protein composition analyses after MCD treatment, there are considerations to be taken: MCD treatment not only alters PM sterol levels, but also leads to a concomitant reorganization of the actin cytoskeleton (Kwik *et al.*, 2003) and impaired clathrin-coated vesicle budding (Rodal *et al.*, 1999; Subtil *et al.*, 1999). Additionally, lateral mobility of raft and non-raft proteins decreased upon MCD application without any great difference (Kenworthy, 2008). A possible explanation for this observation might be loss of cholesterol from the boundary of lipid rafts (Ilangumaran & Hoessli, 1998) and concomitant reorganization of the actin cytoskeleton (Kwik *et al.*, 2003). This leads to the same level of mobility for raft and non-raft proteins in the PM as no sub-compartmentalization by the cytoskeleton is present anymore (Kusumi & Sako, 1996).

The association of the cytoskeleton with sub-compartmentalization processes has not yet been examined for plants. However, for polar growth processes, there might be a connecting link. *A.th.* FH5 represents a tip-located, membrane-anchored actin-nucleating protein, which is strongly involved in the organization of subapical actin structures in rapidly growing pollen tubes (Cheung *et al.*, 2010). As lipid microdomains also play an important role in pollen tube growth (Liu *et al.*, 2009b), polar growth at the pollen tube tips might depend both on the cytoskeleton and lipid microdomains.

4.2 RAFT & NON-RAFT MARKERS

In the mammalian system, availability of specific protein markers which localize in or are excluded from lipid rafts greatly facilitated raft research (Mayor & Rao, 2004). Transferrin and folate receptors represent two GAPs which do not accumulate in DRMs (Hao *et al.*, 2001; Varma & Mayor, 1998) and are suitable non-raft markers. The GAP Thy-1 (Brügger *et al.*, 2004; Friedrichson & Kurzchalia, 1998; Holowka *et al.*, 2000), the transmembrane adaptor protein LAT (Head *et al.*, 2006; Wilson *et al.*, 2004) and the palmitoylated c-Src kinases (Resh, 1999; Simons & Ikonen, 1997; Stulnig *et al.*, 1998) are highly present in DRMs and serve often as mammalian raft markers. Until now, no corresponding raft and non-raft markers for *A.th.* had been identified.

4.2.1. AtRem 1.2 / 1.3 as model lipid raft markers

A plant lipid raft marker would fulfill several expectations: strong presence in Triton X-100 DRMs, strict dependency upon a sterol-rich environment at the PM and microscopic *in vivo* localization in small (< 200 nm) defined compartments at the plant PM. A naturally high expression level and existence of many plant homologues would complete the profile of an ideal lipid raft marker.

The *A.th.* remorins AtRem 1.2 & 1.3 represent such candidates to be plant lipid raft markers. Remorins have already been identified in many plant species like *A.th.* (Alliotte *et al.*, 1989; Bariola *et al.*, 2004), *M.t.* (Lefebvre *et al.*, 2010), *Oryza sativa* (Malakshah *et al.*, 2007) and *S.t.* (Bariola *et al.*, 2004; Raffaele *et al.*, 2007). AtRem 1.2 & 1.3 are among the 10 % most highly expressed genes in *A.th.* (Raffaele *et al.*, 2007) which facilitated their proteomic identification in many studies analyzing Triton X-100 DRMs (Kierszniowska *et al.*, 2008; Minami *et al.*, 2009; Shahollari *et al.*, 2004).

A strict sterol dependency of these *A.th.* remorins was observed in *A.th.* cell cultures (Kierszniowska *et al.*, 2008) and *A.th.* leaves. Upon MCD application, AtRem 1.2 & 1.3 dislocated from Triton X-100 DRMs and could be detected in the MCD supernatant (Kierszniowska *et al.*, 2008). This strict sterol dependency has also been observed for the *Solanum tuberosum* remorin StRem 1.3 (Raffaele *et al.*, 2009a). MCD treatment perturbed StRem 1.3 localization in DRMs and StRem 1.3 clustering in immunogold-labeled electron microscopic structures (Raffaele *et al.*, 2009a). Accordingly, there is evidence in this study that AtRem 1.2 & 1.3 behave in a similar manner like the established lipid raft marker StRem 1.3 from *Solanum tuberosum*. MCD treatment depleted both AtRem 1.2 & 1.3 from DRMs as observed in immunological assays (figure 3.13, p. 98) and mass spectrometric analyses (tables 3.5, p. 91 and 3.6, p. 95).

Examining the localization of fluorescently labeled AtRem 1.2 & 1.3 in *A.th.* epidermal cells by transient co-expression displayed patchy, small structures at the PM (Jörg Blachutzik, personal communication). These structures co-localize well with the established lipid raft marker StRem 1.3 which fortifies the lipid raft localization of these two *A.th.* remorin proteins. AtRem 1.2 & 1.3 exhibited a **low** lateral mobility at the plant PM as fluorescence recovery after photobleaching (FRAP) experiments disclosed (Jörg Blachutzik, personal communication). Though a low lateral mobility itself is not a proof for raft localization (Kenworthy *et al.*, 2004), it surely identifies AtRem 1.2 & 1.3 as stable membrane domain members.

All this experimental evidence supports the assumption that AtRem 1.2 & 1.3 represent ideal lipid raft markers: they are strongly present in Triton X-100 DRMs, strictly depend upon sterols and show microscopic localization to small, patchy compartments at the plant PM. A characteristic feature of the *A.th.* and *S.t.* remorins is the lack of any transmembrane domains, yet do they display a strong attachment to the PM. Potato StRem 1.3 was located at the cytosolic leaflet of the PM (Raffaele *et al.*, 2009a). The situation for AtRem 1.2 & 1.3 might be similar, especially as both *A.th.* remorins exhibit palmitoylation sites at their C-terminus (section 1.2.6.4, p. 40). As palmitoylations (cf. 1.1.4.2, p. 8) are a frequently encountered lipid modification in animal lipid raft proteins (Resh, 2006), this might also render *A.th.* remorins into the cytosolic leaflet of lipid rafts.

Though no clear functional, physiological role for remorin proteins has been attributed yet, an involvement in plant-pathogen (Raffaele *et al.*, 2009a) and plant-symbiotic interactions (Lefebvre *et al.*, 2010) seems favorable. The high expression level of the *A.th.* remorins 1.2 & 1.3 (Raffaele *et al.*, 2007) represents another piece of evidence for an important role of AtRem 1.2 & 1.3 and might ameliorate our knowledge of their enigmatic function in the nearby future.

4.2.2. AtLipocalin as a non-raft marker

Searching for a non-raft marker in plants, AtLipocalin (At5g58070) seemed to be a reasonable candidate. In this investigation AtLipocalin was detected in the PM but not in DRMs. Similar results were obtained by Minami *et al.* (2009) who studied alterations in the DRM protein composition upon cold acclimation: AtLipocalin did not localize to DRMs though it is supposed to be a temperature-induced protein (Charron *et al.*, 2002) which acts against lipid per-oxidation (Chi *et al.*, 2009) and oxidative stress (Charron *et al.*, 2008).

Immunoblot analysis uncovered AtLipocalin to be not located in Triton X-100 DRMs (figure 3.13, p. 98). Co-localization analysis revealed a strong separation between fluorescently labeled, transiently expressed AtRem 1.3 and AtLipocalin (figure 3.14, p. 101). Thus, it may be suitable to suggest AtLipocalin as a non-raft marker to be used in further investigations.

4.3 ABI1, CPK21 & SLAH3 FORM A DRM-RESIDENT PROTEIN COMPLEX

Drought stress represents a major challenge for sessile organisms such as plants. Therefore, regulation of drought stress signaling in plants is finely regulated. A key role in this regulation cascade is occupied by the plant hormone ABA (Zhu, 2002). In the 1990s the protein phosphatases ABI1 and ABI2 were discovered to be key components in the drought stress response via ABA (Leung *et al.*, 1994, 1997; Meyer *et al.*, 1994). ABI1 is a negative regulator of ABA responses and *abi1-1* mutants displayed ABA-resistance (Gosti *et al.*, 1999). ABA acts through alterations in further signaling cascades (Ma & Wu, 2007; Yoshida *et al.*, 2006) and membrane transport systems (Becker *et al.*, 2003; Geiger *et al.*, 2010b; Trouverie *et al.*, 2008).

4.3.1. Regulation of stomatal closure

Controlling stomatal closure is a key point in drought stress regulation where ABA is strongly involved. Recent investigations disclosed that fast stomatal closure in guard cells depends on the activity of the anion channel SLAC1 (Negi *et al.*, 2008). SLAC1 represents an S-type anion channel (Brault *et al.*, 2004) mediating chloride and nitrate ion transport through the plasma membrane in guard cells (Vahisalu *et al.*, 2008). Homologues of SLAC1 (SLAH1-4) have been identified which are also expressed in other tissues than guard cells, for instance SLAH3 which is strongly expressed in mesophyll cells (Negi *et al.*, 2008).

The activity of ion channels is often regulated by cytosolic Ca^{2+} (Hedrich & Neher, 1987), hence, it is not surprising that SLAC1 is also regulated by CPKs (Geiger *et al.*, 2010b). CPK21 and CPK23 both activated, regulated and interacted with SLAC1, but only CPK21 displayed a strong Ca^{2+} -dependency (Geiger *et al.*, 2009). If SLAC1 was heterologously expressed in *Xenopus laevis* oocytes without addition of CPK21 or CPK23, no transport activity could be observed (Geiger *et al.*, 2009). Thus, CPK21 plays an important role in activating the anion channel SLAC1 in guard cells. For SLAH3, a similar interaction with CPK21 could be observed electrophysiologically (Geiger *et al.*, 2010a).

Negative regulation of anion channel activity is mediated by ABI1 which diminishes SLAC1 (Geiger *et al.*, 2009) and SLAH3 currents (Geiger *et al.*, 2010a) in the absence of ABA. ABA is perceived by the cytosolic ABA receptors of the PYR/PYL/RCAR family (Fujii *et al.*, 2009), which interact with the protein phosphatase ABI1 (Nishimura *et al.*, 2009). The binding pockets of these PYR/PYL/RCAR receptors are occupied by ABA which subsequently leads to tight binding to ABI1 via hydrophobic interactions (Miyazono *et al.*, 2009). It has been

4.3. ABI1, CPK21 & SLAH3 FORM A DRM-RESIDENT PROTEIN COMPLEX

shown that RCAR1 is functionally active as a dimer where only one half is binding ABA (Santiago *et al.*, 2009).

Regulation of ABI1 is not only performed via the PYR/PYL/RCAR receptors but also by lipid signaling molecules like phosphatidic acid (Jacob *et al.*, 1999). Phosphatidic acid (PA) is generated by phospholipase D α 1 (Zhang *et al.*, 2004) and tethers the cytosolic protein phosphatase ABI1 to the PM thereby deactivating ABI1 phosphatase activity and promoting stomatal closure. Phospholipase D α 1 and PA act together with the heterotrimeric GTP-binding protein subunit G_{α} in regulation of stomatal closure (Mishra *et al.*, 2006). G_{α} bound to GTP inhibits stomatal opening whereas G_{α} bound to GDP interacts with phospholipase D α to promote stomatal opening (Mishra *et al.*, 2006). Mutations in the G_{α} subunit (*gpa1*) led to impaired ABA inhibition of guard cell inward K^{+} currents (Wang *et al.*, 2001).

Taken together, stomatal closure is finely regulated by a network of proteins which interact with the plant hormone ABA. Protein phosphatase ABI1 plays a key role in the regulation of ion channels (e.g. SLAH3) and their activating protein kinases (e.g. CPK21). ABI1 itself is regulated by the ABA receptors of the PYR/PYL/RCAR family.

4.3.2. ABI1, CPK21 & SLAH3 are located in DRMs

This complex network of ABA-regulated processes which induce stomatal closure can be (partially) connected with signaling & transport complexes in plant lipid rafts. Members of the CPK family have been spotted in Brij-98 and Triton X-100 DRMs (CPK10, 21 & 32, see section A, p. 186 for complete lists). CPK21 displayed the highest identification confidence in mass spectrometric measurements and was detected to be strictly sterol-dependent by MCD treatment in immunoblotting (figure 3.17, p. 104) and mass spectrometric (table 3.5, p. 91) assays. ABI1 was also identified among the MCD affected Triton X-100 DRM proteins (table 3.6, p. 95) and was strongly present in Triton X-100 DRMs.

Spotting two proteins involved in the regulation of stomatal closure through anion channels (Geiger *et al.*, 2009, 2010b) led to the assumption that there is a signaling and transport complex present in Triton X-100 DRMs which is dependent upon a sterol-rich environment and contributes to drought stress tolerance. Thus, transient (co-)expression analyses of ABI1, CPK21 and SLAH3 in *N.b.* leaves were performed. Only CPK21 located in DRMs indicating an intrinsic localization of CPK21 in lipid rafts. Co-expressing CPK21 with SLAH3 resulted in a sterol-dependent localization of both proteins in Triton X-100 DRMs.

Additional co-expression of ABI1 led to the dislocation of SLAH3 from DRMs (figure 3.18, p. 105) into the DSF (figure 3.19, p. 106). Heterologous expression of CPK21 and SLAH3 in *Xenopus laevis* oocytes displayed strong inward currents which were abolished by additional injection of ABI1 (Demir *et al.*, 2010; Geiger *et al.*, 2010a).

Thus, it may be tempting to propose a relationship between the localization of SLAH3 in DRMs and functional anion transport. CPK21 is highly expressed in mesophyll cells (Geiger *et al.*, 2010a) and has been located in plant DRMs for the first time. This kinase is double acylated via myristate + palmitate lipidations and seem to represent an ideal plant equivalent for the mammalian c-Src protein tyrosine kinases (Resh, 2006).

C-Src kinases display double acylations, are attached to the cytosolic leaflet of the PM and represent prominent members of mammalian DRMs (Ottico *et al.*, 2003; Trouet *et al.*, 2001a). They are highly susceptible to sterol-depletion by MCD application (Ottico *et al.*, 2003). CPK21 is comparable to this c-Src protein kinase family, especially as c-Src kinases are also involved in the regulation of anion channels (Trouet *et al.*, 2001a).

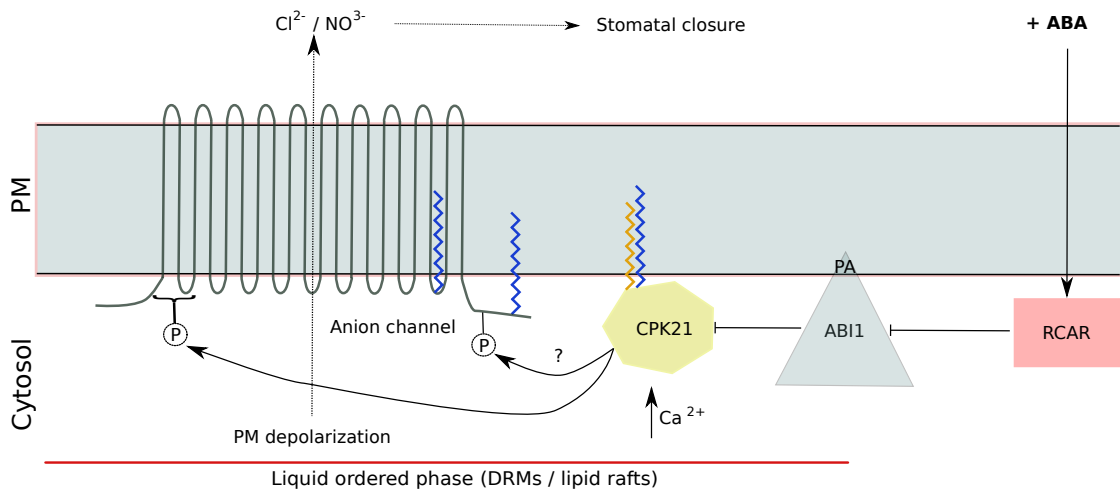


Figure 4.4.: **Hypothetical interactions among ABI1, CPK21 & SLAH3 at the plant plasma membrane.** CPK21 is a protein kinase attached to *A.th.* lipid rafts via myristoylation and palmitoylation lipid anchors. Upon ABA presence, the kinase activity of CPK21 renders SLAH3 active in lipid rafts which leads to chloride & nitrate efflux and concomitant membrane depolarization. Subsequently K^+ efflux induces stomatal closure. ABI1 remains inactive and tethered to the plasma membrane via attachment to phosphatidic acid. Without ABA, the cytosolic ABA receptors of the RCAR family do not inhibit the protein phosphatase ABI1. ABI1 itself inhibits the autophosphorylation of CPK21 and prevents activation and lipid raft localization of the anion channel SLAH3.

Abbreviations: ABI1 = ABA insensitive 1, CPK21 = Ca^{2+} -dependent protein kinase 21, PA = phosphatidic acid, PLD α 1 = phospholipase D α 1, RCAR = regulatory component of ABA receptor, SLAH3 = *SLAC1* homologue 3.

4.3. ABI1, CPK21 & SLAH3 FORM A DRM-RESIDENT PROTEIN COMPLEX

CPKs have already been studied to be involved in the response to drought stress in *A.th.* (Hrabak *et al.*, 2003; Ma & Wu, 2007). For instance, CPK3 and CPK6 directly regulate guard cell S-type anion channels (Mori *et al.*, 2006). Other members of the *A.th.* CPK family are involved in the initial steps of MAMP signaling and thus play a key role in plant defense signaling (Boudsocq *et al.*, 2010). The regulation of polarized growth also depends strongly on Ca²⁺ and CPKs: CPK17 & CPK34 are important for the pollen tube tip growth (Myers *et al.*, 2009). Therefore, directed / polar growth and drought stress responses seem to be mediated by CPKs and interacting proteins (DeFalco *et al.*, 2010).

The hereby investigated protein kinase CPK21 may activate the anion channel SLAH3 at multiple phosphorylation sites at the N- (Geiger *et al.*, 2010a) and C-terminus (Nühse *et al.*, 2003), thus triggering SLAH3 activation and transition into lipid rafts upon presence of ABA. SLAH3 mediates chloride & nitrate efflux in lipid rafts which leads to PM depolarization and stomatal closure (figure 4.4). SLAH3 features three putative palmitoylation sites among which two palmitoylation sites are present at the C-terminus near the last TMD. Palmitoylation sites at the vicinity of TMDs are putative triggers for lipid raft localization as investigations on viral haemagglutinin (HA) revealed (Scolari *et al.*, 2009). It may be advisable to further study the lipid raft localization of SLAH3 in terms of putative palmitoylation and phosphorylation sites.

However, if ABI1 is present and active, no localization of SLAH3 in lipid rafts is detectable and no nitrate flux can be measured (Demir *et al.*, 2010). ABI1 suppresses CPK21 autophosphorylation & activation and thus inhibits phosphorylation of SLAH3 (figure 4.4). Deactivation of the protein phosphatase ABI1 can be performed by direct binding of the ABA receptor RCAR1 to ABI1 upon ABA presence (Miyazono *et al.*, 2009). In summary, CPK21 and SLAH3 build a lipid raft-localized signaling & transport complex mediating stomatal closure upon presence of ABA. Hence, this complex mediates the plants' drought stress response in presence of the desiccation signal ABA. Without ABA, the protein phosphatase ABI1 is active, inhibiting CPK21 kinase activity and suppressing lipid raft localization of SLAH3.

A similar protein complex is found in the epithelium of mammalian lungs. There, the chloride channel cystic fibrosis transmembrane receptor (CFTR) was located in lipid rafts together with the protein tyrosine kinase c-Src (Dudez *et al.*, 2008). The amount of DRM-localized CFTR strongly correlated with the amount of c-Src kinase in DRMs. Comparable to the interaction between the transmembrane anion channel SLAH3 and the PM-attached CPK21, these proteins mediate chloride transport in mammals. Thus, it might be a general principle to localize anion channels and their respective regulative protein kinases in protein complexes within lipid rafts.

5

Summary

Arabidopsis thaliana (*A.th.*) mesophyll cells play a pivotal role in the regulation of the drought stress response. The signaling & transport components involved in drought stress regulation within lipid rafts of the plasma membrane were investigated by DRM isolation from highly purified plasma membranes.

Detergent treatment with Brij-98 and Triton X-100 resulted in a total of 246 DRM proteins which were identified by nano HPLC-MS/MS. The majority of these proteins could be isolated by Triton X-100 treatment (78.5 %) which remains the "golden" standard for the isolation of DRMs. Comparing in-gel and in-solution digestion approaches disclosed additional protein identifications for each method but the in-gel approach clearly delivered the majority of the identified proteins (81.8 %). Functionally, a clear bias on signaling proteins was visible – almost $\frac{1}{3}$ of the detected DRM proteins belonged to the group of kinases, phosphatases and other signaling proteins. Especially leucine-rich repeat receptor-like protein kinases and calcium-dependent protein kinases were present in Brij-98 & Triton X-100 DRMs, for instance the calcium-dependent protein kinase CPK21. Another prominent member of DRMs was the protein phosphatase 2C 56, ABI1, which is a key regulator of the ABA-mediated drought stress response in *A.th.*.

The lipid raft localization of the identified DRM proteins was confirmed by sterol-depletion with the chemical drug MCD. Proteins which depend upon a sterol-rich environment are depleted from DRMs by MCD application. Especially signaling proteins exhibited a strong sterol-dependency. They represented the vast majority (41.5 %) among the Triton X-100 DRM proteins which were no longer detected following MCD treatment. AtRem 1.2 & 1.3 could be shown to be sterol-dependent in mesophyll cells as well as two CPKs (CPK10 & CPK21) and the protein phosphatase ABI1.

AtRem 1.2 & 1.3 could be proven to represent ideal plant lipid raft marker proteins due to their strong presence in Triton X-100 DRMs and dependency upon a sterol-rich environment.

When fluorescence labeled AtRem 1.2 & 1.3 were transiently expressed in *A.th.* leaves, they localized to small, patchy structures at the plasma membrane.

CPK21 was an intrinsic member of Triton X-100 DRMs and displayed extreme susceptibility to sterol-depletion by MCD in immunological and proteomic assays. Calcium-dependent protein kinases (CPKs) have already been studied to be involved in drought stress regulation, for instance at the regulation of S-type anion channels in guard cells. Hence, further transient expression studies with the anion channel SLAH3, protein kinase CPK21 and its counterpart, protein phosphatase ABI1 were performed in *Nicotiana benthamiana*.

Transient co-expression of CPK21 and the anion channel SLAH3, a highly mesophyll-specific homologue of the guard cell anion channel SLAC1, resulted in a combined, sterol-dependent localization of both proteins in DRMs. Supplementary co-expression of the counterpart protein phosphatase ABI1 induced dislocation of SLAH3 from DRMs, probably by inactivation of the protein kinase CPK21. CPK21 is known to regulate the anion channel SLAH3 by phosphorylation. ABI1 dephosphorylates CPK21 thus leading to deactivation and dislocation of SLAH3 from DRMs.

All this regulative events are taking place in DRMs of *A.th.* mesophyll cells. This study presents the first evidence for a lipid raft-resident protein complex combining signaling and transport functions in *A.th.*.

Future perspectives for lipid raft research might target investigations on the lipid raft localization of candidate DRM proteins under presence of abiotic and biotic stress factors. For instance, which alterations in the DRM protein composition are detectable upon exogenous application of the plant hormone ABA? Quantitative proteomics approaches will surely increase our knowledge of the post-transcriptional regulation of gene activity under drought stress conditions.

6

Zusammenfassung

Mesophyllzellen spielen eine sehr wichtige Rolle bei der Regulierung der Trockenstress-Antwort in der Pflanze *Arabidopsis thaliana* (*A.th.*). Um die an der Trockenstress-Antwort beteiligten Signaltransduktions- und Transportproteine zu identifizieren, die sich in Lipid Rafts der pflanzlichen Plasmamembran befinden, wurden Detergent-Resistant Membranes (DRMs) aus hochreinen *Arabidopsis* Plasmamembran-Präparationen isoliert.

Behandlung dieser hochreinen Plasmamembran mit den Detergentien Brij-98 und Triton X-100 führte zur Identifikation von 246 DRM Proteinen, die mittels der nano HPLC-MS/MS Technologie detektiert wurden. Hierbei war festzustellen, daß das Detergens Triton X-100 eindeutig **den** Standard für die Isolierung von DRMs darstellt. Die große Mehrheit (78,5 %) der identifizierten DRM Proteine konnte nämlich mit Triton X-100 aufgereinigt werden. Vergleichende Anwendung verschiedener Verdauungsmethoden (In-Gel und In-Lösung Verdau) zeigte auf, daß jede Methode einen unterschiedlichen Pool an Proteinen identifiziert. Das Gros der analysierten Proteine (81,8 %) konnte jedoch auch alleine durch In-Gel Verdau ermittelt werden.

Unter den identifizierten DRM Proteinen stellten Proteine, die an der Signaltransduktion beteiligt sind, fast $\frac{1}{3}$ dar. Diese Proteingruppe wurde hauptsächlich durch Kinasen und Phosphatasen vertreten. Insbesondere leucin-reiche rezeptor-artige and calcium-abhängige Proteinkinasen waren in Brij-98 & Triton X-100 DRMs zu beobachten, z.B. die calcium-abhängige Proteinkinase CPK21. Ebenso in Triton X-100 DRMs wurde die Proteinphosphatase 2C 56 (ABI1) lokalisiert, die eine zentrale Rolle bei der ABA-vermittelten Antwort auf Trockenstress in *A.th.* inne hat.

Zur Bestätigung der Lipid Raft Lokalisation der identifizierten DRM Proteine wurden Sterole aus der Plasmamembran mittels der Chemikalie Methyl- β -D-cyclodextrin entfernt. Besonders Proteine, die an der Signalweiterleitung beteiligt sind, zeigten eine starke Abhängigkeit von der Präsenz der Sterole. Sie waren besonders betroffen von der Reduzierung des Sterolgehalts in der Plasmamembran: 41,5 % der Proteine, die nach MCD Behandlung nicht mehr in

DRMs identifiziert wurden, gehörten zur Gruppe der Signaltransduktionsproteine. Beispiele waren sowohl die calcium-abhängigen Proteinkinasen CPK10 & CPK21, als auch die Proteinphosphatase ABI1.

Die *A.th.* Remorine AtRem 1.2 & 1.3 stellen ideale Kandidaten für pflanzliche Lipid Raft Markerproteine dar, da beide sowohl ziemlich stark in Triton X-100 DRMs vertreten, als auch im besonderen Maße auf die Präsenz von Sterolen in DRMs angewiesen sind. Fluoreszenzmarkierte AtRem 1.2 & 1.3 Fusionskonstrukte lokalisierten bei transienter Expression in *A.th.* Blättern in kleinen, punktförmigen Strukturen an der Plasmamembran. Diese Strukturen zeigten frappierende Ähnlichkeit zu bereits bekannten Mustern von Lipid Raft Proteinen in Hefen und Säugetieren.

CPK21 stellte ein besonderes Mitglied der Triton X-100 DRMs dar, welches ebenfalls stark auf die Präsenz von Sterolen in DRMs angewiesen war. Dies konnte durch immunologische and massenspektrometrische Experimente nachgewiesen werden. Calcium-abhängige Proteinkinasen (CPKs) sind an der Regulierung der Trockenstress-Antwort in Pflanzen beteiligt, z.B. bei der Aktivierung von S-typ Anionenkanälen in Schließzellen von *A.th.* Aufgrund dieser Beteiligung an der Trockenstress-Antwort, wurden transiente Co-Expressionsstudien des Anionenkanals SLAH3, der Proteinkinase CPK21 und ihrem Gegenspieler, der Proteinphosphatase ABI1 in *Nicotiana benthamiana* Blättern durchgeführt.

Transiente Co-Expression von CPK21 und SLAH3, einem zum schließzell-spezifischen Anionenkanal SLAC1 homologen Protein in Mesophyllzellen, resultierte in einer sterol-abhängigen Co-Lokalisation beider Proteine in DRMs. Zusätzliche Gabe vom Gegenspieler ABI1 führte zum Verschwinden von SLAH3 aus DRMs, was möglicherweise auf die Inaktivierung der Proteinkinase CPK21 durch ABI1 zurückzuführen ist. Für CPK21 konnte schon aufgezeigt werden, daß es den Anionenkanal SLAH3 durch Phosphorylierung aktiviert. ABI1 hingegen dephosphoryliert die Proteinkinase CPK21 und führt zur Deaktivierung vom Anionenkanal SLAH3, welcher dann auch nicht mehr in DRMs lokalisierbar ist.

Diese streng regulierten Prozesse im Rahmen der Trockenstress-Antwort spielen sich in DRMs von *A.th.* Mesophyllzellen ab. Die vorliegende Arbeit ist der erste Bericht eines Lipid Raft-lokalisierten Proteinkomplexes, der Signalweiterleitung und Transportprozesse in *Arabidopsis* Lipid Rafts vereint.

Zukünftige Lipid Raft Studien könnten sich mit der Lokalisation von putativen DRM Proteinen nach Anwendung von abiotischen und biotischen Stressfaktoren befassen. So könnte man sich die Frage stellen, inwiefern sich die Proteinzusammensetzung in DRMs von der Zugabe des pflanzlichen Hormons Abscisinsäure (ABA) beeinflussen läßt. Insbesondere quantitative Proteomstudien werden in Zukunft mit Sicherheit unser Wissen über die posttranskriptionelle Regulation der Genaktivität bei Trockenstress erweitern.

7

Bibliography

- ABRAMOFF M, MAGELHAES P & RAM S (2004). Image Processing with ImageJ. *Biophotonics International*, **11** (7):36–42.
- ACASANDREI MA, DALE RE, VANDEVEN M & AMELOOT M (2006). Two-dimensional Förster resonance energy transfer (2-D FRET) and the membrane raft hypothesis. *Chemical Physics Letters*, **419** (4-6):469 – 473.
- AHMED SN, BROWN DA & LONDON E (1997). On the origin of sphingolipid/cholesterol-rich detergent-insoluble cell membranes: physiological concentrations of cholesterol and sphingolipid induce formation of a detergent-insoluble, liquid-ordered lipid phase in model membranes. *Biochemistry*, **36** (36):10944–10953.
- ALEXANDERSSON E, SAALBACH G, LARSSON C & KJELLBOM P (2004). Arabidopsis plasma membrane proteomics identifies components of transport, signal transduction and membrane trafficking. *Plant & cell physiology*, **45** (11):1543–1556.
- ALLIOTTE T, TIRÉ C, ENGLER G, PELEMAN J, CAPLAN A, VAN MONTAGU M & INZÉ D (1989). An Auxin-Regulated Gene of *Arabidopsis thaliana* Encodes a DNA-Binding Protein. *Plant Physiology*, **89** (3):743–752.
- DE ALMEIDA RFM, FEDOROV A & PRIETO M (2003). Sphingomyelin/phosphatidylcholine/cholesterol phase diagram: boundaries and composition of lipid rafts. *Biophys J*, **85** (4):2406–2416.
- DE ALMEIDA RFM, LOURA LMS, FEDOROV A & PRIETO M (2005). Lipid rafts have different sizes depending on membrane composition: a time-resolved fluorescence resonance energy transfer study. *J Mol Biol*, **346** (4):1109–1120.
- ALVAREZ FJ, DOUGLAS LM & KONOPKA JB (2007). Sterol-rich plasma membrane domains in fungi. *Eukaryot Cell*, **6** (5):755–763.

7. Bibliography

- ASSAAD FF, QIU JL, YOUNGS H, EHRHARDT D, ZIMMERLI L, KALDE M, WANNER G, PECK SC, EDWARDS H, RAMONELL K, SOMERVILLE CR & THORDAL-CHRISTENSEN H (2004). The PEN1 syntaxin defines a novel cellular compartment upon fungal attack and is required for the timely assembly of papillae. *Mol Biol Cell*, **15** (11):5118–5129.
- AYLLÓN V, FLEISCHER A, CAYLA X, GARCÍA A & REBOLLO A (2002). Segregation of Bad from lipid rafts is implicated in the induction of apoptosis. *J Immunol*, **168** (7):3387–3393.
- BAGNAT M & SIMONS K (2002). Cell surface polarization during yeast mating. *Proc Natl Acad Sci U S A*, **99** (22):14183–14188.
- BAGNAT M, CHANG A & SIMONS K (2001). Plasma membrane proton ATPase Pma1p requires raft association for surface delivery in yeast. *Mol Biol Cell*, **12** (12):4129–4138.
- BARIOLA PA, RETELSKA D, STASIAK A, KAMMERER RA, FLEMING A, HIJRI M, FRANK S & FARMER EE (2004). Remorins form a novel family of coiled coil-forming oligomeric and filamentous proteins associated with apical, vascular and embryonic tissues in plants. *Plant Mol Biol*, **55** (4):579–594.
- BECK JG, MATHIEU D, LOUDET C, BUCHOUX S & DUFOURC EJ (2007). Plant sterols in "rafts": a better way to regulate membrane thermal shocks. *FASEB J*, **21** (8):1714–1723.
- BECKER D, HOTH S, ACHE P, WENKEL S, ROELFSEMA MRG, MEYERHOFF O, HARTUNG W & HEDRICH R (2003). Regulation of the ABA-sensitive Arabidopsis potassium channel gene GORK in response to water stress. *FEBS Lett*, **554** (1-2):119–126.
- BENTING J, RIETVELD A, ANSORGE I & SIMONS K (1999). Acyl and alkyl chain length of GPI-anchors is critical for raft association in vitro. *FEBS Lett*, **462** (1-2):47–50.
- BERGELSON LD & BARSUKOV LI (1977). Topological asymmetry of phospholipids in membranes. *Science*, **197** (4300):224–230.
- BHAT RA, MIKLIS M, SCHMELZER E, SCHULZE-LEFERT P & PANSTRUGA R (2005). Recruitment and interaction dynamics of plant penetration resistance components in a plasma membrane microdomain. *Proc Natl Acad Sci U S A*, **102** (8):3135–3140.

- BIRNBOIM HC & DOLY J (1979). A rapid alkaline extraction procedure for screening recombinant plasmid DNA. *Nucleic Acids Res*, **7** (6):1513–1523.
- BLUM H, BEIER H & GROSS HJ (1987). Improved silver staining of plant proteins, RNA and DNA in polyacrylamide gels. *Electrophoresis*, **8** (2):93–99.
- BORNER GHH, LILLEY KS, STEVENS TJ & DUPREE P (2003). Identification of glycosylphosphatidylinositol-anchored proteins in Arabidopsis. A proteomic and genomic analysis. *Plant Physiol*, **132** (2):568–577.
- BORNER GHH, SHERRIER DJ, WEIMAR T, MICHAELSON LV, HAWKINS ND, MACASKILL A, NAPIER JA, BEALE MH, LILLEY KS & DUPREE P (2005). Analysis of detergent-resistant membranes in Arabidopsis. Evidence for plasma membrane lipid rafts. *Plant Physiol*, **137** (1):104–116.
- BOUDSOCQ M, WILLMANN MR, MCCORMACK M, LEE H, SHAN L, HE P, BUSH J, CHENG SH & SHEEN J (2010). Differential innate immune signalling via Ca(2+) sensor protein kinases. *Nature*, **464** (7287):418–422.
- BRADFORD MM (1976). A rapid and sensitive method for the quantitation of microgram quantities of protein utilizing the principle of protein-dye binding. *Anal Biochem*, **72**:248–254.
- BRAULT M, AMIAR Z, PENNARUN AM, MONESTIEZ M, ZHANG Z, CORNEL D, DELLIS O, KNIGHT H, BOUTEAU F & RONA JP (2004). Plasma membrane depolarization induced by abscisic acid in Arabidopsis suspension cells involves reduction of proton pumping in addition to anion channel activation, which are both Ca²⁺ dependent. *Plant Physiol*, **135** (1):231–243.
- BRAY EA (2002). Abscisic acid regulation of gene expression during water-deficit stress in the era of the Arabidopsis genome. *Plant Cell Environ*, **25** (2):153–161.
- BRETSCHER MS & RAFF MC (1975). Mammalian plasma membranes. *Nature*, **258** (5530):43–49.
- BROWN D (1993). The tyrosine kinase connection: how GPI-anchored proteins activate T cells. *Curr Opin Immunol*, **5** (3):349–354.
- BROWN DA (2006). Lipid rafts, detergent-resistant membranes, and raft targeting signals. *Physiology (Bethesda)*, **21**:430–439.

7. Bibliography

- BROWN DA & ROSE JK (1992). Sorting of GPI-anchored proteins to glycolipid-enriched membrane subdomains during transport to the apical cell surface. *Cell*, **68** (3):533–544.
- BRÜGGER B, GRAHAM C, LEIBRECHT I, MOMBELLI E, JEN A, WIELAND F & MORRIS R (2004). The membrane domains occupied by glycosylphosphatidylinositol-anchored prion protein and Thy-1 differ in lipid composition. *J Biol Chem*, **279** (9):7530–7536.
- CABIB E & POLACHECK I (1984). Protein assay for dilute solutions. *Methods Enzymol*, **104**:415–416.
- CAMPBELL S, GAUS K, BITTMAN R, JESSUP W, CROWE S & MAK J (2004). The raft-promoting property of virion-associated cholesterol, but not the presence of virion-associated Brij 98 rafts, is a determinant of human immunodeficiency virus type 1 infectivity. *J Virol*, **78** (19):10556–10565.
- CASEY PJ (1995). Protein lipidation in cell signaling. *Science*, **268** (5208):221–225.
- CHAMBERLAIN LH (2004). Detergents as tools for the purification and classification of lipid rafts. *FEBS Lett*, **559** (1-3):1–5.
- CHARRON JBF, BRETON G, BADAWI M & SARHAN F (2002). Molecular and structural analyses of a novel temperature stress-induced lipocalin from wheat and Arabidopsis. *FEBS Lett*, **517** (1-3):129–132.
- CHARRON JBF, OUELLET F, HOUDE M & SARHAN F (2008). The plant Apolipoprotein D ortholog protects Arabidopsis against oxidative stress. *BMC Plant Biol*, **8**:86.
- CHAZAL N & GERLIER D (2003). Virus entry, assembly, budding, and membrane rafts. *Microbiol Mol Biol Rev*, **67** (2):226–37, table of contents.
- CHEN S & HARMON AC (2006). Advances in plant proteomics. *Proteomics*, **6** (20):5504–5516.
- CHEN Y, HOEHENWARTER W & WECKWERTH W (2010). Comparative analysis of phytohormone-responsive phosphoproteins in Arabidopsis thaliana using TiO-phosphopeptide enrichment and mass accuracy precursor alignment. *Plant J*, **63** (1):1–17.
- CHEN Z (2001). A superfamily of proteins with novel cysteine-rich repeats. *Plant Physiol*, **126** (2):473–476.

- CHEUNG AY, NIROOMAND S, ZOU Y & WU HM (2010). A transmembrane formin nucleates subapical actin assembly and controls tip-focused growth in pollen tubes. *Proc Natl Acad Sci U S A*, **107** (37):16390–16395.
- CHI WT, FUNG RWM, LIU HC, HSU CC & CHARNG YY (2009). Temperature-induced lipocalin is required for basal and acquired thermotolerance in Arabidopsis. *Plant Cell Environ*, **32** (7):917–927.
- CHINCHILLA D, ZIPFEL C, ROBATZEK S, KEMMERLING B, NÜRNBERGER T, JONES JDG, FELIX G & BOLLER T (2007). A flagellin-induced complex of the receptor FLS2 and BAK1 initiates plant defence. *Nature*, **448** (7152):497–500.
- CHOO-SMITH LP, GARZON-RODRIGUEZ W, GLABE CG & SUREWICZ WK (1997). Acceleration of amyloid fibril formation by specific binding of Abeta-(1-40) peptide to ganglioside-containing membrane vesicles. *J Biol Chem*, **272** (37):22987–22990.
- CHRISTIAN AE, HAYNES MP, PHILLIPS MC & ROTHBLAT GH (1997). Use of cyclodextrins for manipulating cellular cholesterol content. *J Lipid Res*, **38** (11):2264–2272.
- COHEN AW, HNASKO R, SCHUBERT W & LISANTI MP (2004). Role of caveolae and caveolins in health and disease. *Physiol Rev*, **84** (4):1341–1379.
- COLLINS TJ (2007). ImageJ for microscopy. *Biotechniques*, **43** (1 Suppl):25–30.
- CONNER SD & SCHMID SL (2003). Regulated portals of entry into the cell. *Nature*, **422** (6927):37–44.
- DEFALCO TA, BENDER KW & SNEDDEN WA (2010). Breaking the code: Ca²⁺ sensors in plant signalling. *Biochem J*, **425** (1):27–40.
- DEMIR F, BLACHUTZIK J, SCHERZER S, REINDERS Y, AL-RASHEID KA, HARMS G, HEDRICH R, GEIGER D & KREUZER I (2010). Arabidopsis nanodomain-delimited ABA signalling regulates ion channel SLAH3. *In submission to Nature*.
- DIETRICH C, BAGATOLLI LA, VOLOVYK ZN, THOMPSON NL, LEVI M, JACOBSON K & GRATTON E (2001). Lipid rafts reconstituted in model membranes. *Biophys J*, **80** (3):1417–1428.
- DIETRICH C, YANG B, FUJIWARA T, KUSUMI A & JACOBSON K (2002). Relationship of lipid rafts to transient confinement zones detected by single particle tracking. *Biophys J*, **82** (1 Pt 1):274–284.

7. Bibliography

- DIVECHA N & IRVINE RF (1995). Phospholipid signaling. *Cell*, **80** (2):269–278.
- DIZHOOR AM, CHEN CK, OLSHEVSKAYA E, SINELNIKOVA VV, PHILLIPOV P & HURLEY JB (1993). Role of the acylated amino terminus of recoverin in Ca(2+)-dependent membrane interaction. *Science*, **259** (5096):829–832.
- DRAB M, VERKADE P, ELGER M, KASPER M, LOHN M, LAUTERBACH B, MENNE J, LINDSCHAU C, MENDE F, LUFT FC, SCHEDL A, HALLER H & KURZCHALIA TV (2001). Loss of caveolae, vascular dysfunction, and pulmonary defects in caveolin-1 gene-disrupted mice. *Science*, **293** (5539):2449–2452.
- DREVOT P, LANGLET C, GUO XJ, BERNARD AM, COLARD O, CHAUVIN JP, LASSERRE R & HE HT (2002). TCR signal initiation machinery is pre-assembled and activated in a subset of membrane rafts. *The EMBO journal*, **21** (8):1899–1908.
- DUDEZ T, BOROT F, HUANG S, KWAK BR, BACCHETTA M, OLLERO M, STANTON BA & CHANSON M (2008). CFTR in a lipid raft-TNFR1 complex modulates gap junctional intercellular communication and IL-8 secretion. *Biochim Biophys Acta*, **1783** (5):779–788.
- EGGELING C, RINGEMANN C, MEDDA R, SCHWARZMANN G, SANDHOFF K, POLYAKOVA S, BELOV VN, HEIN B, VON MIDDENDORFF C, SCHÖNLE A & HELL SW (2009). Direct observation of the nanoscale dynamics of membrane lipids in a living cell. *Nature*, **457** (7233):1159–1162.
- EISENHABER B, BORK P & EISENHABER F (1999). Prediction of potential GPI-modification sites in proprotein sequences. *J Mol Biol*, **292** (3):741–758.
- ELORTZA F, NÜHSE TS, FOSTER LJ, STENSALLE A, PECK SC & JENSEN ON (2003). Proteomic analysis of glycosylphosphatidylinositol-anchored membrane proteins. *Mol Cell Proteomics*, **2** (12):1261–1270.
- ELORTZA F, MOHAMMED S, BUNKENBORG J, FOSTER LJ, NÜHSE TS, BRODBECK U, PECK SC & JENSEN ON (2006). Modification-specific proteomics of plasma membrane proteins: identification and characterization of glycosylphosphatidylinositol-anchored proteins released upon phospholipase D treatment. *J Proteome Res*, **5** (4):935–943.

- EROGLU C, BRUGGER B, WIELAND F & SINNING I (2003). Glutamate-binding affinity of *Drosophila* metabotropic glutamate receptor is modulated by association with lipid rafts. *Proc Natl Acad Sci U S A*, **100** (18):10219–10224.
- FERRO M, SEIGNEURIN-BERNY D, ROLLAND N, CHAPEL A, SALVI D, GARIN J & JOYARD J (2000). Organic solvent extraction as a versatile procedure to identify hydrophobic chloroplast membrane proteins. *Electrophoresis*, **21** (16):3517–3526.
- FLOWER DR (1996). The lipocalin protein family: structure and function. *Biochem J*, **318** (Pt 1):1–14.
- FOSTER LJ, HOOG CLD & MANN M (2003). Unbiased quantitative proteomics of lipid rafts reveals high specificity for signaling factors. *Proc Natl Acad Sci U S A*, **100** (10):5813–5818.
- FRENCH AP, MILLS S, SWARUP R, BENNETT MJ & PRIDMORE TP (2008). Colocalization of fluorescent markers in confocal microscope images of plant cells. *Nat. Protocols*, **3** (4):619–628.
- FRIEDRICHSON T & KURZCHALIA TV (1998). Microdomains of GPI-anchored proteins in living cells revealed by crosslinking. *Nature*, **394** (6695):802–805.
- FROMHERZ P (1988). Self-organization of the fluid mosaic of charged channel proteins in membranes. *Proc. Natl. Acad. Sci. U. S. A.*, **85** (17):6353–6357.
- FUJII H, CHINNUSAMY V, RODRIGUES A, RUBIO S, ANTONI R, PARK SY, CUTLER SR, SHEEN J, RODRIGUEZ PL & ZHU JK (2009). In vitro reconstitution of an abscisic acid signalling pathway. *Nature*, **462** (7273):660–664.
- FUJIKI Y, HUBBARD AL, FOWLER S & LAZAROW PB (1982). Isolation of intracellular membranes by means of sodium carbonate treatment: application to endoplasmic reticulum. *The Journal of cell biology*, **93** (1):97–102.
- FURUCHI T & ANDERSON RG (1998). Cholesterol depletion of caveolae causes hyperactivation of extracellular signal-related kinase (ERK). *J Biol Chem*, **273** (33):21099–21104.
- GALLOVÁ J, UHRÍKOVÁ D, KUCERKA N, TEIXEIRA J & BALGAVÝ P (2008). Hydrophobic thickness, lipid surface area and polar region hydration in monounsaturated diacylphosphatidylcholine bilayers: SANS study of effects of cholesterol and beta-sitosterol in unilamellar vesicles. *Biochim Biophys Acta*, **1778** (11):2627–2632.

7. Bibliography

- GAO M, WANG X, WANG D, XU F, DING X, ZHANG Z, BI D, CHENG YT, CHEN S, LI X & ZHANG Y (2009). Regulation of cell death and innate immunity by two receptor-like kinases in Arabidopsis. *Cell Host Microbe*, **6** (1):34–44.
- GARCÍA-SÁEZ AJ, CHIANTIA S & SCHWILLE P (2007). Effect of line tension on the lateral organization of lipid membranes. *J Biol Chem*, **282** (46):33537–33544.
- GASPARI M, ABBONANTE V & CUDA G (2007). Gel-free sample preparation for the nanoscale LC-MS/MS analysis and identification of low-nanogram protein samples. *J Sep Sci*, **30** (14):2210–2216.
- GEIGER D, SCHERZER S, MUMM P, STANGE A, MARTEN I, BAUER H, ACHE P, MATSCHI S, LIESE A, AL-RASHEID KAS, ROMEIS T & HEDRICH R (2009). Activity of guard cell anion channel SLAC1 is controlled by drought-stress signaling kinase-phosphatase pair. *Proc Natl Acad Sci U S A*, **106** (50):21425–21430.
- GEIGER D, MAIERHOFER T, AL-RASHEID KAS, SCHERZER S, MUMM P, ACHE P, GRILL E, MARTEN I & HEDRICH R (2010a). Fast abscisic acid signalling of stomatal closure via guard cell anion channel SLAH3 and ABA-receptor RCAR1. *Under revision in Science signaling*.
- GEIGER D, SCHERZER S, MUMM P, MARTEN I, ACHE P, MATSCHI S, LIESE A, WELLMANN C, AL-RASHEID KAS, GRILL E, ROMEIS T & HEDRICH R (2010b). Guard cell anion channel SLAC1 is regulated by CDPK protein kinases with distinct Ca²⁺ affinities. *Proc Natl Acad Sci U S A*, **107** (17):8023–8028.
- GEU-FLORES F, NOUR-ELDIN HH, NIELSEN MT & HALKIER BA (2007). USER fusion: a rapid and efficient method for simultaneous fusion and cloning of multiple PCR products. *Nucleic Acids Res*, **35** (7):–55.
- GHOSH S, STRUM JC & BELL RM (1997). Lipid biochemistry: functions of glycerolipids and sphingolipids in cellular signaling. *FASEB J*, **11** (1):45–50.
- GIBALA M, KICIA M, SAKAMOTO W, GOLA EM, KUBRAKIEWICZ J, SMAKOWSKA E & JANSKA H (2009). The lack of mitochondrial AtFtsH4 protease alters Arabidopsis leaf morphology at the late stage of rosette development under short-day photoperiod. *Plant J*, **59** (5):685–699.
- GIL C, CUBÍ R, BLASI J & AGUILERA J (2006). Synaptic proteins associate with a subset of lipid rafts when isolated from nerve endings at physiological temperature. *Biochem Biophys Res Commun*, **348** (4):1334–1342.

- GORTER E & GREDEL F (1925). On Bimolecular Layers Of Lipoids On The Chromocytes Of The Blood. *J Exp Med*, **41** (4):439–443.
- GOSTI F, BEAUDOIN N, SERIZET C, WEBB AA, VARTANIAN N & GIRAUDAT J (1999). ABI1 protein phosphatase 2C is a negative regulator of abscisic acid signaling. *Plant Cell*, **11** (10):1897–1910.
- GRANDMOUGIN-FERJANI A, SCHULER-MULLER I & HARTMANN MA (1997). Sterol Modulation of the Plasma Membrane H⁺-ATPase Activity from Corn Roots Reconstituted into Soybean Lipids. *Plant Physiol*, **113** (1):163–174.
- GRIEBEL T & ZEIER J (2010). A role for beta-sitosterol to stigmasterol conversion in plant-pathogen interactions. *Plant J*, **63** (2):254–268.
- GROSSMANN G, OPEKAROVA M, NOVAKOVA L, STOLZ J & TANNER W (2006). Lipid raft-based membrane compartmentation of a plant transport protein expressed in *Saccharomyces cerevisiae*. *Eukaryot Cell*, **5** (6):945–953.
- GROSSMANN G, OPEKAROVÁ M, MALINSKY J, WEIG-MECKL I & TANNER W (2007). Membrane potential governs lateral segregation of plasma membrane proteins and lipids in yeast. *The EMBO journal*, **26** (1):1–8.
- GROSSMANN G, MALINSKY J, STAHLSCHEIDT W, LOIBL M, WEIG-MECKL I, FROMMER WB, OPEKAROVÁ M & TANNER W (2008). Plasma membrane microdomains regulate turnover of transport proteins in yeast. *J Cell Biol*, **183** (6):1075–1088.
- GUPTA N, WOLLSCHIED B, WATTS JD, SCHEER B, AEBERSOLD R & DEFranco AL (2006). Quantitative proteomic analysis of B cell lipid rafts reveals that ezrin regulates antigen receptor-mediated lipid raft dynamics. *Nat Immunol*, **7** (6):625–633.
- GÓMEZ-GÓMEZ L & BOLLER T (2000). FLS2: an LRR receptor-like kinase involved in the perception of the bacterial elicitor flagellin in *Arabidopsis*. *Mol Cell*, **5** (6):1003–1011.
- HAC-WYDRO K, FLASIŃSKI M, BRONIATOWSKI M, DYNAROWICZ-LATKA P & MAJEWSKI J (2010). Comparative studies on the influence of beta-sitosterol and stigmasterol on model sphingomyelin membranes: a grazing-incidence X-ray diffraction study. *J Phys Chem B*, **114** (20):6866–6871.

7. Bibliography

- HAILSTONES D, SLEER LS, PARTON RG & STANLEY KK (1998). Regulation of caveolin and caveolae by cholesterol in MDCK cells. *J Lipid Res*, **39** (2):369–379.
- HANCOCK JF (2006). Lipid rafts: contentious only from simplistic standpoints. *Nat Rev Mol Cell Biol*, **7** (6):456–462.
- HANCOCK JF, MAGEE AI, CHILDS JE & MARSHALL CJ (1989). All ras proteins are polyisoprenylated but only some are palmitoylated. *Cell*, **57** (7):1167–1177.
- HAO M, MUKHERJEE S & MAXFIELD FR (2001). Cholesterol depletion induces large scale domain segregation in living cell membranes. *Proc Natl Acad Sci U S A*, **98** (23):13072–13077.
- HARDER T & SIMONS K (1997). Caveolae, DIGs, and the dynamics of sphingolipid-cholesterol microdomains. *Curr Opin Cell Biol*, **9** (4):534–542.
- HARDER T, SCHEIFFELE P, VERKADE P & SIMONS K (1998). Lipid domain structure of the plasma membrane revealed by patching of membrane components. *J Cell Biol*, **141** (4):929–942.
- HARTMANN MA (1998). Plant sterols and the membrane environment. *Trends Plant Sci.*, **3** (5):170–175.
- HAVEL RJ, EDER HA & BRAGDON JH (1955). The distribution and chemical composition of ultracentrifugally separated lipoproteins in human serum. *J Clin Invest*, **34** (9):1345–1353.
- HEAD BP, PATEL HH, ROTH DM, MURRAY F, SWANEY JS, NIESMAN IR, FARQUHAR MG & INSEL PA (2006). Microtubules and actin microfilaments regulate lipid raft/caveolae localization of adenylyl cyclase signaling components. *J Biol Chem*, **281** (36):26391–26399.
- HEDRICH R & NEHER E (1987). Cytoplasmic calcium regulates voltage-dependent ion channels in plant vacuoles. *Nature*, **329**:833–836.
- HEERKLOTZ H (2002). Triton promotes domain formation in lipid raft mixtures. *Biophys J*, **83** (5):2693–2701.
- HEESE A, HANN DR, GIMENEZ-IBANEZ S, JONES AME, HE K, LI J, SCHROEDER JI, PECK SC & RATHJEN JP (2007). The receptor-like kinase SERK3/BAK1 is a central regulator of innate immunity in plants. *Proc Natl Acad Sci U S A*, **104** (29):12217–12222.

- HEFFER-LAUC M, VILJETIĆ B, VAJN K, SCHNAAR RL & LAUC G (2007). Effects of detergents on the redistribution of gangliosides and GPI-anchored proteins in brain tissue sections. *The journal of histochemistry and cytochemistry : official journal of the Histochemistry Society*, **55** (8):805–812.
- HEIN B, WILLIG KI & HELL SW (2008). Stimulated emission depletion (STED) nanoscopy of a fluorescent protein-labeled organelle inside a living cell. *Proc Natl Acad Sci U S A*, **105** (38):14271–14276.
- HELL SW (2003). Toward fluorescence nanoscopy. *Nat Biotechnol*, **21** (11):1347–1355.
- (2007). Far-field optical nanoscopy. *Science*, **316** (5828):1153–1158.
- HEMLER ME (2005). Tetraspanin functions and associated microdomains. *Nat Rev Mol Cell Biol*, **6** (10):801–811.
- HENDERSON R & UNWIN PN (1975). Three-dimensional model of purple membrane obtained by electron microscopy. *Nature*, **257** (5521):28–32.
- HESKETH JE (1996). Sorting of messenger RNAs in the cytoplasm: mRNA localization and the cytoskeleton. *Exp Cell Res*, **225** (2):219–236.
- HOLLOWKA D, SHEETS ED & BAIRD B (2000). Interactions between Fc(epsilon)RI and lipid raft components are regulated by the actin cytoskeleton. *J Cell Sci*, **113** (Pt 6):1009–1019.
- HORTON P, PARK KJ, OBAYASHI T, FUJITA N, HARADA H, ADAMS-COLLIER CJ & NAKAI K (2007). WoLF PSORT: protein localization predictor. *Nucleic Acids Res*, **35** (Web Server issue):W585–W587.
- HRABAK EM, CHAN CWM, GRIBSKOV M, HARPER JF, CHOI JH, HALFORD N, KUDLA J, LUAN S, NIMMO HG, SUSSMAN MR, THOMAS M, WALKER-SIMMONS K, ZHU JK & HARMON AC (2003). The Arabidopsis CDPK-SnRK superfamily of protein kinases. *Plant Physiol*, **132** (2):666–680.
- HURKMAN WJ & TANAKA CK (1986). Solubilization of Plant Membrane Proteins for Analysis by Two-Dimensional Gel Electrophoresis. *Plant Physiol*, **81** (3):802–806.
- ILANGUMARAN S & HOESSLI DC (1998). Effects of cholesterol depletion by cyclodextrin on the sphingolipid microdomains of the plasma membrane. *Biochem J*, **335** (Pt 2):433–440.

7. Bibliography

- ISHIHAMA Y, ODA Y, TABATA T, SATO T, NAGASU T, RAPPSILBER J & MANN M (2005). Exponentially modified protein abundance index (emPAI) for estimation of absolute protein amount in proteomics by the number of sequenced peptides per protein. *Mol Cell Proteomics*, **4** (9):1265–1272.
- ISHIHAMA Y, SCHMIDT T, RAPPSILBER J, MANN M, HARTL FU, KERNER MJ & FRISHMAN D (2008). Protein abundance profiling of the Escherichia coli cytosol. *BMC Genomics*, **9**:102.
- JACINTO T, FARMER EE & RYAN CA (1993). Purification of Potato Leaf Plasma Membrane Protein pp34, a Protein Phosphorylated in Response to Oligogalacturonide Signals for Defense and Development. *Plant Physiol*, **103** (4):1393–1397.
- JACOB T, RITCHIE S, ASSMANN SM & GILROY S (1999). Abscisic acid signal transduction in guard cells is mediated by phospholipase D activity. *Proc Natl Acad Sci U S A*, **96** (21):12192–12197.
- JACOBS AK, LIPKA V, BURTON RA, PANSTRUGA R, STRIZHOV N, SCHULZE-LEFERT P & FINCHER GB (2003). An Arabidopsis Callose Synthase, GSL5, Is Required for Wound and Papillary Callose Formation. *Plant Cell*, **15** (11):2503–2513.
- JACOBS J & ROE JL (2005). SKS6, a multicopper oxidase-like gene, participates in cotyledon vascular patterning during Arabidopsis thaliana development. *Planta*, **222** (4):652–666.
- JACOBSON K & DIETRICH C (1999). Looking at lipid rafts? *Trends Cell Biol*, **9** (3):87–91.
- JACOBSON K, SHEETS ED & SIMSON R (1995). Revisiting the fluid mosaic model of membranes. *Science*, **268** (5216):1441–1442.
- JACOBSON K, MOURITSEN OG & ANDERSON RGW (2007). Lipid rafts: at a crossroad between cell biology and physics. *Nat Cell Biol*, **9** (1):7–14.
- JAIN E, BAIROCH A, DUVAUD S, PHAN I, REDASCHI N, SUZEK BE, MARTIN MJ, MCGARVEY P & GASTEIGER E (2009). Infrastructure for the life sciences: design and implementation of the UniProt website. *BMC Bioinformatics*, **10**:136.
- JONES AME, MACLEAN D, STUDHOLME DJ, SERNA-SANZ A, ANDREASSON E, RATHJEN JP & PECK SC (2009). Phosphoproteomic analysis of nuclei-enriched fractions from Arabidopsis thaliana. *J Proteomics*, **72** (3):439–451.

- JOURNOT-CATALINO N, SOMSSICH IE, ROBY D & KROJ T (2006). The transcription factors WRKY11 and WRKY17 act as negative regulators of basal resistance in *Arabidopsis thaliana*. *Plant Cell*, **18** (11):3289–3302.
- KARACSONYI C, BEDKE T, HINRICHSSEN N, SCHWINZER R & LINDNER R (2005). MHC II molecules and invariant chain reside in membranes distinct from conventional lipid rafts. *J Leukoc Biol*, **78** (5):1097–1105.
- KELLER P & SIMONS K (1998). Cholesterol is required for surface transport of influenza virus hemagglutinin. *J Cell Biol*, **140** (6):1357–1367.
- KENWORTHY AK (2008). Have we become overly reliant on lipid rafts? Talking Point on the involvement of lipid rafts in T-cell activation. *EMBO Rep*, **9** (6):531–535.
- KENWORTHY AK & EDIDIN M (1998). Distribution of a glycosylphosphatidylinositol-anchored protein at the apical surface of MDCK cells examined at a resolution of ≤ 100 Å using imaging fluorescence resonance energy transfer. *J Cell Biol*, **142** (1):69–84.
- KENWORTHY AK, NICHOLS BJ, REMMERT CL, HENDRIX GM, KUMAR M, ZIMMERBERG J & LIPPINCOTT-SCHWARTZ J (2004). Dynamics of putative raft-associated proteins at the cell surface. *J Cell Biol*, **165** (5):735–746.
- KIERSZNIOWSKA S, SEIWERT B & SCHULZE WX (2008). Definition of Arabidopsis sterol-rich membrane microdomains by differential treatment with methyl-beta-cyclodextrin and quantitative proteomics. *Mol Cell Proteomics*, **8** (4):612–623.
- KILSDONK EP, YANCEY PG, STOUTD GW, BANGERTER FW, JOHNSON WJ, PHILLIPS MC & ROTHBLAT GH (1995). Cellular cholesterol efflux mediated by cyclodextrins. *J Biol Chem*, **270** (29):17250–17256.
- KITTEL RJ, WICHMANN C, RASSE TM, FOUQUET W, SCHMIDT M, SCHMID A, WAGH DA, PAWLU C, KELLNER RR, WILLIG KI, HELL SW, BUCHNER E, HECKMANN M & SIGRIST SJ (2006). Bruchpilot promotes active zone assembly, Ca²⁺ channel clustering, and vesicle release. *Science*, **312** (5776):1051–1054.
- KLEIN TM, FROMM M, WEISSINGER A, TOMES D, SCHAAF S, SLETTEN M & SANFORD JC (1988a). Transfer of foreign genes into intact maize cells with high-velocity microprojectiles. *Proc Natl Acad Sci U S A*, **85** (12):4305–4309.

7. Bibliography

- KLEIN TM, HARPER EC, SVAB Z, SANFORD JC, FROMM ME & MALIGA P (1988b). Stable genetic transformation of intact *Nicotiana* cells by the particle bombardment process. *Proc Natl Acad Sci U S A*, **85** (22):8502–8505.
- KLEIN U, GIMPL G & FAHRENHOLZ F (1995). Alteration of the myometrial plasma membrane cholesterol content with beta-cyclodextrin modulates the binding affinity of the oxytocin receptor. *Biochemistry*, **34** (42):13784–13793.
- KOBAE Y, SEKINO T, YOSHIOKA H, NAKAGAWA T, MARTINOIA E & MAESHIMA M (2006). Loss of AtPDR8, a plasma membrane ABC transporter of *Arabidopsis thaliana*, causes hypersensitive cell death upon pathogen infection. *Plant Cell Physiol*, **47** (3):309–318.
- KOHN WD, MANT CT & HODGES RS (1997). Alpha-helical protein assembly motifs. *J Biol Chem*, **272** (5):2583–2586.
- KORN ED (1966). Structure of biological membranes. *Science*, **153** (743):1491–1498.
- KOSTREWA D & WINKLER FK (1995). Mg²⁺ binding to the active site of EcoRV endonuclease: a crystallographic study of complexes with substrate and product DNA at 2 Å resolution. *Biochemistry*, **34** (2):683–696.
- KURAS R, SAINT-MARCOUX D, WOLLMAN FA & DE VITRY C (2007). A specific c-type cytochrome maturation system is required for oxygenic photosynthesis. *Proc Natl Acad Sci U S A*, **104** (23):9906–9910.
- KUSUMI A & SAKO Y (1996). Cell surface organization by the membrane skeleton. *Curr Opin Cell Biol*, **8** (4):566–574.
- KWIK J, BOYLE S, FOOKSMAN D, MARGOLIS L, SHEETZ MP & EDIDIN M (2003). Membrane cholesterol, lateral mobility, and the phosphatidylinositol 4,5-bisphosphate-dependent organization of cell actin. *Proc Natl Acad Sci U S A*, **100** (24):13964–13969.
- KYHSE-ANDERSEN J (1984). Electroblotting of multiple gels: a simple apparatus without buffer tank for rapid transfer of proteins from polyacrylamide to nitrocellulose. *J Biochem Biophys Methods*, **10** (3-4):203–209.
- KYTE J & DOOLITTLE RF (1982). A simple method for displaying the hydrophobic character of a protein. *J Mol Biol*, **157** (1):105–132.

- LAEMMLI UK (1970). Cleavage of structural proteins during the assembly of the head of bacteriophage T4. *Nature*, **227** (5259):680–685.
- LALOI M, PERRET AM, CHATRE L, MELSER S, CANTREL C, VAULTIER MN, ZACHOWSKI A, BATHANY K, SCHMITTER JM, VALLET M, LESSIRE R, HARTMANN MA & MOREAU P (2007). Insights into the role of specific lipids in the formation and delivery of lipid microdomains to the plasma membrane of plant cells. *Plant Physiol*, **143** (1):461–472.
- LARSSON K (1988). Lipid phase transitions in membranes involving intrinsic periodic curvature. *Chem Phys Lipids*, **49** (1-2):65–67.
- LAUWERS E & ANDRÉ B (2006). Association of yeast transporters with detergent-resistant membranes correlates with their cell-surface location. *Traffic*, **7** (8):1045–1059.
- LEE CW, EFETOVA M, ENGELMANN JC, KRAMELL R, WASTERNAK C, LUDWIG-MÜLLER J, HEDRICH R & DEEKEN R (2009a). *Agrobacterium tumefaciens* promotes tumor induction by modulating pathogen defense in *Arabidopsis thaliana*. *Plant Cell*, **21** (9):2948–2962.
- LEE SC, LAN W, BUCHANAN BB & LUAN S (2009b). A protein kinase-phosphatase pair interacts with an ion channel to regulate ABA signaling in plant guard cells. *Proc Natl Acad Sci U S A*, **106** (50):21419–21424.
- LEFEBVRE B, TIMMERS T, MBENGUE M, MOREAU S, HERVÉ C, TÓTH K, BITTENCOURT-SILVESTRE J, KLAUS D, DESLANDES L, GODIARD L, MURRAY JD, UDVARDI MK, RAFFAELE S, MONGRAND S, CULLIMORE J, GAMAS P, NIEBEL A & OTT T (2010). A remorin protein interacts with symbiotic receptors and regulates bacterial infection. *Proceedings of the National Academy of Sciences*, **107** (5):2343–2348.
- LEUNG J, BOUVIER-DURAND M, MORRIS PC, GUERRIER D, CHEFDOR F & GIRAUDAT J (1994). *Arabidopsis* ABA response gene *ABI1*: features of a calcium-modulated protein phosphatase. *Science*, **264** (5164):1448–1452.
- LEUNG J, MERLOT S & GIRAUDAT J (1997). The *Arabidopsis* ABSCISIC ACID-INSENSITIVE2 (*ABI2*) and *ABI1* genes encode homologous protein phosphatases 2C involved in abscisic acid signal transduction. *Plant Cell*, **9** (5):759–771.

7. Bibliography

- LI J, WEN J, LEASE KA, DOKE JT, TAX FE & WALKER JC (2002). BAK1, an Arabidopsis LRR receptor-like protein kinase, interacts with BRI1 and modulates brassinosteroid signaling. *Cell*, **110** (2):213–222.
- LI XM, MOMSEN MM, SMABY JM, BROCKMAN HL & BROWN RE (2001). Cholesterol decreases the interfacial elasticity and detergent solubility of sphingomyelins. *Biochemistry*, **40** (20):5954–5963.
- LICHTENBERG D, GOÑI FM & HEERKLOTZ H (2005). Detergent-resistant membranes should not be identified with membrane rafts. *Trends Biochem Sci*, **30** (8):430–436.
- LILLEMEIER BF, PFEIFFER JR, SURVILADZE Z, WILSON BS & DAVIS MM (2006). Plasma membrane-associated proteins are clustered into islands attached to the cytoskeleton. *Proc Natl Acad Sci U S A*, **103** (50):18992–18997.
- LILLEY KS & DUPREE P (2007). Plant organelle proteomics. *Curr Opin Plant Biol*, **10** (6):594–599.
- LINGWOOD D & SIMONS K (2007). Detergent resistance as a tool in membrane research. *Nat Protoc*, **2** (9):2159–2165.
- LIPKA U, FUCHS R & LIPKA V (2008). Arabidopsis non-host resistance to powdery mildews. *Curr Opin Plant Biol*, **11** (4):404–411.
- LIU J, ELMORE JM, FUGLSANG AT, PALMGREN MG, STASKAWICZ BJ & COAKER G (2009a). RIN4 functions with plasma membrane H⁺-ATPases to regulate stomatal apertures during pathogen attack. *PLoS Biol*, **7** (6):e1000139.
- LIU P, YING Y & ANDERSON RG (1997). Platelet-derived growth factor activates mitogen-activated protein kinase in isolated caveolae. *Proc Natl Acad Sci U S A*, **94** (25):13666–13670.
- LIU P, LI RL, ZHANG L, WANG QL, NIEHAUS K, BALUŠKA F, SAMAJ J & LIN JX (2009b). Lipid microdomain polarization is required for NADPH oxidase-dependent ROS signaling in *Picea meyeri* pollen tube tip growth. *Plant J*, **60** (2):303–313.
- LÜTHJE S, HOPFF D, SCHMITT A, MEISRIMLER CN & MENCKHOFF L (2009). Hunting for low abundant redox proteins in plant plasma membranes. *J Proteomics*, **72** (3):475–483.
- MA SY & WU WH (2007). AtCPK23 functions in Arabidopsis responses to drought and salt stresses. *Plant Mol Biol*, **65** (4):511–518.

- MADORE N, SMITH KL, GRAHAM CH, JEN A, BRADY K, HALL S & MORRIS R (1999). Functionally different GPI proteins are organized in different domains on the neuronal surface. *EMBO J*, **18** (24):6917–6926.
- MAEDA Y, TASHIMA Y, HOUJOU T, FUJITA M, YOKO-O T, JIGAMI Y, TAGUCHI R & KINOSHITA T (2007). Fatty acid remodeling of GPI-anchored proteins is required for their raft association. *Mol Biol Cell*, **18** (4):1497–1506.
- MALAKSHAH SN, REZAEI MH, HEIDARI M & SALEKDEH GH (2007). Proteomics reveals new salt responsive proteins associated with rice plasma membrane. *Biosci Biotechnol Biochem*, **71** (9):2144–2154.
- MALÍNSKÁ K, MALÍNSKÝ J, OPEKAROVÁ M & TANNER W (2003). Visualization of protein compartmentation within the plasma membrane of living yeast cells. *Mol Biol Cell*, **14** (11):4427–4436.
- MARMAGNE A, ROUET MA, FERRO M, ROLLAND N, ALCON C, JOYARD J, GARIN J, BARBIER-BRYGOO H & EPHRITIKHINE G (2004). Identification of new intrinsic proteins in Arabidopsis plasma membrane proteome. *Mol Cell Proteomics*, **3** (7):675–691.
- MARMAGNE A, FERRO M, MEINNEL T, BRULEY C, KUHN L, GARIN J, BARBIER-BRYGOO H & EPHRITIKHINE G (2007). A high content in lipid-modified peripheral proteins and integral receptor kinases features in the arabidopsis plasma membrane proteome. *Mol Cell Proteomics*, **6** (11):1980–1996.
- MARTENS JR, NAVARRO-POLANCO R, COPPOCK EA, NISHIYAMA A, PARSHLEY L, GROBASKI TD & TAMKUN MM (2000). Differential targeting of Shaker-like potassium channels to lipid rafts. *J Biol Chem*, **275** (11):7443–7446.
- MARTZ F, WILCZYNSKA M & KLECZKOWSKI LA (2002). Oligomerization status, with the monomer as active species, defines catalytic efficiency of UDP-glucose pyrophosphorylase. *Biochem J*, **367** (Pt 1):295–300.
- MAYOR S & RAO M (2004). Rafts: scale-dependent, active lipid organization at the cell surface. *Traffic*, **5** (4):231–240.
- MCLAUGHLIN S & ADEREM A (1995). The myristoyl-electrostatic switch: a modulator of reversible protein-membrane interactions. *Trends Biochem Sci*, **20** (7):272–276.

7. Bibliography

- MEDALIA O, WEBER I, FRANGAKIS AS, NICASTRO D, GERISCH G & BAUMEISTER W (2002). Macromolecular architecture in eukaryotic cells visualized by cryoelectron tomography. *Science*, **298** (5596):1209–1213.
- VAN MEER G & SIMONS K (1988). Lipid polarity and sorting in epithelial cells. *J Cell Biochem*, **36** (1):51–58.
- MELKONIAN KA, OSTERMEYER AG, CHEN JZ, ROTH MG & BROWN DA (1999). Role of lipid modifications in targeting proteins to detergent-resistant membrane rafts. Many raft proteins are acylated, while few are prenylated. *J Biol Chem*, **274** (6):3910–3917.
- MEN S, BOUTTÉ Y, IKEDA Y, LI X, PALME K, STIERHOF YD, HARTMANN MA, MORITZ T & GREBE M (2008). Sterol-dependent endocytosis mediates post-cytokinetic acquisition of PIN2 auxin efflux carrier polarity. *Nat Cell Biol*, **10** (2):237–244.
- MEYER K, LEUBE MP & GRILL E (1994). A protein phosphatase 2C involved in ABA signal transduction in *Arabidopsis thaliana*. *Science*, **264** (5164):1452–1455.
- MINAMI A, FUJIWARA M, FURUTO A, FUKAO Y, YAMASHITA T, KAMO M, KAWAMURA Y & UEMURA M (2009). Alterations in detergent-resistant plasma membrane microdomains in *Arabidopsis thaliana* during cold acclimation. *Plant Cell Physiol*, **50** (2):341–359.
- MISHRA G, ZHANG W, DENG F, ZHAO J & WANG X (2006). A bifurcating pathway directs abscisic acid effects on stomatal closure and opening in *Arabidopsis*. *Science*, **312** (5771):264–266.
- MITRA SK, CLOUSE SD & GOSHE MB (2009). Enrichment and preparation of plasma membrane proteins from *Arabidopsis thaliana* for global proteomic analysis using liquid chromatography-tandem mass spectrometry. *Methods Mol Biol*, **564**:341–355.
- MIYAZONO KI, MIYAKAWA T, SAWANO Y, KUBOTA K, KANG HJ, ASANO A, MIYAUCHI Y, TAKAHASHI M, ZHI Y, FUJITA Y, YOSHIDA T, KODAIRA KS, YAMAGUCHI-SHINOZAKI K & TANOKURA M (2009). Structural basis of abscisic acid signalling. *Nature*, **462** (7273):609–614.
- MOFFETT S, BROWN DA & LINDER ME (2000). Lipid-dependent targeting of G proteins into rafts. *J Biol Chem*, **275** (3):2191–2198.

- MONGRAND S, MOREL J, LAROCHE J, CLAVEROL S, CARDE JP, HARTMANN MA, BONNEU M, SIMON-PLAS F, LESSIRE R & BESSOULE JJ (2004). Lipid rafts in higher plant cells: purification and characterization of Triton X-100-insoluble microdomains from tobacco plasma membrane. *The Journal of biological chemistry*, **279** (35):36277–36286.
- MORANDAT S & EL KIRAT K (2006). Membrane resistance to Triton X-100 explored by real-time atomic force microscopy. *Langmuir : the ACS journal of surfaces and colloids*, **22** (13):5786–5791.
- MOREL J, CLAVEROL S, MONGRAND S, FURT F, FROMENTIN J, BESSOULE JJ, BLEIN JP & SIMON-PLAS F (2006). Proteomics of plant detergent-resistant membranes. *Mol Cell Proteomics*, **5** (8):1396–1411.
- MORI IC, MURATA Y, YANG Y, MUNEMASA S, WANG YF, ANDREOLI S, TIRIAC H, ALONSO JM, HARPER JF, ECKER JR, KWAK JM & SCHROEDER JI (2006). CDPKs CPK6 and CPK3 function in ABA regulation of guard cell S-type anion- and Ca(2+)-permeable channels and stomatal closure. *PLoS Biol*, **4** (10):e327.
- MORONE N, FUJIWARA T, MURASE K, KASAI RS, IKE H, YUASA S, USUKURA J & KUSUMI A (2006). Three-dimensional reconstruction of the membrane skeleton at the plasma membrane interface by electron tomography. *J Cell Biol*, **174** (6):851–862.
- MORSOMME P & BOUTRY M (2000). The plant plasma membrane H(+)-ATPase: structure, function and regulation. *Biochim Biophys Acta*, **1465** (1-2):1–16.
- MYERS C, ROMANOWSKY SM, BARRON YD, GARG S, AZUSE CL, CURRAN A, DAVIS RM, HATTON J, HARMON AC & HARPER JF (2009). Calcium-dependent protein kinases regulate polarized tip growth in pollen tubes. *Plant J*, **59** (4):528–539.
- NAM KH & LI J (2002). BRI1/BAK1, a receptor kinase pair mediating brassinosteroid signaling. *Cell*, **110** (2):203–212.
- NEGI J, MATSUDA O, NAGASAWA T, OBA Y, TAKAHASHI H, KAWAI-YAMADA M, UCHIMIYA H, HASHIMOTO M & IBA K (2008). CO₂ regulator SLAC1 and its homologues are essential for anion homeostasis in plant cells. *Nature*, **452** (7186):483–486.

7. Bibliography

- NELSON CJ, HEGEMAN AD, HARMS AC & SUSSMAN MR (2006). A quantitative analysis of Arabidopsis plasma membrane using trypsin-catalyzed (18)O labeling. *Mol Cell Proteomics*, **5** (8):1382–1395.
- NEUFELD EB, COONEY AM, PITHA J, DAWIDOWICZ EA, DWYER NK, PENTCHEV PG & BLANCHETTE-MACKIE EJ (1996). Intracellular trafficking of cholesterol monitored with a cyclodextrin. *J Biol Chem*, **271** (35):21604–21613.
- NICOLAU DV, BURRAGE K, PARTON RG & HANCOCK JF (2006). Identifying optimal lipid raft characteristics required to promote nanoscale protein-protein interactions on the plasma membrane. *Mol Cell Biol*, **26** (1):313–323.
- NIELSEN BL & BROWN LR (1984). The basis for colored silver-protein complex formation in stained polyacrylamide gels. *Anal Biochem*, **141** (2):311–315.
- NIITTYLÄ T, FUGLSANG AT, PALMGREN MG, FROMMER WB & SCHULZE WX (2007). Temporal analysis of sucrose-induced phosphorylation changes in plasma membrane proteins of Arabidopsis. *Mol Cell Proteomics*, **6** (10):1711–1726.
- NISHIMURA N, SARKESHIK A, NITO K, PARK SY, WANG A, CARVALHO P, LEE S, CADDELL DF, CUTLER SR, CHORY J, III JRY & SCHROEDER JI (2009). PYR/PYL/RCAR family members are major in vivo ABI1 protein phosphatase 2C-interacting proteins in Arabidopsis. *Plant J*, **61** (2):290–299.
- NISOLE S, KRUST B & HOVANESSIAN AG (2002). Anchorage of HIV on permissive cells leads to coaggregation of viral particles with surface nucleolin at membrane raft microdomains. *Exp Cell Res*, **276** (2):155–173.
- NOUR-ELDIN HH, HANSEN BG, NØRHOLM MH, JENSEN JK & HALKIER BA (2006). Advancing uracil-excision based cloning towards an ideal technique for cloning PCR fragments. *Nucleic Acids Res*, **34** (18):–122.
- NYDEGGER S, KHURANA S, KREMENTSOV DN, FOTI M & THALI M (2006). Mapping of tetraspanin-enriched microdomains that can function as gateways for HIV-1. *J Cell Biol*, **173** (5):795–807.
- NÜHSE TS, BOLLER T & PECK SC (2003). A plasma membrane syntaxin is phosphorylated in response to the bacterial elicitor flagellin. *The Journal of biological chemistry*, **278** (46):45248–45254.

- NÜHSE TS, STENSBALLE A, JENSEN ON & PECK SC (2004). Phosphoproteomics of the Arabidopsis plasma membrane and a new phosphorylation site database. *The Plant cell*, **16** (9):2394–2405.
- OHVO H, OLSIO C & SLOTTE JP (1997). Effects of sphingomyelin and phosphatidylcholine degradation on cyclodextrin-mediated cholesterol efflux in cultured fibroblasts. *Biochim Biophys Acta*, **1349** (2):131–141.
- OKAMOTO T, SCHLEGEL A, SCHERER PE & LISANTI MP (1998). Caveolins, a family of scaffolding proteins for organizing "preassembled signaling complexes" at the plasma membrane. *J Biol Chem*, **273** (10):5419–5422.
- OLDFIELD E & CHAPMAN D (1972). Dynamics of lipids in membranes: Heterogeneity and the role of cholesterol. *FEBS Lett*, **23** (3):285–297.
- OTTICO E, PRINETTI A, PRIONI S, GIANNOTTA C, BASSO L, CHIGORNO V & SONNINO S (2003). Dynamics of membrane lipid domains in neuronal cells differentiated in culture. *J Lipid Res*, **44** (11):2142–2151.
- PAGE MD, KROPAT J, HAMEL PP & MERCHANT SS (2009). Two *Chlamydomonas* CTR copper transporters with a novel cys-met motif are localized to the plasma membrane and function in copper assimilation. *Plant Cell*, **21** (3):928–943.
- PANDIT SA, JAKOBSSON E & SCOTT HL (2004a). Simulation of the early stages of nano-domain formation in mixed bilayers of sphingomyelin, cholesterol, and dioleoylphosphatidylcholine. *Biophys J*, **87** (5):3312–3322.
- PANDIT SA, VASUDEVAN S, CHIU SW, MASHL RJ, JAKOBSSON E & SCOTT HL (2004b). Sphingomyelin-cholesterol domains in phospholipid membranes: atomistic simulation. *Biophys J*, **87** (2):1092–1100.
- PARTON RG & SIMONS K (2007). The multiple faces of caveolae. *Nat Rev Mol Cell Biol*, **8** (3):185–194.
- PECK SC (2005). Update on proteomics in Arabidopsis. Where do we go from here? *Plant Physiol*, **138** (2):591–599.
- PELKMANS L, BÜRLI T, ZERIAL M & HELENIUS A (2004). Caveolin-stabilized membrane domains as multifunctional transport and sorting devices in endocytic membrane traffic. *Cell*, **118** (6):767–780.

7. Bibliography

- PESKAN T, WESTERMANN M & OELMÜLLER R (2000). Identification of low-density Triton X-100-insoluble plasma membrane microdomains in higher plants. *European journal of biochemistry / FEBS*, **267** (24):6989–6995.
- PIKE LJ (2006). Rafts defined: a report on the Keystone Symposium on Lipid Rafts and Cell Function. *J Lipid Res*, **47** (7):1597–1598.
- PIMPL P, MOVAFEGHI A, COUGHLAN S, DENECKE J, HILLMER S & ROBINSON DG (2000). In situ localization and in vitro induction of plant COPI-coated vesicles. *Plant Cell*, **12** (11):2219–2236.
- PINGOUD A & JELTSCH A (2001). Structure and function of type II restriction endonucleases. *Nucleic Acids Res*, **29** (18):3705–3727.
- PODELL S & GRIBSKOV M (2004). Predicting N-terminal myristoylation sites in plant proteins. *BMC Genomics*, **5** (1):37.
- PRALLE A, KELLER P, FLORIN EL, SIMONS K & HÖRBER JK (2000). Sphingolipid-cholesterol rafts diffuse as small entities in the plasma membrane of mammalian cells. *J Cell Biol*, **148** (5):997–1008.
- PRINS A, VAN HEERDEN PDR, OLMOS E, KUNERT KJ & FOYER CH (2008). Cysteine proteinases regulate chloroplast protein content and composition in tobacco leaves: a model for dynamic interactions with ribulose-1,5-bisphosphate carboxylase/oxygenase (Rubisco) vesicular bodies. *J Exp Bot*, **59** (7):1935–1950.
- PRIOR IA, HARDING A, YAN J, SLUIMER J, PARTON RG & HANCOCK JF (2001). GTP-dependent segregation of H-ras from lipid rafts is required for biological activity. *Nat Cell Biol*, **3** (4):368–375.
- QI Y & KATAGIRI F (2009). Purification of low-abundance Arabidopsis plasma-membrane protein complexes and identification of candidate components. *Plant J*, **57** (5):932–944.
- RAFF MC, MIRSKY R, FIELDS KL, LISAK RP, DORFMAN SH, SILBERBERG DH, GREGSON NA, LEIBOWITZ S & KENNEDY MC (1978). Galactocerebroside is a specific cell-surface antigenic marker for oligodendrocytes in culture. *Nature*, **274** (5673):813–816.
- RAFFAELE S, MONGRAND S, GAMAS P, NIEBEL A & OTT T (2007). Genome-wide annotation of remorins, a plant-specific protein family: evolutionary and functional perspectives. *Plant Physiol*, **145** (3):593–600.

- RAFFAELE S, BAYER E, LAFARGE D, CLUZET S, RETANA SG, BOUBEKEUR T, LEBORGNE-CASTEL N, CARDE JP, LHERMINIER J, NOIROT E, SATIAT-JEUNEMAÎTRE B, LAROCHE-TRAINEAU J, MOREAU P, OTT T, MAULE AJ, REYMOND P, SIMON-PLAS F, FARMER EE, BESSOULE JJ & MONGRAND S (2009a). Remorin, a Solanaceae Protein Resident in Membrane Rafts and Plasmodesmata, Impairs Potato virus X Movement. *Plant Cell*, **21** (5):1541–1555.
- RAFFAELE S, BAYER E & MONGRAND S (2009b). Upregulation of the plant protein remorin correlates with dehiscence and cell maturation: a link with the maturation of plasmodesmata? *Plant Signal Behav*, **4** (10):915–919.
- RAJAGOPALAN S, WACHTLER V & BALASUBRAMANIAN M (2003). Cytokinesis in fission yeast: a story of rings, rafts and walls. *Trends Genet*, **19** (7):403–408.
- REN J, WEN L, GAO X, JIN C, XUE Y & YAO X (2008). CSS-Palm 2.0: an updated software for palmitoylation sites prediction. *Protein Eng Des Sel*, **21** (11):639–644.
- RESH MD (1994). Myristylation and palmitoylation of Src family members: the fats of the matter. *Cell*, **76** (3):411–413.
- (1999). Fatty acylation of proteins: new insights into membrane targeting of myristoylated and palmitoylated proteins. *Biochim Biophys Acta*, **1451** (1):1–16.
- (2006). Trafficking and signaling by fatty-acylated and prenylated proteins. *Nat Chem Biol*, **2** (11):584–590.
- REUVENI M, EVENOR D, ARTZI B, PERL A & ERNER Y (2001). Decrease in vacuolar pH during petunia flower opening is reflected in the activity of tonoplast H⁺-ATPase. *Journal of Plant Physiology*, **158** (8):991 – 998.
- REVEREY H, VEIT M, PONIMASKIN E & SCHMIDT MF (1996). Differential fatty acid selection during biosynthetic S-acylation of a transmembrane protein (HEF) and other proteins in insect cells (Sf9) and in mammalian cells (CV1). *J Biol Chem*, **271** (39):23607–23610.
- REYMOND P, KUNZ B, PAUL-PLETZER K, GRIMM R, ECKERSKORN C & FARMER EE (1996). Cloning of a cDNA encoding a plasma membrane-associated, uronide binding phosphoprotein with physical properties similar to viral movement proteins. *The Plant cell*, **8** (12):2265–2276.

7. Bibliography

- REYMOND P, WEBER H, DAMOND M & FARMER EE (2000). Differential gene expression in response to mechanical wounding and insect feeding in *Arabidopsis*. *Plant Cell*, **12** (5):707–720.
- RIETVELD A & SIMONS K (1998). The differential miscibility of lipids as the basis for the formation of functional membrane rafts. *Biochim Biophys Acta*, **1376** (3):467–479.
- RINIA HA, SNEL MM, VAN DER EERDEN JP & DE KRUIJFF B (2001). Visualizing detergent resistant domains in model membranes with atomic force microscopy. *FEBS Lett*, **501** (1):92–96.
- ROBATZEK S (2007). Vesicle trafficking in plant immune responses. *Cell Microbiol*, **9** (1):1–8.
- ROBATZEK S, CHINCHILLA D & BOLLER T (2006). Ligand-induced endocytosis of the pattern recognition receptor FLS2 in *Arabidopsis*. *Genes Dev*, **20** (5):537–542.
- ROCHE Y, GERBEAU-PISSOT P, BUHOT B, THOMAS D, BONNEAU L, GRETI J, MONGRAND S, PERRIER-CORNET JM & SIMON-PLAS F (2008). Depletion of phytosterols from the plant plasma membrane provides evidence for disruption of lipid rafts. *FASEB J*, **22** (11):3980–3991.
- RODAL SK, SKRETTING G, GARRED O, VILHARDT F, VAN DEURS B & SANDVIG K (1999). Extraction of cholesterol with methyl-beta-cyclodextrin perturbs formation of clathrin-coated endocytic vesicles. *Mol Biol Cell*, **10** (4):961–974.
- ROMEIS T, LUDWIG AA, MARTIN R & JONES JD (2001). Calcium-dependent protein kinases play an essential role in a plant defence response. *EMBO J*, **20** (20):5556–5567.
- ROTHBERG KG, HEUSER JE, DONZELL WC, YING YS, GLENNEY JR & ANDERSON RG (1992). Caveolin, a protein component of caveolae membrane coats. *Cell*, **68** (4):673–682.
- ROY S, LUETTERFORST R, HARDING A, APOLLONI A, ETHERIDGE M, STANG E, ROLLS B, HANCOCK JF & PARTON RG (1999). Dominant-negative caveolin inhibits H-Ras function by disrupting cholesterol-rich plasma membrane domains. *Nat Cell Biol*, **1** (2):98–105.
- SANGER F, NICKLEN S & COULSON AR (1977). DNA sequencing with chain-terminating inhibitors. *Proc Natl Acad Sci U S A*, **74** (12):5463–5467.

- SANTIAGO J, DUPEUX F, ROUND A, ANTONI R, PARK SY, JAMIN M, CUTLER SR, RODRIGUEZ PL & MÁRQUEZ JA (2009). The abscisic acid receptor PYR1 in complex with abscisic acid. *Nature*, **462** (7273):665–668.
- SASLOWSKY DE, LAWRENCE J, REN X, BROWN DA, HENDERSON RM & EDWARDS JM (2002). Placental alkaline phosphatase is efficiently targeted to rafts in supported lipid bilayers. *J Biol Chem*, **277** (30):26966–26970.
- SCHEIFFELE P, ROTH MG & SIMONS K (1997). Interaction of influenza virus haemagglutinin with sphingolipid-cholesterol membrane domains via its transmembrane domain. *EMBO J*, **16** (18):5501–5508.
- SCHRAW W, LI Y, McCLAIN MS, VAN DER GOOT FG & COVER TL (2002). Association of *Helicobacter pylori* vacuolating toxin (VacA) with lipid rafts. *J Biol Chem*, **277** (37):34642–34650.
- SCHROEDER R, LONDON E & BROWN D (1994). Interactions between saturated acyl chains confer detergent resistance on lipids and glycosylphosphatidylinositol (GPI)-anchored proteins: GPI-anchored proteins in liposomes and cells show similar behavior. *Proc Natl Acad Sci U S A*, **91** (25):12130–12134.
- SCHUCK S, HONSHO M, EKROOS K, SHEVCHENKO A & SIMONS K (2003). Resistance of cell membranes to different detergents. *Proc Natl Acad Sci U S A*, **100** (10):5795–5800.
- SCHULER I, MILON A, NAKATANI Y, OURISSON G, ALBRECHT AM, BENVENISTE P & HARTMAN MA (1991). Differential effects of plant sterols on water permeability and on acyl chain ordering of soybean phosphatidylcholine bilayers. *Proc Natl Acad Sci U S A*, **88** (16):6926–6930.
- SCHÜTZ GJ, KADA G, PASTUSHENKO VP & SCHINDLER H (2000). Properties of lipid microdomains in a muscle cell membrane visualized by single molecule microscopy. *EMBO J*, **19** (5):892–901.
- SCOLARI S, ENGEL S, KREBS N, PLAZZO AP, ALMEIDA RFMD, PRIETO M, VEIT M & HERRMANN A (2009). Lateral distribution of the transmembrane domain of influenza virus hemagglutinin revealed by time-resolved fluorescence imaging. *J Biol Chem*, **284** (23):15708–15716.

7. Bibliography

- SEDBROOK JC, CARROLL KL, HUNG KF, MASSON PH & SOMERVILLE CR (2002). The Arabidopsis SKU5 gene encodes an extracellular glycosyl phosphatidylinositol-anchored glycoprotein involved in directional root growth. *Plant Cell*, **14** (7):1635–1648.
- SHAHOLLARI B, PESKAN-BERGHÖFER T & OELMÜLLER R (2004). Receptor kinases with leucine-rich repeats are enriched in Triton X-100 insoluble plasma membrane microdomains from plants. *PHYSIOLOGIA PLANTARUM*, **122**:397–403.
- SHAHOLLARI B, VARMA A & OELMÜLLER R (2005). Expression of a receptor kinase in Arabidopsis roots is stimulated by the basidiomycete *Piriformospora indica* and the protein accumulates in Triton X-100 insoluble plasma membrane microdomains. *Journal of plant physiology*, **162** (8):945–958.
- SHAHOLLARI B, VADASSERY J, VARMA A & OELMÜLLER R (2007). A leucine-rich repeat protein is required for growth promotion and enhanced seed production mediated by the endophytic fungus *Piriformospora indica* in Arabidopsis thaliana. *The Plant journal : for cell and molecular biology*, **50** (1):1–13.
- SHAUL PW, SMART EJ, ROBINSON LJ, GERMAN Z, YUHANNA IS, YING Y, ANDERSON RG & MICHEL T (1996). Acylation targets endothelial nitric-oxide synthase to plasmalemmal caveolae. *J Biol Chem*, **271** (11):6518–6522.
- SHERRIER DJ, PRIME TA & DUPREE P (1999). Glycosylphosphatidylinositol-anchored cell-surface proteins from Arabidopsis. *Electrophoresis*, **20** (10):2027–2035.
- SHEVCHENKO A, JENSEN ON, PODTELEJNIKOV AV, SAGLIOCCO F, WILM M, VORM O, MORTENSEN P, BOUCHERIE H & MANN M (1997). Linking genome and proteome by mass spectrometry: large-scale identification of yeast proteins from two dimensional gels. *Proc Natl Acad Sci U S A*, **93** (25):14440–14445.
- SILVIUS JR (2003). Role of cholesterol in lipid raft formation: lessons from lipid model systems. *Biochim Biophys Acta*, **1610** (2):174–183.
- (2005). Partitioning of membrane molecules between raft and non-raft domains: insights from model-membrane studies. *Biochim Biophys Acta*, **1746** (3):193–202.
- SIMON-PLAS F, ELMAYAN T & BLEIN JP (2002). The plasma membrane oxidase NtrbohD is responsible for AOS production in elicited tobacco cells. *Plant J*, **31** (2):137–147.

- SIMONS K & EHEHALT R (2002). Cholesterol, lipid rafts, and disease. *J Clin Invest*, **110** (5):597–603.
- SIMONS K & IKONEN E (1997). Functional rafts in cell membranes. *Nature*, **387** (6633):569–572.
- SIMONS K & TOOMRE D (2000). Lipid rafts and signal transduction. *Nat Rev Mol Cell Biol*, **1** (1):31–39.
- SIMONS K & VAZ WLC (2004). Model systems, lipid rafts, and cell membranes. *Annu Rev Biophys Biomol Struct*, **33**:269–295.
- SIMONS M, KELLER P, STROOPER BD, BEYREUTHER K, DOTTI CG & SIMONS K (1998). Cholesterol depletion inhibits the generation of beta-amyloid in hippocampal neurons. *Proc Natl Acad Sci U S A*, **95** (11):6460–6464.
- SINGER SJ & NICOLSON GL (1972). The fluid mosaic model of the structure of cell membranes. *Science*, **175** (23):720–731.
- SIVARAMAN T, KUMAR TK, JAYARAMAN G & YU C (1997). The mechanism of 2,2,2-trichloroacetic acid-induced protein precipitation. *J Protein Chem*, **16** (4):291–297.
- SMITH PK, KROHN RI, HERMANSON GT, MALLIA AK, GARTNER FH, PROVENZANO MD, FUJIMOTO EK, GOEKE NM, OLSON BJ & KLENK DC (1985). Measurement of protein using bicinchoninic acid. *Anal Biochem*, **150** (1):76–85.
- SOMERVILLE C & BROWSE J (1991). Plant lipids: metabolism, mutants, and membranes. *Science*, **252** (5002):80–87.
- STANEVA G, SEIGNEURET M, KOUMANOV K, TRUGNAN G & ANGELOVA MI (2005). Detergents induce raft-like domains budding and fission from giant unilamellar heterogeneous vesicles: a direct microscopy observation. *Chem Phys Lipids*, **136** (1):55–66.
- STANISLAS T, BOUYSSIE D, ROSSIGNOL M, VESA S, FROMENTIN J, MOREL J, PICHEREAUX C, MONSARRAT B & SIMON-PLAS F (2009). Quantitative proteomics reveals a dynamic association of proteins to detergent resistant membranes upon elicitor signaling in tobacco. *Mol Cell Proteomics*, **8** (9):2186–2198.
- STEIN M, DITTMEN J, SÁNCHEZ-RODRÍGUEZ C, HOU BH, MOLINA A, SCHULZE-LEFERT P, LIPKA V & SOMERVILLE S (2006). Arabidopsis PEN3/PDR8, an

7. Bibliography

- ATP binding cassette transporter, contributes to nonhost resistance to inappropriate pathogens that enter by direct penetration. *The Plant cell*, **18** (3):731–746.
- STILLWELL W, CHENG YF & WASSALL SR (1990). Plant sterol inhibition of abscisic acid-induced perturbations in phospholipid bilayers. *Biochim Biophys Acta*, **1024** (2):345–351.
- STULNIG TM, BERGER M, SIGMUND T, RAEDERSTORFF D, STOCKINGER H & WALDHÄUSL W (1998). Polyunsaturated fatty acids inhibit T cell signal transduction by modification of detergent-insoluble membrane domains. *J Cell Biol*, **143** (3):637–644.
- SUBTIL A, GAIDAROV I, KOBYLARZ K, LAMPSON MA, KEEN JH & MCGRAW TE (1999). Acute cholesterol depletion inhibits clathrin-coated pit budding. *Proc Natl Acad Sci U S A*, **96** (12):6775–6780.
- SUSSMAN MR (1994). Molecular Analysis of Proteins in the Plant Plasma Membrane. *Annual Review of Plant Physiology and Plant Molecular Biology*, **45** (1):211–234.
- SWARBRECK D, WILKS C, LAMESCH P, BERARDINI TZ, GARCIA-HERNANDEZ M, FOERSTER H, LI D, MEYER T, MULLER R, PLOETZ L, RADENBAUGH A, SINGH S, SWING V, TISSIER C, ZHANG P & HUALA E (2008). The Arabidopsis Information Resource (TAIR): gene structure and function annotation. *Nucleic Acids Res*, **36** (Database issue):D1009–D1014.
- SYROVÝ I & HODNÝ Z (1991). Staining and quantification of proteins separated by polyacrylamide gel electrophoresis. *J Chromatogr*, **569** (1-2):175–196.
- SÁEZ-CIRIÓN A, NIR S, LORIZATE M, AGIRRE A, CRUZ A, PÉREZ-GIL J & NIEVA JL (2002). Sphingomyelin and cholesterol promote HIV-1 gp41 pretransmembrane sequence surface aggregation and membrane restructuring. *J Biol Chem*, **277** (24):21776–21785.
- TE J, MELCHER U, HOWARD A & VERCHOT-LUBICZ J (2005). Soilborne wheat mosaic virus (SBWMV) 19K protein belongs to a class of cysteine rich proteins that suppress RNA silencing. *Virology*, **2**:18.
- THOMAS DS, HOSSACK JA & ROSE AH (1978). Plasma-membrane lipid composition and ethanol tolerance in *Saccharomyces cerevisiae*. *Arch Microbiol*, **117** (3):239–245.

- TITAPIWATANAKUN B, BLAKESLEE JJ, BANDYOPADHYAY A, YANG H, MRAVEC J, SAUER M, CHENG Y, ADAMEC J, NAGASHIMA A, GEISLER M, SAKAI T, FRIML J, PEER WA & MURPHY AS (2009). ABCB19/PGP19 stabilises PIN1 in membrane microdomains in Arabidopsis. *Plant J*, **57** (1):27–44.
- TROUET D, CARTON I, HERMANS D, DROOGMANS G, NILIUS B & EGGERMONT J (2001a). Inhibition of VRAC by c-Src tyrosine kinase targeted to caveolae is mediated by the Src homology domains. *Am J Physiol Cell Physiol*, **281** (1):C248–C256.
- TROUET D, HERMANS D, DROOGMANS G, NILIUS B & EGGERMONT J (2001b). Inhibition of volume-regulated anion channels by dominant-negative caveolin-1. *Biochem Biophys Res Commun*, **284** (2):461–465.
- TROUVERIE J, VIDAL G, ZHANG Z, SIRICHANDRA C, MADIONA K, AMIAR Z, PRIOUL JL, JEANNETTE E, RONA JP & BRAULT M (2008). Anion channel activation and proton pumping inhibition involved in the plasma membrane depolarization induced by ABA in Arabidopsis thaliana suspension cells are both ROS dependent. *Plant Cell Physiol*, **49** (10):1495–1507.
- TRUERNIT E & SAUER N (1995). The promoter of the Arabidopsis thaliana SUC2 sucrose-H⁺ symporter gene directs expression of beta-glucuronidase to the phloem: evidence for phloem loading and unloading by SUC2. *Planta*, **196** (3):564–570.
- UEMURA M, JOSEPH RA & STEPONKUS PL (1995). Cold Acclimation of Arabidopsis thaliana (Effect on Plasma Membrane Lipid Composition and Freeze-Induced Lesions). *Plant Physiol*, **109** (1):15–30.
- VAHISALU T, KOLLIST H, WANG YF, NISHIMURA N, CHAN WY, VALERIO G, LAMMINMÄKI A, BROSCHE M, MOLDAU H, DESIKAN R, SCHROEDER JI & KANGASJÄRVI J (2008). SLAC1 is required for plant guard cell S-type anion channel function in stomatal signalling. *Nature*, **452** (7186):487–491.
- VAIN P, KEEN N, MURILLO J, RATHUS C, NEMES C & FINER J (1993). Development of the Particle Inflow Gun. *Plant Cell, Tissue and Organ Culture*, **33** (3):237–246.
- VARMA R & MAYOR S (1998). GPI-anchored proteins are organized in submicron domains at the cell surface. *Nature*, **394** (6695):798–801.
- VEATCH SL & KELLER SL (2003). Separation of liquid phases in giant vesicles of ternary mixtures of phospholipids and cholesterol. *Biophys J*, **85** (5):3074–3083.

7. Bibliography

- VEIT M, REVEREY H & SCHMIDT MF (1996). Cytoplasmic tail length influences fatty acid selection for acylation of viral glycoproteins. *Biochem J*, **318** (Pt 1):163–172.
- VEREB G, SZÖLLOSI J, MATKÓ J, NAGY P, FARKAS T, VIGH L, MÁTYUS L, WALDMANN TA & DAMJANOVICH S (2003). Dynamic, yet structured: The cell membrane three decades after the Singer-Nicolson model. *Proc Natl Acad Sci U S A*, **100** (14):8053–8058.
- VERTOMMEN A, PANIS B, SWENNEN R & CARPENTIER SC (2010). Evaluation of chloroform/methanol extraction to facilitate the study of membrane proteins of non-model plants. *Planta*, **231** (5):1113–1125.
- VOINNET O, RIVAS S, MESTRE P & BAULCOMBE D (2003). An enhanced transient expression system in plants based on suppression of gene silencing by the p19 protein of tomato bushy stunt virus. *Plant J*, **33** (5):949–956.
- WACHTLER V & BALASUBRAMANIAN MK (2006). Yeast lipid rafts? – An emerging view. *Trends Cell Biol*, **16** (1):1–4.
- WACHTLER V, RAJAGOPALAN S & BALASUBRAMANIAN MK (2003). Sterol-rich plasma membrane domains in the fission yeast *Schizosaccharomyces pombe*. *J Cell Sci*, **116** (Pt 5):867–874.
- WANG W, SCALI M, VIGNANI R, SPADAFORA A, SENSI E, MAZZUCA S & CRESTI M (2003). Protein extraction for two-dimensional electrophoresis from olive leaf, a plant tissue containing high levels of interfering compounds. *Electrophoresis*, **24** (14):2369–2375.
- WANG XQ, ULLAH H, JONES AM & ASSMANN SM (2001). G protein regulation of ion channels and abscisic acid signaling in *Arabidopsis* guard cells. *Science*, **292** (5524):2070–2072.
- WARNECKE D & HEINZ E (2003). Recently discovered functions of glucosylceramides in plants and fungi. *Cell Mol Life Sci*, **60** (5):919–941.
- WESSEL D & FLÜGGE UI (1984). A method for the quantitative recovery of protein in dilute solution in the presence of detergents and lipids. *Anal Biochem*, **138** (1):141–143.
- WHITEMAN SA, SERAZETDINOVA L, JONES AME, SANDERS D, RATHJEN J, PECK SC & MAATHUIS FJM (2008). Identification of novel proteins and phosphorylation

- sites in a tonoplast enriched membrane fraction of *Arabidopsis thaliana*. *Proteomics*, **8** (17):3536–3547.
- WIDJAJA I, NAUMANN K, ROTH U, WOLF N, MACKEY D, DANGL JL, SCHEEL D & LEE J (2009). Combining subproteome enrichment and Rubisco depletion enables identification of low abundance proteins differentially regulated during plant defense. *Proteomics*, **9** (1):138–147.
- WILCOX C, HU JS & OLSON EN (1987). Acylation of proteins with myristic acid occurs cotranslationally. *Science*, **238** (4831):1275–1278.
- WILLIG KI, RIZZOLI SO, WESTPHAL V, JAHN R & HELL SW (2006). STED microscopy reveals that synaptotagmin remains clustered after synaptic vesicle exocytosis. *Nature*, **440** (7086):935–939.
- WILSON BS, STEINBERG SL, LIEDERMAN K, PFEIFFER JR, SURVILADZE Z, ZHANG J, SAMELSON LE, YANG LH, KOTULA PG & OLIVER JM (2004). Markers for detergent-resistant lipid rafts occupy distinct and dynamic domains in native membranes. *Mol Biol Cell*, **15** (6):2580–2592.
- XAVIER R, BRENNAN T, LI Q, MCCORMACK C & SEED B (1998). Membrane compartmentation is required for efficient T cell activation. *Immunity*, **8** (6):723–732.
- XU Z, XIE Q & ZHOU HM (2003). Trichloroacetic acid-induced molten globule state of aminoacylase from pig kidney. *J Protein Chem*, **22** (7-8):669–675.
- YAMADA E (1955). The fine structure of the gall bladder epithelium of the mouse. *J Biophys Biochem Cytol*, **1** (5):445–458.
- YAMADA H, HANAKI N, IMAMURA A, UEGUCHI C & MIZUNO T (1998). An *Arabidopsis* protein that interacts with the cytokinin-inducible response regulator, ARR4, implicated in the His-Asp phosphorylay signal transduction. *FEBS Lett*, **436** (1):76–80.
- YANCEY PG, RODRIGUEZA WV, KILSDONK EP, STOUT GW, JOHNSON WJ, PHILLIPS MC & ROTHBLAT GH (1996). Cellular cholesterol efflux mediated by cyclodextrins. Demonstration Of kinetic pools and mechanism of efflux. *J Biol Chem*, **271** (27):16026–16034.
- YOSHIDA R, UMEZAWA T, MIZOGUCHI T, TAKAHASHI S, TAKAHASHI F & SHINOZAKI K (2006). The regulatory domain of SRK2E/OST1/SnRK2.6 interacts with ABI1 and integrates abscisic acid (ABA) and osmotic stress signals controlling stomatal closure in *Arabidopsis*. *J Biol Chem*, **281** (8):5310–5318.

7. Bibliography

- YOSHIDA S, UEMURA M, NIKI T, SAKAI A & GUSTA LV (1983). Partition of Membrane Particles in Aqueous Two-Polymer Phase System and Its Practical Use for Purification of Plasma Membranes from Plants. *Plant Physiol*, **72** (1):105–114.
- YUAN C, FURLONG J, BURGOS P & JOHNSTON LJ (2002). The size of lipid rafts: an atomic force microscopy study of ganglioside GM1 domains in sphingomyelin/DOPC/cholesterol membranes. *Biophys J*, **82** (5):2526–2535.
- ZAJCHOWSKI LD & ROBBINS SM (2002). Lipid rafts and little caves. Compartmentalized signalling in membrane microdomains. *Eur J Biochem*, **269** (3):737–752.
- ZAPPEL NF & PANSTRUGA R (2008). Heterogeneity and lateral compartmentalization of plant plasma membranes. *Curr Opin Plant Biol*, **11** (6):632–640.
- ZHANG FL & CASEY PJ (1996). Protein prenylation: molecular mechanisms and functional consequences. *Annu Rev Biochem*, **65**:241–269.
- ZHANG W, QIN C, ZHAO J & WANG X (2004). Phospholipase D alpha 1-derived phosphatidic acid interacts with ABI1 phosphatase 2C and regulates abscisic acid signaling. *Proc Natl Acad Sci U S A*, **101** (25):9508–9513.
- ZHANG Y, ZHU H, ZHANG Q, LI M, YAN M, WANG R, WANG L, WELTI R, ZHANG W & WANG X (2009). Phospholipase Dalpha1 and Phosphatidic Acid Regulate NADPH Oxidase Activity and Production of Reactive Oxygen Species in ABA-Mediated Stomatal Closure in Arabidopsis. *Plant Cell*, **21** (8):2357–2377.
- ZHU J, LEE BH, DELLINGER M, CUI X, ZHANG C, WU S, NOTHNAGEL EA & ZHU JK (2010). A cellulose synthase-like protein is required for osmotic stress tolerance in Arabidopsis. *Plant J*, **63** (1):128–140.
- ZHU JK (2002). Salt and drought stress signal transduction in plants. *Annu Rev Plant Biol*, **53**:247–273.

A

Protein lists

Treatment with the non-ionic detergents Brij-98 and Triton X-100 resulted in complex lists of protein identifications. The following lists represent all *Arabidopsis thaliana* mesophyll DRM proteins which were identified either in Brij-98 DRMs (table A.3, p. 194) or Triton X-100 DRMs (table A.2, p. 186) with a false discovery rate (fdr) < 5 %. The protein composition of the PM, which was used to generate the Brij-98 & Triton X-100 DRMs, was also investigated (table A.1, p. 162). DRM proteins were grouped by functional classification and sorted by ascending *Arabidopsis* Gene Identifiers (AGIs) whereas PM proteins were just sorted by AGIs.

Corresponding PM preparations were precipitated by chloroform / methanol (cf. 2.2.4.2, p. 58) or the method of Wang *et al.* (2003) (cf. 2.2.4.4, p. 59) before mass spectrometric protein identification was conducted.

Methyl- β -D-cyclodextrin investigations of sterol-dependency were only performed with Triton X-100 DRMs. Detailed results have already been presented in tables 3.5 (p. 91) and 3.6 (p. 95). Previous protein identifications after detergent-treatment with Brij-98 or Triton X-100 were not subjected to MCD treatment (first experimental setup).

The following protein lists represent pooled protein identification data from 2 independent proteomic experiments. Triton X-100 treatment was performed within all experiments whereas the non-ionic detergent Brij-98 was only used in the first experimental setup. The effects of in-gel and in-solution assisted digestion were also studied only in this first experimental setup. However, MCD sterol-depletion effects were investigated in the second experimental setup where only Triton X-100 DRMs were isolated.

Data evaluation and database searching were conducted against the TAIR9 database using the Mascot daemon software (Mascot algorithm, version 2.2) by Matrix Science Ltd., London, UK (cf. section 2.3.2.3, p. 64).

Table A.1.: PM proteins identified via mass spectrometry (MS); the corresponding DRMs were isolated from these PM isolations

AGI	Uniprot	Name	MW [kDa]	TMD	GRAVY	Precipitation methods		
						CHCl ₃ /MeOH	Wang	-
At1g01100	Q8LCW9	60S acidic ribosomal protein P1-1	11.2	0	0.21	•		
At1g01620	Q08733	Aquaporin PIP1-3	30.6	6	0.38	•	•	•
At1g02130	P28188	Ras-related protein RABD2A	22.6	0	-0.37		•	
At1g02520	Q9FWX7	ABC transporter B family member 11 (PGP11)	137.7	12	0.15		•	
At1g02780	Q9SRX2	60S ribosomal protein L19-1	24.6	0	-0.99	•	•	
At1g02930	P42760	Glutathione S-transferase 1	23.5	0	-0.22	•		
At1g03130	Q9SA56	Photosystem I reaction center subunit II-2 (chloroplastic)	22.3	0	-0.39		•	
At1g03870	Q9ZWA8	Fasciclin-like arabinogalactan protein 9 (Fla9)	26.1	0	0	•	•	•
At1g04270	Q08112	40S ribosomal protein S15-1	17.2	0	-0.35		•	
At1g04410	P93819	Malate dehydrogenase (cytoplasmic) 1	35.6	0	0.01	•		
At1g04750	Q9ZTW3	Vesicle-associated membrane protein 721 (AtVAMP721)	24.8	1	-0.12		•	•
At1g04820	P29510	Tubulin alpha-2/alpha-4 chain	49.5	0	-0.2	•	•	
At1g05150	O23052	Uncharacterized TPR repeat-containing protein At1g05150	90.2	0	-0.42		•	
At1g05190	O23049	50S ribosomal protein L6 (chloroplastic)	24.7	0	-0.44		•	•
At1g05500	Q9ZVY8	Synaptotagmin homologue E (AtSytE)	59.2	0	-0.01		•	
At1g06400	P28185	Ras-related protein RABA1a	23.9	0	-0.31		•	
At1g06700	Q8H1G6	Serin/threonin protein kinase	39.8	0	-0.33	•	•	
At1g07320	O50061	50S ribosomal protein L4 (chloroplastic)	30.6	0	-0.4			•
At1g07890	Q05431	L-ascorbate peroxidase 1, cytosolic	27.6	0	-0.39	•		
At1g07930	P13905	Elongation factor 1-alpha	49.5	0	-0.33			•
At1g08360	Q8VZB9	60S ribosomal protein L10a-1	24.5	0	-0.42		•	
At1g08830	P24704	Superoxide dismutase [Cu-Zn]	15.1	0	-0.08	•		
At1g09100	O04019	26S protease regulatory subunit 6A homolog	46.7	0	-0.4		•	
At1g09160	O80492	Probable protein phosphatase 2C 5	45.8	0	-0.15		•	
At1g09310	Q9ZPZ4	Putative uncharacterized protein	19.9	0	-0.37	•		
At1g09420	Q93ZW0	Glucose-6-phosphate 1-dehydrogenase 4 (chloroplastic)	70.2	0	-0.31	•		
At1g09590	Q43291	60S ribosomal protein L21-1	18.7	0	-0.69			•

Continued on next page ...

AGI	Uniprot	Name	MW [kDa]	TMD	GRAVY	Precipitation methods		
						CHCl ₃ /MeOH	Wang	-
At1g09630	O04486	Ras-related protein RABA2a	24.1	0	-0.34		•	
At1g10290	Q9SE83	Dynamin-2A	99.2	0	-0.49		•	
At1g10630	Q6ID97	ADP-ribosylation factor A1F	20.6	0	-0.19			•
At1g10840	Q9C5Z2	Eukaryotic translation initiation factor 3 subunit H	38.4	0	-0.34	•		
At1g11260	P23586	Sugar transport protein 1 (STP1)	57.6	12	0.48	•	•	•
At1g11310	Q9SXB6	MLO-like protein 2	65.5	7	-0.1	•		
At1g12110	Q05085	Nitrate/chlorate transporter	64.9	12	0.36	•	•	
At1g12310	Q94AZ4	Probable calcium-binding protein CML13	16.5	0	-0.34	•		
At1g12900	Q9LPW0	GAPA-2	42.8	0	-0.05		•	
At1g13210	Q9SAF5	Putative phospholipid-transporting ATPase 11	136.6	10	-0.08		•	
At1g13440	Q9FX54	Putative glyceraldehyde-3-phosphate dehydrogenase	36.9	0	-0.14	•	•	
At1g13470	Q56XU1	Uncharacterized protein	31	0	-0.61			•
At1g13930	Q9XI93	Similar to nodulin-related	16.2	0	-0.88	•		
At1g14320	Q93VT9	60S ribosomal protein L10-1	24.9	0	-0.45		•	
At1g14870	Q9LQU4	Uncharacterized protein At1g14870	16.7	1	-0.13	•		
At1g14880	Q9LQU2	F10B6.29	16.5	0	-0.11	•	•	•
At1g15210	Q7PC86	ABC transporter G family member 35 (PDR7)	162.6	13	0.05		•	
At1g15690	P31414	Pyrophosphate-energized vacuolar membrane proton pump 1	80.9	13	0.62	•	•	•
At1g16030	Q9S9N1	Heat shock protein 70B (Hsp70b)	70.9	0	-0.38		•	
At1g16260	Q9SA25	Wall-associated receptor kinase-like 8	81.2	1	-0.24		•	
At1g16670	Q93YN1	Putative uncharacterized protein At1g16670	43.3	0	-0.32		•	
At1g16860	Q9FZ45	Uncharacterized membrane protein At1g16860	50.6	2	-0.11		•	
At1g17260	Q43128	ATPase 10, plasma membrane-type	104.8	10	0.14		•	
At1g17620	Q9LNP3	Similar to Heavy metal transport/detoxification protein (Harpin-induced 1)	28.3	0	-0.02		•	
At1g18210	Q9LE22	Probable calcium-binding protein CML27	18.4	0	-0.45	•		
At1g18540	Q9FZ76	60S ribosomal protein L6-1	26.2	0	-0.59		•	
At1g19110	Q8L798	Putative uncharacterized protein At1g19110	83	0	-0.13		•	
At1g19570	Q9FWR4	Glutathione S-transferase DHAR1, mitochondrial	23.6	0	-0.17	•		
At1g19870	Q9FXI5	Protein IQ-DOMAIN 32	86.9	0	-0.89	•		
At1g20010	P29513	Tubulin beta-5 chain	50.3	0	-0.36	•	•	
At1g20370	Q9LN29	tRNA pseudouridine synthase family protein	61.5	0	-0.6	•		

Continued on next page ...

AGI	Uniprot	Name	MW [kDa]	TMD	GRAVY	Precipitation methods		
						CHCl ₃ /MeOH	Wang	-
At1g20440	P31168	Dehydrin COR47	29.9	0	-1.25	•	•	
At1g20450	P42759	Dehydrin ERD10	29.5	0	-1.35	•	•	
At1g20780	Q9LM76	U-box domain-containing protein 44	88.4	0	-0.02			•
At1g21080	Q9LPU3	DNAJ heat shock N-terminal domain-containing protein	43.9	0	-0.6	•		
At1g21210	Q9LMN6	Wall-associated receptor kinase 4	81.7	1	-0.3			•
At1g21230	Q9LMN7	Wall-associated receptor kinase 5	82.2	1	-0.28			•
At1g21240	Q9LMN8	Wall-associated receptor kinase 3	82.7	1	-0.26			•
At1g21250	Q39191	Wall-associated receptor kinase 1	81.2	1	-0.26	•		
At1g21270	Q9LMP1	Wall-associated receptor kinase 2	81.6	1	-0.3			•
At1g21750	Q9XI01	Protein disulfide-isomerase 5	55.6	0	-0.33	•		
At1g21880	Q93ZH0	LysM domain-containing GPI-anchored protein 1	43.5	0	0.29	•		
At1g22280	Q9LME4	Probable protein phosphatase 2C 9	30.7	0	-0.41	•		•
At1g22300	P48347	14-3-3-like protein GF14 epsilon (GRF10)	28.9	0	-0.64	•		•
At1g22530	Q56Z12	Patellin-2	76	0	-0.53	•		•
At1g22710	Q39231	Sucrose transport protein SUC2	54.5	12	0.48	•		•
At1g22740	O04157	Ras-related protein Rab7	22.9	0	-0.37			•
At1g22780	P34788	40S ribosomal protein S18	17.5	0	-0.68			•
At1g23080	Q940Y5	Auxin efflux carrier component 7 (AtPIN7)	67.6	10	0.14	•		•
At1g23410	P59263	Ubiquitin	8.5	0	-0.45			•
At1g23490	Q9SRC3	ADP-ribosylation factor 2	20.6	0	-0.19			•
At1g25490	Q38845	Serine/threonine-protein phosphatase 2A 65 kDa regulatory subunit A α	65.5	0	0.15	•		
At1g26830	Q9ZVH4	Cullin 3a	85.3	0	-0.54	•		
At1g27190	O04567	Probable inactive receptor kinase At1g27190	65.4	1	-0.01	•		•
At1g27950	Q9C7F7	LTPG1	19.8	0	0.23	•		•
At1g29910	P04777	Chlorophyll a-b binding protein 165/180 (chloroplastic)	28.3	3	0.02			•
At1g30360	Q9C8G5	Dehydrin ERD4	81.9	0	0.3	•		•
At1g30690	Q94C59	Patellin-4	61.2	0	-0.59			•
At1g31330	Q9SHE8	Photosystem I reaction center subunit III (chloroplastic)	24.2	1	-0.01	•		•
At1g31340	Q9SHE7	NEDD8-like protein RUB1	8.9	0	-0.29			•
At1g32050	Q9C6X2	Secretory carrier-associated membrane protein 4	30.1	4	0.23	•		•
At1g32990	Q9MAP3	50S ribosomal protein L11 (chloroplastic)	23.1	0	0.1			•

Continued on next page ...

AGI	Uniprot	Name	MW [kDa]	TMD	GRAVY	Precipitation methods		
						CHCl ₃ /MeOH	Wang	-
At1g33120	P49209	60S ribosomal protein L9-1	22	0	-0.35		•	
At1g34210	Q9XIC7	Somatic embryogenesis receptor kinase 2 (AtSERK2)	69.4	1	-0.1		•	
At1g34750	Q9S9Z7	Probable protein phosphatase 2C 10	30.1	0	-0.4		•	
At1g35620	Q94F09	Protein disulfide-isomerase 5-like 2	49.9	0	-0.16		•	
At1g35680	P51412	50S ribosomal protein L21 (chloroplastic)	24	0	-0.15			•
At1g35720	Q9SYT0	Annexin D1	36.2	0	-0.6	•	•	•
At1g42550	Q8VY94	Plastid movement impaired 1 (PMI1)	78.9	0	-0.63		•	
At1g42970	P25857	Glyceraldehyde-3-phosphate dehydrogenase B (chloroplastic)	47.7	0	0		•	
At1g43170	P17094	60S ribosomal protein L3-1	44.6	0	-0.58		•	
At1g43890	Q23657	AtRab18	23.5	0	-0.28		•	
At1g44100	Q8GUM3	Amino acid permease, putative	52.6	0	0.49	•		
At1g47550	Q9SX85	Exocyst complex component SEC3A	100.1	0	-0.33	•		
At1g48240	Q9LNH6	Novel plant SNARE 12	29.9	1	-0.54	•	•	
At1g48440	Q8LDS7	At1g48440	14.1	0	0.32	•		
At1g48480	Q9LP77	Probable inactive receptor kinase At1g48480	71.1	1	-0.19	•	•	
At1g49040	Q8RXA7	Stomatal cytokinesis defective	131.6	0	-0.16	•		
At1g49240	Q96293	Actin-8	41.9	0	-0.18		•	
At1g49300	Q9XI98	AtRABG3E	22.1	0	-0.37		•	
At1g50700	Q9C6P3	Calcium-dependent protein kinase 33 (CPK33)	58.6	0	-0.47		•	
At1g51500	Q9C8K2	ABC transporter G family member 12 (AtWBC12)	76.5	7	0.11	•	•	
At1g51980	Q9ZU25	Probable mitochondrial-processing peptidase subunit alpha-1	54.4	0	-0.13			•
At1g52190	Q9M817	Probable peptide transporter At1g52190	66.9	10	0.24	•	•	
At1g52200	Q9M815	At1g52200	21.2	0	-0.37	•	•	
At1g52280	Q9C820	AtRab72	23.1	0	-0.39		•	
At1g52290	Q9C821	Protein kinase	55.7	0	-0.43	•		
At1g53210	Q8L636	Sodium/calcium exchanger family protein	63.4	0	0.47		•	
At1g53400	Q9MAG2	F12M16.29	12.7	0	-0.63	•		
At1g53730	Q9C8M9	Protein STRUBBELIG-RECEPTOR FAMILY 6	78.1	1	-0.2		•	
At1g53840	Q43867	Pectinesterase 1	64.1	0	-0.21		•	
At1g54270	P41377	Eukaryotic initiation factor 4A-2	46.8	0	-0.22		•	
At1g54610	Q9ZVM9	Putative serine/threonine-protein kinase At1g54610	63.3	0	-0.62		•	

Continued on next page ...

AGI	Uniprot	Name	MW [kDa]	TMD	GRAVY	Precipitation methods		
						CHCl ₃ /MeOH	Wang	-
At1g56330	Q01474	GTP-binding protein SAR1B	21.1	0	-0.12		•	
At1g56410	Q9C7X7	Heat shock cognate 70 kDa protein/HSC70/HSP70	68.4	0	-0.37		•	
At1g57990	Q9C508	Probable purine permease 18	44.2	10	0.44	•		
At1g58360	Q42400	Amino acid permease I	52.9	0	0.42	•		
At1g58380	Q8L8Y0	40S ribosomal protein S2-1	30.7	0	-0.43		•	
At1g58684	Q93VB8	40S ribosomal protein S2-2	30.8	0	-0.43		•	
At1g59610	Q9LQ55	Dynamin-2B	100.2	0	-0.56		•	
At1g59870	Q9XIE2	ABC transporter G family member 36 (PEN3/PDR8)	165.1	14	0.05	•	•	•
At1g61180	Q940K0	Probable disease resistance protein At1g61180	101.7	0	-0.18		•	
At1g61250	Q9M5P2	Secretory carrier-associated membrane protein 3	32.6	4	0.19	•	•	•
At1g61520	Q9SY97	PSI type III chlorophyll a/b-binding protein	29.2	0	-0.01			•
At1g61900	Q8GUI4	Uncharacterized GPI-anchored protein At1g61900	47	0	0.07	•		
At1g63830	Q9CAJ7	Proline-rich family protein	25.7	0	-0.08	•	•	
At1g64500	Q9SGW5	Glutaredoxin family protein	41	0	-0.7		•	
At1g64760	Q6NKW9	Putative glucan endo-1,3-beta-glucosidase 8	52.3	0	0.03	•	•	
At1g65260	O80796	Probable membrane-associated 30 kDa protein (chloroplastic)	36.4	0	-0.56	•	•	
At1g65690	Q8LD98	Harpin-induced protein-like	28.6	0	-0.26			•
At1g66100	Q9C8D6	Probable thionin-2.4 [Cleaved into: Probable thionin-2.4; Acidic protein]	14.1	0	0.25	•		
At1g66150	P43298	Putative receptor protein kinase TMK1	102.4	1	-0.13		•	
At1g66940	Q9FZI4	Serin/threonin protein kinase	36.7	0	-0.06		•	
At1g66950	Q7PC84	ABC transporter G family member 39 (PDR11)	165.2	15	0.03		•	
At1g66970	Q7Y208	Probable glycerophosphoryl diester phosphodiesterase 3	83.8	0	-0.02	•	•	•
At1g67090	P10795	Ribulose biphosphate carboxylase small chain 1A (chloroplastic)	20.3	0	-0.27	•	•	•
At1g68220	Q9C9F7	Putative uncharacterized protein	21.4	0	0.39	•		
At1g68570	Q9SX20	Proton-dependent oligopeptide transport (POT) family protein	66.2	0	0.24	•		
At1g68710	Q9SX33	Putative phospholipid-transporting ATPase 9	136	10	-0.06		•	
At1g69840	Q9CAR7	Hypersensitive-induced response protein	31.4	0	-0.22	•	•	•
At1g69960	O04951	Serine/threonine-protein phosphatase PP2A-5 catalytic subunit	35	0	-0.3	•		
At1g70410	Q94CE4	Carbonic anhydrase	30.8	0	-0.17	•	•	•
At1g70530	Q9CAL2	Cysteine-rich receptor-like protein kinase 3	71.6	1	-0.13		•	
At1g70810	Q9SSL1	C2 domain-containing protein	18.7	0	-0.29	•		

Continued on next page ...

AGI	Uniprot	Name	MW [kDa]	TMD	GRAVY	Precipitation methods		
						CHCl ₃ /MeOH	Wang	-
At1g70940	Q9S7Z8	Auxin efflux carrier component 3 (AtPIN3)	69.5	10	0.14	•	•	
At1g71820	Q94A16	SEC6	85.7	0	-0.32		•	
At1g71880	Q39232	Sucrose transport protein SUC1	54.9	12	0.47	•	•	•
At1g72150	Q56WK6	Patellin-1	64	0	-0.54	•	•	•
At1g72160	Q56Z59	Patellin-3	56.1	0	-0.64		•	
At1g72230	Q9C7T2	Blue copper protein, putative	18.4	0	0.25	•	•	
At1g72370	Q08682	40S ribosomal protein Sa-1	32.3	0	-0.32	•	•	
At1g72730	Q9CAI7	Eukaryotic initiation factor 4A-3	46.8	0	-0.22		•	
At1g73390	Q9FX34	At1g73390	46.8	0	-0.36		•	
At1g73650	Q3ECD5	Oxidoreductase, acting on the CH-CH group of donors	33.1	0	0.52			•
At1g74050	Q9C9C5	60S ribosomal protein L6-3	26.1	0	-0.56		•	
At1g74060	Q9C9C6	60S ribosomal protein L6-2	26	0	-0.56		•	
At1g74790	Q9SSG3	HIPL1 protein	75.2	0	-0.31	•	•	
At1g75680	Q8LCP6	Endoglucanase 10	57.9	0	-0.33	•	•	•
At1g75780	P12411	Tubulin beta-1 chain	50.2	0	-0.38		•	
At1g76010	Q93VA8	Nucleic-acid binding	37.4	0	-1.21		•	•
At1g76040	Q8RWL2	Calcium-dependent protein kinase 29 (CPK29)	60.5	0	-0.53	•		
At1g76180	P42763	Dehydrin ERD14	20.8	0	-1.27		•	•
At1g76400	Q9SFX3	Putative dolichyl-diphosphooligosaccharide-protein glycosyltransferase	68.7	0	-0.12		•	
At1g77210	Q8GW61	Sugar transport protein 14 (STP14)	55.4	12	0.52	•		
At1g78200	Q8L714	Probable protein phosphatase 2C 17	30.9	0	-0.41		•	
At1g78300	Q01525	14-3-3-like protein GF14 omega (GRF2)	29.2	0	-0.48	•		
At1g78630	Q9SYL9	50S ribosomal protein L13 (chloroplastic)	26.8	0	-0.47	•		•
At1g78880	Q9ZVA7	Balbani ring 1-related	50.1	0	-0.16		•	
At1g78900	O23654	V-type proton ATPase catalytic subunit A	68.8	0	-0.17	•	•	
At1g80180	Q9SSC1	At1g80180/F18B13_26	15.2	0	-1.01		•	
At1g80660	Q42556	ATPase 9, plasma membrane-type	105.2	10	0.01		•	
At2g01180	Q9ZU49	Lipid phosphate phosphatase 1	36.7	6	0.1	•		
At2g01420	Q8RWZ6	Auxin efflux carrier component 4 (AtPIN4)	66.7	10	0.2		•	
At2g01820	Q9SIT1	Leucine-rich repeat receptor-like protein kinase	101.1	0	-0.18		•	
At2g02100	Q39182	Defensin-like protein 2	8.5	0	0.2	•		

Continued on next page ...

AGI	Uniprot	Name	MW [kDa]	TMD	GRAVY	Precipitation methods		
						CHCl ₃ /MeOH	Wang	-
At2g03440	Q9ZQ80	Putative uncharacterized protein At2g03440	19.7	0	-1.08	•		
At2g03530	Q9ZQ89	Ureide permease 2	43.5	10	0.43	•		
At2g04390	P49205	40S ribosomal protein S17-1	16	0	-0.58		•	•
At2g04780	Q9SJ81	Fasciclin-like arabinogalactan protein 7 (Fla7)	26.8	0	0.16	•		•
At2g05220	Q9SJ36	40S ribosomal protein S17-2	15.1	0	-0.59		•	
At2g07560	Q9SH76	ATPase 6, plasma membrane-type	105.1	10	0.03		•	
At2g13790	Q9SKG5	Somatic embryogenesis receptor kinase 4 (AtSERK4)	68.7	1	-0.19		•	
At2g16360	Q9SIW5	40S ribosomal protein S25-1	11.1	0	-0.72		•	
At2g16600	Q38900	Peptidyl-prolyl cis-trans isomerase CYP19-1	18.5	0	-0.32	•		
At2g16850	Q9ZVX8	Probable aquaporin PIP2-8	29.5	6	0.52	•		
At2g17120	Q23006	LysM domain-containing GPI-anchored protein 2	37.7	0	0.04	•	•	•
At2g17290	Q38872	Calcium-dependent protein kinase 6 (CPK6)	61.1	0	-0.32	•		
At2g17360	Q93VH9	40S ribosomal protein S4-1	29.8	0	-0.53	•	•	•
At2g17390	Q7XJS6	Ankyrin repeat-containing 2b	36.9	0	-0.57	•		
At2g18020	P46286	60S ribosomal protein L8-1	27.9	0	-0.47		•	
At2g18730	Q8VZG1	Diacylglycerol kinase, putative	53.9	0	-0.25	•	•	
At2g18960	P20649	ATPase 1, plasma membrane-type	104.2	10	0.08	•	•	•
At2g19580	Q9ZUN5	Tetraspanin 2	30.1	4	0.36	•		
At2g19730	O82204	60S ribosomal protein L28-1	15.9	0	-0.62	•	•	
At2g20260	Q9S714	Photosystem I reaction center subunit IV B (chloroplastic)	15.2	0	-0.13		•	
At2g20630	Q9SIU8	Probable protein phosphatase 2C 20	31.8	0	-0.32	•	•	
At2g20840	Q9SKT3	Secretory carrier-associated membrane protein 1	31.1	4	0.18	•		
At2g20990	Q9SKR2	Synaptotagmin A	61.7	0	-0.26	•	•	•
At2g21160	P45434	Translocon-associated protein subunit alpha	28.2	1	0.03	•	•	
At2g21330	Q9SJU4	Probable fructose-bisphosphate aldolase 1 (chloroplastic)	42.9	0	-0.12	•	•	
At2g21410	Q9SJT7	Putative vacuolar proton-ATPase subunit	93.1	0	0.05		•	
At2g21620	Q94II5	RD2 protein	21.3	0	-0.13	•		
At2g21660	Q03250	Glycine-rich RNA-binding protein 7	16.9	0	-0.76	•		
At2g23120	Q8S8R1	Expressed protein	8.5	0	-1	•		
At2g23140	O22193	U-box domain-containing protein 4	88.3	0	-0.33		•	
At2g23200	O22187	Putative uncharacterized protein At2g23200	93.4	0	-0.28	•	•	

Continued on next page ...

AGI	Uniprot	Name	MW [kDa]	TMD	GRAVY	Precipitation methods		
						CHCl ₃ /MeOH	Wang	-
At2g23810	O64822	Tetraspanin 8	22.1	4	-0.18	•		•
At2g24420	Q9ZQ26	DNA repair ATPase-related	50.4	0	-0.65			•
At2g24520	Q9SJB3	ATPase 5, plasma membrane-type	104.7	10	0.07			•
At2g24940	Q9SK39	Putative steroid-binding protein 3	11	0	-0.58	•		
At2g26510	Q8GZD4	Nucleobase-ascorbate transporter 3	60.2	12	0.49	•		
At2g26730	O48788	Probable inactive receptor kinase At2g26730	71.8	1	-0.19	•		•
At2g26975	Q8GWP3	Putative copper transport protein	15.8	0	0.51	•		
At2g27500	Q9ZQG9	Putative glucan endo-1,3-beta-glucosidase 14	44.1	0	-0.08	•		
At2g27720	P51407	60S acidic ribosomal protein P2-1	11.5	0	-0.17	•		
At2g27810	Q3E7D0	Nucleobase-ascorbate transporter 12	76.7	12	0.2	•		•
At2g28790	Q9ZV34	Osmotin-like protein	27	0	-0.06			•
At2g30520	Q2V443	Root phototropism 2	60.6	0	-0.23			•
At2g30560	O04339	Putative glycine-rich protein	14.3	0	-0.77	•		
At2g30730	O49338	Putative serine/threonine protein kinase	37.6	0	-0.19			•
At2g30740	O49339	Putative PTI1-like protein tyrosine kinase	40.5	0	-0.4	•		•
At2g30930	O80858	Expressed protein	16.9	0	-0.25	•		•
At2g31610	Q9SIP7	40S ribosomal protein S3-1	27.5	0	-0.08			•
At2g31680	Q9SIP0	Putative Ras superfamily GTP-binding protein	24.4	0	-0.39	•		
At2g31880	Q9SKB2	Leucine-rich repeat receptor-like protein kinase	71.1	0	-0.16	•		•
At2g31960	Q9SL03	Callose synthase 2	226.1	16	-0.11	•		
At2g32240	Q8S8J6	Putative myosin heavy chain	86.2	0	-0.78			•
At2g32450	Q8S8L9	Calcium-binding EF hand family protein	90.2	0	-0.41			•
At2g32680	O48849	Receptor Like Protein 23 (AtRLP23)	98.5	0	-0.06	•		•
At2g33050	O49328	Receptor Like Protein 26 (AtRLP26)	89.1	0	-0.03			•
At2g33120	P47192	Vesicle-associated membrane protein 722	24.9	1	-0.12	•		•
At2g33580	O22808	Peptidoglycan-binding LysM domain-containing protein	72.6	0	-0.12			•
At2g33870	P93020	Putative GTP-binding protein	24.5	0	-0.36			•
At2g34480	P51418	60S ribosomal protein L18a-2	21.3	0	-0.73			•
At2g34510	O64696	Putative uncharacterized protein At2g34510	43.9	0	-0.09	•		•
At2g34585	Q8S8R9	At2g34585	8.6	0	-0.13	•		
At2g35190	Q944A9	Novel plant SNARE 11	29.9	1	-0.48	•		

Continued on next page ...

AGI	Uniprot	Name	MW [kDa]	TMD	GRAVY	Precipitation methods		
						CHCl ₃ /MeOH	Wang	-
At2g35635	Q8RUC6	NEDD8-like protein RUB2	8.6	0	-0.26		•	
At2g35980	Q9SJ52	NDR1/HIN1-like	25.7	0	-0.07			•
At2g36160	Q9SIH0	40S ribosomal protein S14-1	16.3	0	-0.47		•	•
At2g36380	Q7PC87	ABC transporter G family member 34 (PDR6)	164.2	13	0.05		•	
At2g36620	Q42347	60S ribosomal protein L24-1	18.9	0	-1.02	•		
At2g36910	Q9ZR72	ABC transporter B family member 1 (MDR1/PGP1)	140.6	12	0.07		•	
At2g37170	P43287	Aquaporin PIP2-2	30.5	6	0.46	•	•	•
At2g37180	P30302	Aquaporin PIP2-3	30.4	6	0.5	•	•	•
At2g37190	P50883	60S ribosomal protein L12-1	17.9	0	-0.33		•	•
At2g37270	Q9ZUT9	40S ribosomal protein S5-1	22.1	0	-0.18	•		
At2g37620	P10671	Actin-1/3	41.8	0	-0.2		•	
At2g37710	O80939	Putative receptor protein kinase	75.5	0	-0.13	•	•	•
At2g38290	Q9M6N7	Ammonium transporter 2 (AtAMT2)	50.8	11	0.54	•		
At2g38480	Q8LE26	UPF0497 membrane protein At2g38480	20.9	4	0.12	•		
At2g38750	Q9ZVJ6	Annexin D4	36.2	0	-0.44	•		
At2g38940	Q96303	Inorganic phosphate transporter 1-4	58.6	12	0.32	•		
At2g39010	Q9ZV07	Probable aquaporin PIP2-6	31	6	0.46	•	•	•
At2g39210	O80960	Nodulin-like protein	66	0	0.51	•	•	
At2g39330	O80948	Myrosinase-binding protein-like At2g39330	50.4	0	-0.38		•	
At2g39460	Q8LD46	60S ribosomal protein L23a-1	17.4	0	-0.76	•	•	
At2g39480	Q8LPT1	ABC transporter B family member 6 (MDR6/PGP6)	155.9	12	0.07		•	
At2g39730	P10896	Ribulose biphosphate carboxylase/oxygenase activase (chloroplastic)	51.1	0	-0.31		•	•
At2g40300	Q9S756	Ferritin-4 (chloroplastic)	29	0	-0.27	•		•
At2g40410	Q3EBI8	Ca(2+)-dependent nuclease, putative	37.3	0	-0.44	•		
At2g40510	Q8LPJ7	40S ribosomal protein S26-2	14.8	0	-0.82			•
At2g40590	P49206	40S ribosomal protein S26-1	14.7	0	-0.88			•
At2g41840	P49688	40S ribosomal protein S2-3	30.9	0	-0.41			•
At2g42590	Q96299	14-3-3-like protein GF14 mu (GRF9)	29.5	0	-0.5	•		
At2g42740	P42795	60S ribosomal protein L11-1	20.8	0	-0.46			•
At2g42800	Q9SJH6	AtRLP29 (Receptor Like Protein 29)	50.8	0	0.01	•	•	
At2g43030	Q9SKX4	50S ribosomal protein L3-1 (chloroplastic)	29.4	0	-0.17		•	•

Continued on next page ...

AGI	Uniprot	Name	MW [kDa]	TMD	GRAVY	Precipitation methods		
						CHCl ₃ /MeOH	Wang	-
At2g43230	Q9ZW72	Protein kinase	45.4	0	-0.47	•	•	
At2g44060	O80576	LEA family protein	36	0	-0.31		•	
At2g44290	O64864	Non-specific lipid-transfer protein	21.6	0	0.16	•		
At2g44610	O80501	Ras-related protein RABH1B	23.1	0	-0.14	•		
At2g44790	O80517	Uclacyanin-2	20.4	0	0.02	•	•	•
At2g45140	Q9SHC8	Putative VAMP-associated protein	26.4	0	-0.47	•		
At2g45470	O22126	Fasciclin-like arabinogalactan protein 8 (Fla8)	43.1	0	0.13	•		•
At2g45820	O80837	AtRemorin 1.3	20.1	0	-0.81	•	•	•
At2g45960	Q06611	Aquaporin PIP1-2	30.6	6	0.41	•	•	•
At2g46650	Q9ZNV4	Putative cytochrome b5	14.9	0	-0.23	•		
At2g47000	O80725	ABC transporter B family member 4 (MDR4/PGP4)	139	12	0.11		•	
At2g47060	Q27GL0	Serin/threonin protein kinase	43.8	0	-0.35	•	•	
At2g47110	P59232	40S ribosomal protein S27a-2	9.3	0	-1.01		•	
At2g47170	P36397	ADP-ribosylation factor 1	20.6	0	-0.21		•	
At2g47470	O22263	Probable protein disulfide-isomerase A6	39.5	0	-0.29	•	•	
At2g47610	P49692	60S ribosomal protein L7a-1	29.1	0	-0.56		•	
At3g01050	Q9MAB9	Membrane-anchored ubiquitin-fold protein 1	12.8	0	-0.45	•		
At3g01290	Q9SRH6	Hypersensitive-induced response protein	31.4	0	-0.07	•	•	•
At3g01500	P27140	Carbonic anhydrase (chloroplastic)	37.4	0	-0.01	•	•	
At3g02520	Q96300	14-3-3-like protein GF14 nu (GRF7)	29.8	0	-0.5	•	•	
At3g02740	Q9M8R6	Putative aspartyl protease	52.8	0	-0.02	•		
At3g02880	Q9M8T0	Probable inactive receptor kinase At3g02880	67.8	2	-0.09	•	•	•
At3g04120	P25858	Glyceraldehyde-3-phosphate dehydrogenase, cytosolic	36.9	0	-0.13		•	•
At3g04840	Q9CAV0	40S ribosomal protein S3a-1	29.9	0	-0.52		•	
At3g04920	Q9SS17	40S ribosomal protein S24-1	15.4	0	-0.81	•		
At3g05530	Q9SEI2	26S proteasome AAA-ATPase subunit RPT5a	47.5	0	-0.44		•	
At3g05560	Q9M9W1	60S ribosomal protein L22-2	14	0	-0.65		•	•
At3g05590	P42791	60S ribosomal protein L18-2	20.9	0	-0.43		•	•
At3g06035	Q84MC0	Uncharacterized GPI-anchored protein At3g06035	22.1	0	0.02	•		
At3g06270	Q7XJ53	Probable protein phosphatase 2C 35	38.4	0	-0.36		•	
At3g06400	Q8RWY3	Putative chromatin-remodeling complex ATPase chain	122.6	0	-0.83	•		

Continued on next page ...

AGI	Uniprot	Name	MW [kDa]	TMD	GRAVY	Precipitation methods		
						CHCl ₃ /MeOH	Wang	-
At3g07020	Q9M8Z7	UDP-glucose:sterol glucosyltransferase	69.3	0	-0.24	•	•	
At3g07110	Q9SFU1	60S ribosomal protein L13a-1	23.5	0	-0.39		•	
At3g07160	Q9SFU6	Callose synthase 9	222.1	16	-0.01	•	•	
At3g07230	Q9SFV3	Putative wound-induced basic protein	5.3	0	-1.34	•		
At3g07390	Q94BT2	Auxin-induced in root cultures protein 12 (AIR12)	25.6	0	0.17	•		•
At3g08510	Q39033	Phosphoinositide phospholipase C 2	66.1	0	-0.47	•		•
At3g08580	P31167	ADP,ATP carrier protein 1, mitochondrial	41.5	6	-0.12			•
At3g08600	Q9C9Z6	At3g08600/F17O14.7	34.7	0	-0.09		•	
At3g08710	Q9C9Y6	Thioredoxin H-type 9	15.3	0	-0.23	•		
At3g08940	Q9XF88	Chlorophyll a-b binding protein CP29.2 (chloroplastic)	31.2	3	-0.06	•		
At3g09440	O65719	Heat shock cognate 70 kDa protein 3	71.1	0	-0.39	•	•	
At3g09500	Q9SF53	60S ribosomal protein L35-1	14.3	0	-0.76			•
At3g09630	Q9SF40	60S ribosomal protein L4-1	44.7	0	-0.38		•	
At3g09740	Q9SF29	Syntaxin-71	29.1	1	-0.52	•	•	•
At3g09900	Q9SF91	Putative Ras-like GTP-binding protein	24.3	0	-0.38	•	•	
At3g09980	Q8RXZ8	At3g09980	20.6	0	-0.86	•		
At3g10260	Q9SS37	Reticulon-like protein B8	27.9	3	0.13	•		
At3g10380	Q93YU5	Probable exocyst complex component 4	116.6	0	-0.27		•	
At3g10610	Q9SQZ1	40S ribosomal protein S17-3	16	0	-0.57		•	
At3g11250	P57691	60S acidic ribosomal protein P0-3	34.4	0	0.02	•		
At3g11510	Q9CAX6	40S ribosomal protein S14-2	16.3	0	-0.5	•	•	
At3g11660	Q9SRN0	NDR1-HIN1-like 1	23.7	0	0.05		•	•
At3g11730	Q9ZRE2	Ras-related protein RABD1	22.7	0	-0.31		•	
At3g11770	Q9SF21	Nucleic-acid binding	22.1	0	-0.11			•
At3g11820	Q9ZSD4	Syntaxin-121 (PEN1)	37.1	1	-0.57	•	•	•
At3g12110	P53496	Actin-11	41.7	0	-0.18		•	•
At3g12160	Q9LH50	GTP-binding protein-like	24.7	0	-0.28		•	
At3g12580	Q9LHA8	70 kDa heat shock protein	71.1	0	-0.43		•	
At3g13530	Q9LJD8	MAP3K epsilon protein kinase	151.2	0	-0.36		•	
At3g13560	Q94CD8	Putative glucan endo-1,3-beta-glucosidase 4	54.4	0	0.05	•		
At3g13920	P41376	Eukaryotic initiation factor 4A-1	46.7	0	-0.22	•	•	

Continued on next page ...

AGI	Uniprot	Name	MW [kDa]	TMD	GRAVY	Precipitation methods		
						CHCl ₃ /MeOH	Wang	–
At3g14350	Q9LUL4	Protein STRUBBELIG-RECEPTOR FAMILY 7	77.6	1	-0.23	•	•	
At3g14840	Q9LH71	Receptor-like serine/threonine kinase	114.7	2	-0.22			•
At3g15060	Q9LK99	GTP-binding protein-like	24.3	0	-0.28			•
At3g15480	Q9LDK1	At3g15480/MJK13_14	19.4	0	0.55	•		
At3g15730	Q38882	Phospholipase D alpha 1	91.8	0	-0.4	•		
At3g16100	Q9LW76	AtRab73	22.1	0	-0.34			•
At3g16240	Q41951	Aquaporin TIP2-1	25	6	0.97	•		
At3g16340	Q94A18	ABC transporter G family member 29 (PDR1)	160.3	13	0.06			•
At3g16950	Q9M5K5	Dihydrolipoyl dehydrogenase	60.8	0	-0.01			•
At3g17410	Q9LUT0	Putative uncharacterized protein At3g17410	39.6	0	-0.3	•		•
At3g17440	Q9LRP1	Novel plant SNARE 13	30.4	1	-0.55	•		•
At3g17840	Q9LVI6	Probable inactive receptor kinase RLK902	70.4	1	-0.07	•		•
At3g18780	Q96292	Actin-2	41.9	0	-0.18	•		•
At3g18820	Q9LS94	AtRab71	23.1	0	-0.41			•
At3g18830	Q8VZ80	Polyol transporter 5 (AtPLT5)	58.1	12	0.34			•
At3g19340	Q8RWC3	Putative uncharacterized protein At3g19340	56.8	0	-0.31			•
At3g19930	Q39228	Sugar transport protein 4 (STP4)	57.1	12	0.56	•		
At3g19960	Q9LHE9	Myosin-like protein	131.2	0	-0.42			•
At3g20410	Q38868	Calcium-dependent protein kinase 9 (CPK9)	60.4	0	-0.46	•		
At3g21180	Q9LU41	Calcium-transporting ATPase 9, plasma membrane-type	118.8	10	0.06			•
At3g22560	Q9LJ90	Alanine acetyl transferase-like protein	19.1	0	-0.29	•		
At3g23750	Q9LK43	Similarity to receptor protein kinase	99.1	0	-0.1	•		•
At3g24550	Q9LV48	AtPERK1 (Proline Extensin-Like Receptor Kinase 1)	69.3	0	-0.56	•		•
At3g24830	Q9LRX8	60S ribosomal protein L13a-2	23.5	0	-0.34			•
At3g25070	Q8GYN5	RPM1-interacting protein 4	23.4	0	-1.41	•		•
At3g25220	Q38935	Peptidyl-prolyl cis-trans isomerase	16.4	0	-0.24	•		
At3g25290	Q9LSE7	Auxin-responsive family protein	42.6	0	0.2	•		•
At3g25610	Q9LI83	Putative phospholipid-transporting ATPase 10	136.3	10	-0.08			•
At3g25860	Q9SQI8	Dihydrolipoamide S-acetyltransferase	50.1	0	0.05			•
At3g25920	P25873	50S ribosomal protein L15 (chloroplastic)	29.7	0	-0.47			•
At3g26520	Q41963	Aquaporin TIP1-2	25.8	6	0.79	•		

Continued on next page ...

AGI	Uniprot	Name	MW [kDa]	TMD	GRAVY	Precipitation methods		
						CHCl ₃ /MeOH	Wang	–
At3g26650	P25856	Glyceraldehyde-3-phosphate dehydrogenase A (chloroplastic)	42.5	0	-0.02	•	•	•
At3g27390	Q8GUM4	Uncharacterized membrane protein At3g27390	65.5	7	0.24	•	•	
At3g28220	Q9LHA6	MATH-domain containing protein	42.9	0	-0.43			•
At3g28450	Q9LSI9	Leucine-rich repeat receptor-like protein kinase	66.9	0	-0.1	•	•	
At3g28860	Q9LJX0	ABC transporter B family member 19 (MDR11/PGP19)	136.8	11	0.13	•	•	•
At3g42640	Q9M2A0	ATPase 8, plasma membrane-type	104.2	10	0.08		•	
At3g44110	Q94AW8	Chaperone protein dnaJ 3	46.5	0	-0.78	•		
At3g44890	P25864	50S ribosomal protein L9 (chloroplastic)	22.1	0	-0.32			•
At3g45140	P38418	Lipoxygenase 2 (chloroplastic) (AtLOX2)	102.1	0	-0.47		•	
At3g45600	Q9M1E7	Tetraspanin 3	31.9	4	0.25	•	•	•
At3g45780	O48963	Phototropin-1	111.7	0	-0.64	•	•	
At3g46060	P28186	Ras-related protein ARA-3	23.8	0	-0.3		•	•
At3g46290	Q9LX66	Probable receptor-like protein kinase At3g46290	91.5	1	-0.18		•	
At3g46520	P53497	Actin-12	41.8	0	-0.22		•	
At3g46830	Q96283	Ras-related protein RABA2c	23.8	0	-0.28	•	•	
At3g47950	Q9SU58	ATPase 4, plasma membrane-type	105.7	10	0.13		•	
At3g47960	Q94K82	Putative peptide transporter protein	67.4	0	0.3		•	
At3g48740	Q9SMM5	MTN3-like protein	31.9	0	0.57	•	•	
At3g48870	Q9M2Z6	AtClpC	105.8	0	-0.31		•	
At3g48890	Q9M2Z4	Membrane steroid-binding protein 2	25.4	1	-0.46	•	•	
At3g49010	P41127	60S ribosomal protein L13-1	23.8	0	-0.92		•	
At3g49870	Q8VY57	ADP-ribosylation factor-like protein	20.4	0	-0.03		•	
At3g49910	P51414	60S ribosomal protein L26-1	16.9	0	-0.95		•	
At3g50360	O82659	Probable calcium-binding protein CML20	19.4	0	-0.86	•	•	
At3g51550	Q9SCZ4	Receptor-protein kinase-like protein	98.1	0	-0.26	•	•	
At3g52400	Q9SVC2	Syntaxin-122	37.8	1	-0.54	•	•	
At3g52580	P42036	40S ribosomal protein S14-3	16.2	0	-0.49		•	
At3g52930	Q9LF98	Fructose-bisphosphate aldolase	38.5	0	-0.23	•		
At3g53420	P43286	Aquaporin PIP2-1	30.5	6	0.51	•	•	•
At3g53430	Q9LFH5	60S ribosomal protein L12-2	17.1	0	-0.33		•	
At3g53610	O24466	AtRAB8	23.9	0	-0.35		•	

Continued on next page ...

AGI	Uniprot	Name	MW [kDa]	TMD	GRAVY	Precipitation methods		
						CHCl ₃ /MeOH	Wang	-
At3g53870	Q9M339	40S ribosomal protein S3-2	27.3	0	-0.05		•	
At3g54030	Q9M324	Protein kinase-like protein	54.8	0	-0.32		•	
At3g54140	Q9M390	Peptide transporter PTR1	64	10	0.14	•	•	
At3g54200	Q9M386	Putative uncharacterized protein At3g54200	25.8	0	0.11		•	
At3g54210	Q9M385	50S ribosomal protein L17 (chloroplastic)	23.5	0	-0.33			•
At3g55280	Q9M3C3	60S ribosomal protein L23a-2	17.4	0	-0.63		•	
At3g55320	Q9M3B9	ABC transporter B family member 20 (MDR14/PGP20)	155.2	12	0.09		•	
At3g55440	P48491	Triosephosphate isomerase, cytosolic	27.2	0	0.08	•		
At3g55450	Q8H186	Serine/threonine-specific protein kinase-like	43.1	0	-0.26		•	
At3g55940	Q9LY51	Phosphoinositide phospholipase C 7	66.5	0	-0.45		•	
At3g56090	Q9LYN2	Ferritin-3 (chloroplastic)	28.8	0	-0.29	•	•	
At3g56190	Q9SPE6	Alpha-soluble NSF attachment protein 2	32.8	0	-0.52	•	•	
At3g56240	O82089	Copper homeostasis factor	12.1	0	-0.51	•		
At3g56340	Q9LYK9	40S ribosomal protein S26-3	14.6	0	-0.88	•	•	
At3g56910	Q9LER7	50S ribosomal protein 5 (chloroplastic)	16.4	0	-0.47			•
At3g58730	Q9XGM1	V-type proton ATPase subunit D	29.1	0	-0.24		•	
At3g59350	Q940H1	Protein kinase-like protein	40.7	0	-0.37		•	
At3g60190	Q9FNX5	Dynamin-related protein 1E	69.8	0	-0.33		•	
At3g60330	Q9LY32	ATPase 7, plasma membrane-type	105.5	10	0.06		•	
At3g60950	Q9LDM1	Putative uncharacterized protein T27115_120	66.8	0	-0.08		•	•
At3g61050	Q9LEX1	CaLB protein	55.1	0	0.02	•	•	
At3g61110	Q9M2F1	40S ribosomal protein S27-2	9.6	0	-0.3	•		
At3g61260	Q9M2D8	AtRemorin 1.2	23.1	0	-0.77	•	•	•
At3g61430	P61837	Aquaporin PIP1-1	30.7	6	0.37			•
At3g62150	Q9M1Q9	ABC transporter B family member 21 (MDR17/PGP21)	139.8	11	0.1	•	•	
At3g62220	Q9M1Q2	Serine/threonine protein kinase-like protein	38.1	0	-0.29		•	
At3g62250	P59233	40S ribosomal protein S27a-3	9.3	0	-0.91		•	
At3g62290	Q9M1P5	ADP-ribosylation factor-like protein	20.6	0	-0.22		•	
At3g62560	Q8VYP7	Putative Sar1 GTP binding protein	21.9	0	-0.13	•	•	
At3g63080	Q9LYB4	Probable glutathione peroxidase 5	19.3	0	-0.34	•		
At3g63160	Q9M1X3	Putative uncharacterized protein F16M2_10	7.3	0	-0.16	•	•	

Continued on next page ...

AGI	Uniprot	Name	MW [kDa]	TMD	GRAVY	Precipitation methods		
						CHCl ₃ /MeOH	Wang	-
At3g63260	O22100	Arabidopsis thaliana MLK/Raf-related protein kinase 1 (ATMRK1)	42.6	0	-0.3	•	•	
At3g63420	Q9FDX9	Heterotrimeric G protein gamma-subunit	10.9	0	-0.32	•		
At3g63490	Q9LY66	50S ribosomal protein L1 (chloroplastic)	37.6	0	-0.25			•
At3g63520	O65572	Carotenoid cleavage dioxygenase 1	60.9	0	-0.25	•	•	•
At4g00430	Q39196	Probable aquaporin PIP1-4	30.7	6	0.38	•		•
At4g00710	Q8W4L3	Putative uncharacterized protein At4g00710	54.9	0	-0.37		•	
At4g01310	O04603	50S ribosomal protein L5 (chloroplastic)	28.3	0	-0.28		•	•
At4g02050	O04249	Sugar transport protein 7 (STP7)	55.8	12	0.51	•	•	
At4g02080	O04834	GTP-binding protein SAR1A	22	0	-0.17		•	
At4g02520	P46422	Glutathione S-transferase PM24	24.1	0	-0.32			•
At4g02770	Q9S7H1	Photosystem I reaction center subunit II-1 (chloroplastic)	22.6	0	-0.37	•	•	•
At4g02890	Q8H0Y0	Polyubiquitin	25.7	0	-0.43		•	
At4g03550	Q9ZT82	Callose synthase 12	206.9	16	-0.03		•	
At4g04020	O81439	Probable plastid-lipid-associated protein 1 (chloroplastic)	34.9	0	-0.27		•	
At4g04570	Q9SYS3	Cysteine-rich receptor-like protein kinase 40	73.2	1	-0.18	•		
At4g04720	Q9ZSA2	Calcium-dependent protein kinase 21 (CPK21)	59.9	0	-0.47	•	•	
At4g05120	Q9M0Y3	AtENT3 (FUR1)	46.2	0	0.42	•		
At4g05180	Q41932	Oxygen-evolving enhancer protein 3-2 (chloroplastic)	24.6	0	-0.24	•	•	
At4g09000	P42643	14-3-3-like protein GF14 chi (GRF1)	29.9	0	-0.44	•	•	•
At4g10340	Q9XF89	Chlorophyll a-b binding protein CP26 (chloroplastic)	30.2	3	-0.03			•
At4g10930	Q8L7I1	Uncharacterized protein At4g10930	108.1	0	-0.78	•		
At4g11070	Q8H0Y8	Probable WRKY transcription factor 41	34.9	0	-0.56	•		
At4g11460	Q9LDT0	Putative cysteine-rich receptor-like protein kinase 30	77.8	1	-0.13			•
At4g11470	Q9LDM5	Putative cysteine-rich receptor-like protein kinase 31	74.7	1	-0.2			•
At4g11480	Q9LDS6	Putative cysteine-rich receptor-like protein kinase 32	73.7	1	-0.2			•
At4g11530	Q9LDQ3	Putative cysteine-rich receptor-like protein kinase 35	74.1	1	-0.11			•
At4g11850	Q9T053	Phospholipase D gamma 1	95.6	0	-0.35			•
At4g12420	Q9SU40	Putative monocopper oxidase (AtSku5)	65.7	0	-0.24	•	•	•
At4g12730	Q9SU13	Fasciclin-like arabinogalactan protein 2 (Fla2)	43.5	0	-0.08	•		•
At4g12800	Q9SUI4	Photosystem I reaction center subunit XI (chloroplastic)	23.1	2	0.31			•
At4g12980	Q9SV71	Auxin-responsive protein, putative	42.2	0	0.24		•	

Continued on next page ...

AGI	Uniprot	Name	MW [kDa]	TMD	GRAVY	Precipitation methods		
						CHCl ₃ /MeOH	Wang	-
At4g13010	Q9SV68	Putative quinone-oxidoreductase homolog (chloroplastic)	34.4	0	0.04	•		
At4g13170	Q9SVR0	60S ribosomal protein L13a-3	23.6	0	-0.48		•	
At4g13510	P54144	Ammonium transporter 1 member 1 (AtAMT1;1)	53.6	9	0.36	•	•	
At4g13770	P48421	Cytochrome P450 83A1	57.4	1	-0.26		•	
At4g14880	P47998	Cysteine synthase	33.8	0	0.09	•		
At4g14960	P29511	Tubulin alpha-6 chain	49.5	0	-0.2		•	
At4g15630	Q8L8Z1	UPF0497 membrane protein At4g15630	20.1	4	0.66	•		
At4g16155	Q9M5K4	Dihydrolipoyl dehydrogenase	60.1	0	0.03			•
At4g16370	O23482	Probable oligopeptide transporter 3 (AtOPT3)	82.1	16	0.38	•	•	•
At4g17170	P92963	GTP-binding RAB2A like protein	23.2	0	-0.23	•	•	
At4g17270	Q9M0M4	Putative MO25-like protein At4g17270	39.7	0	-0.32		•	
At4g17390	Q8VYF1	60S ribosomal protein L15-2	24.3	0	-1.12	•		
At4g17530	Q9SEH3	Ras-related small GTP-binding protein RAB1c	22.3	0	-0.27			•
At4g17560	Q8W463	50S ribosomal protein L19-1 (chloroplastic)	25.5	0	-0.32			•
At4g18100	P49211	60S ribosomal protein L32-1	15.5	0	-0.72			•
At4g18430	O49513	Membrane-bound small GTP-binding-like protein	24.3	0	-0.31	•	•	•
At4g18760	Q9SN38	Leucine-rich repeat receptor-like protein kinase	46.1	0	0.02	•	•	
At4g18800	Q9SN35	Putative Ras-related GTP binding protein	23.9	0	-0.34	•	•	
At4g20260	Q96262	Plasma-membrane associated cation-binding protein 1	24.6	0	-0.71	•	•	•
At4g20360	P17745	Elongation factor Tu (chloroplastic)	51.6	0	-0.12		•	
At4g21150	Q93Z16	HAPLESS 6 (HAP6)	74.7	0	0.17		•	
At4g21280	Q9XFT3	Oxygen-evolving enhancer protein 3-1 (chloroplastic)	23.9	0	-0.31	•		
At4g21740	Q9SVS3	At4g21740	17.2	0	-0.21	•		
At4g21940	O49717	Calcium-dependent protein kinase 15 (CPK15)	62.6	0	-0.45			•
At4g22290	O49634	Ubiquitin thiolesterase	109.1	0	-0.29			•
At4g22710	O49652	Cytochrome P450 - like protein	59.4	0	-0.18			•
At4g23140	Q9C5S9	Cysteine-rich receptor-like protein kinase 6	74.5	1	-0.14			•
At4g23150	Q8L7G3	Cysteine-rich receptor-like protein kinase 7	73.9	1	-0.21			•
At4g23160	O65468	Cysteine-rich receptor-like protein kinase 8	75.4	1	-0.16			•
At4g23180	Q8GYA4	Cysteine-rich receptor-like protein kinase 10	72.1	1	-0.14	•	•	•
At4g23190	Q9ZP16	Cysteine-rich receptor-like protein kinase 11	74.1	1	-0.29			•

Continued on next page ...

AGI	Uniprot	Name	MW [kDa]	TMD	GRAVY	Precipitation methods		
						CHCl ₃ /MeOH	Wang	–
At4g23200	O65472	Putative cysteine-rich receptor-like protein kinase 12	77.4	1	0.03		•	
At4g23220	Q8H199	Cysteine-rich receptor-like protein kinase 14	73.9	1	-0.08	•	•	
At4g23230	Q8W4G6	Cysteine-rich receptor-like protein kinase 15	69.7	1	-0.07		•	
At4g23250	Q8L710	Cysteine-rich receptor-like protein kinase 17	76.4	1	-0.15		•	
At4g23260	Q8RX80	Cysteine-rich receptor-like protein kinase 18	72.8	1	-0.06		•	
At4g23290	Q3E9X6	Cysteine-rich receptor-like protein kinase 21	76.9	1	-0.24	•	•	
At4g23300	Q6NQ87	Cysteine-rich receptor-like protein kinase 22	73.8	1	-0.18		•	
At4g23400	Q8LAA6	Probable aquaporin PIP1-5	30.6	6	0.4	•	•	•
At4g23650	Q42479	Calcium-dependent protein kinase 3 (CPK3)	59.3	0	-0.53		•	
At4g23850	Q9T0A0	Long chain acyl-CoA synthetase 4	74.5	0	-0.14	•	•	
At4g24990	Q9SW27	Membrane-anchored ubiquitin-fold protein 3	12.8	0	-0.1	•		
At4g25240	Q8VXX5	Monocopper oxidase-like protein SKS1	65.9	0	-0.17		•	
At4g25390	Q9STJ8	Receptor kinase-like protein	72.2	0	-0.46	•		
At4g26080	P49597	Protein phosphatase 2C 56 (ABI1)	47.5	0	-0.32			•
At4g26530	O65581	Fructose-bisphosphate aldolase	38.3	0	-0.12	•		
At4g26690	Q9SZ11	Probable glycerophosphoryl diester phosphodiesterase 2	82.6	0	0.05	•		•
At4g27090	Q9T043	60S ribosomal protein L14-2	15.5	0	-0.35	•	•	
At4g27520	Q9T076	Early nodulin-like protein 2	35.1	0	-0.31	•		•
At4g28050	Q9SUD4	Tetraspanin 7	29.9	4	0.2	•		
At4g28100	Q9SUC9	Uncharacterized GPI-anchored protein At4g28100	33.1	0	0.04	•	•	
At4g28400	Q93YW5	Probable protein phosphatase 2C 58	31	0	-0.32		•	
At4g28750	Q9S831	Photosystem I reaction center subunit IV A (chloroplastic)	14.1	0	-0.18		•	•
At4g29900	Q9SZR1	Putative calcium-transporting ATPase 10, plasma membrane-type	116.9	10	0.04	•	•	
At4g30190	P19456	ATPase 2, plasma membrane-type	104.4	10	0.1	•	•	•
At4g31140	Q9M088	Putative glucan endo-1,3-beta-glucosidase 5	52.7	0	0.06	•	•	•
At4g31500	O65782	Cytochrome P450 83B1	56.8	1	-0.12		•	
At4g31700	O48549	40S ribosomal protein S6-1	28.4	0	-0.9	•	•	
At4g31750	Q8RXV3	Probable protein phosphatase 2C 59	33.2	0	-0.28		•	
At4g33430	Q94F62	BRI 1-associated receptor kinase 1 (BAK1)	68.2	1	-0.19	•	•	
At4g33700	Q8VZ12	CBS domain-containing protein	47.1	0	0.18		•	
At4g34150	Q945K9	C2 domain-containing protein	27.1	0	-0.64	•		

Continued on next page ...

AGI	Uniprot	Name	MW [kDa]	TMD	GRAVY	Precipitation methods		
						CHCl ₃ /MeOH	Wang	-
At4g34460	P49177	Guanine nucleotide-binding protein subunit beta	41	0	-0.23		•	
At4g34555	Q8GYL5	40S ribosomal protein S25-3	12	0	-0.8		•	
At4g34670	Q42262	40S ribosomal protein S3a-2	29.8	0	-0.56		•	
At4g35060	O49613	Heavy-metal-associated domain-containing protein	17.2	0	-0.39	•		
At4g35100	P93004	Aquaporin PIP2-7	29.7	6	0.45	•	•	•
At4g35230	Q944A7	Putative serine/threonine-protein kinase At4g35230	56.8	0	-0.48	•	•	
At4g35450	Q9SAR5	Ankyrin repeat domain-containing protein 2	36.1	0	-0.53	•		
At4g35470	Q9SVW8	Plant intracellular Ras-group-related LRR protein 4	60.1	0	-0.27	•	•	
At4g35790	Q9C5Y0	Phospholipase D delta	98.1	0	-0.4	•	•	•
At4g35860	Q38922	ATRA2C (GTP-binding protein GB2)	23.2	0	-0.25	•	•	
At4g35900	Q84JK2	Protein FD (bZIP transcription factor 14)	31.4	0	-0.97	•		
At4g36130	Q42064	60S ribosomal protein L8-3	27.9	0	-0.45		•	
At4g36750	O23207	Quinone reductase family	28.8	0	-0.21	•	•	
At4g37300	O23157	Maternal effect embryo arrest 59 (MEE59)	18.8	0	-1.02	•		
At4g38580	Q9SZN7	Farnesylated protein (ATFP6)	17	0	-0.42		•	
At4g38690	Q9SZP6	1-phosphatidylinositol phosphodiesterase-related	36.3	0	-0.41	•		
At4g38970	Q944G9	Probable fructose-bisphosphate aldolase 2 (chloroplastic)	42.9	0	-0.17	•		
At4g39080	Q8W4S4	Vacuolar proton ATPase subunit VHA-a isoform 3	92.8	0	0.03		•	
At4g39200	Q9T029	40S ribosomal protein S25-4	12.1	0	-0.76		•	
At4g39260	Q03251	Glycine-rich RNA-binding protein 8	16.6	0	-0.82	•		
At4g39400	O22476	Protein BRasSINOSTEROID INSENSITIVE 1 (BRI1)	130.5	1	-0.09		•	
At4g39990	Q9SMQ6	GTP-binding protein GB3	24.4	0	-0.33	•	•	
At5g01240	Q9LFB2	Auxin transporter-like protein 1 (AUX1)	54.6	11	0.41	•		
At5g01600	Q39101	Ferritin-1 (chloroplastic)	28.2	0	-0.25	•		•
At5g01750	Q9LZX1	UPF0706 protein At5g01750	24.3	0	-0.21	•		
At5g02290	P43293	Probable serine/threonine-protein kinase NAK	43.5	0	-0.36		•	
At5g02490	P22954	Heat shock cognate 70 kDa protein 2	71.4	0	-0.42		•	
At5g02500	P22953	Heat shock cognate 70 kDa protein 1	71.4	0	-0.44	•	•	
At5g02870	P49691	60S ribosomal protein L4-2	44.7	0	-0.38		•	
At5g03300	Q9LZG0	Adenosine kinase 2	37.8	0	-0.17	•		
At5g03340	Q9LZF6	Cell division control protein 48 homolog E	89.1	0	-0.38	•		

Continued on next page ...

AGI	Uniprot	Name	MW [kDa]	TMD	GRAVY	Precipitation methods		
						CHCl ₃ /MeOH	Wang	-
At5g03520	Q9LZD4	GTP-binding protein-like	24	0	-0.3	•	•	
At5g03540	Q9LZD3	AtEXO70A1 (Exocyst subunit)	72.3	0	-0.4		•	
At5g04800	Q9LZ17	40S ribosomal protein S17-4	16	0	-0.6	•	•	
At5g06320	Q9FNH6	Harpin-induced protein-like (NHL3)	25.9	0	-0.09	•	•	•
At5g06530	Q93YS4	ABC transporter G family member 22 (AtWBC23)	82.9	6	0.05		•	
At5g07090	P49204	40S ribosomal protein S4-2	29.9	0	-0.52		•	
At5g07300	Q94EW4	BONZAI2	64	0	-0.13		•	
At5g07910	Q8RWI2	Putative uncharacterized protein At5g07910	29.1	0	-0.24		•	
At5g08080	Q8VZU2	Syntaxin-132	34.2	1	-0.56	•	•	•
At5g09500	Q9FY65	40S ribosomal protein S15-3	16.7	0	-0.2		•	
At5g09510	Q9FY64	40S ribosomal protein S15-4	17.1	0	-0.32		•	
At5g09660	Q9ZP05	Malate dehydrogenase, glyoxysomal	37.4	0	0.1	•		
At5g09810	P53492	Actin-7	41.7	0	-0.18	•	•	
At5g10360	P51430	40S ribosomal protein S6-2	28.2	0	-0.81		•	
At5g10450	P48349	14-3-3-like protein GF14 lambda (GRF6)	27.1	0	-0.36	•		
At5g10470	Q9LX99	Geminivirus Rep-interacting motor protein	141	0	-0.4	•	•	
At5g12140	Q945Q1	Cysteine proteinase inhibitor 1	11.3	0	-0.47	•		
At5g12370	Q8RVQ5	Exocyst complex component 5	89.7	0	-0.17	•	•	
At5g12480	Q38873	Calcium-dependent protein kinase 7 (CPK7)	60.3	0	-0.48	•		
At5g13850	Q6ICZ8	Nascent polypeptide-associated complex subunit alpha-like protein 3	22.1	0	-0.68	•		
At5g14670	Q9LYJ3	ADP-ribosylation factor-like protein	21.5	0	-0.21		•	
At5g14740	P42737	Carbonic anhydrase 2	28.3	0	-0.07	•	•	•
At5g15200	Q9LXG1	40S ribosomal protein S9-1	23	0	-0.78			•
At5g15350	Q39131	Lamin-like protein	19.4	0	0.01	•		
At5g15970	P31169	Stress-induced protein KIN2	6.6	0	-0.46	•		
At5g16050	P42645	14-3-3-like protein GF14 epsilon (GRF5)	30.2	0	-0.46	•		
At5g16590	Q9FMD7	Probable inactive receptor kinase At5g16590	67.5	1	-0.03	•	•	
At5g16840	Q9LFD5	BPA1 (Binding partner of ACD11 1)	27.3	0	-0.33		•	
At5g16880	Q9LFL3	VHS domain-containing protein / GAT domain-containing protein	45.3	0	-0.53	•		
At5g18500	Q8LEB6	Serine/threonine protein kinase-like protein	54.2	0	-0.5	•	•	
At5g19230	Q8GUL8	Uncharacterized GPI-anchored protein At5g19230	20.5	0	0.24	•	•	

Continued on next page ...

AGI	Uniprot	Name	MW [kDa]	TMD	GRAVY	Precipitation methods		
						CHCl ₃ /MeOH	Wang	-
At5g19240	Q84VZ5	Uncharacterized GPI-anchored protein At5g19240	21.3	0	0.09	•		•
At5g19450	Q42438	Calcium-dependent protein kinase 8 (CPK8)	59.9	0	-0.42		•	
At5g19770	P20363	Tubulin alpha-3/alpha-5 chain	49.7	0	-0.15	•	•	•
At5g19990	Q9C5U3	26S proteasome AAA-ATPase subunit	47.2	0	-0.39		•	
At5g20000	Q94BQ2	Putative 26S proteasome AAA-ATPase subunit RPT6a	47.2	0	-0.36		•	
At5g20230	Q07488	Blue copper protein	20.1	0	0.2	•	•	
At5g20290	Q93VG5	40S ribosomal protein S8-1	24.1	0	-0.92	•	•	•
At5g20500	Q8LFQ6	Glutaredoxin-C4	14.8	0	0.08	•		
At5g22440	P59231	60S ribosomal protein L10a-3	24.5	0	-0.36		•	
At5g25610	Q08298	Dehydration-responsive protein RD22	42.3	0	-0.3			•
At5g25980	Q9C5C2	Putative myosinase TGG2	62.7	0	-0.44			•
At5g26000	P37702	Myosinase TGG1	61.1	0	-0.4	•		
At5g26340	Q94AZ2	Sugar transport protein 13 (STP13)	57.4	12	0.52	•	•	
At5g27850	Q940B0	60S ribosomal protein L18-3	20.1	0	-0.42		•	
At5g28540	Q9LKR3	Luminal-binding protein 1 (BiP1)	73.6	0	-0.46	•	•	
At5g35180	Q8W553	Phosphoinositide binding	87	0	-0.46		•	
At5g35530	Q9FJA6	40S ribosomal protein S3-3	27.5	0	-0.12	•	•	
At5g35630	Q43127	Glutamine synthetase (chloroplastic)/mitochondrial	47.5	0	-0.41	•		
At5g35735	Q9FKH6	Auxin-responsive family protein	43.9	0	0.02			•
At5g37640	Q9FHQ6	Polyubiquitin	36.3	0	-0.28		•	
At5g38410	P10798	Ribulose biphosphate carboxylase small chain 3B (chloroplastic)	20.3	0	-0.18		•	
At5g38420	P10797	Ribulose biphosphate carboxylase small chain 2B (chloroplastic)	20.4	0	-0.21	•	•	•
At5g38480	P42644	14-3-3-like protein GF14 psi (GRF3)	28.6	0	-0.4	•	•	
At5g38990	Q9FID9	Receptor protein kinase-like protein	97.1	0	-0.16		•	
At5g39000	Q9FID8	Receptor-like protein kinase	97.2	0	-0.18		•	
At5g39410	Q8LGI2	Probable mitochondrial saccharopine dehydrogenase At5g39410	49.7	0	-0.18	•	•	
At5g39570	Q9FKA5	Uncharacterized protein At5g39570	43.5	0	-1.93	•		
At5g40780	Q9FKS8	Amino acid permease	49.8	0	0.48	•	•	
At5g40950	Q9FLN4	50S ribosomal protein L27 (chloroplastic)	21.7	0	-0.5			•
At5g41260	Q9FHD7	Putative serine/threonine-protein kinase At5g41260	54.6	0	-0.41		•	
At5g42080	P42697	Dynamin-related protein 1A	68.2	0	-0.28	•	•	

Continued on next page ...

AGI	Uniprot	Name	MW [kDa]	TMD	GRAVY	Precipitation methods		
						CHCl ₃ /MeOH	Wang	-
At5g42720	Q8VY12	Putative beta-1,3-glucanase	47.2	0	-0.02	•		
At5g42980	Q42403	Thioredoxin H-type 3	13.2	0	0.16	•		
At5g43470	Q8W4J9	Disease resistance protein RPP8	104.7	0	-0.28		•	
At5g44020	Q9FNC4	Vegetative storage protein-like	31.1	0	-0.33			•
At5g44130	Q9FFH6	Fasciclin-like arabinogalactan protein 13 (Fla13)	26.3	0	0.02	•		
At5g44340	P24636	Tubulin beta-4 chain	49.8	0	-0.35	•		
At5g45750	Q9FK68	Ras-related protein RABA1c	23.9	0	-0.29		•	
At5g46570	Q9LS26	Protein kinase-like protein	54.1	0	-0.4		•	
At5g47010	Q9FJR0	Regulator of nonsense transcripts 1 homolog (LBA1, ATUPF1)	136.9	0	-0.45	•		
At5g47070	Q9LTC0	Protein serine/threonine kinase-like	46.8	0	-0.65		•	
At5g47100	Q9LTB8	Calcineurin B-like protein 9	24.5	0	-0.22	•		
At5g47180	Q9LVU1	Putative VAMP	24.7	0	-0.51	•	•	
At5g47190	Q8RXX5	50S ribosomal protein L19-2 (chloroplastic)	25.5	0	-0.26			•
At5g47200	Q9FPJ4	Putative Ras-related small GTP-binding protein	22.3	0	-0.29		•	
At5g47540	Q9FGK3	Putative MO25-like protein At5g47540	39.5	0	-0.35		•	
At5g47910	Q9FIJ0	Respiratory burst oxidase homolog protein D (AtRBOHD)	103.9	6	-0.24	•	•	
At5g47960	Q9FE79	Ras superfamily GTP-binding protein-like	24.9	0	-0.32		•	
At5g48380	Q9ASS4	Leucine-rich repeat receptor-like protein kinase	69.1	0	-0.07		•	
At5g48810	Q9ZWT2	Cytochrome b5	15.1	0	-0.07	•	•	
At5g49630	P92934	Amino acid permease 6	53	0	0.37	•	•	
At5g49760	Q8GZ99	Leucine-rich repeat receptor-like protein kinase	104.7	0	-0.13	•	•	•
At5g49770	Q9LT96	Leucine-rich repeat receptor-like protein kinase	104.5	0	-0.23		•	
At5g49780	Q9LT95	Receptor protein kinase-like	111.8	0	-0.22		•	
At5g49830	Q9LTB0	AT5g49830/K21G20.4	82.7	0	-0.26	•		
At5g50000	Q9FGB1	Protein kinase	42.7	0	-0.35		•	
At5g50020	Q8VYS8	Probable S-acyltransferase	47.1	4	-0.31		•	
At5g50920	Q9FI56	ATP-dependent Clp protease	103.5	0	-0.4		•	
At5g51570	Q9FHM7	Hypersensitive-induced protein	32.4	0	-0.12	•		
At5g52240	Q9XFM6	Membrane steroid-binding protein 1	24.4	1	-0.38	•		
At5g53550	Q2EF88	Metal-nicotianamine transporter YSL3	74.1	14	0.44	•		
At5g53560	Q42342	Cytochrome b5 isoform 1	15.1	1	-0.34	•	•	

Continued on next page ...

AGI	Uniprot	Name	MW [kDa]	TMD	GRAVY	Precipitation methods		
						CHCl ₃ /MeOH	Wang	-
At5g53660	Q9FJB8	AtGRF7 (Growth-regulation factor)	40.5	0	-0.67	•		
At5g54380	Q9LK35	Receptor-protein kinase-like protein	93.3	0	-0.04		•	
At5g54500	Q9LSQ5	1,4-benzoquinone reductase-like protein	21.8	0	-0.11	•	•	
At5g54600	P92959	50S ribosomal protein L24 (chloroplastic)	21.1	0	-0.32			•
At5g55480	Q9FJ62	Probable glycerophosphoryl diester phosphodiesterase 1	84.2	0	-0.05	•		
At5g55730	Q9FM65	Fasciclin-like arabinogalactan protein 1 (Fla1)	44.8	0	-0.04	•		
At5g55850	O22633	NOI protein	8.3	0	-0.98	•		
At5g56170	Q9FKT1	Putative uncharacterized protein At5g56170	18.5	0	0.12	•		
At5g56590	Q9FJU9	Putative glucan endo-1,3-beta-glucosidase 13	55.6	0	-0.16	•	•	
At5g57110	Q9LF79	Calcium-transporting ATPase 8, plasma membrane-type	116.2	10	0.03	•	•	•
At5g57290	Q9LVC9	60S acidic ribosomal protein P3-2	11.9	0	-0.21	•		
At5g57350	P20431	ATPase 3, plasma membrane-type	104.4	10	0.05		•	
At5g58060	Q9ZRD6	VAMP-like protein YKT61 (Geranylgeranylated protein 1)	22.5	0	-0.41	•		
At5g58070	Q9FGT8	Outer membrane lipoprotein-like (AtTIL/AtLipocalin)	21.4	0	-0.68	•	•	•
At5g58090	Q93Z08	Putative glucan endo-1,3-beta-glucosidase 6	52.2	0	-0.04	•	•	
At5g58140	P93025	Phototropin-2	102.5	0	-0.56	•	•	
At5g58290	Q9SEI4	26S protease regulatory subunit 6B homolog	45.8	0	-0.34		•	
At5g58420	Q8VYK6	40S ribosomal protein S4-3	29.8	0	-0.5		•	
At5g58640	Q8W1E5	Selenoprotein-related	24.1	0	0.03	•		
At5g58670	Q39032	Phosphoinositide phospholipase C 1	64.3	0	-0.49	•		
At5g58800	Q9LUX9	1,4-benzoquinone reductase-like	22.7	0	-0.19	•		
At5g59010	Q9FIL1	Protein kinase-like protein	54.9	0	-0.35		•	
At5g59150	Q9FIF9	GTP-binding protein rab11	23.8	0	-0.22		•	
At5g59240	Q9FIF3	40S ribosomal protein S8-2	23.8	0	-0.88		•	
At5g59370	P53494	Actin-4	41.8	0	-0.21		•	
At5g59670	Q9FN94	Receptor-like protein kinase At5g59670	97	1	-0.22		•	
At5g59840	Q9FJF1	Putative GTP-binding protein ara-3	23.8	0	-0.3	•	•	
At5g60390	P13905	Elongation factor 1-alpha	49.5	0	-0.33		•	
At5g60660	Q9FF53	Probable aquaporin PIP2-4	30.1	6	0.49		•	
At5g60670	Q9FF52	60S ribosomal protein L12-3	17.8	0	-0.28	•	•	
At5g60860	Q9FJH0	GTP-binding protein, Ras-like	24.3	0	-0.25		•	

Continued on next page ...

AGI	Uniprot	Name	MW [kDa]	TMD	GRAVY	Precipitation methods		
						CHCl ₃ /MeOH	Wang	-
At5g61130	Q9FNQ2	PD callose binding protein 1	20.4	0	-0.12	•		
At5g61520	Q8L7R8	Sugar transport protein 3 (STP3)	55.9	12	0.45	•	•	
At5g61790	P29402	Calnexin homolog 1	60.5	1	-0.76	•	•	
At5g61900	Q9FH53	BONZAI2	63.1	0	-0.06			•
At5g62390	Q9LVA0	AtBag7 (Bcl-2-associated athanogene)	51.6	0	-0.81			•
At5g62630	Q94F08	HIPL2 protein	75.6	0	-0.37	•	•	
At5g62670	Q9LV11	ATPase 11, plasma membrane-type	105.2	10	0.12	•	•	
At5g62680	Q9LV10	Peptide transporter	67.9	0	0.28	•		
At5g62740	Q9FM19	Hypersensitive-induced response protein	31.4	0	-0.1	•	•	•
At5g63880	Q8GXN6	Vacuolar protein sorting-associated protein 20 homolog 1	24.8	0	-0.69		•	
At5g64330	Q9FMF5	Root phototropism protein 3	81.8	0	-0.36		•	
At5g64410	Q9FME8	Oligopeptide transporter 4 (AtOPT4)	81.8	16	0.43	•		
At5g64440	Q9FGF2	Similarity to glutamyl-tRNA amidotransferase subunit A	66.1	0	-0.11		•	
At5g65020	Q9XEE2	Annexin D2	36.3	0	-0.53	•		
At5g65220	Q9FJP3	50S ribosomal protein L29 (chloroplastic)	19.4	0	-0.64	•	•	•
At5g65270	Q9FJN8	GTP-binding protein AtRABA4a	24.8	0	-0.26	•	•	
At5g65430	P48348	14-3-3-like protein GF14 kappa (GRF8)	28	0	-0.32	•		
At5g66210	Q9FKW4	Calcium-dependent protein kinase 28 (CPK28)	58.1	0	-0.43		•	
At5g66570	P23321	Oxygen-evolving enhancer protein 1-1 (chloroplastic)	35.1	0	-0.33			•
At5g66680	Q944K2	Defective glycoylation 1 (DGL1)	48.7	0	-0.08		•	
At5g67130	Q93XX5	PI-PLC X domain-containing protein At5g67130	46.6	0	-0.05	•		
At5g67560	Q93Y31	ADP-ribosylation factor-like protein	20.4	0	-0.05		•	
AtCg00120	P56757	ATP synthase subunit alpha (chloroplastic)	55.3	0	-0.05		•	•
AtCg00340	P56767	Photosystem I P700 chlorophyll a apoprotein A2	82.5	11	0.12	•		•
AtCg00350	P56766	Photosystem I P700 chlorophyll a apoprotein A1	83.2	11	0.25			•
AtCg00380	P56799	30S ribosomal protein S4 (chloroplastic)	23.3	0	-0.5			•
AtCg00480	P19366	ATP synthase subunit beta (chloroplastic)	53.9	0	-0.09		•	•
AtCg00490	O03042	Ribulose biphosphate carboxylase large chain	52.1	0	-0.27	•	•	•
AtCg00540	P56771	Apocytochrome f	35.4	1	-0.09	•		•
AtCg00770	P56801	30S ribosomal protein S8 (chloroplastic)	15.5	0	-0.34		•	•
AtCg00780	P56792	50S ribosomal protein L14 (chloroplastic)	13.6	0	-0.07	•	•	

Continued on next page ...

AGI	Uniprot	Name	MW [kDa]	TMD	GRAVY	Precipitation methods		
						CHCl ₃ /MeOH	Wang	-
AtCg00790	P56793	50S ribosomal protein L16 (chloroplastic)	15.3	0	-0.49		•	•
AtCg00800	P56798	30S ribosomal protein S3 (chloroplastic)	25.2	0	-0.35		•	
AtCg00830	P56791	50S ribosomal protein L2 (chloroplastic)	29.9	0	-0.52		•	•
AtCg00900	P61841	30S ribosomal protein S7 (chloroplastic)	17.4	0	-0.58			•
AtMg00280	P93292	Putative uncharacterized mitochondrial protein	12.7	0	-0.49		•	

Table A.2.: Identified proteins in Triton X-100 DRMs. Methyl- β -D-cyclodextrin treatment effects are valuable determinants if a given Protein represents an intrinsic lipid raft protein. Stars (*) indicate DRM proteins which were not identified yet in proteomic publications handling plant DRMs. Proteins **in bold** were exclusively identified with Triton X-100 and not within Brij-98 DRMs.

AGI	Uniprot	Name	MW [kDa]	TMD	GRAVY	Digestion techniques		MCD [†]	MCD resp.*
						In-gel	In-solution		
Signaling (52)									
At1g05150	O23052	Uncharacterized TPR repeat-containing protein	90.2	0	-0.42	•			
At1g18890	Q9M9V8	Calcium-dependent protein kinase 10 (CPK10)	61.5	0	-0.34	•		•	*
At1g70530	Q9CAL2	Cysteine-rich receptor-like protein kinase 3	71.6	1	-0.13	•			*
At2g47060	Q27GL0	Serine/threonine protein kinase	43.8	0	-0.35		•		○ *
At3g02520	Q96300	14-3-3-like protein GF14 nu (GRF7)	29.8	0	-0.5	•		•	*
At3g25070	Q8GYN5	RPM1-interacting protein 4	23.4	0	-1.41		•		*
At4g00710	Q8W4L3	Putative uncharacterized protein	54.9	0	-0.37	•			○ *
At4g11530	Q9LDQ3	Putat. cysteine-rich receptor-like protein kinase 35	74.1	1	-0.11	•		•	*
At4g12980	Q9SV71	Auxin-responsive protein, putative	42.2	0	0.24	•			*
At4g17530	Q9SEH3	Ras-related small GTP-binding protein RAB1c	22.3	0	-0.27		•		○
At4g26080	P49597	Protein phosphatase 2C 56 (ABI1)	47.5	0	-0.32	•			*
At1g06700	Q8H1G6	Serine/threonine protein kinase	39.8	0	-0.33	•	•		○ *
At1g21250	Q39191	Wall-associated receptor kinase 1	81.2	1	-0.26	•	•	•	*
At1g22280	Q9LME4	Probable protein phosphatase 2C 9	30.7	0	-0.41	•	•		○ *
At1g27190	O04567	Probable inactive receptor kinase	65.4	1	-0.01	•			○ *
At1g30360	Q9C8G5	Dehydrin ERD4	81.9	0	0.3	•	•	○	
At1g51805	Q9C8I7	Leucine-rich repeat receptor-like protein kinase	95.8	0	-0.14	•	•	•	*
At1g53430	Q9LPF9	Leucine-rich repeat receptor-like protein kinase	104.3	0	-0.2	•	•		*
At1g53440	Q9LPG0	Leucine-rich repeat receptor-like protein kinase	108.8	2	-0.21	•		•	*
At1g69840	Q9CAR7	Hypersensitive-induced response protein	31.4	0	-0.22	•	•		○
At1g76180	P42763	Dehydrin ERD14	20.8	0	-1.27	•	•	○	• *
At2g20990	Q9SKR2	Synaptotagmin A	61.7	0	-0.26	•	•	○	
At2g26730	O48788	Probable inactive receptor kinase	71.8	1	-0.19	•	•		
At2g31880	Q9SKB2	Leucine-rich repeat receptor-like protein kinase	71.1	0	-0.16	•	•	•	*

Continued on next page ...

AGI	Uniprot	Name	MW [kDa]	TMD	GRAVY	Digestion techniques			MCD resp.*
						In-gel	In-solution	MCD†	
At2g37710	O80939	Putative receptor protein kinase	75.5	0	-0.13	●	●	●	
At2g45820	O80837	AtRemorin 1.3 *	20.1	0	-0.81	●	●	○	●
At3g01290	Q9SRH6	Hypersensitive-induced response protein	31.4	0	-0.07	●	●	·	○
At3g02880	Q9M8T0	Probable inactive receptor kinase	67.8	2	-0.09	●	●	·	
At3g08510	Q39033	Phosphoinositide phospholipase C 2	66.1	0	-0.47	●	●	○	● *
At3g14840	Q9LH71	Receptor-like serine/threonine kinase	114.7	2	-0.22	●	●	○	*
At3g17410	Q9LUT0	Putative uncharacterized protein	39.6	0	-0.3	●	●		
At3g24550	Q9LV48	Proline Extensin-Like Receptor Kinase 1	69.3	0	-0.56	●	●	●	○ *
At3g28450	Q9LSI9	Leucine-rich repeat receptor-like protein kinase	66.9	0	-0.1	●	●		*
At3g45780	O48963	Phototropin-1	111.7	0	-0.64	●	●	●	*
At3g51550	Q9SCZ4	Receptor-protein kinase-like protein	98.1	0	-0.26	●	●	●	○ *
At3g54200	Q9M386	Putative uncharacterized protein	25.8	0	0.11	●			
At3g57530	Q6NLQ6	Calcium-dependent protein kinase 32 (CPK32)	60.9	0	-0.51	●	●		*
At3g61260	Q9M2D8	AtRemorin 1.2 *	23.1	0	-0.77	●	●	●	●
At3g63260	O22100	A.th. MLK/Raf-related protein kinase 1	42.6	0	-0.3	●	●	●	● *
At4g04720	Q9ZSA2	Calcium-dependent protein kinase 21 (CPK21)	59.9	0	-0.47	●		●	
At4g08850	Q8VZG8	Leucine-rich repeat receptor-like protein kinase	115.4	2	-0.19	●	●	●	○ *
At4g20260	Q96262	PM associated cation-binding protein 1	24.6	0	-0.71	●	●		○
At4g23180	Q8GYA4	Cysteine-rich receptor-like protein kinase 10	72.1	1	-0.14	●	●	·	*
At4g35230	Q944A7	Putative serine/threonine-protein kinase	56.8	0	-0.48	●	●		
At4g35790	Q9C5Y0	Phospholipase D δ	98.1	0	-0.4	●	●	○	
At5g06320	Q9FNH6	Harpin-induced protein-like (NHL3)	25.9	0	-0.09	●	●	·	
At5g16590	Q9FMD7	Probable inactive receptor kinase	67.5	1	-0.03	●	●		
At5g38990	Q9FID9	Receptor protein kinase-like protein	97.1	0	-0.16	●	●		*
At5g48380	Q9ASS4	Leucine-rich repeat receptor-like protein kinase	69.1	0	-0.07	●	●	●	○ *
At5g49760	Q8GZ99	Leucine-rich repeat receptor-like protein kinase	104.7	0	-0.13	●	●	●	● *
At5g58140	P93025	Phototropin-2	102.5	0	-0.56	●	●		*
At5g62740	Q9FM19	Hypersensitive-induced response protein	31.4	0	-0.1	●	●		○
Transport (28)									
At1g13210	Q9SAF5	Putative phospholipid-transporting ATPase 11	136.6	10	-0.08	●			*

Continued on next page ...

AGI	Uniprot	Name	MW [kDa]	TMD	GRAVY	Digestion techniques			MCD resp.*
						In-gel	In-solution	MCD [†]	
At5g06530	Q93YS4	ABC transporter G family # 22 (AtWBC23)	82.9	6	0.05		•		*
At1g01620	Q08733	Aquaporin PIP1-3	30.6	6	0.38	•		.	
At1g11260	P23586	Sugar transport protein 1 (STP1)	57.6	12	0.48	•	•		
At1g22710	Q39231	Sucrose transport protein SUC2	54.5	12	0.48	•	•	•	*
At1g52190	Q9M817	Probable peptide transporter At1g52190	66.9	10	0.24	•	•		*
At1g57990	Q9C508	Probable purine permease 18	44.2	10	0.44	•			*
At1g59870	Q9XIE2	ABC transporter G family # 36 (PEN3/PDR8)	165.1	14	0.05	•	•	○	○
At1g70940	Q9S7Z8	Auxin efflux carrier component 3 (AtPIN3)	69.5	10	0.14	•	•		• *
At2g18960	P20649	ATPase 1, PM-type	104.2	10	0.08	•	•	○	○
At2g37170	P43287	Aquaporin PIP2-2	30.5	6	0.46	•	•	○	
At2g37180	P30302	Aquaporin PIP2-3	30.4	6	0.5	•			
At2g39010	Q9ZV07	Probable aquaporin PIP2-6	31	6	0.46	•	•	.	
At2g45960	Q06611	Aquaporin PIP1-2	30.6	6	0.41	•	•	.	○
At3g19930	Q39228	Sugar transport protein 4 (STP4)	57.1	12	0.56	•			*
At3g28860	Q9LJX0	ABC transporter B family # 19 (MDR11/PGP19)	136.8	11	0.13	•	•	○	*
At3g53420	P43286	Aquaporin PIP2-1	30.5	6	0.51	•	•	.	
At3g61430	P61837	Aquaporin PIP1-1	30.7	6	0.37	•		.	○
At3g62150	Q9M1Q9	ABC transporter B family # 21 (MDR17/PGP21)	139.8	11	0.1	•	•		*
At4g00430	Q39196	Probable aquaporin PIP1-4	30.7	6	0.38	•			
At4g13510	P54144	Ammonium transporter 1 member 1 (AtAMT1;1)	53.6	9	0.36				• *
At4g23400	Q8LAA6	Probable aquaporin PIP1-5	30.6	6	0.4	•	•	.	
At4g29900	Q9SZR1	Putative calcium-transporting ATPase 10, PM-type	116.9	10	0.04	•	•		○ *
At4g30190	P19456	ATPase 2, PM-type	104.4	10	0.1	•	•	○	•
At4g35100	P93004	Aquaporin PIP2-7	29.7	6	0.45	•	•	○	
At5g57110	Q9LF79	Calcium-transporting ATPase 8, PM-type	116.2	10	0.03	•	•	•	• *
At5g57350	P20431	ATPase 3, PM-type	104.4	10	0.05	•		•	○ *
At5g62670	Q9LV11	ATPase 11, PM-type	105.2	10	0.12	•	•	•	○
Structure (17)									
At1g04820	P29510	Tubulin alpha-2/alpha-4 chain	49.5	0	-0.2	•		○	○
At1g49240	Q96293	Actin-8	41.9	0	-0.18	•		•	○

Continued on next page ...

AGI	Uniprot	Name	MW [kDa]	TMD	GRAVY	Digestion techniques		MCD [†]	MCD resp.*
						In-gel	In-solution		
At4g14960	P29511	Tubulin alpha-6 chain	49.5	0	-0.2	●			○
At5g09810	P53492	Actin-7	41.7	0	-0.18	●		●	○
At1g03870	Q9ZWA8	Fasciclin-like arabinogalactan protein 9 (Fla9)	26.1	0	0	●			● ★
At1g20010	P29513	Tubulin beta-5 chain	50.3	0	-0.36	●	●		
At1g35720	Q9SYT0	Annexin D1	36.2	0	-0.6	●	●		★
At1g75680	Q8LCP6	Endoglucanase 10	57.9	0	-0.33	●	●		○ ★
At2g23810	O64822	Tetraspanin 8	22.1	0	-0.18	●		●	★
At2g45470	O22126	Fasciclin-like arabinogalactan protein 8 (Fla8)	43.1	0	0.13	●	●	·	●
At3g07160	Q9SFU6	Callose synthase 9	222.1	16	-0.01	●	●	●	○
At3g18780	Q96292	Actin-2	41.9	0	-0.18	●	●		
At4g03550	Q9ZT82	Callose synthase 12	206.9	16	-0.03	●	●		○
At4g12420	Q9SU40	Putative monocopper oxidase (AtSku5)	65.7	0	-0.24	●	●	·	●
At5g19770	P20363	Tubulin alpha-3/alpha-5 chain	49.7	0	-0.15	●			○
At5g44340	P24636	Tubulin beta-4 chain	49.8	0	-0.35	●	●		
At5g55730	Q9FM65	Fasciclin-like arabinogalactan protein 1 (Fla1)	44.8	0	-0.04	●			● ★
Trafficking (17)									
At1g04750	Q9ZTW3	Vesicle-associated membrane protein 721 (VAMP721)	24.8	1	-0.12	●		○	★
At1g10630	Q6ID97	ADP-ribosylation factor A1F	20.6	0	-0.19	●		·	○ ★
At1g16920	Q39222	Ras-related protein RABA1b	24	0	-0.34	●			★
At3g09900	Q9SF91	Putative Ras-like GTP-binding protein	24.3	0	-0.38	●		·	★
At1g05500	Q9ZVY8	Synaptotagmin homologue E (AtSytE)	59.2	0	-0.01	●	●		
At1g22530	Q56ZL2	Patellin-2	76	0	-0.53	●	●		○
At1g23490	Q9SRC3	ADP-ribosylation factor 2	20.6	0	-0.19	●	●		★
At1g59610	Q9LQ55	Dynamin-2B	100.2	0	-0.56	●	●		○
At1g61250	Q9M5P2	Secretory carrier-associated membrane protein 3	32.6	4	0.19	●	●		★
At1g72150	Q56WK6	Patellin-1	64	0	-0.54	●	●	●	○
At3g09740	Q9SF29	Syntaxin-71	29.1	1	-0.52	●	●	●	○
At3g10380	Q93YU5	Probable exocyst complex component 4	116.6	0	-0.27		●		★
At3g11820	Q9ZSD4	Syntaxin-121 (PEN1)	37.1	1	-0.57	●	●	○	★

Continued on next page ...

AGI	Uniprot	Name	MW [kDa]	TMD	GRAVY	Digestion techniques		MCD [†]	MCD resp.*
						In-gel	In-solution		
At3g52400	Q9SVC2	Syntaxin-122	37.8	1	-0.54	•	•		*
At3g61050	Q9LEX1	CaLB protein	55.1	0	0.02	•	•		
At5g08080	Q8VZU2	Syntaxin-132	34.2	1	-0.56	•	•		*
At5g42080	P42697	Dynamin-related protein 1A	68.2	0	-0.28	•	•		
Other / Unknown (11)									
At1g23410	P59263	Ubiquitin	8.5	0	-0.45	•		•	*
At4g05050	P59263	Ubiquitin 11	8.5	0	-0.45	•			*
At4g22485	A8MRQ5	Uncharacterized protein	68.2	0	-1.07	•		•	*
At1g13470	Q56XU1	Uncharacterized protein	31	0	-0.61	•	•		*
At1g14880	Q9LQU2	F10B6.29	16.5	0	-0.11	•	•		*
At1g17620	Q9LNP3	Similar to Heavy metal transport/detoxification protein (Harpin-induced 1)	28.3	0	-0.02	•			
At1g66970	Q7Y208	Probable glycerophosphoryl diester phosphodiesterase 3 (SHV3-LIKE 2)	83.8	0	-0.02	•	•		*
At1g73650	Q3ECD5	Oxidoreductase, acting on the CH-CH group of donors	33.1	0	0.52	•			
At3g07570	Q9SSF3	Membrane protein, putative	50.4	0	0.13	•			*
At3g08600	Q9C9Z6	At3g08600/F17O14.7	34.7	0	-0.09	•			
At4g36750	O23207	Quinone reductase family	28.8	0	-0.21	•	•		• *
Ribosomal (25)									
At1g02780	Q9SRX2	60S ribosomal protein L19-1	24.6	0	-0.99		•		○ *
At1g48830	Q9C514	40S ribosomal protein S7-1	21.9	0	-0.47		•		*
At2g01250	P60040	60S ribosomal protein L7-2	28.2	0	-0.57	•		•	○ *
At2g24090	Q8VZ55	50S ribosomal protein L35	16.1	0	-0.43		•		*
At2g36620	Q42347	60S ribosomal protein L24-1	18.9	0	-1.02		•		*
At2g39460	Q8LD46	60S ribosomal protein L23a-1	17.4	0	-0.76	•			○ *
At2g47610	P49692	60S ribosomal protein L7a-1	29.1	0	-0.56		•		○ *
At3g04840	Q9CAV0	40S ribosomal protein S3a-1	29.9	0	-0.52	•			*
At3g09630	Q9SF40	60S ribosomal protein L4-1	44.7	0	-0.38		•		○ *
At3g49010	P41127	60S ribosomal protein L13-1	23.8	0	-0.92		•		○ *

Continued on next page ...

AGI	Uniprot	Name	MW [kDa]	TMD	GRAVY	Digestion techniques		MCD [†]	MCD resp.*
						In-gel	In-solution		
At3g60770	P59223	40S ribosomal protein S13-1	17.1	0	-0.51		•		○ *
At4g34555	Q8GYL5	40S ribosomal protein S25-3	12	0	-0.8	•			*
At4g36130	Q42064	60S ribosomal protein L8-3	27.9	0	-0.45		•		*
At4g39200	Q9T029	40S ribosomal protein S25-4	12.1	0	-0.76		•		*
At5g09510	Q9FY64	40S ribosomal protein S15-4	17.1	0	-0.32	•			*
At5g60670	Q9FF52	60S ribosomal protein L12-3	17.8	0	-0.28	•			*
At2g17360	Q93VH9	40S ribosomal protein S4-1	29.8	0	-0.53	•	•		○ *
At2g20450	Q9SIM4	60S ribosomal protein L14-1	15.5	0	-0.23	•			*
At2g36160	Q9SIH0	40S ribosomal protein S14-1	16.3	0	-0.47	•	•		○ *
At2g41840	P49688	40S ribosomal protein S2-3	30.9	0	-0.41	•	•		*
At3g11510	Q9CAX6	40S ribosomal protein S14-2	16.3	0	-0.5	•	•		*
At3g56340	Q9LYK9	40S ribosomal protein S26-3	14.6	0	-0.88	•	•		*
At4g31700	O48549	40S ribosomal protein S6-1	28.4	0	-0.9	•	•	•	○ *
At5g20290	Q93VG5	40S ribosomal protein S8-1	24.1	0	-0.92	•	•		○ *
At5g27850	Q940B0	60S ribosomal protein L18-3	20.1	0	-0.42	•			*
Contaminations (43)									
At1g07320	O50061	50S ribosomal protein L4 (chloroplastic)	30.6	0	-0.4		•		*
At1g07930	P13905	Elongation factor 1-alpha	49.5	0	-0.33	•			*
At1g11530	Q8LDI5	Thioredoxin-like 4	13.3	0	0.14	•			*
At1g31330	Q9SHE8	Photosystem I reaction center subunit III	24.2	1	-0.01		•		*
At1g61520	Q9SY97	PSI type III chlorophyll a/b-binding protein	29.2	0	-0.01		•		○ *
At1g67090	P10795	Ribulose biphosphate carboxylase small chain 1A	20.3	0	-0.27	•			*
At1g78630	Q9SYL9	50S ribosomal protein L13 (chloroplastic)	26.8	0	-0.47		•		*
At3g09440	O65719	Heat shock cognate 70 kDa protein 3	71.1	0	-0.39	•		•	○
At3g11130	Q0WM81	Clathrin heavy chain, putative	27.6	0	-0.39	•	•	•	○
At3g13920	P41376	Eukaryotic initiation factor 4A-1	46.7	0	-0.22		•		○ *
At3g19340	Q8RWC3	Putative uncharacterized protein At3g19340	56.8	0	-0.31	•			*
At3g25920	P25873	50S ribosomal protein L15 (chloroplastic)	29.7	0	-0.47	•	•	○	*
At3g28220	Q9LHA6	MATH-domain containing protein	42.9	0	-0.43	•			*
At3g45140	P38418	Lipoxygenase 2 (chloroplastic) (AtLOX2)	102.1	0	-0.47	•	•	•	*

Continued on next page ...

AGI	Uniprot	Name	MW [kDa]	TMD	GRAVY	Digestion techniques			MCD resp.*
						In-gel	In-solution	MCD [†]	
At3g46060	P28186	Ras-related protein ARA-3	23.8	0	-0.3	●			★
At4g01310	O04603	50S ribosomal protein L5 (chloroplastic)	28.3	0	-0.28	●		○	★
At4g20360	P17745	Elongation factor Tu (chloroplastic)	51.6	0	-0.12		●		○ ★
At5g40950	Q9FLN4	50S ribosomal protein L27 (chloroplastic)	21.7	0	-0.5		●		★
At5g44020	Q9FNC4	Vegetative storage protein-like	31.1	0	-0.33	●		●	★
At5g56000	O03986	Heat shock protein (HSP81-4)	80.1	0	-0.59	●		●	○ ★
At5g61790	P29402	Calnexin homolog 1	60.5	1	-0.76	●			○ ★
At5g62390	Q9LVA0	AtBag7 (Bcl-2-associated athanogene)	51.6	0	-0.81		●		○ ★
At5g65220	Q9FJP3	50S ribosomal protein L29 (chloroplastic)	19.4	0	-0.64		●		★
AtCg00770	P56801	30S ribosomal protein S8 (chloroplastic)	15.5	0	-0.34		●		★
At1g12900	Q9LPW0	GAPA-2	42.8	0	-0.05	●	●		★
At1g13440	Q9FX54	Putative glyceraldehyde-3-phosphate dehydrogenase	36.9	0	-0.14	●	●	●	○ ★
At1g15690	P31414	Pyrophosphate-energized vacuolar membrane proton pump 1	80.9	13	0.62	●	●	○	● ★
At1g70410	Q94CE4	Carbonic anhydrase	30.8	0	-0.17	●	●	○	★
At2g39730	P10896	RuBisCO activase	51.1	0	-0.31	●	●	●	★
At2g43030	Q9SKX4	50S ribosomal protein L3-1 (chloroplastic)	29.4	0	-0.17	●	●	○	★
At3g08580	P31167	ADP,ATP carrier protein 1, mitochondrial	41.5	6	-0.12	●	●	○	○ ★
At3g16240	Q41951	Aquaporin TIP2-1	25	6	0.97	●			● ★
At3g26650	P25856	Glyceraldehyde-3-phosphate dehydrogenase A	42.5	0	-0.02	●		●	★
At4g02770	Q9S7H1	Photosystem I reaction center subunit II-1	22.6	0	-0.37	●	●		★
At5g02500	P22953	Heat shock cognate 70 kDa protein 1	71.4	0	-0.44	●	●		○
At5g14740	P42737	Carbonic anhydrase 2	28.3	0	-0.07	●	●		★
At5g28540	Q9LKR3	Luminal-binding protein 1 (BiP1)	73.6	0	-0.46	●			○ ★
At5g43470	Q8W4J9	Disease resistance protein RPP8	104.7	0	-0.28	●	●	●	★
At5g60390	P13905	Elongation factor 1-alpha	49.5	0	-0.33	●	●		★
AtCg00340	P56767	Photosystem I P700 chlorophyll a apoprotein A2	82.5	11	0.12	●	●	·	★
AtCg00490	O03042	Ribulose bisphosphate carboxylase large chain	52.1	0	-0.27	●	●	○	★
AtCg00790	P56793	50S ribosomal protein L16 (chloroplastic)	15.3	0	-0.49		●		★
AtCg00830	P56791	50S ribosomal protein L2 (chloroplastic)	29.9	0	-0.52	●	●	●	★

†Proteins affected by Methyl- β -D-cyclodextrin application were classified as followed: removed due to the MCD application (●), negatively affected in the proteomic identification parameters (◦) and unaffected or enriched (·). Triton X-100 DRM proteins not subjected to MCD treatment but identified in previous experiments do not have any special mark.

*MCD responsive proteins according to Kierszniowska *et al.* (2008). Filled circles (●): proteins negatively affected, empty circles (◦): unaffected proteins.

Table A.3.: Identified proteins in Brij-98 DRMs. Proteins exclusively identified with Brij-98 and not within Triton X-100 DRMs are marked **in bold**. Stars (*) indicate novel identified DRM proteins.

AGI	Uniprot	Name	MW [kDa]	TMD	GRAVY	Digestion techniques		MCD [†]	MCD resp.*
						In-gel	In-solution		
Signaling (58)									
At1g11330	Q9SXB8	S-locus lectin protein kinase family protein	88.8	0	-0.24	•			*
At1g19870	Q9FXI5	Protein IQ-DOMAIN 32	86.9	0	-0.89		•		*
At1g20450	P42759	Dehydrin ERD10	29.5	0	-1.35		•		*
At1g48210	Q93Y19	Serine/threonine protein kinase-like protein	39.6	0	-0.33		•		*
At1g63500	Q9SH35	Protein kinase	69.7	0	-0.21	•			
At2g17120	O23006	LysM domain-containing GPI-anchored protein 2	37.7	0	0.04	•		•	*
At2g37050	Q2V2T0	Uncharacterized protein	79.3	0	-0.21		•		*
At3g07390	Q94BT2	Auxin-induced in root cultures protein 12 (AIR12)	25.6	0	0.17	•		•	*
At3g17840	Q9LVI6	Probable inactive receptor kinase RLK902	70.4	1	-0.07	•	•		○
At3g23750	Q9LK43	Similarity to receptor protein kinase	99.1	0	-0.1	•	•		○
At4g18760	Q9SN38	Leucine-rich repeat receptor-like protein kinase	46.1	0	0.02	•			○
At4g23160	O65468	Cysteine-rich receptor-like protein kinase 8	75.4	1	-0.16		•		*
At4g23220	Q8H199	Cysteine-rich receptor-like protein kinase 14	73.9	1	-0.08		•		*
At4g23250	Q8L710	Cysteine-rich receptor-like protein kinase 17	76.4	1	-0.15		•		*
At5g10020	Q0WR59	Probable inactive receptor kinase	114.7	1	-0.17		•		*
At5g41260	Q9FHD7	Putative serine/threonine-protein kinase	54.6	0	-0.41		•		
At5g59010	Q9FIL1	Protein kinase-like protein	54.9	0	-0.35		•		*
At1g06700	Q8H1G6	Serine/threonine protein kinase	39.8	0	-0.33	•	•		○
At1g21250	Q39191	Wall-associated receptor kinase 1	81.2	1	-0.26	•	•	•	*
At1g22280	Q9LME4	Probable protein phosphatase 2C 9	30.7	0	-0.41	•	•		○
At1g27190	O04567	Probable inactive receptor kinase At1g27190	65.4	1	-0.01	•			○
At1g30360	Q9C8G5	Dehydrin ERD4	81.9	0	0.3	•	•	○	
At1g51805	Q9C8I7	Leucine-rich repeat receptor-like protein kinase	95.8	0	-0.14	•	•	•	*
At1g53430	Q9LPF9	Leucine-rich repeat receptor-like protein kinase	104.3	0	-0.2	•	•		*
At1g53440	Q9LPG0	Leucine-rich repeat receptor-like protein kinase	108.8	2	-0.21	•		•	*

Continued on next page ...

AGI	Uniprot	Name	MW [kDa]	TMD	GRAVY	Digestion techniques			
						In-gel	In-solution	MCD†	MCD resp.*
At1g69840	Q9CAR7	Hypersensitive-induced response protein	31.4	0	-0.22	●	●		○
At1g76180	P42763	Dehydrin ERD14	20.8	0	-1.27	●	●	○	● ★
At2g20990	Q9SKR2	Synaptotagmin A	61.7	0	-0.26	●	●	○	
At2g26730	O48788	Probable inactive receptor kinase At2g26730	71.8	1	-0.19	●	●		
At2g31880	Q9SKB2	Leucine-rich repeat receptor-like protein kinase	71.1	0	-0.16	●	●	●	★
At2g37710	O80939	Putative receptor protein kinase	75.5	0	-0.13	●	●	●	
At2g45820	O80837	AtRemorin 1.3	20.1	0	-0.81	●	●	○	●
At3g01290	Q9SRH6	Hypersensitive-induced response protein	31.4	0	-0.07	●	●	·	○
At3g02880	Q9M8T0	Probable inactive receptor kinase At3g02880	67.8	2	-0.09	●	●	·	
At3g08510	Q39033	Phosphoinositide phospholipase C 2	66.1	0	-0.47	●	●	○	● ★
At3g14840	Q9LH71	Receptor-like serine/threonine kinase	114.7	2	-0.22	●	●	○	★
At3g17410	Q9LUT0	Putative uncharacterized protein	39.6	0	-0.3	●	●		
At3g24550	Q9LV48	Proline Extensin-Like Receptor Kinase 1	69.3	0	-0.56	●	●	●	○ ★
At3g28450	Q9LSI9	Leucine-rich repeat receptor-like protein kinase	66.9	0	-0.1	●	●		★
At3g45780	O48963	Phototropin-1	111.7	0	-0.64	●	●	●	★
At3g51550	Q9SCZ4	Receptor-protein kinase-like protein	98.1	0	-0.26	●	●	●	○ ★
At3g54200	Q9M386	Putative uncharacterized protein	25.8	0	0.11	●			
At3g57530	Q6NLQ6	Calcium-dependent protein kinase 32 (CPK32)	60.9	0	-0.51	●	●		★
At3g61260	Q9M2D8	AtRemorin 1.2	23.1	0	-0.77	●	●	●	●
At3g63260	O22100	A.th. MLK/Raf-related protein kinase 1	42.6	0	-0.3	●	●	●	● ★
At4g04720	Q9ZSA2	Calcium-dependent protein kinase 21 (CPK21)	59.9	0	-0.47	●		●	
At4g08850	Q8VZG8	Leucine-rich repeat receptor-like protein kinase	115.4	2	-0.19	●	●	●	○ ★
At4g20260	Q96262	PM associated cation-binding protein 1	24.6	0	-0.71	●	●		○
At4g23180	Q8GYA4	Cysteine-rich receptor-like protein kinase 10	72.1	1	-0.14	●	●	·	★
At4g35230	Q944A7	Putative serine/threonine-protein kinase	56.8	0	-0.48	●	●		
At4g35790	Q9C5Y0	Phospholipase D δ	98.1	0	-0.4	●	●	○	
At5g06320	Q9FNH6	Harpin-induced protein-like (NHL3)	25.9	0	-0.09	●	●	·	
At5g16590	Q9FMD7	Probable inactive receptor kinase	67.5	1	-0.03	●	●		
At5g38990	Q9FID9	Receptor protein kinase-like protein	97.1	0	-0.16	●	●		★
At5g48380	Q9ASS4	Leucine-rich repeat receptor-like protein kinase	69.1	0	-0.07	●	●	●	○ ★
At5g49760	Q8GZ99	Leucine-rich repeat receptor-like protein kinase	104.7	0	-0.13	●	●	●	● ★

Continued on next page ...

AGI	Uniprot	Name	MW [kDa]	TMD	GRAVY	Digestion techniques		MCD†	MCD resp.*	
						In-gel	In-solution			
At5g58140	P93025	Phototropin-2	102.5	0	-0.56	•	•			★
At5g62740	Q9FM19	Hypersensitive-induced response protein	31.4	0	-0.1	•	•		○	
Transport (32)										
At1g71880	Q39232	Sucrose transport protein SUC1	54.9	12	0.47	•				★
At2g36910	Q9ZR72	ABC transporter B family # 1 (MDR1/PGP1)	140.6	12	0.07	•				★
At2g39480	Q8LPT1	ABC transporter B family # 6 (MDR6/PGP6)	155.9	12	0.07		•			★
At3g18830	Q8VZ80	Polyol transporter 5 (AtPLT5)	58.1	12	0.34	•				★
At4g16370	O23482	Probable oligopeptide transporter 3 (AtOPT3)	82.1	16	0.38	•				★
At5g26340	Q94AZ2	Sugar transport protein 13 (STP13)	57.4	12	0.52	•	•		○	
At1g01620	Q08733	Aquaporin PIP1-3	30.6	6	0.38	•				
At1g11260	P23586	Sugar transport protein 1 (STP1)	57.6	12	0.48	•	•			
At1g22710	Q39231	Sucrose transport protein SUC2	54.5	12	0.48	•	•	•		★
At1g52190	Q9M817	Probable peptide transporter	66.9	10	0.24	•	•			★
At1g57990	Q9C508	Probable purine permease 18	44.2	10	0.44	•				★
At1g59870	Q9XIE2	ABC transporter G family # 36 (PEN3/PDR8)	165.1	14	0.05	•	•	○	○	
At1g70940	Q9S7Z8	Auxin efflux carrier component 3 (AtPIN3)	69.5	10	0.14	•	•		•	★
At2g18960	P20649	ATPase 1, PM-type	104.2	10	0.08	•	•	○	○	
At2g37170	P43287	Aquaporin PIP2-2	30.5	6	0.46	•	•	○		
At2g37180	P30302	Aquaporin PIP2-3	30.4	6	0.5	•				
At2g39010	Q9ZV07	Probable aquaporin PIP2-6	31	6	0.46	•	•			
At2g45960	Q06611	Aquaporin PIP1-2	30.6	6	0.41	•	•		○	
At3g19930	Q39228	Sugar transport protein 4 (STP4)	57.1	12	0.56	•				★
At3g28860	Q9LJX0	ABC transporter B family # 19 (MDR11/PGP19)	136.8	11	0.13	•	•	○		★
At3g53420	P43286	Aquaporin PIP2-1	30.5	6	0.51	•	•			
At3g61430	P61837	Aquaporin PIP1-1	30.7	6	0.37	•			○	
At3g62150	Q9M1Q9	ABC transporter B family # 21 (MDR17/PGP21)	139.8	11	0.1	•	•			★
At4g00430	Q39196	Probable aquaporin PIP1-4	30.7	6	0.38	•				
At4g13510	P54144	Ammonium transporter 1 member 1 (AtAMT1;1)	53.6	9	0.36	•			•	★
At4g23400	Q8LAA6	Probable aquaporin PIP1-5	30.6	6	0.4	•	•			
At4g29900	Q9SZR1	Putative calcium-transporting ATPase 10, PM-type	116.9	10	0.04	•	•		○	★

Continued on next page ...

AGI	Uniprot	Name	MW [kDa]	TMD	GRAVY	Digestion techniques			
						In-gel	In-solution	MCD [†]	MCD resp.*
At4g30190	P19456	ATPase 2, PM-type	104.4	10	0.1	●	●	○	●
At4g35100	P93004	Aquaporin PIP2-7	29.7	6	0.45	●	●	○	
At5g57110	Q9LF79	Calcium-transporting ATPase 8, PM-type	116.2	10	0.03	●	●	●	● *
At5g57350	P20431	ATPase 3, PM-type	104.4	10	0.05	●		●	○ *
At5g62670	Q9LV11	ATPase 11, PM-type	105.2	10	0.12	●	●	●	○
Structure (18)									
At3g45600	Q9M1E7	Tetraspanin 3	31.9	0	0.25	●			*
At4g12730	Q9SU13	Fasciclin-like arabinogalactan protein 2 (Fla2)	43.5	0	-0.08	●	●		● *
At4g31140	Q9M088	Putative glucan endo-1,3-beta-glucosidase 5	52.7	0	0.06	●			● *
At5g12250	P29514	Tubulin beta-6 chain	50.6	0	-0.38		●		
At5g44130	Q9FFH6	Fasciclin-like arabinogalactan protein 13 (Fla13)	26.3	0	0.02	●			● *
At1g03870	Q9ZWA8	Fasciclin-like arabinogalactan protein 9 (Fla9)	26.1	0	0	●			● *
At1g20010	P29513	Tubulin beta-5 chain	50.3	0	-0.36	●	●		
At1g35720	Q9SYT0	Annexin D1	36.2	0	-0.6	●	●		*
At1g75680	Q8LCP6	Endoglucanase 10	57.9	0	-0.33	●	●		○ *
At2g23810	O64822	Tetraspanin 8	22.1	0	-0.18	●		●	*
At2g45470	O22126	Fasciclin-like arabinogalactan protein 8 (Fla8)	43.1	0	0.13	●	●		●
At3g07160	Q9SFU6	Callose synthase 9	222.1	16	-0.01	●	●	●	○
At3g18780	Q96292	Actin-2	41.9	0	-0.18	●	●		
At4g03550	Q9ZT82	Callose synthase 12	206.9	16	-0.03	●	●		○
At4g12420	Q9SU40	Putative monocopper oxidase (AtSku5)	65.7	0	-0.24	●	●		●
At5g19770	P20363	Tubulin alpha-3/alpha-5 chain	49.7	0	-0.15	●			○
At5g44340	P24636	Tubulin beta-4 chain	49.8	0	-0.35	●	●		
At5g55730	Q9FM65	Fasciclin-like arabinogalactan protein 1 (Fla1)	44.8	0	-0.04	●			● *
Trafficking (17)									
At1g32050	Q9C6X2	Secretory carrier-associated membrane protein 4	30.1	4	0.23	●			○ *
At3g46830	Q96283	Ras-related protein RABA2c	23.8	0	-0.28		●		○ *
At4g02350	O81298	Exocyst complex subunit Sec15-like family protein	86.5	0	-0.23	●			*
At5g03520	Q9LZD4	GTP-binding protein-like	24	0	-0.3	●	●		*

AGI	Uniprot	Name	MW [kDa]	TMD	GRAVY	Digestion techniques			MCD resp.*
						In-gel	In-solution	MCD†	
At1g05500	Q9ZVY8	Synaptotagmin homologue E (AtSytE)	59.2	0	-0.01	•	•		
At1g22530	Q56ZL2	Patellin-2	76	0	-0.53	•	•		○
At1g23490	Q9SRC3	ADP-ribosylation factor 2	20.6	0	-0.19	•	•		★
At1g59610	Q9LQ55	Dynamin-2B	100.2	0	-0.56	•	•		○
At1g61250	Q9M5P2	Secretory carrier-associated membrane protein 3	32.6	4	0.19	•	•		★
At1g72150	Q56WK6	Patellin-1	64	0	-0.54	•	•	•	○
At3g09740	Q9SF29	Syntaxin-71	29.1	1	-0.52	•	•	•	○
At3g10380	Q93YU5	Probable exocyst complex component 4	116.6	0	-0.27		•		★
At3g11820	Q9ZSD4	Syntaxin-121 (PEN1)	37.1	1	-0.57	•	•	○	★
At3g52400	Q9SVC2	Syntaxin-122	37.8	1	-0.54	•	•		★
At3g61050	Q9LEX1	CaLB protein	55.1	0	0.02	•	•		
At5g08080	Q8VZU2	Syntaxin-132	34.2	1	-0.56	•	•		★
At5g42080	P42697	Dynamin-related protein 1A	68.2	0	-0.28	•	•		
Other / Unknown (14)									
At3g09790	Q39256	Polyubiquitin	71.8	0	-0.29	•	•		★
At4g26690	Q9SZ11	Probable glycerophosphoryl diester phosphodiesterase 2 (MRH5/SHV3)	82.6	0	0.05	•	•		• ★
At4g27520	Q9T076	Early nodulin-like protein 2	35.1	0	-0.31	•	•		• ★
At5g19240	Q84VZ5	Uncharacterized GPI-anchored protein At5g19240	21.3	0	0.09	•	•		★
At5g20230	Q07488	Blue copper protein	20.1	0	0.2		•		★
At5g55480	Q9FJ62	Probable glycerophosphoryl diester phosphodiesterase 1 (SHV3-LIKE 1)	84.2	0	-0.05	•			•
At1g13470	Q56XU1	Uncharacterized protein	31	0	-0.61	•	•		★
At1g14880	Q9LQU2	F10B6.29	16.5	0	-0.11	•	•		★
At1g17620	Q9LNP3	Similar to Heavy metal transport/detoxification protein (Harpin-induced 1)	28.3	0	-0.02	•			
At1g66970	Q7Y208	Probable glycerophosphoryl diester phosphodiesterase 3 (SHV3-LIKE 2)	83.8	0	-0.02	•	•		★
At1g73650	Q3ECD5	Oxidoreductase, acting on the CH-CH group of donors	33.1	0	0.52	•			
At3g07570	Q9SSF3	Membrane protein, putative	50.4	0	0.13	•			★

Continued on next page ...

AGI	Uniprot	Name	MW [kDa]	TMD	GRAVY	Digestion techniques			MCD resp.*
						In-gel	In-solution	MCD†	
At3g08600	Q9C9Z6	At3g08600/F17O14_7	34.7	0	-0.09	●			
At4g36750	O23207	Quinone reductase family	28.8	0	-0.21	●	●		● ★
Ribosomal (11)									
At4g34670	Q42262	40S ribosomal protein S3a-2	29.8	0	-0.56		●		○ ★
At5g02870	P49691	60S ribosomal protein L4-2	44.7	0	-0.38	●	●		★
At2g17360	Q93VH9	40S ribosomal protein S4-1	29.8	0	-0.53	●	●		○ ★
At2g20450	Q9SIM4	60S ribosomal protein L14-1	15.5	0	-0.23	●			★
At2g36160	Q9SIH0	40S ribosomal protein S14-1	16.3	0	-0.47	●	●		○ ★
At2g41840	P49688	40S ribosomal protein S2-3	30.9	0	-0.41	●	●		★
At3g11510	Q9CAX6	40S ribosomal protein S14-2	16.3	0	-0.5	●	●		★
At3g56340	Q9LYK9	40S ribosomal protein S26-3	14.6	0	-0.88	●	●		★
At4g31700	O48549	40S ribosomal protein S6-1	28.4	0	-0.9	●	●	●	○ ★
At5g20290	Q93VG5	40S ribosomal protein S8-1	24.1	0	-0.92	●	●		○ ★
At5g27850	Q940B0	60S ribosomal protein L18-3	20.1	0	-0.42	●			★
Contaminations (32)									
At2g23200	O22187	Putative uncharacterized protein	93.4	0	-0.28	●	●		★
At2g34420	Q39141	Photosystem II type I chlorophyll a/b binding protein	28.1	0	-0.01		●		★
At3g07020	Q9M8Z7	UDP-glucose:sterol glucosyltransferase	69.3	0	-0.24	●	●		★
At3g08530	Q0WLB5	Clathrin heavy chain, putative	193.3	0	-0.17	●	●		
At3g26520	Q41963	Aquaporin TIP1-2	25.8	6	0.79	●			★
At3g47470	P27521	Chlorophyll a-b binding protein 4	27.7	2	-0.16	●			★
At3g50360	O82659	Probable calcium-binding protein CML20	19.4	0	-0.86		●		★
At3g53780	Q3EAK1	Rhomboid-like protein	29.4	0	0.55	●			★
At4g28750	Q9S831	Photosystem I reaction center subunit IV A	14.1	0	-0.18	●			★
At4g39080	Q8W4S4	Vacuolar proton ATPase subunit VHA-a isoform 3	92.8	0	0.03	●			
AtCg00280	P56778	Photosystem II CP43 chlorophyll apoprotein	50.3	6	0.27	●			○ ★
AtCg00480	P19366	ATP synthase subunit beta (chloroplastic)	53.9	0	-0.09	●			★

Continued on next page ...

AGI	Uniprot	Name	MW [kDa]	TMD	GRAVY	Digestion techniques			MCD resp.*
						In-gel	In-solution	MCD [†]	
AtCg00680	Q8HS55	Photosystem II CP47 protein	51.1	0	0.08	●	●		★
At1g12900	Q9LPW0	GAPA-2	42.8	0	-0.05	●	●		★
At1g13440	Q9FX54	Putative glyceraldehyde-3-phosphate dehydrogenase	36.9	0	-0.14	●	●	●	○ ★
At1g15690	P31414	Pyrophosphate-energized vacuolar membrane proton pump 1	80.9	13	0.62	●	●	○	● ★
At1g70410	Q94CE4	Carbonic anhydrase	30.8	0	-0.17	●	●	○	★
At2g39730	P10896	RuBisCO activase	51.1	0	-0.31	●	●	●	★
At2g43030	Q9SKX4	50S ribosomal protein L3-1 (chloroplastic)	29.4	0	-0.17	●	●	○	★
At3g08580	P31167	ADP,ATP carrier protein 1, mitochondrial	41.5	6	-0.12	●	●	○	○ ★
At3g16240	Q41951	Aquaporin TIP2-1	25	6	0.97	●			● ★
At3g26650	P25856	Glyceraldehyde-3-phosphate dehydrogenase A	42.5	0	-0.02	●		●	★
At4g02770	Q9S7H1	Photosystem I reaction center subunit II-1	22.6	0	-0.37	●	●		★
At5g02500	P22953	Heat shock cognate 70 kDa protein 1	71.4	0	-0.44	●	●		○
At5g14740	P42737	Carbonic anhydrase 2	28.3	0	-0.07	●	●		★
At5g28540	Q9LKR3	Luminal-binding protein 1 (BiP1)	73.6	0	-0.46	●			○ ★
At5g43470	Q8W4J9	Disease resistance protein RPP8	104.7	0	-0.28	●	●	●	★
At5g60390	P13905	Elongation factor 1-alpha	49.5	0	-0.33	●	●		★
AtCg00340	P56767	Photosystem I P700 chlorophyll a apoprotein A2	82.5	11	0.12	●	●	.	★
AtCg00490	O03042	Ribulose biphosphate carboxylase large chain	52.1	0	-0.27	●	●	○	★
AtCg00790	P56793	50S ribosomal protein L16 (chloroplastic)	15.3	0	-0.49		●		★
AtCg00830	P56791	50S ribosomal protein L2 (chloroplastic)	29.9	0	-0.52	●	●	●	★

[†]Proteins affected by Methyl-β-D-cyclodextrin application. Removed (●), negatively affected (○) and unaffected or enriched (·).

*MCD responsive proteins according to Kierszniowska *et al.* (2008). Filled circles (●): proteins negatively affected, empty circles (○): unaffected proteins.

B

Vector maps

B.1 eGFP::StRem 1.3

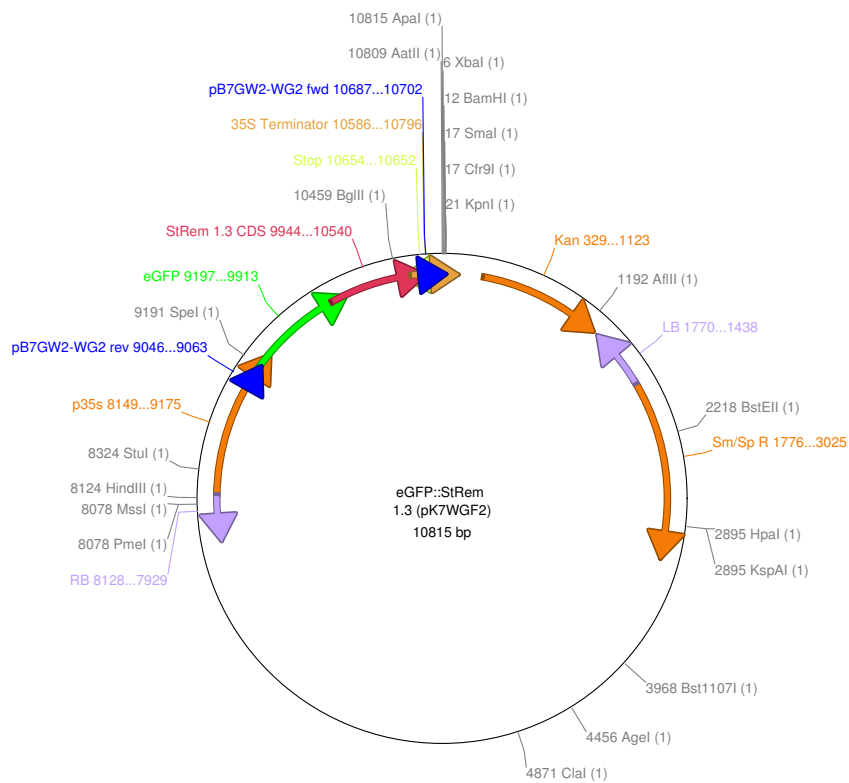


Figure B.1.: Vector map of the eGFP::StRem 1.3 construct in the pK7WGF2 binary vector featuring all unique restriction sites.

StRem 1.3 CDS length: 597 bp. Ideal restriction digest conditions: BglIII & HindIII resulting in 8480 & 2335 bp fragments.

APPENDIX B. VECTOR MAPS

B.2 eGFP::AtRemorin 1.2

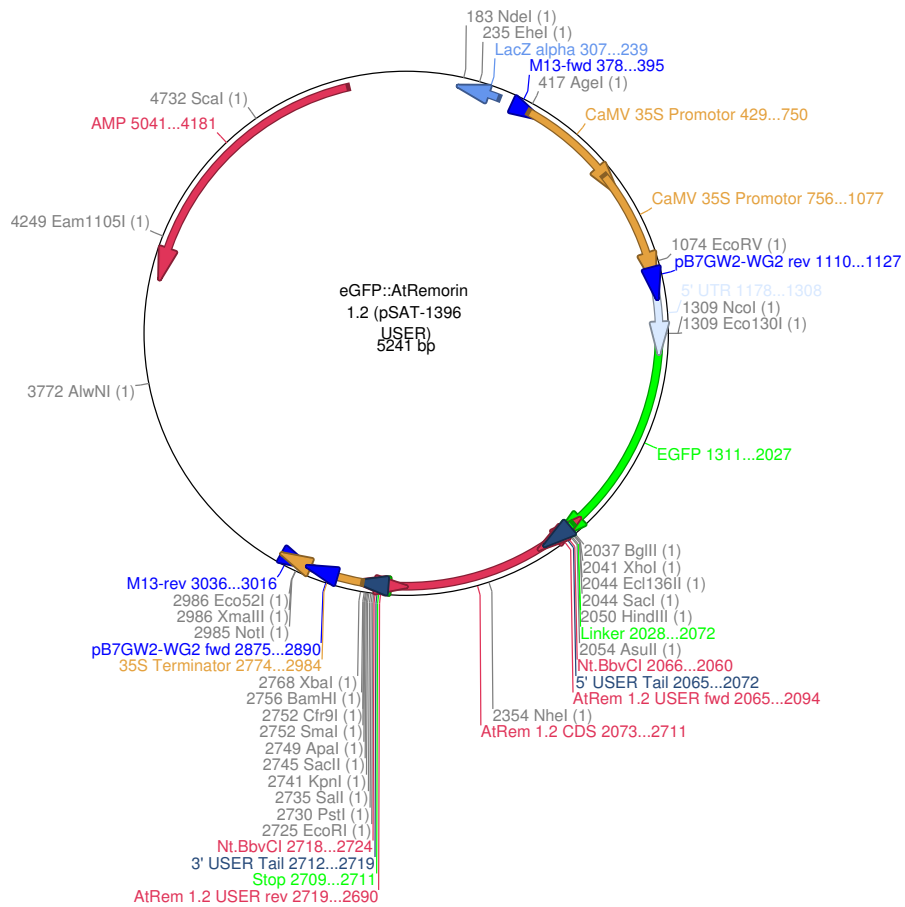


Figure B.2.: Vector map of the eGFP::AtRemorin 1.2 construct in the transient expression vector pSAT 1396 USER featuring all unique restriction sites.

AtRemorin 1.2 CDS length: 639 bp. Ideal restriction digest conditions: EcoRV & NheI resulting in 3961 & 1280 bp fragments.

B.3 DsRed2::AtRemorin 1.3

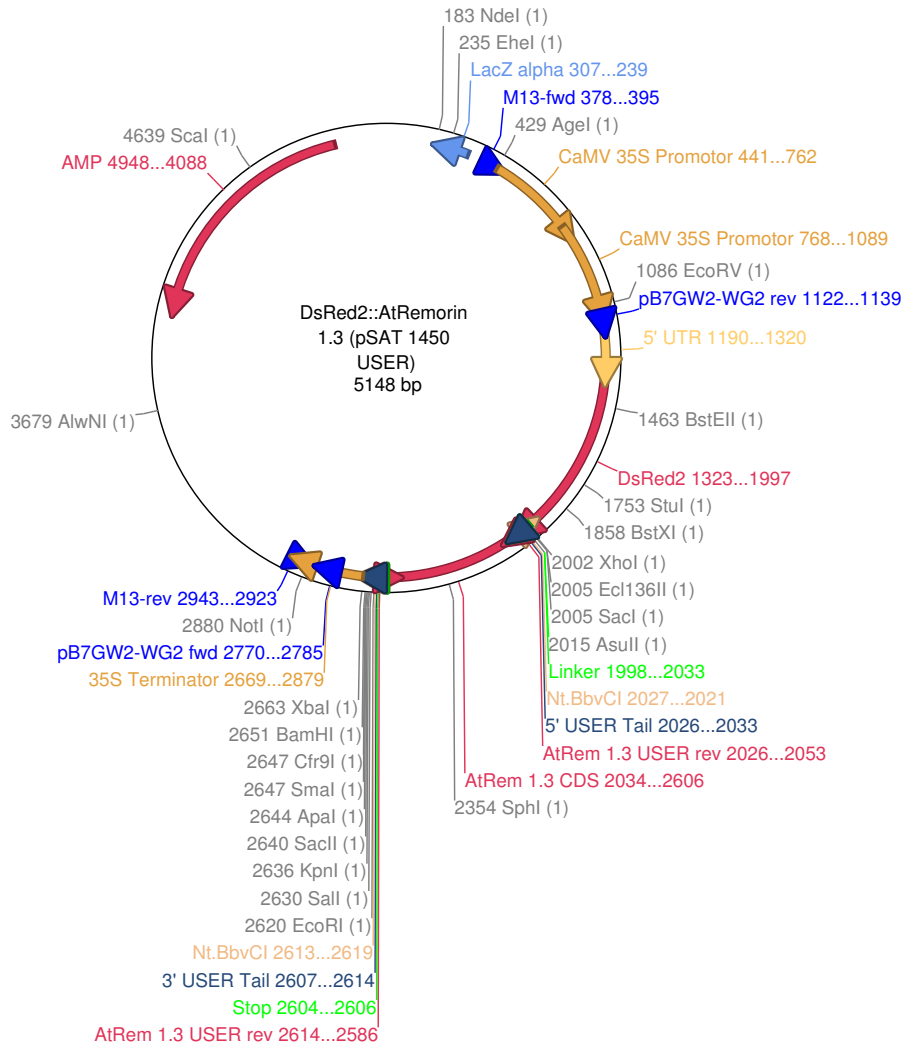


Figure B.3.: Vector map of the DsRed2::AtRemorin 1.3 construct in the transient expression vector pSAT 1450 USER featuring all unique restriction sites. AtRemorin 1.3 CDS length: 573 bp. Ideal restriction digest conditions: EcoRV & SphI resulting in 3880 & 1268 bp fragments.

B.4 eGFP::AtSUC1

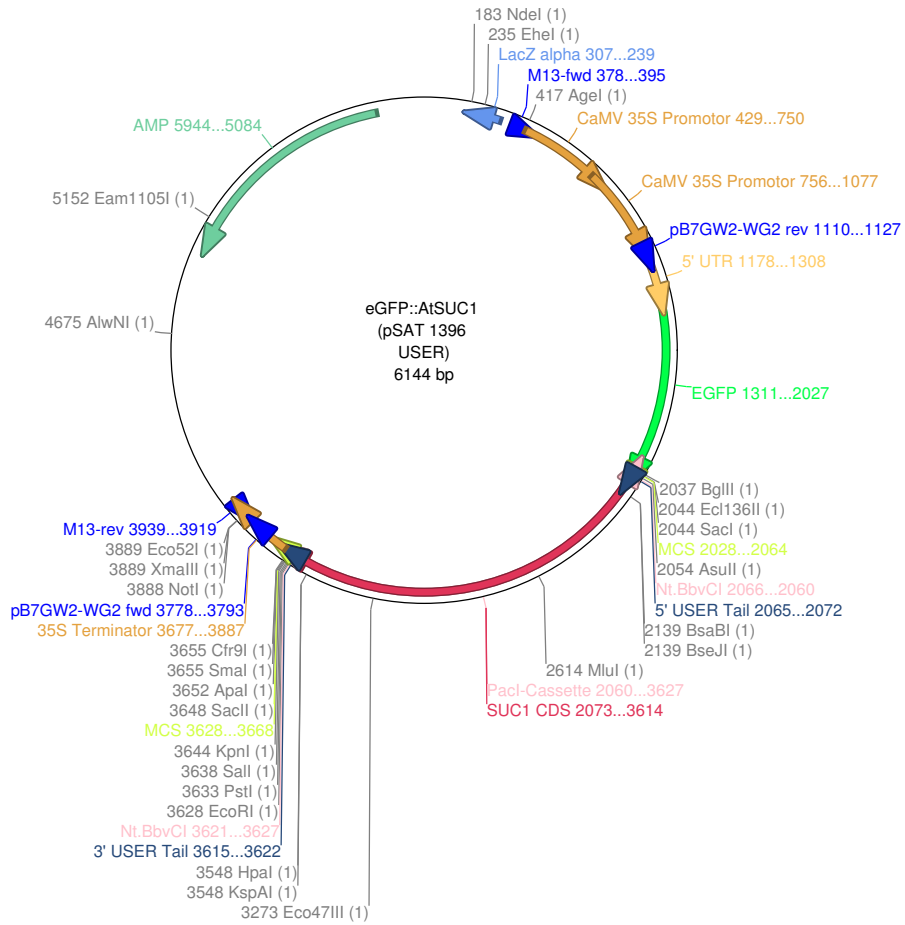


Figure B.4.: Vector map of the eGFP::AtSUC1 construct in the transient expression vector pSAT 1396 USER featuring all unique restriction sites. AtSUC1 CDS length: 1542 bp. Ideal restriction digest conditions: BglIII & Eco47III resulting in 4908 & 1236 bp fragments.

B.5 EGFP::AtSUC2

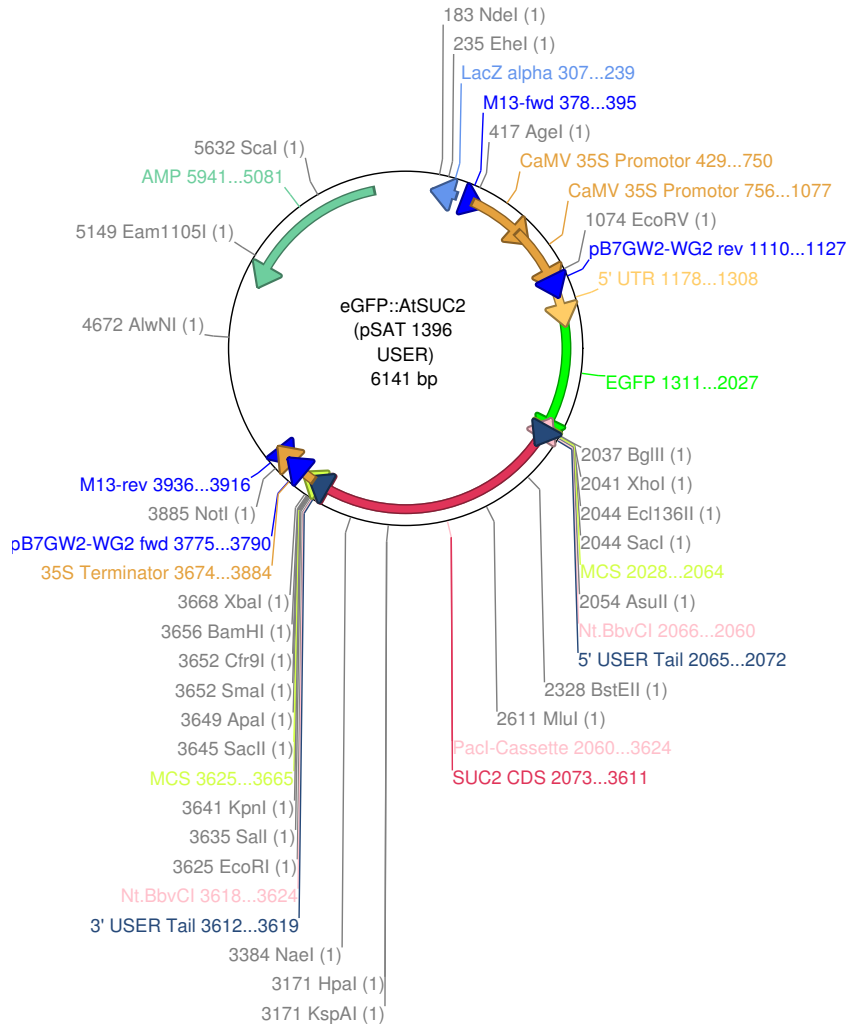


Figure B.5.: Vector map of the eGFP::AtSUC2 construct in the transient expression vector pSAT 1396 USER featuring all unique restriction sites. AtSUC2 CDS length: 1539 bp. Ideal restriction digest conditions: EcoRV & NaeI resulting in 3831 & 2310 bp fragments.

B.6 eGFP::AtLIPOCALIN

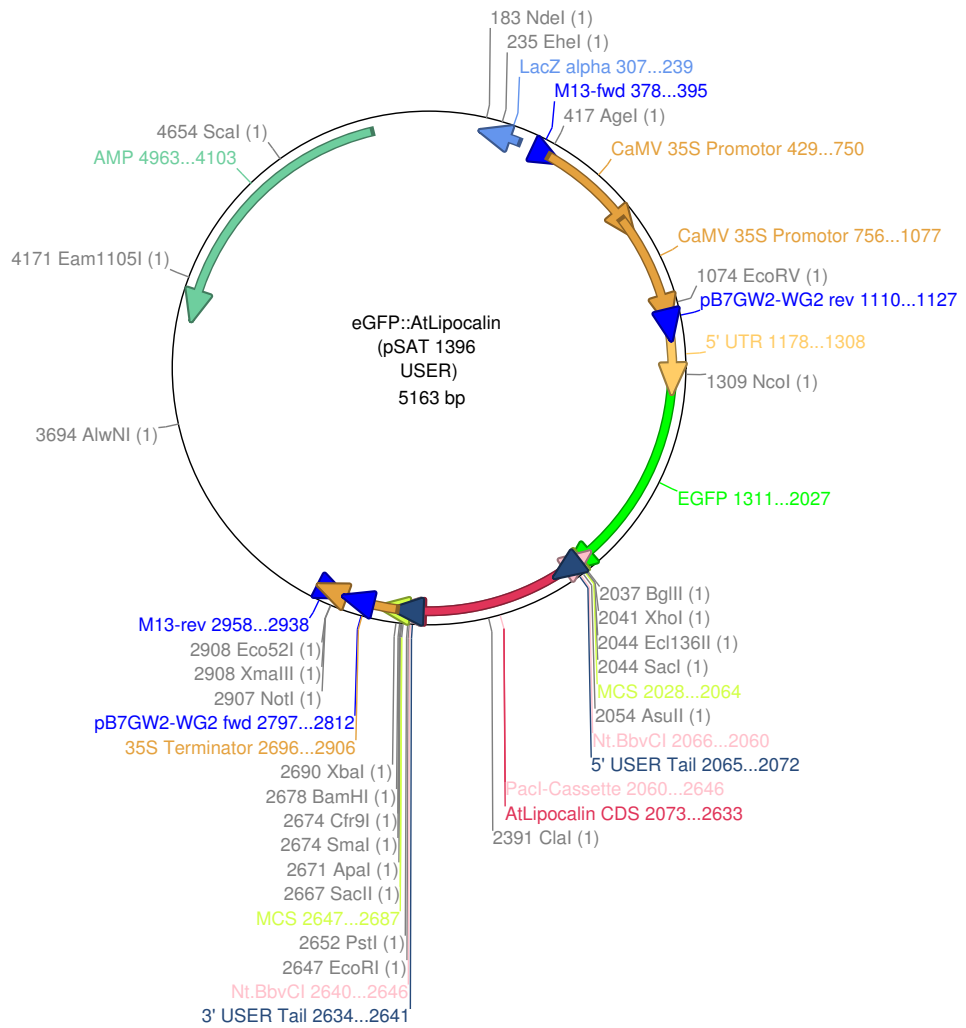


Figure B.6.: Vector map of the eGFP::AtLipocalin construct in the transient expression vector pSAT 1396 USER featuring all unique restriction sites. AtLipocalin (At5g58070) CDS length: 561 bp. Ideal restriction digest conditions: ClaI & NcoI resulting in 4081 & 1082 bp fragments.

B.7 DsRED2::AtLIPOCALIN

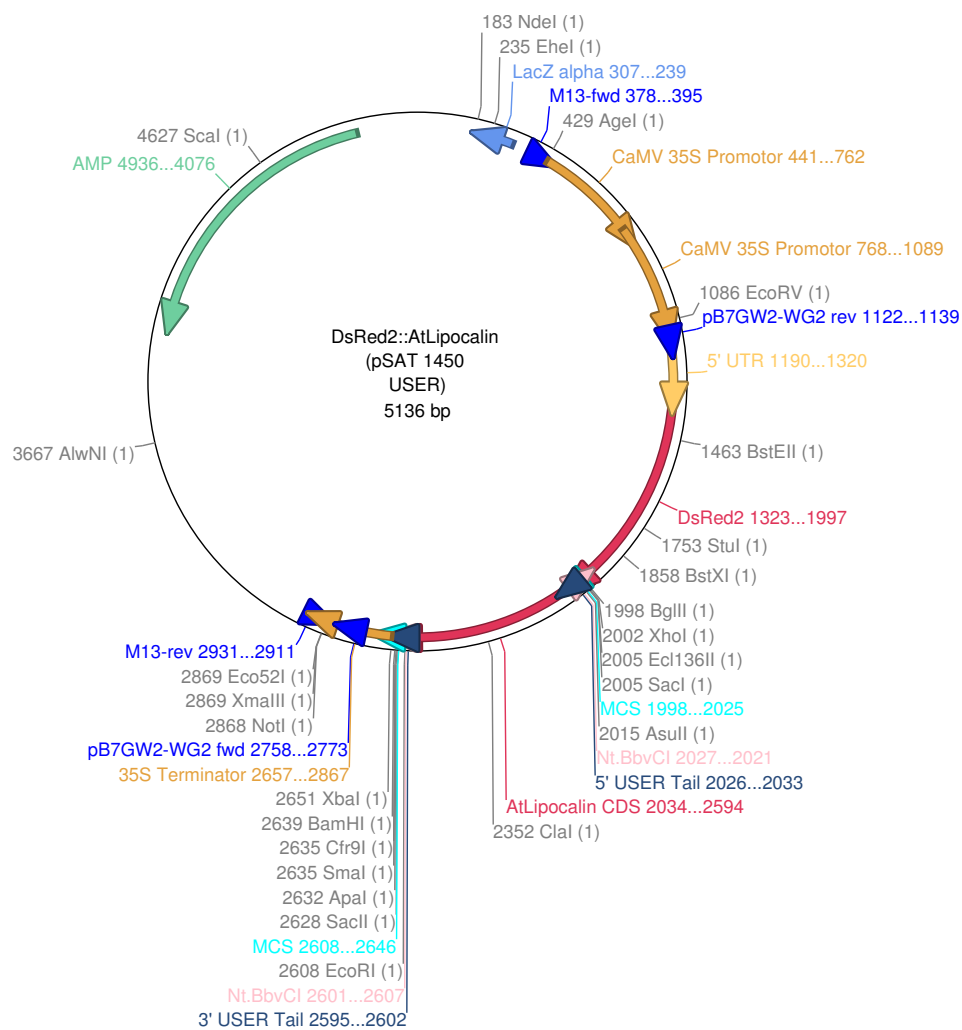


Figure B.7.: Vector map of the DsRed2::AtLipocalin construct in the transient expression vector pSAT 2242 USER featuring all unique restriction sites. AtLipocalin (At5g58070) CDS length: 561 bp. Ideal restriction digest conditions: Clal & EcoRV resulting in 3870 & 1266 bp fragments.

B.8 ABI1::V5

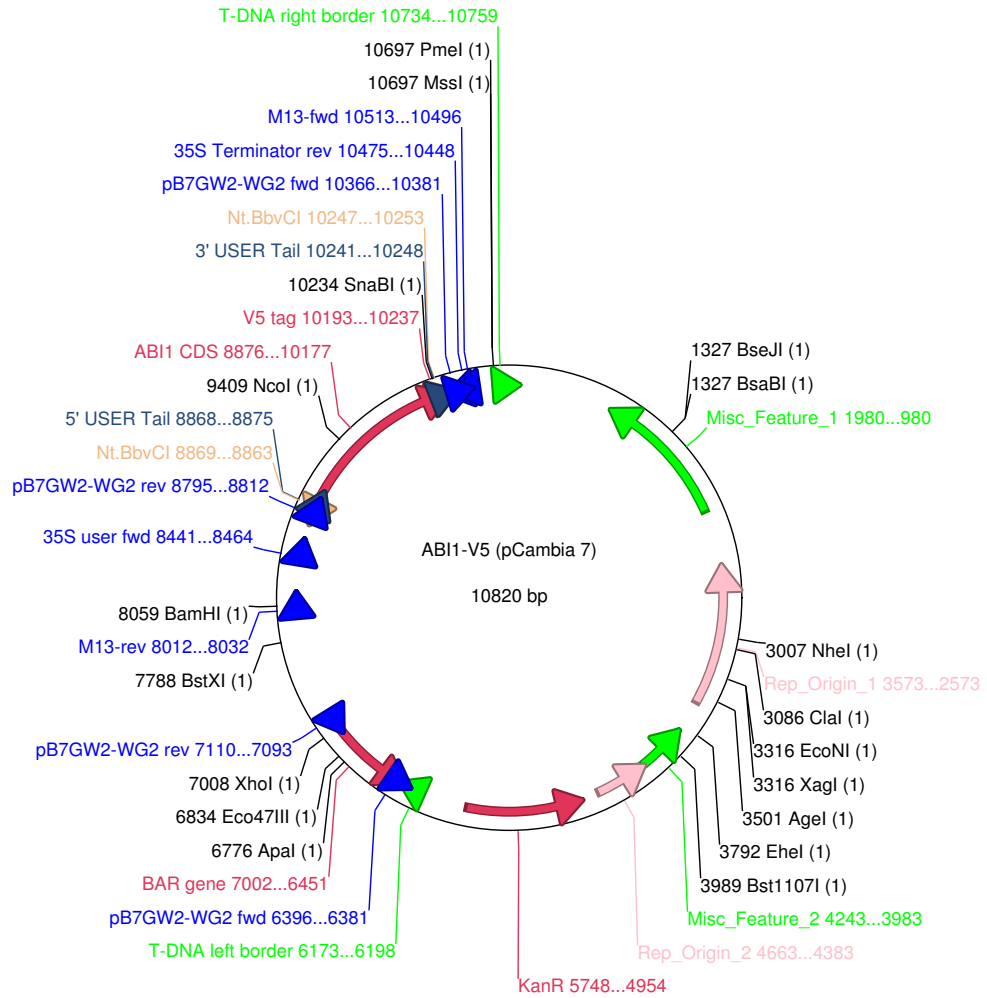


Figure B.8.: Vector map of ABI1::V5 in the binary transformation vector pCambia 7. ABI1 (At4g26080) CDS length: 1302 bp. Ideal restriction digest conditions: NcoI & XhoI resulting in 8419 & 2401 bp fragments.

B.9 CPK21::V5

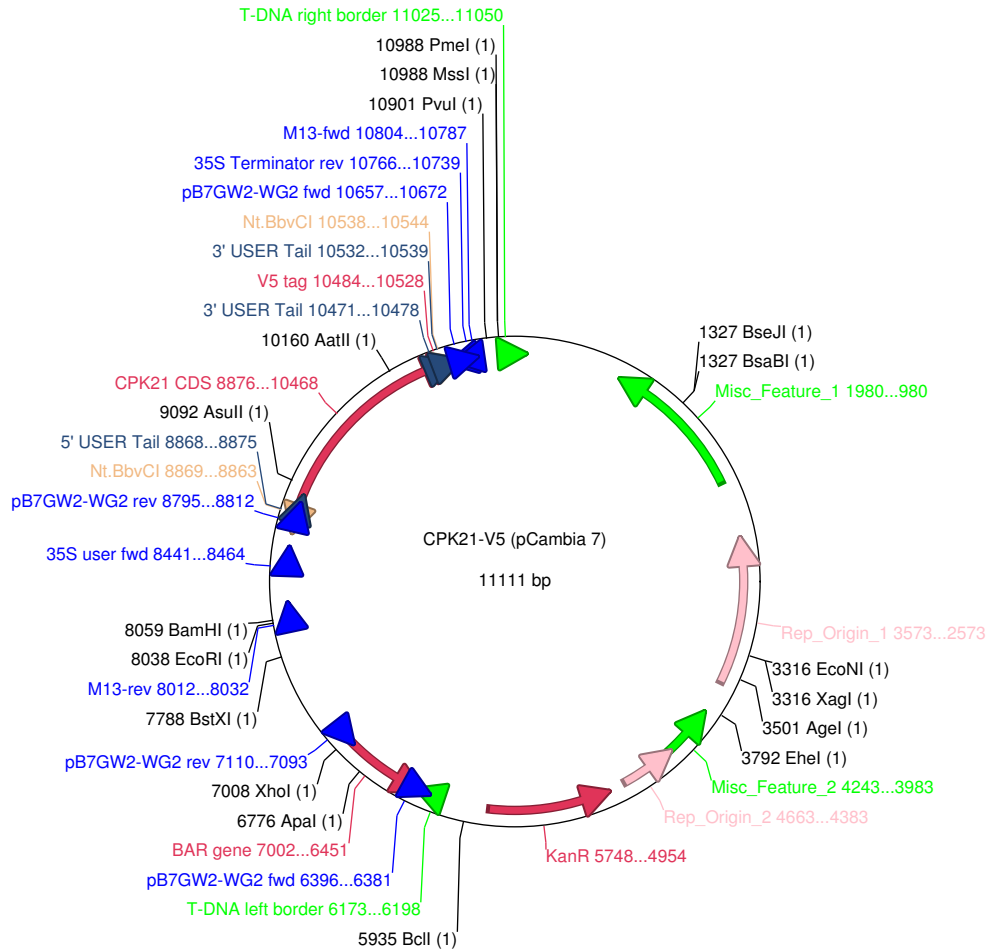


Figure B.9.: Vector map of CPK21::V5 in the binary transformation vector pCambia 7. CPK21 (At4g04720) CDS length: 1593 bp. Ideal restriction digest conditions: AatII & XhoI resulting in 7959 & 3152 bp fragments.

B.10 SLAH3::V5

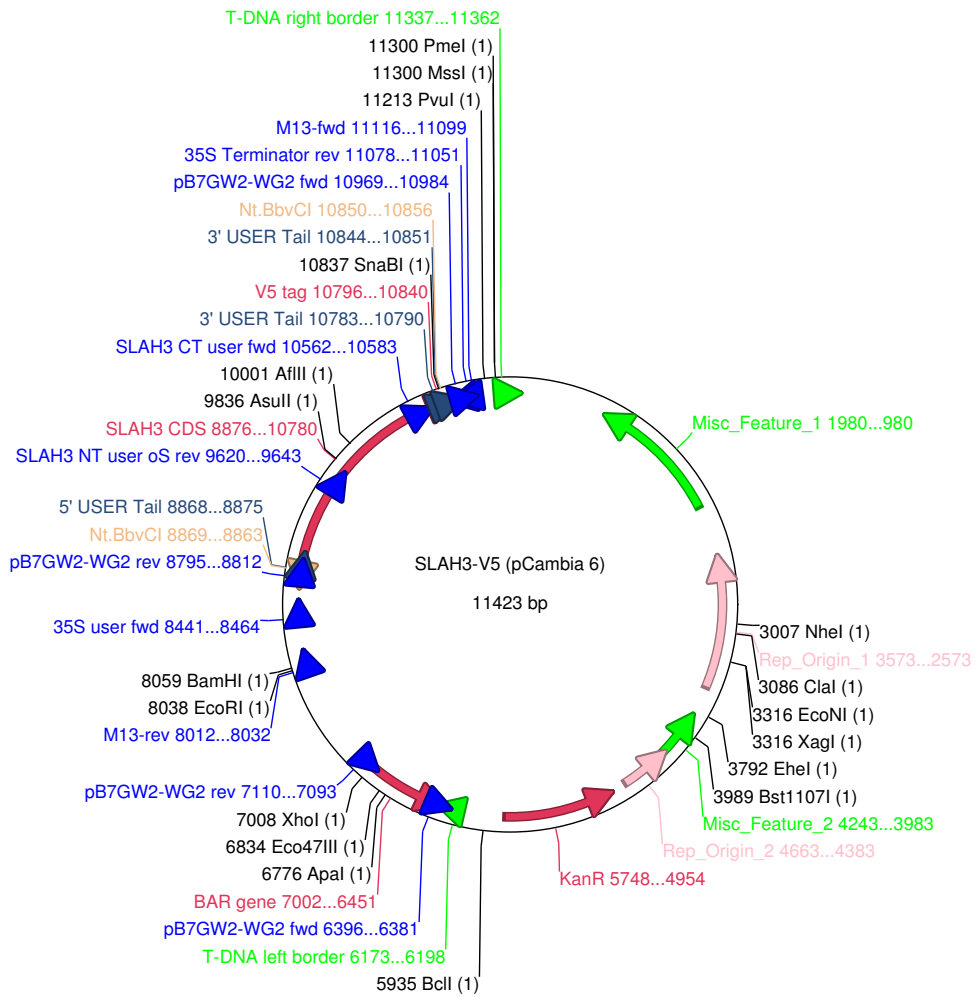
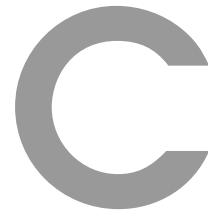


Figure B.10.: Vector map of SLAH3::V5 in the binary transformation vector pCambia 6. SLAH3 (At5g24030) CDS length: 1905 bp. Ideal restriction digest conditions: AflII & XhoI resulting in 8430 & 2993 bp fragments.



Terminology

GLOSSARY

Brij-98

Brij-98 – Non-ionic detergent polyoxyethylene (20) oleyl ether. 24, 34, 44, 49, 79–83, 85–87, 96, 100, 109–112, 114, 117, 121, 125, 127, 161, 186, 194

caveolae

Caveolae – Invaginations of the animal plasma membrane present in many cell types (but not in neurons), formed by the 21 kDa protein caveolin (Rothberg *et al.*, 1992). Functionally participating in endo-/exocytosis and transport processes (Pelkmans *et al.*, 2004). They strictly rely on cholesterol (Hailstones *et al.*, 1998).. 4, 28, 29

Dextran T-500

Dextran T-500 – Dextran polymer with an average molecular chain weight of 500 kDa. 46, 47, 76, 96, 213

DIGE

DIGE – Difference gel electrophoresis, involves multiplexing of multiple protein samples on the same 2D gel for direct comparisons of protein abundance. 37, 39, 112

DRMs

DRMs – Detergent-resistant membranes: biochemical approach to decipher *in vivo* lipid rafts. Isolated via sucrose density gradients after detergent treatment (e.g. with Triton X-100) as a floating opaque band due to their higher buoyancy than the rest of the plasma membrane (because DRMs are enriched in sterols & sphingolipids giving rise to the higher buoyancy). Sometimes also called "microdomains", "detergent-insoluble membranes (DIMs)" or "detergent-insoluble glycoproteins (DIGs)". 3, 6, 10–15, 18, 20–22, 26, 29–32, 34–41, 43, 44, 48, 49, 53, 57, 73, 75–77, 79–85, 87–89, 92–94, 96, 98–101, 103–114, 116–119, 121–123, 125–127, 161, 162

DSF

DSF – Detergent-soluble fraction: the solubilized majority of the plasma membrane proteins residing in the "bottom" of the sucrose gradient thus not floating. 3, 48, 49, 73, 78, 93, 96, 98, 99, 103–108, 116, 121

DTT

Dithiothreitol – general reducing reagent. Also used for reduction of cysteine double bonds of tryptically digestion peptide fragments. 60, 61

ESI-Nano-HPLC MS/MS

Electrospray ionization nano-HPLC tandem mass spectrometry – protein identification technique based upon the separation of tryptically digested peptide fragments (of proteins) by reversed-phase chromatography and additional electrospray ionization of the peptide fragments. These fragments are then analyzed via a tandem mass spectrometer and assigned to the corresponding proteins according to databases. 63

filipin

Filipin – a polyene antibiotic which builds specific complexes with free 3-b-hydroxysterols and sequesters cholesterol in the membrane; when filipin has bound to sterols, a bright white fluorescence can be visualized which can be used to localize sterol-enriched domains in the plasma membrane (usually used at a concentration of $5 \frac{\mu}{L}$). 15, 23, 29, 33

GPI

glycosylphosphatidylinositol. 8, 9, 18, 26, 28, 37, 64, 86, 113, 114

IAA

Iodoacetamide – methylation agent for guarding free cysteine groups on the tryptically digested protein backbone. 60, 61

MCD

Methyl- β -D-cyclodextrin – the most widely used chemical to disrupt sterol-enriched membrane domains; cyclodextrins in general sequester sterols away from the membrane. The water-soluble form methyl- β -D-cyclodextrin is usually used at a concentration of 25 mM. 3, 6, 14, 15, 24–26, 28, 29, 31, 37, 39, 41, 43, 48, 75, 88–90, 92–100, 103, 104, 107, 108, 110, 111, 115–118, 121, 122, 125–127, 161, 186, 192, 200

PEG-3350

Polyethylene glycol 3350 – Polyethylene glycol polymer with an average molecular chain weight of 3350 kDa. 46, 47, 76, 96, 213

PVPP

Polyvinylpyrrolidone – inhibitor of the plant-specific family of phenoloxidase proteases. 45

SCXC

Strong cation exchange chromatography – separation of peptides by ionic interactions with a cation exchange column. 61, 80

APPENDIX C. TERMINOLOGY

TPP

Aqueous two-phase partitioning – purification of membrane fractions with the help of two different polymers (e.g. Dextran T-500 & PEG-3350) in an aqueous two-phase system. 46

Triton X-100

Triton X-100 – non-ionic detergent (Polyethylenglycol-[4-(1,1,3,3-tetramethylbutyl)phenyl]-ether). 6, 10–13, 15, 16, 18, 24, 29, 32, 35–37, 40, 44, 49, 79–82, 84–89, 92–94, 96, 100, 101, 104–107, 109–114, 117–119, 121, 125–127, 161, 186, 194

ACRONYMS

°C

temperature in degrees Celsius. 13, 18, 19, 45–49, 53, 57–62, 65–73, 96, 104, 110, 111

aa

amino acids. 7, 27

ABA

abscisic acid. 11, 12, 41, 84, 94, 103, 120–123, 125–127

ABC

ATP-binding cassette. 94, 110, 111, 113

ABI1

abscisic acid insensitive 1. 84, 93, 94, 103, 106, 107, 116, 120–123, 125–127

AFM

atomic force microscopy. 17, 18

A.p.

Allium porrum. 39

APP

amyloid precursor protein. 25

APS

ammoniumpersulfate. 51

BiFC

bi-molecular fluorescence complementation. 42

bp

base pairs. 70, 201–210

BRI1

BRASSINOSTEROID INSENSITIVE-1. 1

BSA

bovine serum albumin. 53

APPENDIX C. TERMINOLOGY

Ca²⁺

calcium. 7, 11, 12, 120, 123

CCV

clathrin-coated vesicle. 24, 33

CFP

cyan fluorescent protein. 73, 106

CFTR

cystic fibrosis transmembrane receptor. 123

CHO

chinese hamster ovary. 24

Col-0

Arabidopsis thaliana ecotype Columbia-0. 71

CPK

calcium-dependent protein kinase. 12, 44, 80, 84, 92, 110, 113, 116, 120, 121, 123, 125

DAG

diacylglycerol. 4

DGDG

digalactosyldiacylglycerol. 10

DIG

detergent-insoluble glycoprotein. 9

DMSO

dimethylsulfoxide. 60, 61

DOPC

1,2-dioleoyl phosphatidylcholine. 14–18, 29

DPPC

1,2-dipalmitoyl phosphatidylcholine. 18, 20, 29

DsRed2

Discosoma sp. red fluorescent protein 2. 72

ER

endoplasmatic reticulum. 8, 14, 23, 28, 37, 75, 79, 101

EtOH

ethanol. 71

FA

formic acid. 62, 63

fdr

false discovery rate. 161

FLS2

FLAGELLIN SENSITIVE-2. 1, 116, 117

FRAP

fluorescence recovery after photobleaching. 118

FRET

Foerster-resonance energy transfer. 14, 17

fwd

forward (5' → 3' primer). 68

GAP

GPI-anchored protein. 6, 8, 9, 11, 13, 14, 18, 25, 26, 29, 30, 32, 36, 37, 83, 109, 116, 118

 g_{av}

g force units in average. 46–48, 58, 59, 61, 73

GFP

green fluorescent protein. 24, 27, 41, 72–74

GRAVY

grand average of hydropathicity. 64, 82, 87

GTP

guanosine triphosphate. 8, 10, 28, 36, 121

GUV

giant unilamellar vesicle. 16

APPENDIX C. TERMINOLOGY

h

hours. 47, 54, 60, 72, 97

H₂O MQ

Millipore purified H₂O. 53

HB

homogenates buffer. 45

HPLC

high-performance liquid chromatography. 63, 110–112

HRP

horseradish peroxidase. 54, 97

IP₃

inositoltriphosphate. 4

kb

kilo base pairs. 70

kDa

kilo Dalton. 27, 28, 40, 73, 74, 85, 97, 98, 103, 105, 212

LCB

long-chain base. 2

L_d

liquid-disordered. 15–17, 20, 36

LGMD

limb-girdle muscular dystrophy. 28

L_o

liquid-ordered. 15–20, 24, 36

LRR

leucin-rich repeat. 36, 93, 110, 116

MAMP

microbe-associated molecular pattern. 32, 123

MAP

mitogen-activated kinase. 28

MCS

multiple cloning site. 70

MDCK

Madin-Darby canine kidney. 30

MDR

multidrug resistance. 36

MeCN

acetonitrile. 62

MGDG

monogalactosyldiacylglycerol. 10

min

minute. 18, 48, 49, 53, 54, 61–63, 66, 67, 69–73, 96, 104

mL

milliliter. 45–47, 78

mM

millimolar. 45, 46

MS

mass spectrometry. 80, 110–112, 117, 162

M.t.

Medicago truncatula. 42

NC

nitrocellulose. 53

NMT

N-myristoyl transferase. 7

o/n

over night. 49, 53, 54, 58, 66, 73

APPENDIX C. TERMINOLOGY

PA

phosphatidic acid. 11, 94

PAI

protein abundance index. 62

PAMP

pathogen-associated molecular pattern. 32

PAT

palmitoyl acyl transferase. 7

PBS

phosphate-buffered saline. 54

PBS-T

PBS supplied with 0.05 % Tween-20. 53

PC

phosphatidylcholine. 11, 32, 115

PCR

polymerase chain reaction. 68, 69

PDGF

platelet-derived growth factor. 28

Pfu C_x

Pyrococcus furiosus C_x polymerase. 68, 70

PI

phosphatidylinositole. 4

pI

isoelectric point. 82

PIG

particle inflow gun. 67, 71

PIP

plasma membrane intrinsic protein. 93

PLAP

placental alkaline phosphatase. 6, 18, 29

PLD

phospholipase D. 11

PM

plasma membrane. 2, 4, 6, 9–11, 15, 18, 20–28, 30, 32, 33, 36–43, 46–49, 56, 57, 59, 73, 75–79, 81, 83–89, 93, 94, 96–101, 103, 105, 107, 109–119, 121–123, 161, 162

PUFA

polyunsaturated fatty acids. 26

PVDF

polyvinylidene fluoride. 53

rev

reverse (3' → 5') primer. 68

ROS

reactive oxygen species. 38, 83, 94

rpm

rounds per minute. 46

RT

room temperature. 49, 53, 54, 57–62, 65, 68, 72, 97

RuBisCO

ribulose-1,5 bisphosphat-carboxylase / -oxygenase. 81, 93

s

seconds. 65, 70

SD

standard deviation. 3

SDS-PAGE

sodium-dodecylsulfate polyacrylamide gel electrophoresis. 40, 50, 80, 97, 112

SDT

single-dye tracking. 26

APPENDIX C. TERMINOLOGY

SE

standard error. 77, 102

S.I.

Solanum lysopersicum. 41

SLAC

slow anion channel. 12

SLAH

SLAC1 homologue. 12, 44, 123

STED

stimulated emission depletion. 14

SUV

small unilamellar vesicle. 16

TBS

tris-buffered saline. 54

TBS-T

TBS supplied with 0.05 % Tween-20. 53

TCR

T-cell receptor. 9, 29

TFA

trifluoroacetic acid. 63

TMD

transmembrane domain. 10, 15, 40, 86, 87, 111, 123

Tris

tris(hydroxymethyl) aminomethane. 45

V

volt. 60, 66

YFP

yellow fluorescent protein. 73, 106



CV

Personal data

Name	Fatih Demir
Date of birth	June 9 1982
Place of birth	Mannheim (D)
Personal status	Luckily ∅ with Liliana Demir
Nationality	Turkish
EMail	fatih.demir@botanik.uni-wuerzburg.de

Academic education

PhD	2010 – 02/2007	Julius-von-Sachs Institute for Biosciences, Dept. of Botany I, Würzburg, D
-----	----------------	---

Thesis	"Lipid rafts in Arabidopsis thaliana leaves"
Supervisor	Prof. Dr. Rainer Hedrich
Co-supervisors	Dr. Ines Kreuzer & Dr. Jörg Reinders

Diplom (Biology)	December 2006	Heidelberg University, D
------------------	---------------	--------------------------

Thesis	"Untersuchungen zur Identifizierung von rezeptor-interagierenden Proteinen in Ara- bidopsis thaliana" ("Investigations on identification of receptor-interacting pro- teins in Arabidopsis thaliana")
Supervisor	Dr. habil. Giselbert Hinz, HIP

	12/2006 – 10/2001	Heidelberg University, D
--	-------------------	--------------------------

Major	Biochemistry
Minors	Cellular biology and molecular biology

Scholar education

Abitur	June 2001	Elisabeth-Gymnasium, Mannheim, D
--------	-----------	----------------------------------

D.1 PUBLICATION(S)

DEMIR F, BLACHUTZIK J, SCHERZER S, GEIGER D, REINDERS Y, AL-RASHEID K, HARMS G, HEDRICH R & KREUZER I (2010): Arabidopsis nanodomain-delimited ABA signalling regulates ion channel SLAH3. *In submission to Nature.*



Erklärung

Hiermit erkläre ich, dass ich die vorliegende Dissertation in allen Teilen selbst angefertigt und keine anderen als die von mir angegebenen Quellen und Hilfsmittel verwendet habe.

Ich habe die Dissertation weder in gleicher noch in ähnlicher Form in anderen Prüfungsverfahren vorgelegt.

Ich habe bislang noch keine weiteren akademischen Grade erworben oder zu erwerben versucht.

Würzburg, den 30. September 2010

Fatih Demir